AN ABSTRACT OF THE THESIS OF

Jeff Louch for the degree of Doctor of Philosophy

in Chemistry presented on May 17, 1991.

TITLE: Fiber Optic Sensors and Spectrometry for the Detection of Volatile Gem-polyhalogenated Hydrocarbons

Redacted for Privacy

Abstract approved: ____

James D. Ingle, Jr.

A fiber optic fluorometer utilizing a double-fiber optic probe was constructed. The absolute fluorescence signal and effective collection efficiency are approximately one fifth those of typical cuvette fluorometers and agree with those predicted by theory. A quinine sulfate calibration curve shows linearity from a detection limit of 10 pg/mL to 10 µg/mL. Single- and double-fiber probe configurations were also compared. The double-fiber configuration provided better detection limits due to its superior signal-to-background ratio.

A discussion of sensor methodology for the monitoring of reaction intermediates is presented and a simple kinetic model for predicting the time dependent response of such sensors is developed. Two possible mechanisms for the Fujiwara reaction with chloroform are discussed. The effect of pyridine, water, and base concentrations on reaction kinetics was evaluated to develop single-phase Fujiwara reagent mixtures for both fluorometric and spectrophotometric determinations of chloroform. A unique "continuous-exposure"

apparatus allowing vapor phase transport of chloroform from an aqueous sample to a conventional cuvette was constructed. The spectrophotometric detection limit for chloroform is 11 ng/mL and the method was shown to be suitable for the analysis of tap water.

Two fiber optic chemical sensors (FOCS) for the detection of chloroform were developed. An aliquot of the optimized fluorometric reagent solution is held in contact with the fiber optic probe within a light-tight enclosure and is isolated from a bulk sample by a trapped headspace. One FOCS utilizes 1.3 mL of reagent held in a reservoir and the other utilizes a 10-μL drop of reagent suspended on the sensing tips of the fiber optic probe. Chloroform vapor from the sample migrates into the FOCS and reacts with the reagent to produce a fluorescent reaction intermediate which is monitored at 590 nm; the rate of increase in the fluorescence signal is related to chloroform concentration. Both FOCSs give detection limits better than 0.1 ng/mL. The response and total measurement times are comparable for the two FOCSs, and the duration of the linear response is limited by inner-filter effects. The response to a number of volatile GPHHCs including the trihalomethanes are reported. Analyses of tap water for chloroform with the reservoir FOCS and GC/MS were in excellent agreement.

Fiber Optic Sensors and Spectrometry for the Detection of Volatile Gem-polyhalogenated Hydrocarbons

by

Jeff Louch

A THESIS

submitted to

Oregon State University

in partial fulfillment of
the requirements for the
degree of

Doctor of Philosophy

Completed May 17, 1991

Commencement June, 1992

APPROVED:

Redacted for Privacy

Professor of Chemistry in Charge of major

Redacted for Privacy

Chairman of Department of Chemistry

Redacted for Privacy

Dean of Graduate School

Date thesis is presented May 17, 1991

Typed by Jeff Louch for Jeff Louch

TABLE OF CONTENTS

LIST OF FIGURES

LIST OF TABLES

LIST OF APPENDIX FIGURES

LIST OF APPENDIX TABLES

FIBER OPTIC SENSORS AND SPECTROMETRY FOR THE DETECTION OF VOLATILE GEM-POLYHALOGENATED HYDROCARBONS

CHAPTER 1

INTRODUCTION

This project involves the design and application of Fiber Optic Chemical Sensors (FOCS). The Random House Dictionary defines a sensor as a "device sensitive to light, temperature, or radiation that transmits a signal to a measuring or control device" (1). Chemical sensors are devices providing signals related to the concentration or activity of a specific chemical species (or class of compound). Fiber optic chemical sensors are transducers that utilize fiber optics to guide optical radiation to and from a sample and transform (chemical) concentration information into the optical domain as either a fluorescence, absorption, or scattering signal.

As defined, a FOCS is a transducer which provides an optically encoded chemical signal. If the chemical species of interest exhibits quantifiable fluorescence, absorption, or scattering in the appropriate wavelength range (defined by the source emission and the transmission characteristics of the fiber optics), the FOCS may be nothing more than the plain terminations of the fiber optics (immersed in the sample). This simple sensor would provide a continuous signal tracking the monitored concentration, i.e., the

optically encoded signal would increase and decrease with the concentration of the chemical species monitored. When the species of interest is not directly measurable, a miniature chemical reactor capable of providing an appropriate signal must be incorporated in the FOCS; this signal should also be continuous in time and track (on a time scale appropriate to the specific application) changes in the chemical composition of the sample.

Overall, the basic definition of a FOCS is that of a chemical transducer which operates as a peripheral device and provides a continuous (on an appropriate time scale) readout that tracks the concentration of the monitored species. It is the ability of a sensor to function in a location removed from all other required instrumentation that is of utility, as this allows "remote sensing".

The ability to obtain a signal from a remote sample (remote sensing) allows for the potential of performing in situ analyses. That is, if it is no longer necessary to place a sample in an instrument to obtain a measurement, but instead, a sensor can be placed in the sample, the need for the sampling step is removed and an in situ analysis is possible. In principle, this offers many advantages when performing a chemical analysis:

(i) Sample contamination due to handling is avoided,

(ii) Loss of analyte due to sample handling is avoided (due to volatility, adsorption, etc.),

(iii) Shifts in chemical equilibria affecting the analyte (triggered by removing a sample from its environment) are avoided,

(iv) The potential for continuous, real time monitoring exists.

The first three factors are especially important when performing trace or ultra trace analyses, speciation studies, or determinations of highly volatile or reactive species (2-4). The ability to perform real time continuous monitoring is important in biomedical, environmental, and process control applications. In addition to the advantages of performing an in situ analysis, the ability to obtain a measurement from a remote sample is often advantageous. With suitable sensors it is possible to monitor aggressive samples in hazardous or otherwise inaccessible sites. Finally, remote sensing methodology allows for the possibility of multiplexing, utilizing one central instrument to process the data from an array of sensors.

Fiber optic sensors are intrinsically safer than electrochemical sensors in that they are electrically passive. This is an important consideration when monitoring potentially explosive environments or obtaining in vivo clinical measurements. In addition, the electrically passive nature of these devices ensures their immunity from electromagnetic interference. Optical sensors can implement a variety of methodologies including absorption, fluorescence, and scattering measurements. Thus, fiber optic sensors are capable of detecting a wide variety of chemical species. A topical analysis for which in situ remote sensing methodology would be particularly useful is the determination of certain volatile gem-polyhalogenated hydrocarbons in both ground and drinking waters.

Gem-polyhalogenated hydrocarbons (GPHHC) are organic species having two or more halogen atoms bonded to a single carbon. Examples of such compounds are DDT, trichloroethylene, Eldrin, and the trihalomethanes (THMs): chloroform, bromoform, bromodichloromethane, and dibromochloromethane. As a group, GPHHCs are heavily regulated by the federal government. Of the 83 contaminants regulated by the Safe Drinking Water Act (SDWA), 11 are gem-polyhalogenated compounds (5), as are 9 of the 53 compounds on the First Drinking Water Priority List (6). Of the 208 species addressed by the Resource Conservation and Recovery Act (RCRA), 33 are gem-polyhalogenated (7). The importance of these compounds is further stressed by their ranking in the Comprehensive Environmental Response, Compensation, and Liability Act (CERCLA) priority pollutant list (8); six of the 25 category 1 species (those posing the greatest health risk and occurring with the highest frequency) are gem-polyhalogenated, and 21% of the total list belongs to this group. Table 1.1 lists the gem-polyhalogenated hydrocarbons addressed by these pieces of legislation.

To ensure compliance, the EPA has defined specific (approved) analytical procedures for quantitation of all regulated compounds and requires verification of compliance at regular, prescribed intervals. The RCRA mandates that land-based waste disposal sites test underlying ground water for contamination at least twice a year (9). The SDWA requires that finished drinking water be tested on a quarterly basis (6).

The prescribed methodologies for quantitation of the volatile species listed by table 1.1 are all based an gas chromatography. For

TABLE 1.1. Compounds with gem-polyhalogenated functional groups regulated by the Safe Drinking Water Act (SDWA), the Resource Conservation and Recovery Act (RCRA), or the Comprehensive Environmental Response, Compensation,and Liability Act (CERCLA).[a]

Compound	Regulated by:
Aldrin	RCRA, CERCLA
Bromodichloromethane*	RCRA, CERCLA, SDWA
Bromoform*	RCRA, CERCLA, SDWA
Carbon Tetrachloride*	RCRA, CERCLA, SDWA
Chlordane	RCRA, CERCLA, SDWA
Chlorodibromomethane*	RCRA, CERCLA, SDWA
Chloroform*	RCRA, CERCLA, SDWA
1,1-Dichloroethane*	RCRA, CERCLA
1,1-Dichloroethylene*	RCRA, CERCLA, SDWA
4,4'-DDE, DDT, DDD	RCRA, CERCLA
Dichlorodifluoromethane*	RCRA, CERCLA
Dieldrin	RCRA, CERCLA
Endosulfan(s)	RCRA
Endrin	RCRA, CERCLA, SDWA
Fluorotrichloromethane*	RCRA, CERCLA
Heptachlor	RCRA, CERCLA, SDWA
Hexachloroethane*	RCRA, CERCLA
Hexachloropropene	RCRA
Methoxychlor	RCRA, CERCLA
Methylene Bromide	RCRA
Methylene Chloride*	RCRA, CERCLA, SDWA
1,1,2-Trichloroethane*	RCRA, CERCLA, SDWA
1,1,1,2-Tetrachloroethane*	RCRA
1,1,2,2-Tetrachloroethane*	RCRA, CERCLA
Trichloroethylene*	RCRA, CERCLA, SDWA
Tetrachloroethylene*	RCRA, CERCLA, SDWA
1,1,1-Trichloroethane*	RCRA, CERCLA, SDWA

[a]Those species EPA considers to be volatile are marked with an asterisk.

quantitation of the trihalomethanes (only) in drinking water, EPA has specified methods 501.1 (10), 501.2 (11), and 501.3 (12). All of these methods require a preconcentration step (purge-and-trap for 501.1 and 501.3 and solvent extraction for 501.2), and utilize either (Hall) electrolytic conductivity (501.1), electron capture (501.2), or mass spectroscopic (501.3) detection. The approved methodologies for the detection of all volatiles (purgables) are purge-and-trap GC with either electrolytic conductivity (EPA method 601) or mass spectrometer (EPA method 624) detection (13). For greater calibration sensitivity, EPA has also approved a method (1624) based on purge-and-trap isotope dilution GC/MS (13).

Implementation of these prescribed methodologies requires a high degree of operator skill and EPA requires each analyst to demonstrate the ability to "generate acceptable accuracy and precision" (13). This, coupled with the high initial cost of the necessary instrumentation, means that most water treatment and waste disposal facilities contract these analyses to private labs; economic considerations also limit the required frequency of analysis (14,15).

The ability to perform frequent, on-site, analysis for the GPHHCs at a reasonable cost is important for many reasons. Although smaller drinking water facilities (those serving less than ten thousand people) are not required to monitor for trihalomethanes (due to treatment cost) in their finished drinking water, a record of THM concentration would still be valuable for both scientific and legal purposes. By providing simple, cost effective, analytical methodology, more frequent testing at all drinking water facilities becomes possible. Similar considerations also apply to the monitoring of

ground water adjacent to landfills, where more frequent monitoring may prevent the undetected breakthrough of contaminants into ground water supplies. In addition, the ability to perform continuous, in situ, monitoring for these organic species would facilitate the study of ground water transport phenomena.

In this thesis, efforts towards developing remote sensing methodology based on fluorescence sensing capable of continuous, in situ, monitoring of aqueous systems for volatile gem-polyhalogenated hydrocarbons are presented. In addition, sensor methodology is applied for the development of laboratory analyses for the detection of the trihalomethanes in drinking water. Initially (chapter 2), a review of fiber optics is presented along with a detailed discussion and review of Fiber Optic Chemical Sensors (FOCS).

Studies to characterize the relative optical efficiencies of the basic single- and double-fiber fiber optic probe geometries were performed and the implications of the results on overall system performance are discussed (chapter 3). A fluorometer for use specifically with FOCSs was designed and constructed. The characteristics of this instrument were evaluated and compared to those of traditional spectrofluorometers (chapter 4). A unique, modular fiber optic probe system allowing one set of fiber optics to be employed with a variety of interchangeable sensing reactors was designed and constructed (chapter 4).

Chemistry for the kinetic determination of gem-polyhalogenated hydrocarbons in aqueous samples was developed (chapter 5). A unique apparatus allowing vapor-phase analysis for the determination of these species using cuvette spectrometers was constructed (chapter

5). The ability to quantitate chloroform in tap-water at sub µg/mL levels using this apparatus coupled with the reported spectrophotometric reagent is demonstrated (chapter 5).

The design parameters affecting the calibration sensitivity of a FOCS reactor for the detection of volatile species were studied and and two FOCS reactors were constructed (chapter 6). The response of both the FOCS reactors to chloroform were characterized (chapter 6) using a reagent system optimized for the fluorometric detection of chloroform (chapter 5), and the ability to detect chloroform at sub ng/mL levels with both reactors is demonstrated. Using one of the reported FOCSs (the "reservoir" FOCS), an FOCS determination of chloroform is shown to give results equivilant to GC/MS for laboratory tap water (chapter 6).

REFERENCES

1. The Random House Dictionary, Ballantine Books, New York, 1980.

2. Leenheer, J.A. in Minear, R.A. and Keith, L.H., Editors, "Water Analysis; Vol. 3, Organic Species", Academic Press, N.Y., 1984, 83-158.

3. Hertz, H.S.; May, W.E.; Wise, S.A.; Chesler, S.N. Anal. Chem. 1978, 50, 428A-436A.

4. Marr, I.L.; Cresser, M.S. "Environmental Chemical Analysis", Chapman and Hall, N.Y., 1983, 24-33.

5. Drinking Water; Substitution of Contaminants and Drinking Water Priority List of Additional Substances Which May Require Regulation Under the Safe Drinking Water Act Federal Register 1987, 52 (130), 25720-25734.

6. Drinking Water; Substitution of Contaminants and Drinking Water Priority List of Additional Substances Which May Require Regulation Under the Safe Drinking Water Act Federal Register 1988, 53 (14), 1892-1902.

7. List (Phase 1) of Hazardous Constituents for Ground-Water Monitoring Federal Register 1987, 52 (131), 25942-25953.

8. Notice of the First Priority List of Hazardous Substances That Will Be the Subject of Toxicological Profiles Federal Register 1987, 52 (74), 12865-12874.

9. Hazardous Waste Management Systems; Permitting Requirements for Land Disposal Facilities Federal Register 1982, 47 (143), 32273-32388.

10. Warner, B.J.; Cheng, S.C.; Friedman, C.S.; Mitrosky, S.; Snyder, A.D.; McMillin, C.R. "EPA Method Study 23A, Method 501.1, Trihalomethanes by Purge and Trap" 1984, EPA-600/4-84-020.

11. Warner, B.J.; Cheng, S.C.; Finke, J.M.; Friedman, C.S.;Mitrosky, S.; Snyder, A.D.; McMillin, C.R. "EPA Method Study 23B, Method 501.2, Trihalomethanes by Liquid/Liquid Extraction" 1984, EPA-600/4-84-021.

12. Measurement of Trihalomethanes in Drinking Water with Gas Chromatography/Mass Spectrometry and Selected Ion Monitoring Method 501.3, EPA form 1320-4 (Rev. 3-76).

13. Guidelines Establishing Test Procedures for the Analysis of Pollutants Under the Clean Water Act; Final Rule and Interim Final Rule and Proposed Rule Federal Register 1984, 49 (209), 43233-43436.

14. Earley, J.D. J. Environ. Health 1987, 50, 33-34.

15. Miller, K.J. WATER/Engrg. and Management Feb. 1988, 30-32.

CHAPTER 2

FIBER OPTICS AND FIBER OPTIC CHEMICAL SENSORS

Paralleling advancing fiber optic technology has been the growing number of applications for fiber optics in optical spectroscopy. Fiber optics have found use in laboratory instruments for the measurement of absorption (1,2) and fluorescence (1-5). The use of fiber optics allows for greater flexibility in instrument design as fixed line of site optics need not be employed, thus reducing constraints on the sample-instrument interface. In addition to their utility in the laboratory, fiber optics are being increasingly used to construct sensors to perform remote fiber spectroscopy (RFS).

The general principle behind any fiber optic sensor is straightforward; radiation is launched into a fiber optic, transmitted to a location where it is modulated by a measurand, and then returned by another (or the same) fiber optic to be demodulated and detected. A fiber optic sensor can be classified as being either extrinsic or intrinsic (6). An extrinsic sensor utilizes fiber optics only to guide radiation to and from a sampling zone; the actual modulation of the carrier radiation occurs externally from the fiber optic. Intrinsic fiber optic sensors are those in which the measurand interacts directly with the radiation within the fiber. For example, the Crenkov radiation generated within a fiber optic by high energy particles can be used to detect these same particles (6). In this case, radiation is generated within the fiber optic and no source is required. More commonly, the measurand will modulate

the intensity, phase, or polarization of the original "probe" radiation.

As a class, intrinsic sensors are used almost exclusively for the measurement of physical parameters. Intrinsic sensors for the measurement of temperature, pressure, electric current, strain, and magnetic force have been reported. Overall, fiber optic sensors responding to physical parameters are well established and have been reviewed (6-8). Of more interest to the analytical chemist, however, are sensors for the quantitation of chemical species, which are by necessity extrinsic.

Fiber optic chemical sensors, or FOCS, for the determination of H^+, NH_3, O_2, CO_2 and many other species have been reported. Conceptually, FOCS systems are in many respects analogous to traditional spectrometers, as represented in figure 2.1. Outwardly, the only difference between a traditional cuvette spectrometer and a fiber optic spectrometer is the use of fiber optics to transmit radiation to and from the sample. However, fiber optics generally exhibit f-numbers much lower than those of most commercially available optical instrumentation. This, coupled with their small size, means that to obtain maximum signal levels the instrumentation should be designed specifically for use with fiber optics. Other, unique, considerations concern the sensor itself.

The geometry of the sample/fiber interface can take many forms, and the sensor itself can be either an active or a passive device. Passive sensors are those which can only detect species which exhibit native fluorescence, absorption, or scattering. Active sensors implement chemistry to obtain signals from species which do not

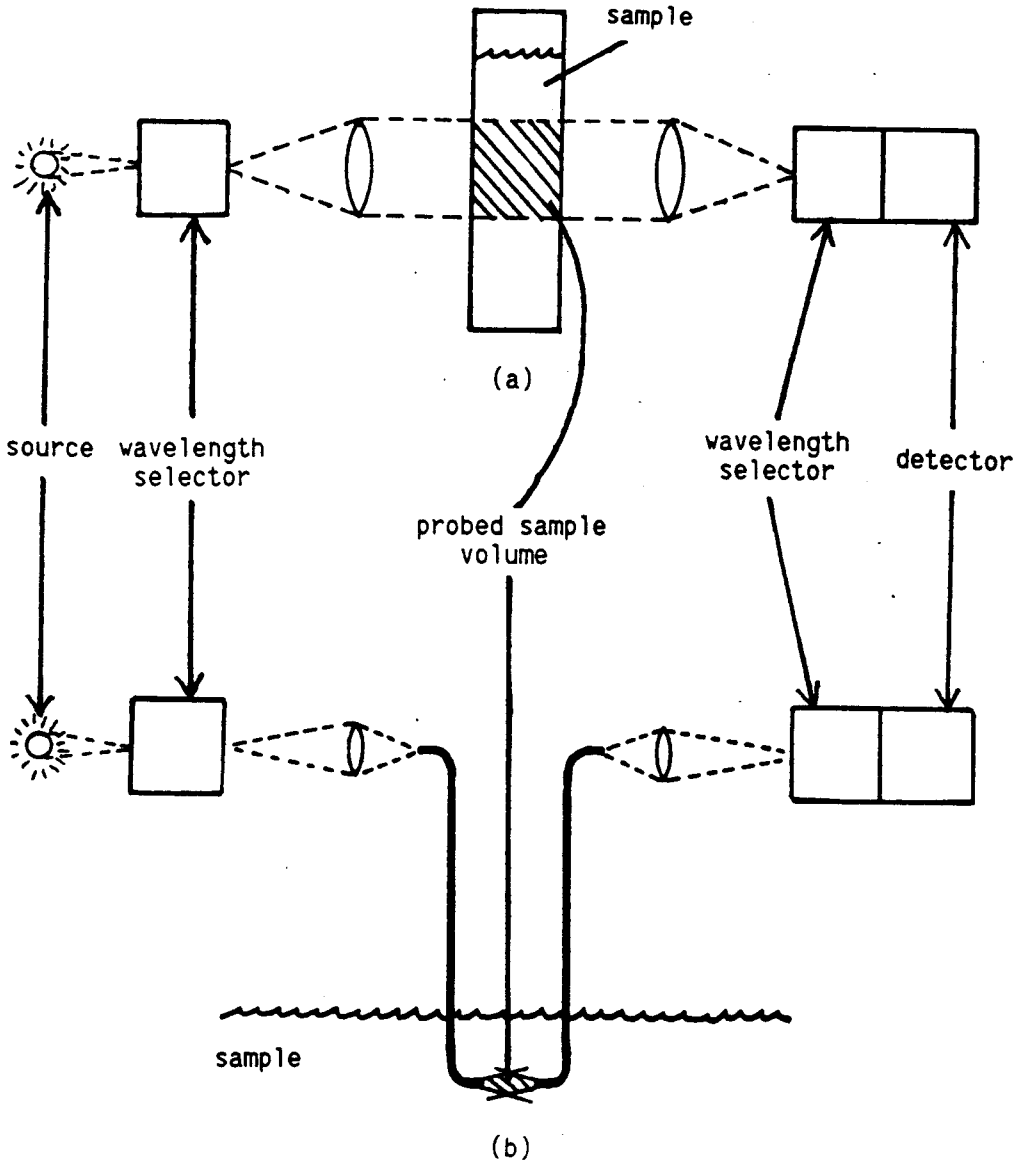

Figure 2.1. Diagram showing the basic configurations of (a), a cuvette spectrometer and (b), a fiber optic spectrometer.

absorb or fluoresce themselves. This points out the most challenging barrier to the development of FOCSs: the difficulty of performing "remote chemistry". In the laboratory, sample preparation can be carried out under controlled conditions and complex chemistry can be used to obtain analyte specific response. This type of methodology is not easily implemented with a sensor, which must be able to obtain an analyte specific signal by simply inserting the sensor into a sample.

This chapter continues with a brief discussion of the properties of fiber optics as they pertain to RFS. Then, the merits of different probe geometries are discussed and their use as passive FOCSs are reviewed. Finally, the chapter ends with a discussion of chemical transduction and a review of active FOCSs.

FIBER OPTICS

Fiber optics utilize the phenomenon of total internal reflection to trap and guide radiation. A representation of a typical step-index fiber optic (for which the refractive indices of both the core (η_1) and cladding (η_2) are constant) is shown in figure 2.2. When a ray of light enters the core of the fiber optic such that the condition $\sin\theta_2 \geq \eta_2/\eta_1$ is met (where θ_2 is the critical angle and η_1 and η_2 are the refractive indices of the core and cladding, respectively), the ray will be totally internally reflected. From this, an expression giving the limiting launch angle, θ_0, (the numerical aperture) can be derived (9)

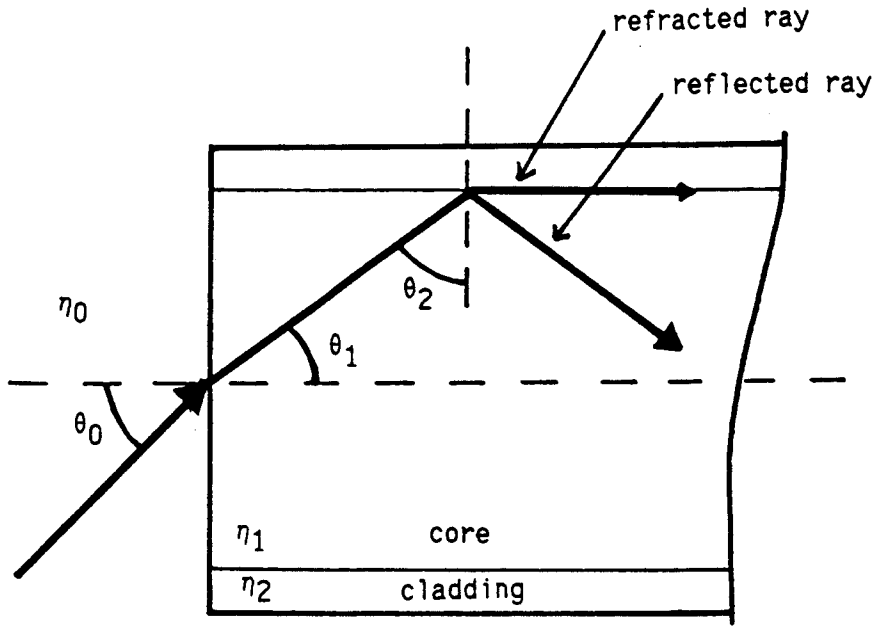

Figure 2.2. Ray path showing the limiting launch angle (θ_0) and the critical angle (θ_2) of a step-index fiber optic (both the reflected and refracted rays at the interface of the core and cladding are shown).

$$NA = \eta_0 \sin\theta_0 = [(\eta_1)^2 - (\eta_2)^2]^{\frac{1}{2}} \qquad (1)$$

where η_0 is the refractive index of the launch medium. Numerical aperture (NA) is a figure of merit representing the light collecting ability of a fiber optic; as the NA increases the angle θ_0 increases and the fiber optic accepts a larger cone of light. Another figure of merit reflecting the light gathering ability of a fiber optic is its f-number, which is defined as

$$F/n = 1/(2 \tan\theta_0) \qquad (2)$$

Because the indices of refraction are a function of wavelength (dispersion), both the NA and F/n of a fiber optic are wavelength dependent. Typical ranges for the NA and F/n are 0.1-0.66 and 0.75-5.0, respectively.

Equations 1 and 2 describe the light gathering ability of step-index fiber optics (10); in addition, graded-index fiber optics are also available. The index of refraction of the core of a graded-index fiber decreases radially from the fiber optics axis (9,10), and the resulting ray paths within a graded-index fiber optic are sinusoidal-like (11); figure 2.3 shows generalized representations of the refractive index profiles and the resulting ray paths for both step- and graded-index fiber optics. For a graded-index fiber optic, the NA (eq. 1) varies with the radial position on the fiber face (9,10) and is greatest on the axis of the fiber optic.

For Lambertian (diffuse) optical sources, the coupling efficiency (source power into fiber optic/total source power) is

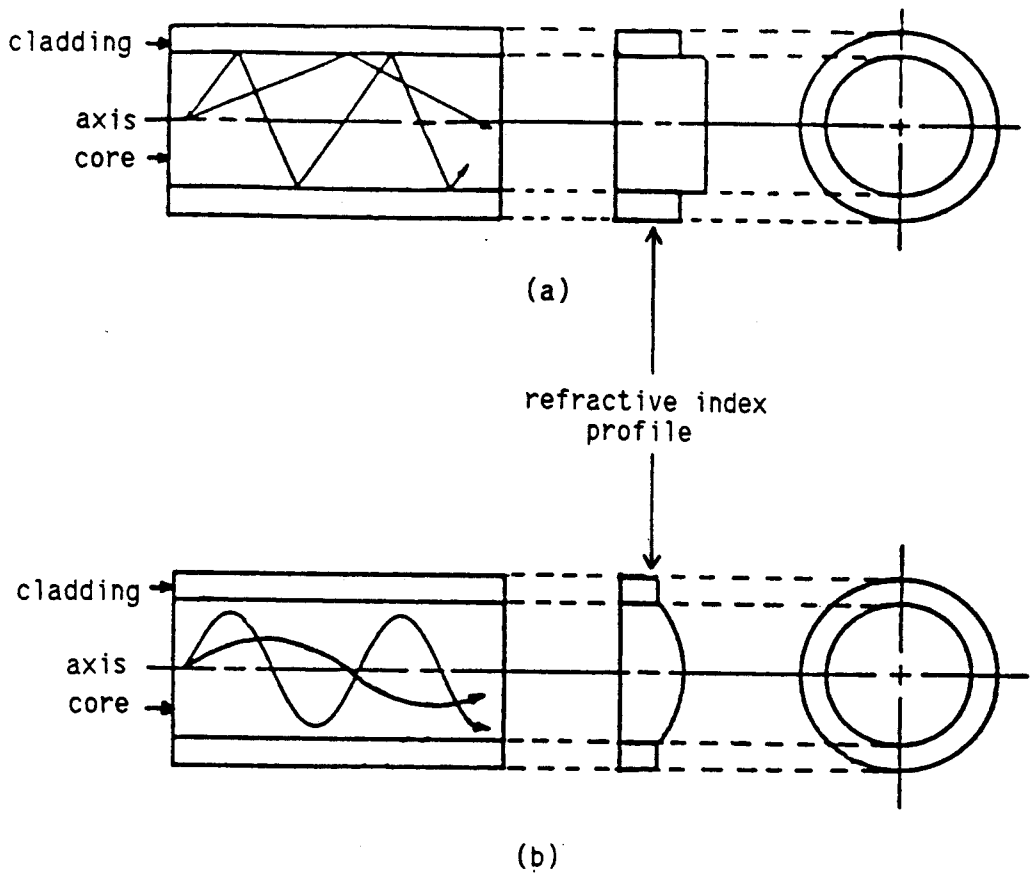

Figure 2.3. Representative ray paths and refractive index profiles of (a), a step-index fiber optic and (b), a graded-index fiber optic. Most graded-index fiber optics have power-law refractive index profiles (10).

proportional to the square of the NA (10,11). Thus (when using a Lambertian source), a graded-index fiber optic exhibiting the same limiting NA (on the fiber optic axis) as a step-index fiber of the same diameter is expected to collect approximately one half the power collected by the step-index fiber optic (11).

Graded-index fiber optics are useful as they reduce pulse dispersion relative to step-index fiber optics, with the extent of dispersion being a function of the refractive index profile (12). Pulse dispersion refers to the temporal broadening of a pulse of radiation as it travels through a fiber optic and is of extreme importance in communications applications as it limits the rate of data transmission. Pulse dispersion must also be considered if fiber optics are to be used in any method requiring temporal resolution (fluorescence lifetime measurements, etc.). There are a number of independent mechanisms causing pulse dispersion in fiber optics (11); their relative contributions depend not only on whether the fiber is a step-index or graded-index fiber but, also, on whether the fiber is a mono-mode or a multi-mode fiber optic.

From figure 2.2, it appears possible to draw an infinite number of unique ray trajectories. However, the number of "allowed" rays is quantized (13,14), each allowed ray corresponding to a standing wave propagating in the fiber optic. Each of these allowed rays is termed a mode. The fundamental mode corresponds to the ray colinear with the fiber optic axis, while the higher order modes are those whose ray representations strike the core/cladding interface at angles approaching the critical angle. The number of modes which can propagate in a given fiber optic is predicted by the relationship

(14)

$$N = V^2/2 \qquad (3)$$

where V is the "waveguide parameter". The parameter V is a function of the fiber optic and wavelength

$$V = (\pi d/\lambda)[(\eta_1)^2 - (\eta_2)^2]^{\frac{1}{2}} \qquad (4)$$

where d is the diameter of the fiber optic core and λ is the free space wavelength (9). A fiber optic is considered to be a multi-mode fiber when $V \gg 1$ and a mono-mode fiber when $V < 2.405$ (although $N \simeq 2.8$ for $V = 2.405$, the two allowed modes are an orthogonal polarization pair). From equation 4, V is proportional to the fiber optics diameter (at a constant wavelength) and thus, typical mono-mode fiber optics have diameters of < 10 μm (for wavelengths in the visible to near-IR region of the spectrum).

A major factor contributing to pulse spreading in fiber optics is intermodal dispersion. This effect is shown (for a step-index fiber) in figure 2.4 and results from the different transit times exhibited by rays following different paths within the fiber optic. Since the index of refraction is constant across the fiber core, all the rays travel at the same speed, and thus, rays with differing trajectories within the core arrive at the distal termination at different times. Because graded-index fibers have refractive indices which decrease radially, rays whose trajectories extend farther from the fiber axis (higher order modes, see figure 2.3) pass through

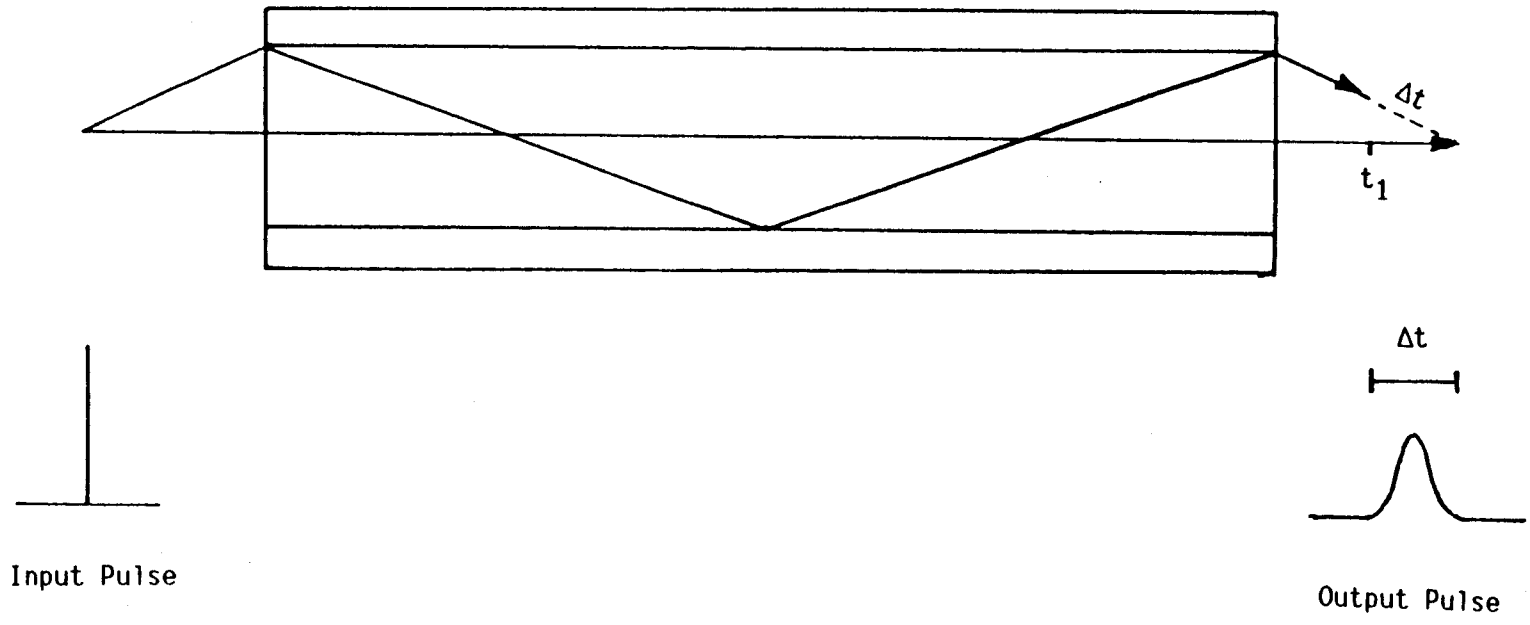

Figure 2.4. Ray trace of the fundamental and a higher order mode (in a step-index fiber opt c) showing the effect of intermodal dispersion on pulse width (both rays are drawn having the same geometric pathlength).

regions of lower refractive indices. This increases their velocity in these regions, equalizing transit times and thus limiting pulse dispersion.

A second factor contributing to pulse spreading is material dispersion resulting from the slight variation of refractive index with wavelength. For fused silica this effect is minimal in the region of 1.2-1.3 μm (15). In addition, as the wavelength range of the guided radiation is decreased, the effect of material dispersion becomes less noticeable (16).

Another factor affecting pulse shape is material absorption (i.e., absorption of the radiation by the fiber optic core and cladding material). This change in pulse shape is partially due to the differences in pathlength (within the core material) experienced by different rays; higher order modes have a longer geometric pathlength within the core and are therefore attenuated (by the core material) to a greater degree than those traveling parallel to the axis. In addition, (for step-index fibers only) these same rays interact with the cladding more frequently, resulting in a greater loss of power to the cladding material.

Overall, the major cause of pulse spreading in a multi-mode fiber optic is intermodal dispersion (16). Typically, step-index fiber optics exhibit dispersion on the order of tens of nanoseconds per kilometer while graded-index fibers exhibit values on the order of nanoseconds, or less, per kilometer (17,18). Interestingly, intermodal dispersion in multi-mode fibers can be reduced by inducing mode coupling. Without mode coupling, the pulse width increases in proportion to fiber length, while with complete mode coupling (a

steady state power distribution among all modes) pulse dispersion is proportional to the square root of fiber length (14,16); however, this will also result in a net loss of power (15,16).

Intermodal dispersion occurs in mono-mode fibers also, although the mechanism is different than that in multi-mode fibers. As previously mentioned, a mono-mode fiber actually supports two modes of mutually orthogonal polarization. If the fiber optic exhibits any birefringence, these two components can travel through the fiber at different velocities resulting in "polarization" dispersion (9); generally, this is a negligible effect (19). This leaves material dispersion as the major cause of pulse broadening in mono-mode fibers. Material dispersion is reported as (ps/(km nm)) and ranges from ca. 400 ps/(km nm) at 500 nm to < 0.1 ps/(km nm) at ca. 1300 nm for fused silica fibers (15). Thus, for mono-mode fused silica fiber optics, the net pulse dispersion is on the order of picoseconds per kilometer in the IR region of the spectrum (16). Of the materials used to fabricate fiber optics, fused silica exhibits the lowest material dispersion (15,16).

Pulse broadening is an extremely important parameter in the communications industry and is also of consequence when implementing temporal measurements for chemical quantitation. A parameter of more universal concern, however, is the attenuation coefficient of the fiber optic in the spectral region of interest. Just as dispersion limits the length over which an accurate temporal measurement is possible, the attenuation by a fiber restricts the distance over which an intensity based measurement is feasible. The attenuation of power guided by a fiber optic is usually expressed in decibels (dB)

where

$$dB = 10 \log_{10} (P_i/P_o) \qquad (5)$$

with P_o being the radiant power exiting a length of fiber optic and P_i the initial radiant power (14); attenuation is usually reported as dB/km.

There are several mechanisms responsible for attenuation in fiber optics. Intrinsic mechanisms are those inherent to the fiber optic materials themselves and are generally grouped under the term material absorption. Material absorption encompasses both absorption and scattering due to the molecular structure of the fiber optic. Mechanisms related to other factors are termed extrinsic. An example would be additional absorption or scattering from defect centers formed on exposing the fiber to ionizing radiation (9,20). In addition, absorption and scattering losses due to chemical impurities (9) and scattering caused by physical artifacts of the manufacturing process (21) are also considered to be extrinsic mechanisms. The fundamental attenuation limit is the sum of the losses due to intrinsic mechanisms (i.e., the losses due to material absorption).

There are three contributions to material absorption: electronic absorption, vibrational absorption, and scattering (9,22). Intrinsic electronic absorption and Rayleigh scattering are due, respectively, to electronic transitions of the species which make up the fiber optic and to refractive index fluctuations due to the random distribution of the individual molecules (9,21). For silica fiber optics, electronic absorption is negligible in the visible and

near-UV regions of the spectrum (14). Rayleigh scattering, on the other hand, increases steadily below 600 nm and represents the fundamental limit to transmission in these regions (9,21,22); the corresponding limit in the IR region is defined by vibrational absorption. Fused silica exhibits strong absorption bands in the approximate range of 9 to 13 μm, with overtones and combination bands appearing down to 3 μm (9). These absorption bands exhibit tails extending down towards 1700 nm (9), and thus, the optimum window for light transmission using fiber optics is traditionally thought of as being between 600 and 1700 nm.

The presence of impurities increases attenuation further; the major impurities found being transition metals and water (21,23). The transition metals copper, iron, nickel, vanadium, chromium, and manganese usually occur in the fiber matrix as ions exhibiting electronic transitions in the visible region of the spectrum (14,21). To keep attenuation at the ions characteristic wavelength of absorbance below 1 dB/km, concentrations should be sub ng/g (14,21). Hydroxyl ion in a fiber exhibits a strong absorption at 2.8 μm (corresponding to a fundamental stretch), and overtones of this band appear at 1.4 μm, 970 nm, and 750 nm (14,21). A concentration of 1 μg/g of water will result in a 1.25 dB/km absorption loss at ca. 970 nm (14).

Another mechanism resulting in the loss of power is waveguide attenuation, a term encompassing mechanisms which are artifacts of the manufacturing process. Manufacturing processes may result in compositional irregularities within the fiber core which can increase loss due to scattering. The cabling process can also lead to

increased attenuation by causing microbending in the fiber, resulting in unwanted mode coupling and an associated loss of power (15). In addition, irregularities at the core/cladding interface can lead to scattering of the guided waves evanescent component, further attenuating power.

The attenuation of radiation in a mono-mode fiber is described by the relationship

$$P(z) = P(0)e^{-2\alpha z} \qquad (6)$$

where P(0) is the initial radiant power (z=0), P(z) is the radiant power at a distance z from the input end, and 2α is a power loss or attenuation coefficient (14). From the relationship

$$dB/km = 4.34(2\alpha) \qquad (7)$$

the attenuation coefficient can be calculated from an experimental measurement of attenuation (14). The exponential relationship (eq. 6) accurately describes power attenuation in a mono-mode fiber or in a multi-mode fiber if only a single mode is excited. As more of the modes of a multi-mode fiber are excited, the simple exponential relationship breaks down because higher order modes are attenuated to a greater extent than low order modes; thus, a single attenuation coefficient is no longer applicable (14). Although a single measurement of attenuation is still possible, this measurement is accurate only for the specific length and launch conditions employed in making the measurement. Over short lengths of fiber, mode mixing compli-

cates the measurements further; however, under conditions of complete mode mixing, an average attenuation coefficient can be approximated and power attenuation again follows the exponential relationship. Still, under most conditions, the loss coefficient depends on mode order; higher order modes usually exhibit larger values than low order modes and the lower order modes carry more power (14). The mechanisms producing this phenomenon can be explained further.

A guided wave (mode) has a well defined spatial structure within the fiber optic core, as shown in figure 2.5. Although not to scale, figure 2.5 shows that the guided wave has a component which extends beyond the core and into the external medium (the cladding material). This "tail" is the evanescent portion of the wave and its amplitude decreases exponentially moving away from the fiber optic (core). The extent to which this field penetrates the cladding (or any external medium) is dependent on its refractive index (relative to the core), the angle of incidence, and the wavelength. The penetration depth (d_p) is defined as the distance over which the field amplitude decays to 1/e of its value at the core surface (25,26). This distance is less than one wavelength and is calculated from

$$d_p = (\lambda/2\pi\eta_1)[\sin^2\theta_2 - (\eta_2/\eta_1)^2]^{-\frac{1}{2}} \qquad (8)$$

where θ_2 is the angle of incidence (see Figures 2.1 and 2.5) and η_1 and η_2 are the refractive indices of the core and the external medium, respectively (25,26). This relationship predicts that at a given wavelength, higher order modes will penetrate any medium

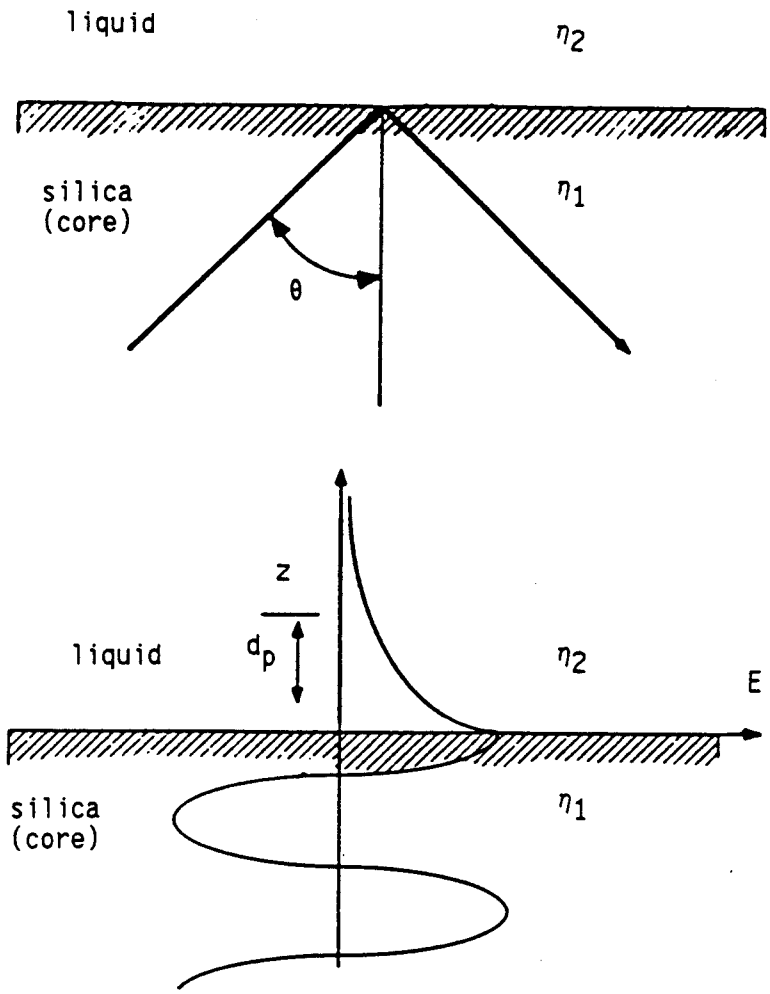

Figure 2.5. Generation of the evanescent wave at the silica-liquid interface of a step-index fiber optic (from ref. 24).

adjacent to the core to a greater extent than lower order modes. In addition, higher order modes will interact with the external medium more frequently than low order modes. The total number of reflections a ray will experience in a fiber optic can be calculated

$$N = (L/d)\cot\theta_2 \qquad (9)$$

where L is the length of the fiber and d is the fiber diameter (25,26). Equation 9 predicts that higher order modes will experience a greater number of reflections per fiber length. Thus, higher order modes lose more power to the cladding (or any external medium) than low order modes because of the greater penetration into the material and the increased frequency of interaction. In addition, these mechanisms partially account for the effects material absorption have on pulse shape, and the often observed decrease in NA of the radiation exiting a fiber optic relative to the launch NA.

Graded-index fiber optics do not suffer from these phenomenon to the same extent as step-index fibers (as the rays are bent, and not reflected at the core/cladding interface). Thus, they typically exhibit slightly lower attenuation coefficients (27).

Another (potential) consequence of this evanescent interrogation of the cladding material (or any external medium) is the injection of unwanted radiation into the fiber optic. Any radiation absorbed by the cladding can potentially excite fluorescence or Raman scattering, a fraction of which is coupled back into the fiber optic core contributing an unwanted background signal. This can be a problem with plastic cladding materials, which are both more absorp-

tive and more fluorescent than glass or silica cladding materials (28).

In the final analysis, material adsorption represents the fundamental limit of power attenuation in a fiber optic. Obviously, higher quality fibers, with a minimum in the level of impurities and number of physical defects, exhibit lower attenuation coefficients. At this time, fused silica fibers provide the lowest attenuation coefficients in the UV-VIS region of the spectrum, and the highest quality fibers are approaching their fundamental limits from this region up into the near-IR region (22).

Figure 2.6 shows typical spectral attenuation plots for both silica and plastic core fiber optics. At 660 nm, the silica fiber optic exhibits an attenuation of ca. 20 dB/km; the corresponding value for a plastic (methylmethacrylate) core fiber optic is ca. 500 dB/km. Glass fiber optics exhibit attenuation coefficients similar to plastic fiber optics (29).

A final consideration in fiber selection is the affect of the fiber optic on the polarization of the guided radiation. In order to preserve the polarization of guided radiation a fiber optic would, ideally, exhibit zero birefringence. Unfortunately, all fiber optics exhibit some birefringence due to incomplete radial symmetry in either refractive index, diameter, or both (31). By spinning the preform while drawing the fiber it is possible to minimize birefringence due to these causes, and mono-mode fibers exhibiting birefringence of less than 2.5°/m have been fabricated (31). Conventionally drawn fiber optics exhibit birefringence on the order of tens of degrees per meter (31), and plane polarized light is

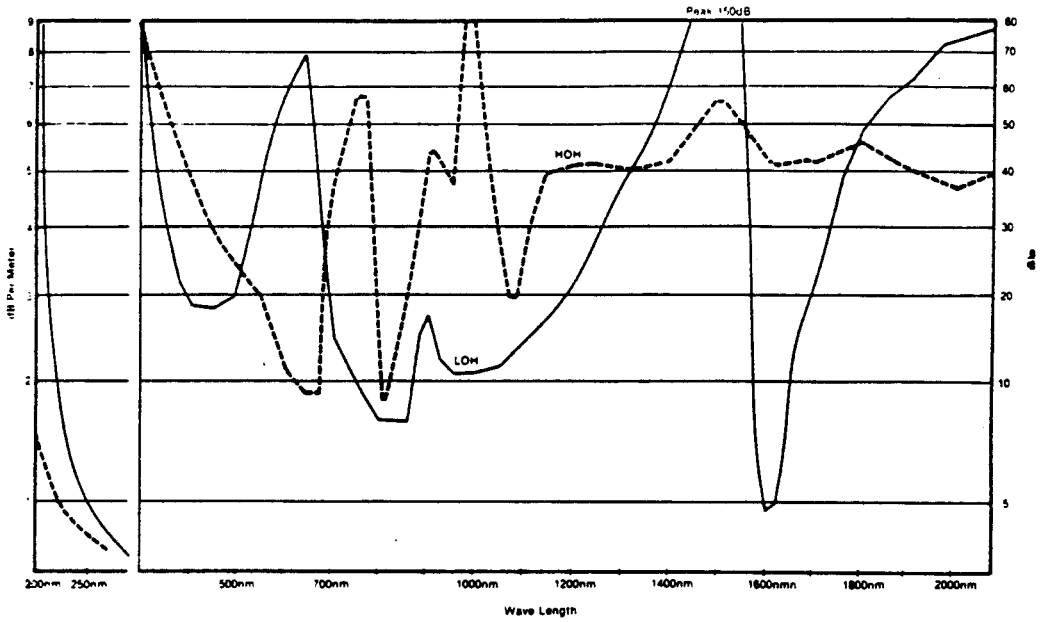

(a)

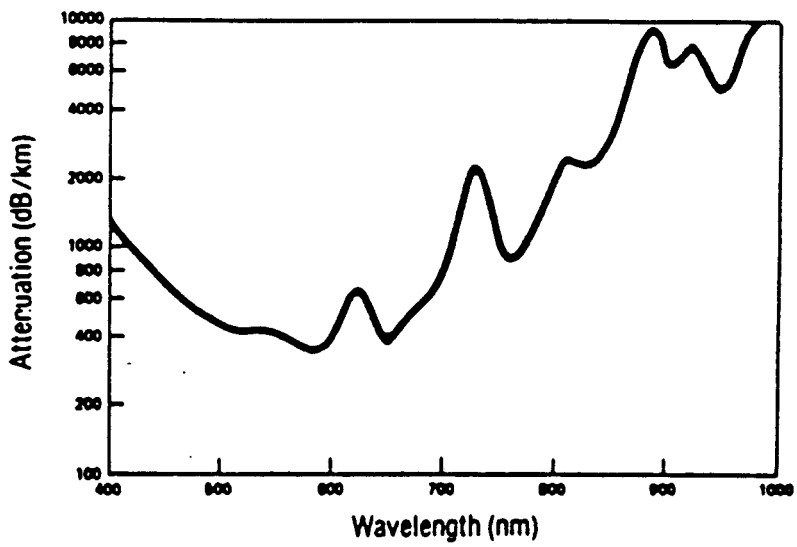

(b)

Figure 2.6. Typical spectral attenuation plots for (a), silica core fiber optic (LOH and HOH are low and high hydroxyl ion content, respectively, from ref. 29) and (b), methylmethacrylate core fiber optic (from ref. 30).

rapidly converted to elliptically polarized light (32).

FIBER OPTIC CHEMICAL SENSORS

The first reported use of fiber optics for chemical sensing appeared in 1962 (33,34). To determine blood oxygen levels, Polanyi and Heir used the common termination of a bifurcated fiber optic bundle immersed in a blood sample to measure attenuated reflectance. Modulated light of two wavelengths was launched into the proximal end of one leg of the fiber bundle while the reflected signal was collected and transmitted to a detector by the other leg. At one wavelength the molar absorptivities of oxyhemoglobin (HbO_2) and reduced hemoglobin (HHb) are different, while at the second they are equal (isobestic pt.). The ratio of the reflected signals at the two wavelengths was shown to be linear with percent oxygen saturation. In later studies the same probe was used for in vivo determinations of percent blood oxygen levels and tracer dye concentrations (35-38). Kapany presented a very similar fiber optic in vivo oximeter in 1964 (39). Since this work, many fiber optic chemical sensors (FOCS) have been reported, and reviews of the FOCS literature have appeared periodically (24,32,40-60). In addition, Analytical Chemistry has recently begun to include a separate FOCS section in their annual Chemical Sensor review (61).

For the purposes of this discussion, each FOCS is defined as being either passive or active. The probe described above is a passive device in that a signal can be obtained only if the species of interest absorbs, fluoresces, or scatters within the wavelength

region transmitted by the fiber optics. If the species of interest cannot be measured directly, the FOCS must implement methodology capable of extracting an optically encoded signal from the analyte. This process has been termed "chemical transduction" (53) and sensors so constructed are active sensors.

Another characteristic differentiating FOCSs is the number of optical channels used to guide radiation to and from the sample. Although it is possible to construct fiber optic probes with any number of fiber optics, all probes implement either the "dual-path" or the "single-path" approach to guiding radiation.

The configuration depicted in figure 2.1 uses one fiber to guide the source radiation to the sample and another to guide the modulated signal from the sample. In this case, the two radiation components travel in two separate optical channels, and the probe is an example of a dual-path probe. Polyani and Hehir's probe is a real example of a passive dual-path probe. Conceptually, any probe consisting of one or more discrete source fibers (guiding the source radiation to the sample) and one or more discrete collection fibers (guiding the modulated signal radiation from the sample to the detection system) is a dual-path probe. It is also possible to utilize a single fiber optic (or bundle) to guide both radiation components. In these cases, a common optical channel is shared and the probes are single-path probes.

All FOCSs can be categorized as being active or passive and dual- or single-path. As passive sensors do not implement any type of chemical transduction, they differ only in their geometric configurations. In this section, a discussion of the different possible

probe configurations is presented first, followed by a summary of their reported applications as passive probes. Subsequent discussions concentrate on chemical transduction and a summary of active probes.

Probe Configurations

Although the probe geometry at the interface between a fiber optic sensor and a sample can have many configurations, there are only two basic modes of interrogation, the transmittive mode and the non-transmittive mode. Transmittive probes monitor the transmission of (source) probe radiation through a volume of sample within an optical path defined by the fiber optics. The instrumental analog to these types of probes would be a spectrophotometer, and this mode is used almost exclusively for the measurement of absorption (see Figure 2.1). Non-transmittive probes launch the probe radiation into a sample collecting a portion of any sample emission, scattering, or reflectance. The instrumental analog to these types of probes would be a fluorometer, and these probes are used to monitor fluorescence, reflectance, or scattering.

Some transmittive probe configurations are shown in figure 2.7. Two variations of the simplest configuration are shown in figures 2.7a and 2.7b. The volume interrogated by these probes is defined by the optical pathlength and the beam diameter (between the two fiber terminations). The sensitivity of these probes can be increased by increasing the pathlength, and in general, the measured absorbance will obey a Beer's Law type relationship (62,63). As shown, both are passive dual-path sensors. Transmittive probes

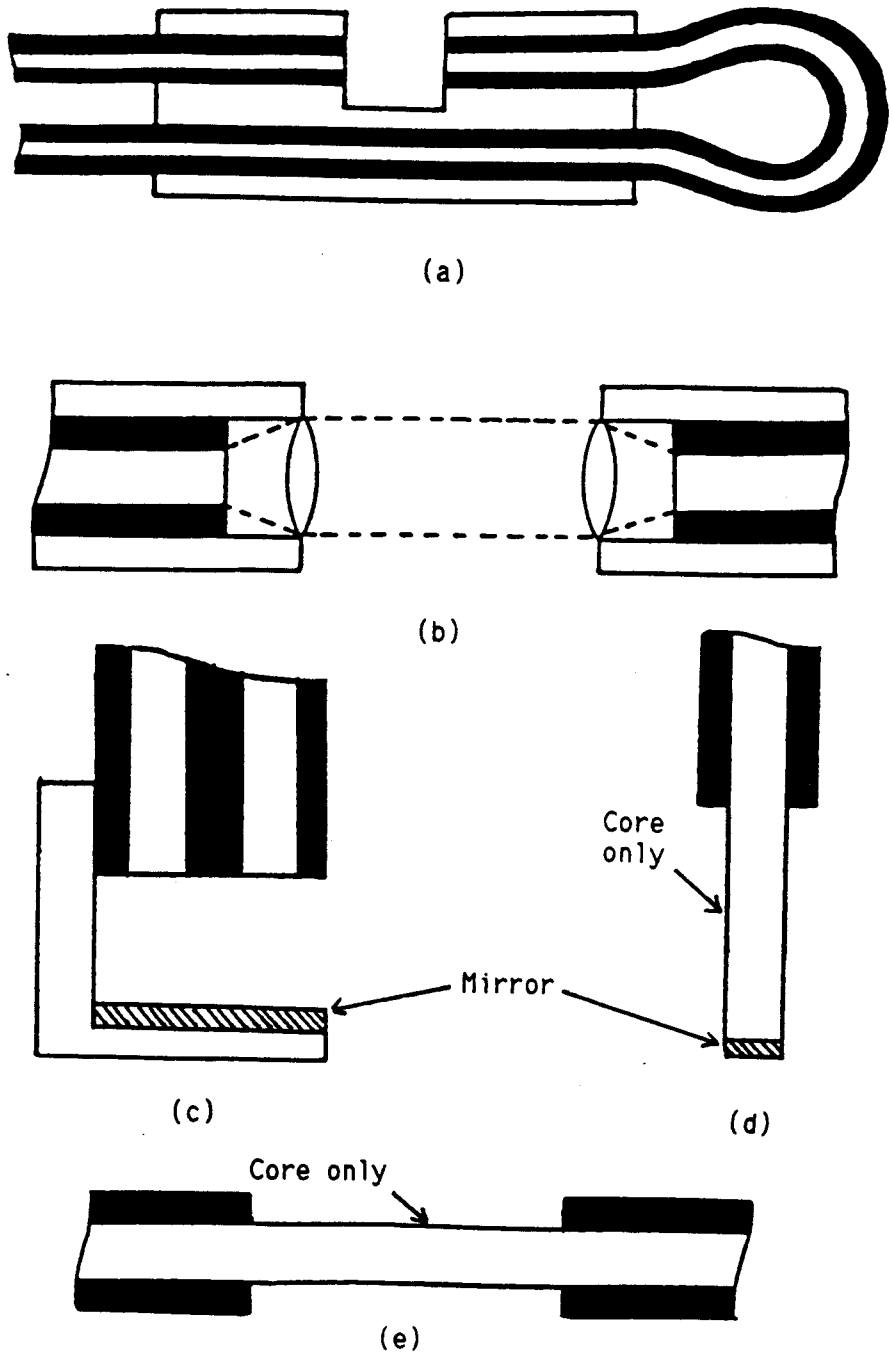

Figure 2.7. Some transmittive fiber optic probe configurations. Configurations 2.7a-2.7c rely on the probe radiation passing through the sample while configurations 2.7d and 2.7e are based on evanescent interrogation of the sample.

similar in configuration to (2.7c) are commercially available (64-66).

The other basic transmittive geometry is the evanescent configuration in which the cladding is removed from a portion of the fiber optic so that the core is in direct contact with the sample; figures 2.7d and 2.7e show the dual- and single-path variations of this type of probe. These configurations rely on the evanescent component of the guided radiation to interrogate the sample volume directly adjacent to the fiber optics surface, and are used to monitor both fluorescence and absorption. This mechanism is conceptually identical to that of ATR (attenuated total reflection) cells used for IR spectroscopy (67).

The sensitivity of an evanescent sensor depends on the ratio of the power of the evanescent wave to that of the total propagating wave (68), and the volume viewed. For a given length of fiber, the viewing volume is a function of penetration depth which, as previously discussed, is greater for the higher order modes when all other factors are equal (Eq. 6). The evanescent power is a function of wavelength and fiber optic dimensions and can be related to the fiber waveguide parameter (V)

$$\eta_p = (P_{ev}/P_t) = 4(2)^{\frac{1}{2}}/(3V) \qquad (10)$$

where η_p is the evanescent-wave ratio, P_{ev} is the net radiant power available in the evanescent components of the guided waves, and P_t is the total guided radiant power (69). Thus, fibers exhibiting lower values of V are predicted to provide greater sensitivity; this

effect has been observed (69).

Love and Slovacek have studied the effects of launch NA on evanescently excited fluorescence (70) and conclude that the fluorescence signal is proportional to the eighth power of launch NA. Although Hirschfeld has also reported this result (71), other workers have reported that the fluorescence signal is proportional to the sixth power of the launch NA (25). Regardless, the trend is clear; by utilizing a larger launch NA, higher order modes are excited increasing the net penetration depth (eq. 8).

Evanescent probes utilizing straight fiber optics have been shown to provide signals linearly related to both concentration (68,69,72,73) and probe length (74). For a straight length of fiber, the observed attenuation by an absorbing species in the external medium is described by a relationship similar to Beer's Law

$$P/P_0 = 10^{-(\eta_p \alpha c L)} \qquad (11)$$

where P_0 is the transmitted radiant power in the absence of the absorber, c and α are the concentration and absorption coefficient of the absorber, respectively, and L is the length of the evanescent field sensor (73). The efficiency of the evanescent field interaction can be increased by coiling the fiber optics, providing an ca. factor of two increase in sensitivity over a straight fiber probe (73). This also makes for a more compact probe when longer lengths of fiber are employed.

The two basic configurations for non-transmittive probes, single- and dual-path, are shown in figure 2.8. Although these

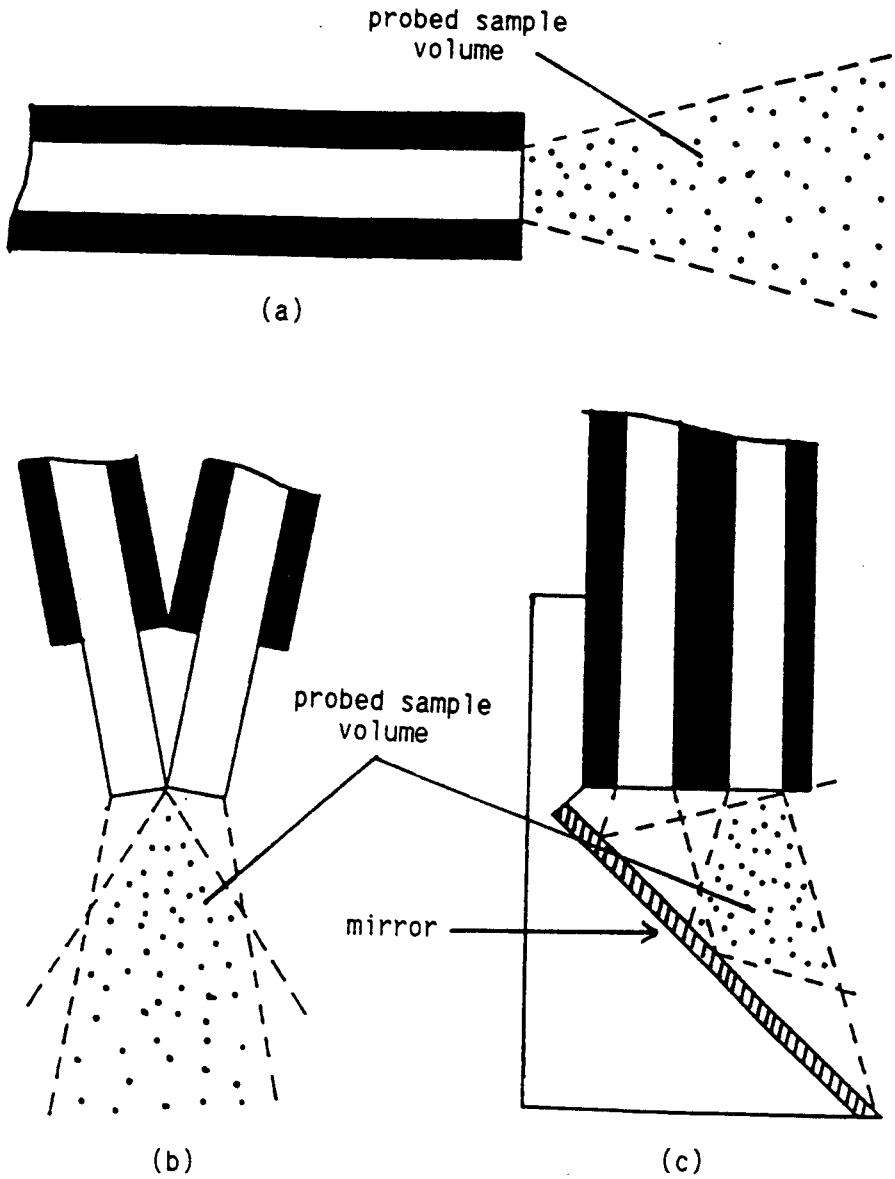

Figure 2.8. Some non-transmittive fiber optic probe configurations. In 2.8a a single-path probe is shown while 2.8b and 2.8c illustrate dual-path probes.

probes cannot measure true transmittance (thus, non-transmittive probes), they can detect absorbing species via attenuated reflectance. These configurations are commonly used to measure fluorescence and scattering, and the probe shown in figure 2.8c is commercially available (66).

Deaton has derived a figure of merit relating the fluorescence collection efficiency of single-path non-transmittive probes (see Figure 2.8a) to the characteristics of the fiber optic (75). The "effective pathlength" is defined (75) as the length, L_E, of a cylinder (of a solution of a fluorophore) having a diameter equal to the diameter of a fiber optic yielding a fluorescence signal equal to the signal actually obtained when the fiber optic probe is inserted into an extended sample (it is assumed that the excitation illumination and fluorescence collection efficiency are both constant throughout this idealized cylindrical volume). The effective pathlength is calculated from

$$L_E = 1.303\ r_o\ \cot\theta_0 \qquad (12)$$

where r_o is the radius of the fiber optic core and θ_0 is the acceptance angle of the fiber (see Figure 2.2). For example, equation 12 predicts an effective pathlength of ca. 1.1 mm for a 600-μm fiber optic exhibiting a NA of 0.33. This results in a (calculated) "viewing volume" of ca. 3.1×10^{-4} mL ($V = L_E \pi r_o^2$). Note that for an extended sample, some fluorescence is collected from solution further from the fiber tip than L_E.

Overall, equation 12 predicts that the effective pathlength

(and thus, viewing volume) is proportional to the fiber's diameter and inversely proportional to its NA ($\cot\theta_0 \propto 1/NA$). However, the increased solid angle of fluorescence collection afforded by a large NA results in a greater (calculated) net fluorescence signal and thus, a greater fluorescence collection efficiency (75). Recently, an arithmetic error has been found in Deaton's derivation which reduces the numerical value of the constant from 1.303 to 1.076 (76).

Modifications to the plain termination single-fiber probe have been proposed to increase sensitivity. By using a sapphire ball as a lens in front of the fiber, as shown in figure 2.9a, the net fluorescence signal obtained has been shown to increase by a factor of ca. 1.6 (43,75). By focusing the excitation radiation into a reflective capillary (see Figure 2.9b), six- to seven-fold fluorescence signal enhancements have been observed (43,75).

Schwab and McCreery have modeled the Raman collection efficiencies of double-fiber non-transmittive probes and predict that collection efficiency increases with fiber NA (77). Plaza has extended this work and developed theory predicting the relative collection efficiencies of a wide range of multi-fiber configurations (78). When identical fibers are employed (the basic double-fiber configuration), a maximum in collection efficiency occurs when the angle of intersection between the core axes of the two fibers is held at some specific angle (see Figure 2.8b). This angle increases with the the fiber's NA. Again, fibers exhibiting larger NAs are expected to provide greater collection efficiencies. In addition, it is predicted that collection efficiencies can be doubled by using a small diameter excitation fiber exhibiting a lower NA in conjunction

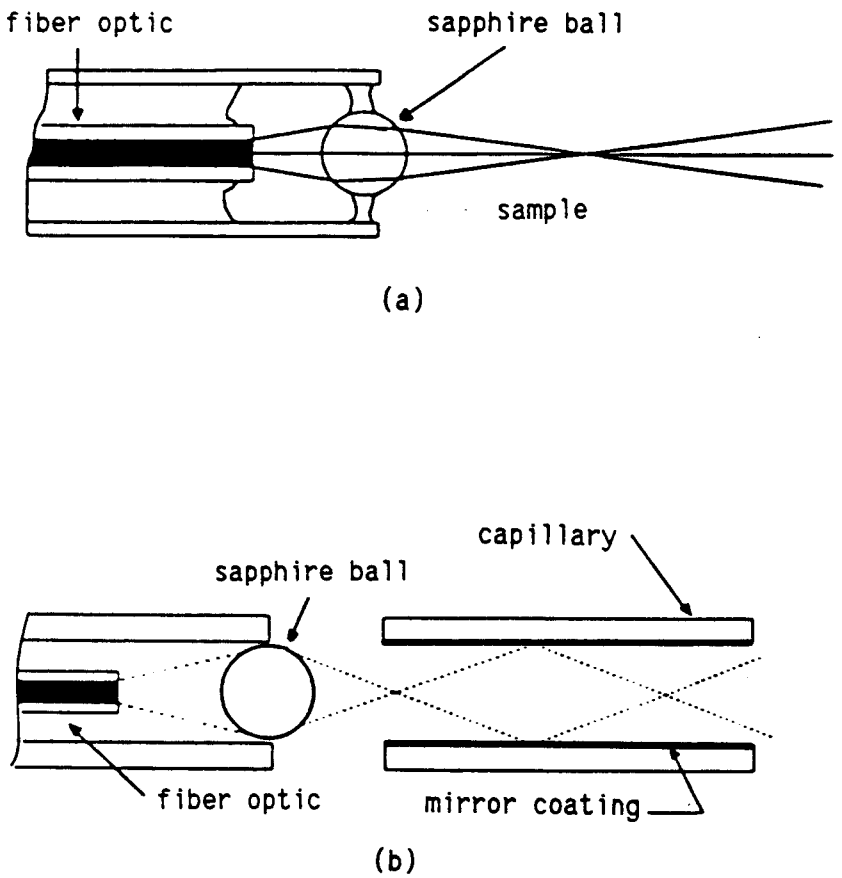

Figure 2.9. Modifications to the basic single-fiber non-transmittive probe configuration to increase calibration sensitivity. In (a), the fiber face is reimaged in the sample solution using a sapphire ball as a lens, and in (b), radiation exiting the fiber optic is focused (using a sapphire ball) into a reflective capillary (from ref. 24).

with a larger diameter collection fiber exhibiting a larger NA. Collection efficiencies can be increased further by using multiple collection fibers (77,78). As the fundamental expressions relating Raman collection efficiencies to instrumental parameters are quite similar to those for fluorescence (79), the results of these studies are generally applicable to fluorescence probes also.

Data have been presented showing that the fluorescence collection efficiency of the basic double-fiber (dual-path) configuration is ca. 30% less than that of the basic single-fiber (single-path) configuration (80). Coupled with the theory of Plaza, this indicates that fully optimized double-fiber probes, and certainly multi-fiber probes, will provide at least the same fluorescence collection efficiencies as single-fiber probes. The two configurations also exhibit different background signal levels. Since single-path probes utilize a single optical path, background levels due to fiber fluorescence and scattering will be higher (at the detector) for single-path probes (81). Data have been presented indicating this effect can result in fluorescence detection limits (DL) for single path probes ranging from one to three orders of magnitude higher than dual path probes when background noise is limiting (80,82). However, polymer clad silica (PCS) fiber optics were employed in both cases, and the use of silica on silica fibers would decrease these background signals (28).

Passive Fiber Optic Chemical Sensors

Inaba et. al. have made extensive use of transmittive probes for the remote detection of combustible gas leaks. With probes

having the configuration shown in figure 2.7b, detection of 0.5 torr of CH_4 and 1 torr of propane over a 2 km length of fiber was demonstrated (83-85). Their system used 50-μm (core) silica fibers coupled with an LED source (ca. 1.33 μm) and a 50-cm pathlength cell. A similar probe geometry has been used to perform continuous in-line absorption monitoring of uranium and plutonium hexafluoride in a flowing gas stream (86). In both these applications, the ability to perform remote, in-situ measurements was important. Inaba has also utilized a multi-path configuration for the detection of NO_2 (87). With a differential absorption measurement scheme in the visible region (496 nm and 514 nm), NO_2 was detected at ppm levels over a distance of 20 m with a cell pathlength of 1 m.

A passive transmittive probe (see Figure 2.7a) has been reported for the monitoring of Cu(II) in plating baths (62). With a 2-mm pathlength probe, the absorbance at 820 nm was linearly related to Cu(II) concentrations over the range 50 to 500 mM.

Milano and Kim used a 250-μm methyl acrylate fiber to construct a miniature probe suitable for the monitoring of hemoglobin absorbance in blood (63). The fiber was heated in boiling water, bent sharply, and inserted into a surgical needle. The end of the loop extending from the needle was cut to form a short pathlength (ca 0.03 mm), dual-path transmittive probe (similar to figure 2.7a). Hemocrit values were determined to 1% precision in 30 s.

DeGranpre and Burgess recently compared absorption spectra of oxizine perchlorate solutions obtained using a dual-path coiled evanescent probe (similar to figure 2.7e, 1.2 m of a 200-μm core PCS fiber coiled with a bend radius of 1.5 cm, cladding left intact) and

a HP8450 spectrometer with a 1-cm pathlength cell (73). The probe did not distort any spectral features (over a 150-nm scan) and provided a peak absorbance ca. 60 times less than that of the cuvette instrument. An approximate 3-fold increase in sensitivity was observed for a straight fiber probe on stripping the cladding and using the bare core in the same (straight) configuration (73). Dual-path, evanescent absorbance probes showing linear responses to Rhodamine 6G (69) and glycine solutions (72) have also been reported.

A passive dual-path evanescent probe for the monitoring of humidity has been reported (88). The attenuation of transmitted intensity resulting from degraded internal reflection (caused by the adsorption of water vapor onto the bare fiber core) was shown to be linear with relative humidity.

A passive single-path evanescent probe has been shown to provide fluorescence signals proportional to sensor length (74). In the same work it was shown that the fluorescence intensity increased in proportion to the square root of time. This suggests that the probe samples only molecules adsorbed onto its surface and that this adsorption is diffusion-limited. It has been suggested that the sampling of a thin layer directly adjacent to the probe surface offers an advantage in that interferences due to sample turbidity and inner-filter effects are minimized (24).

As discussed earlier, the first reported use of an FOCS was the dual-path non-transmittive probe used by Polyani to make in vivo biomedical measurements; other biomedical applications of non-transmittive passive probes have been reported. Mayevsky and Chance used a dual-path fluorescence probe for monitoring NADH, in vivo, during a

study on the effects of oxygen deprivation in gerbils and rats (89). Sepaniak used a single-path fluoroprobe, threaded through a surgical needle, to measure (in vivo) the accumulation of the antitumor drug doxorubicin in mice tumors (90,91). The same probe has been proposed for in vivo absorption measurements and has been demonstrated in vitro (92).

Non-transmittive probes have been used to make in situ fluorescence measurements of chlorophyll in sea water (93,94) and of Na^+ and OH^- in methane flames (95). The probe configuration used by Kychakoff is shown in figure 2.8c. The same probe configuration has been used by Issacs for observing Raman scattering from samples contained in a Helium Dewar suspended in an electromagnetic field (96). Similar dual-path non-transmittive probes, minus the 45° mirror, are available commercially (64-66).

Probes of this configuration (figure 2.8c without the 45° mirror) have been used as both fluorometric (97) and colorimetric (98) endpoint detectors in liquid titrations. This same configuration has also been applied for the detection of natively fluorescent contaminants in ground water and was demonstrated to provide detectability at the ng/mL level (99-101). McCreery compared the Raman collection efficiencies of this configuration to that of a traditional Raman spectrometer and found it to provide ca. one tenth the signal level of the traditional 90° sampling geometry (102). In a later report, the Raman collection efficiency of a multi-fiber probe, utilizing 1 excitation and 18 concentric collection fibers, was compared to that of a Spex capillary system with an elliptical collector and focused input beam (77). This probe provided ca. the

same signal level as the capillary system with no base line shift or spectral distortion.

The feasibility of performing fluorescence lifetime measurements with fiber optics has been studied (103). Using a dual-path non-transmittive probe, Vickers et. al. studied the effects of launch NA on the accuracy of fluorescence lifetime measurements of rhodamine-B and rose bengal. Precision on the order of 0.05 ns was obtained over a 16-m length of multi-mode fiber when a launch NA of ca. 0.02 was employed. Further, calculations indicate that by utilizing small launch NAs, fiber lengths approaching 1 km can be used with no significant loss of accuracy or precision (103).

Using a fluoroprobe consisting of a randomized, bifurcated, fiber optic bundle, Mitchell et. al. demonstrated that these probes are less sensitive to pre-filter effects than are cuvette fluorometers (3). A net sample absorbance of 0.25 (absorbance measured with a Beckman spectrophotometer, unspecified pathlength) resulted in a 63% loss of fluorescence signal with the cuvette fluorometer and only a 21% reduction with the fiber optic fluorometer.

The detectability achieved with a flow cell utilizing a randomized, bifurcated, fiber optic as a fluoroprobe has been compared to that obtained with a commercial fluorometric flow cell unit (4). The detection limits (S/N = 2) for protoporphyrin were 0.061 µg/L for the commercial system (Aminco J4-7413, 0.11 mL) and 0.057 µg/L for the fiber optic system (0.14 mL).

Chemical Transduction

Species which do not exhibit native absorption or fluorescence

within an appropriate wavelength range (defined by the source emission and the transmission characteristics of the fiber optics) cannot be directly detected with a passive fiber optic probe. However, these species can be measured if they can modulate an optical signal derived from some other reagent system, or if they react with some reagent system producing a quantifiable product. This process is called chemical transduction, and a chemical transducer is a reactor capable of fulfilling this function. Active FOCSs utilize chemical transduction to obtain analyte specific signals from species not directly measurable.

The basic requirement of any chemical transducer is that it provide some measurable signal related to analyte concentration. An additional constraint for a FOCS is that this signal tracks analyte concentration, just as a passive probe would. This is necessary if the sensor is to be useful for continuous monitoring, where analyte concentrations may rise and fall in time.

Figure 2.10 shows a generalized configuration for an active FOCS chemical transducer. A reagent system is held in view of the fiber optics and is isolated from the bulk sample by some selective barrier, which defines an interface between the reagent and sample phases (in some cases, there is no barrier and the sample solution and the reagent phase are in direct contact). The analyte diffuses across (through) this interface into the reagent phase and reacts with the reagent system in a manner that can be detected spectrometrically. The analyte concentration in the reagent phase ($[A]_r$) can be greater, less than, or equal to the analyte concentration in the bulk sample phase ($[A]_s$) depending on the rate

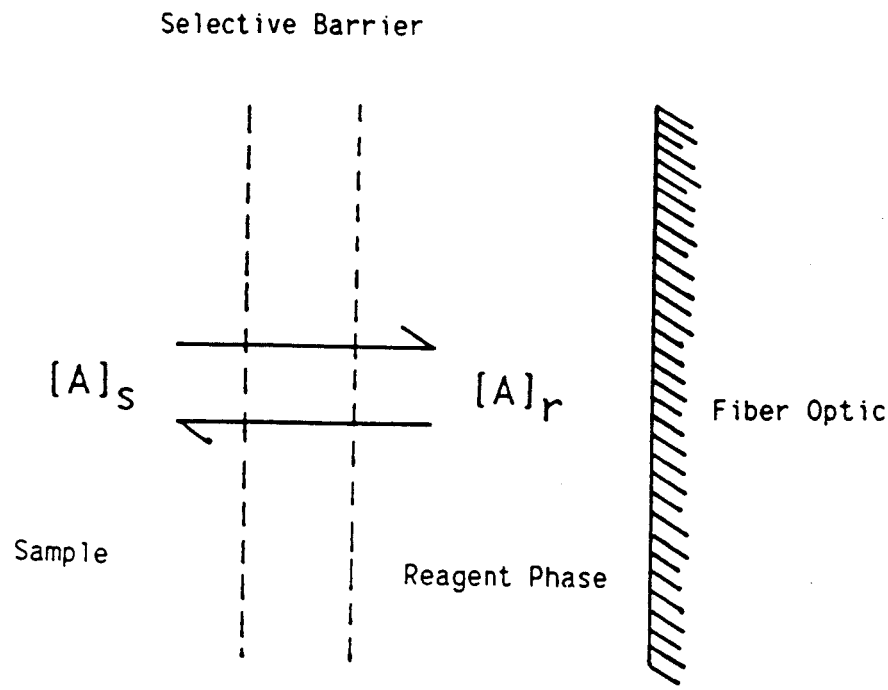

Figure 2.10 Generalized schematic of an active FOCS chemical transducer.

of diffusion (of the analyte into the reagent), the distribution coefficient (for the analyte) between the sample and reagent phases, and the rate of the reaction between the reagent(s) and the analyte.

A chemical transducer can be considered on two levels: first, the basic mechanism, or mode, of interaction (reaction) between an analyte and a reagent system, and second, the reactor implementing this mechanism at the distal termination of a fiber optic. This section addresses the possible modes of chemical transduction and reviews reactor design.

The reaction between an analyte and a reagent system can be reversible or irreversible. Thus, the two basic modes of chemical transduction are reversible and irreversible chemical reaction. The simplest irreversible reaction (denoted a derivatization for this discussion) is one between the analyte (A) and a single reagent (R) forming a single product (P)

$$A + R \rightarrow P \qquad (13)$$

where P is the monitored species.

Traditionally, derivatization reactions are used in batch mode analyses in which an aliquot of a sample solution is mixed with an aliquot of a reagent solution; after the reaction is complete, the change in [P] is measured and related to the analyte concentration in the initial sample via a calibration curve. The mode of operation of a true sensor is not that of a batch analysis because the sample is being "sampled" continuously. Proper reactor design ensures that the analyte concentration in the bulk sample is not depleted during an

analysis. This is accomplished by limiting the volume of the reagent phase (relative to the sample volume), the rate of chemical reaction, and/or the rate of transport (of the analyte into the reagent phase). Under these conditions, the analyte concentration in the bulk sample can be considered to be constant (57), and the response of the sensor is limited (at a specific analyte concentration) by either the rate of the chemical reaction, the rate of transport (flux) of the analyte into the reagent phase, or a combination of both.

If reaction kinetics are the limiting factor, an equilibrium is established between the analyte concentrations in the bulk sample and in the reagent phase

$$[A]_r \rightleftharpoons [A]_s \qquad (14)$$

and $[A]_r$ can be considered a constant. The concentration of the analyte in the sensor reagent phase is related to that in the bulk sample by the relationship

$$K_p = [A]_r/[A]_s \qquad (15)$$

where K_p is the partition coefficient between the two phases. The response of a sensor utilizing a derivatization reaction depends on the concentration of the analyte in the sensor reagent phase. Thus, sensitivity increases with K_p.

On formation, the product P can either remain in the reagent phase or it can migrate back into the sample. If the product is

trapped within the viewed reagent phase the FOCS is an integrating device. Under these conditions, [P] will increase in time at a rate related to analyte concentration by the expression

$$d[P]/dt = k(K_p[A]_s)[R] \qquad (16)$$

where k is the reaction rate constant. For the initial time period during which the reagent concentration can be considered a constant, equation 16 becomes

$$d[P]/dt = K'[A]_s \qquad (17)$$

where the term K' includes the constants k, K_p, and [R]. Equation 17 describes a pseudo-zero-order reaction suitable for use in an initial-rate kinetic determination (104); during the period of time over which reagent concentration can be considered a constant, the observed rate of change in [P] is proportional to analyte concentration in the sample. Furthermore, if $[A]_s$ changes, the rate of formation of P tracks $[A]_s$.

If the rate of transport (of the analyte into the reagent phase) limits the rate of product formation, in general, $[A]_s \gg [A]_r \simeq 0$ and

$$d[P]/dt = F/V \qquad (18)$$

where F is the rate of transport of the analyte into the reagent phase (flux, mol/s) and V is the volume of the reagent phase. If the

rate of transport is proportional to the concentration gradient across the sample-reagent interface, the rate of product formation is proportional to $[A]_s$ and equation 17 applies (where K' depends on the net flux of A and on [R]).

For intermediate cases, a steady-state concentration $[A]_r$ is eventually achieved when the transport rate equals the rate of product formation. Again, a simple linear relationship between d[P]/dt and $[A]_s$ is predicted.

If the product (P) is free to diffuse away from the reagent phase back into the sample, P can no longer be monitored kinetically. However, a steady-state concentration ([P]) will eventually be established when the rate of diffusion (of P) into the sample increases (with increasing [P]) to the point where it equals the rate of product formation. Thus, $[A]_s$ would be monitored via the steady-state signal of P (which will be proportional to $[A]_s$).

Overall, any derivatization reaction can be used for chemical transduction if conditions can be arranged such that equation 17 is obeyed and a product is formed that can be spectrometrically monitored. It is also necessary that the product concentration be in a range that provides a signal linearly related to [P] (e.g., no inner-filter effects, etc.), and the rate of the transducer reaction under the conditions of the analysis must be sufficiently large to produce a detectable change in signal over a reasonable period of time (dependent on the specific application).

For a FOCS, it is generally preferred that the chemistry occurs in a single reagent phase (i.e., a multiple reagent system can be employed only if all reagents are misicible and stable when

combined). Many derivatization reactions used in the laboratory require sequential additions of reagents, separation steps, and/or heating; due to the difficulty of performing these tasks at the distal termination of a fiber optic probe, these chemistries are not generally suitable for use in a FOCS.

There exists a large body of literature describing many derivatization reactions potentially useful in FOCSs. Derivatization reactions producing fluorescent products for quantitative determinations of non-fluorescent organic molecules (105,106), metal ions (105), and inorganic anions (107) have been reviewed. In addition, many compendia of colorimetric derivatization reactions have been published (108-113). Reactions for the detection of organics can be specific to an individual molecule or to functional group. A good source for functional-group specific chemistry is the literature of both pre- and post-column derivatization in LC (114-116).

Reversible reactions exhibiting very large formation constants will provide responses effectively equivalent to those obtained using irreversible (derivatization) reactions. Highly specific molecular response can be obtained using enzymatic (105,106) and antibody-antigen reactions. Other ligand-receptor reactions, such as metal-chelate systems, can also be useful.

A drawback to using derivatization reactions in a sensor is their finite useful lifetime; furthermore, the calibration sensitivity of the resulting device will be inversely proportional to this useful lifetime (i.e., there is a trade-off between sensitivity and longevity due to reagent consumption). If calibration sensitivity is increased by increasing the rate of transport of the

analyte into the reagent phase or manipulating the chemistry to increase the reaction rate, reagent consumption will increase, reducing the period over which (17) is valid.

To avoid this compromise associated with the use of derivatization reactions in FOCSs, a reversible reaction as described by equation 19 can be utilized

$$A + R \rightleftharpoons P \qquad (19)$$

To be useful, either the complex or the free reagent must absorb or fluoresce. When the complex between the analyte and the reagent provides the optical signal, the expression relating the monitored species to the concentration of the analyte in the sample is

$$[P] = \frac{K_f K_p [A]_s}{1 + K_f K_p [A]_s} [R]_t \qquad (20)$$

where K_f is the formation constant

$$K_f = [P]/[A][R] \qquad (21)$$

and $[R]_t$ equals the sum of [P] and [R]. A nonlinear response to $[A]_s$ is predicted when the product P is the monitored species. When the reagent is monitored the corresponding relationship is

$$[R] = \frac{[R]_t}{K_f K_p [A]_s + 1} \qquad (22)$$

and a nonlinear relationship between [R] and $[A]_s$ is (also)

predicted. However, when $(K_f K_p [A]_s) \ll 1$, both equations can be reduced

$$[P] = K_f K_p [A]_s [R]_t \qquad (23)$$

$$[R] = [R]_t (1 - K_f K_p [A]_s) \qquad (24)$$

and a linear response to $[A]_s$ is predicted in both cases.

Regardless of whether the product P or the reagent R is the monitored species, the calibration sensitivity is proportional to both K_f (and K_p) and $[R]_t$ at low analyte concentrations (eqs. 23 and 24). For a given value of K_f, the calibration sensitivity increases with $[R]_t$ with no effect on the linear dynamic range. For a given value of $[R]_t$, the calibration sensitivity increases with K_f; however, as K_f increases, the concentration range ($[A]_s$) over which the assumption that $K_f K_p [A]_s \ll 1$ is true decreases. In order to ensure linearity to within one percent, the product $(K_f K_p [A]_s)$ should be maintained at values ≤ 0.01. In any case, the maximum calibration sensitivities correspond to the regions of linear response.

A special case arises when both P and R give resolvable signals; the ratio of the two signals (equations 20 and 22)

$$[P]/[R] = K_f K_p [A]_s \qquad (25)$$

is directly proportional to analyte concentration. Again, cali-

bration sensitivity is proportional to K_f (and K_p). Note that even as K_f increases beyond the range where the change in either [P] or [R] is linearly related to $[A]_S$ ($K_fK_p[A]_S \leq 0.01$), the ratioed response is still linearly related to $[A]_S$. Thus, the linear dynamic range obtainable with this measurement scheme extends to the extreme of reagent saturation. This ratioed measurement can also help compensate some types of instrumental drift and any slow loss of reagent. A practical limitation to this approach is that both [R] and [P] must be large enough to measure with good precision; if $K_fK_p[A]_S < 0.01$ or $K_fK_p[A]_S > 100$, it is difficult to determine [P]/[R] accurately. For this reason, the value of K_f is often chosen so that $1/K_f$ is approximately equal to the mean analyte concentration. Thus, for pH monitoring, the indicator selected would have a $pK_a \simeq pH$ ($K_f[A]_S \simeq 1$).

A factor which may limit the utility of a reversible (equilibrium) reaction in a FOCS is the kinetics of the reaction. As the rate constants of either formation or dissociation decrease, the sensors response time to increases or decreases (respectively) in analyte concentration will increase. Although these rate constants do not affect the final equilibrium of the system, and thus have no effect on the final signal, the resulting response time may be too long for a specific application. If the ratio of the rate constants (formation/dissociation) is very large, the chemistry may be useful as an "irreversible" transducer.

Reactions useful in reversible chemical transduction include those based on acid/base indicators, enzyme-substrate, antibody-antigen, and metal-chelate reactions exhibiting small binding

constants. In addition, the dynamic quenching of the native fluorescence of a reagent (by an analyte) is a reversible process obeying the Stern-Volmer equation (116). The Stern-Volmer equation is functionally equivalent to Equation 22, and the observed response is subject to the same considerations (vide supra).

If no reaction suitable for the direct determination of an analyte is available, it is still possible to quantitate the analyte via competitive-binding methodology (57). Competitive-binding schemes utilize two reactions in which the analyte competes for the binding sites of a reagent with another ligand

$$A + R \rightleftharpoons AR, \qquad K_A = [AR]/[A][R] \qquad (26)$$

$$L + R \rightleftharpoons LR, \qquad K_L = [LR]/[L][R] \qquad (27)$$

and either the competing ligand, L, or the ligand-reagent complex, LR, is monitored. Expressions relating analyte concentration to the observed species (either L or LR) have been derived and predict a nonlinear relationship (57).

Competitive-binding chemical transduction is directly related to immunoassay methodology where (A) is the analyte antigen and (L) is the tagged (competing) antigen (117). Probably the most useful methodology for use with FOCSs is that of a homogeneous fluorescence immunoassay, where the static quenching (or enhancement) of the fluorescence of a (bound) tagged antigen is monitored (117,118). Other immunoassays which are of potential use are based on energy transfer or fluorescence lifetime effects (117,118); enzyme-subsrate

reactions are also useful. Consideration of how to implement these techniques at the distal termination of a fiber optic leads to a discussion of reactor design.

Reactor Design

The major consideration when designing a reactor is how to contain the reagent system in the viewing volume (of the fiber optic) while simultaneously allowing transport between this volume and the sample. The common approaches are immobilization and containment. The simplest approach is containment.

Figure 2.11a depicts a "reservoir" FOCS in which the reagent phase is contained within a reservoir isolated from the external sample by a semi-permeable membrane. The membrane is selected based on its relative permeability to the reagent and the analyte; transport of reagent(s) across the membrane should be restricted while the analyte is allowed to migrate freely. This type of reactor is useful for implementing any of the modes of chemical transduction previously discussed; multiple reagent chemistries can be employed, and figure 2.11a represents the implementation of a (fluorescence) homogeneous competitive-binding scheme. In this case, both the competing ligand (L) and the receptor (R) are held in view of the fiber optic termination, while the analyte (A) migrates freely across the membrane. The analyte within the reservoir competes for the binding sites of R (with L), resulting in a net displacement of L. The species monitored can be either the free ligand or the ligand-receptor complex, and in either case, the measured signal can be an increase or decrease in observed fluorescence intensity.

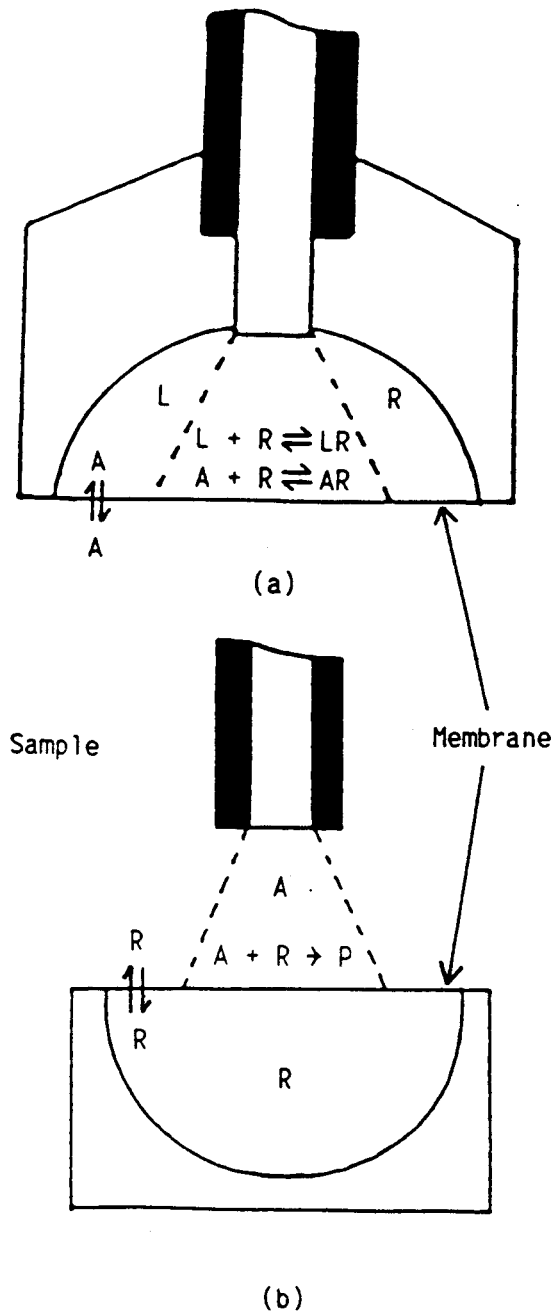

Figure 2.11 Two variations of a reservoir FOCS utilizing membranes as a selective barrier (see figure 2.10). In 2.11a., the analyte diffuses through the membrane into the reagent phase, and in 2.11b, the reagents diffuse through the membrane into the sample.

Another variation of the reagent reservoir approach involves the controlled release of a reagent, as depicted by figure 2.11b. In this case, reagent is allowed to seep, slowly, into the sample solution in view of the fiber optic. The fiber optic monitors the sample side of the membrane surface and detects any changes in the optical properties due to reaction of the reagent with the analyte. The requirements for the membrane are that it be permeable only to the reagent. Competitive-binding assays are difficult to implement with this type of system and, in addition, the reagent released into the sample should be benign.

The critical component of a reservoir reactor is the membrane. There are two basic mechanisms regulating transport across membrane materials, solution-diffusion and size exclusion (119). Solution-diffusion is a three step process beginning with the dissolution of the permeant into the membrane material at one surface, followed by diffusion through the bulk membrane, and finishing with desorption of the permeant from the membrane at the opposite surface. Selectivity is provided by the relative solubilities of different permeants in the membrane material, with those species most similar in chemical composition to the membrane material being more soluble. Generally, membranes used in dialysis, electrodialysis, reverse osmosis, gas separations, and controlled release technology are of this type (119). Size exclusion involves the selective migration of molecules through pores in the membrane material based on their size relative to the mean pore size of the membrane. Micro-filtration membranes work on this principle and are available in controlled pore sizes ranging from 0.01 to 10 μm (120).

Other factors to consider, in addition to selectivity, are the effects a membrane has on response time and sensitivity. For a specific membrane, the rate of transport (flux) is proportional to specific factors including: membrane surface area, membrane thickness, and the magnitude of the concentration gradient driving the migration across the membrane (121). Generally, the analyte is the migrating species and the concentration gradient is a function of the sample and the kinetics of the transducer reaction. Thus, response time is shortened by maximizing membrane surface area and minimizing membrane thickness.

When performing a kinetic analysis, the use of a membrane generally reduces the calibration sensitivity. However (ignoring boundary layer effects), analyte flux across a membrane of a given thickness and area is directly proportional to the concentration gradient (121). Thus, the kinetic response is still linearly related to $[A]_S$. Overall, calibration sensitivity and response time are both optimized by maximizing membrane surface area and minimizing membrane thickness.

In addition to their roles in reservoir sensors, membranes can also be used as substrates on which to immobilize a reagent. The immobilization of a reagent on a substrate can be accomplished via adsorption or covalent bonding. Techniques for covalently bonding enzymes and other proteins to both synthetic and natural membrane materials are found in the immunoassay literature (122). The preparation of bonded phase chromatography packings also makes extensive use of covalent linkages (123). Reagent immobilization via adsorption depends on the nature of the surface and the reagent;

binding may be the result of ionic interactions or physical adsorption. Again, this technique has found extensive applications in the preparation of immunoassay substrates (122).

The physical form of the reagent phase depends on the form of the substrate onto which the reagent is immobilized. Figure 2.12 shows some of the possible sensors resulting when different substrate materials are used. For the sensor shown in figure 2.12d, the fiber optic itself is the substrate. In this case, silianization chemistry is used to bond the reagent directly to the fiber optic (123).

Immobilization can also be accomplished via entrapment. Entrapment, or occlusion, refers to the trapping of the reagent within the interstitial spaces of some polymer matrix. Potential matrices include polyacrylamide, silicone rubber, polyvinyl alcohol, and silica gel (121). Typically, the reagent is mixed with the polymer precursors and the still fluid mixture is spread on some solid support, forming a thin skin. Next, polymerization is initiated and, on the setting of the polymer, this skin is peeled. This skin can then be held on the end of a fiber optic, giving a sensor analogous to that shown figure 2.11a. It is also possible to allow polymerization to occur on the fiber optic directly, resulting in sensors analogous to figures 2.11c and 2.11d.

Sensors based on immobilized reagents can implement either irreversible (derivatization) or reversible based chemical transduction. If the reagent of an irreversible derivatization (eq. 13) is immobilized in view of the fiber optic, a kinetic signal results as the resulting product is also bound in view of the fiber optic. The immobilized reagent can be a single-substrate enzyme with

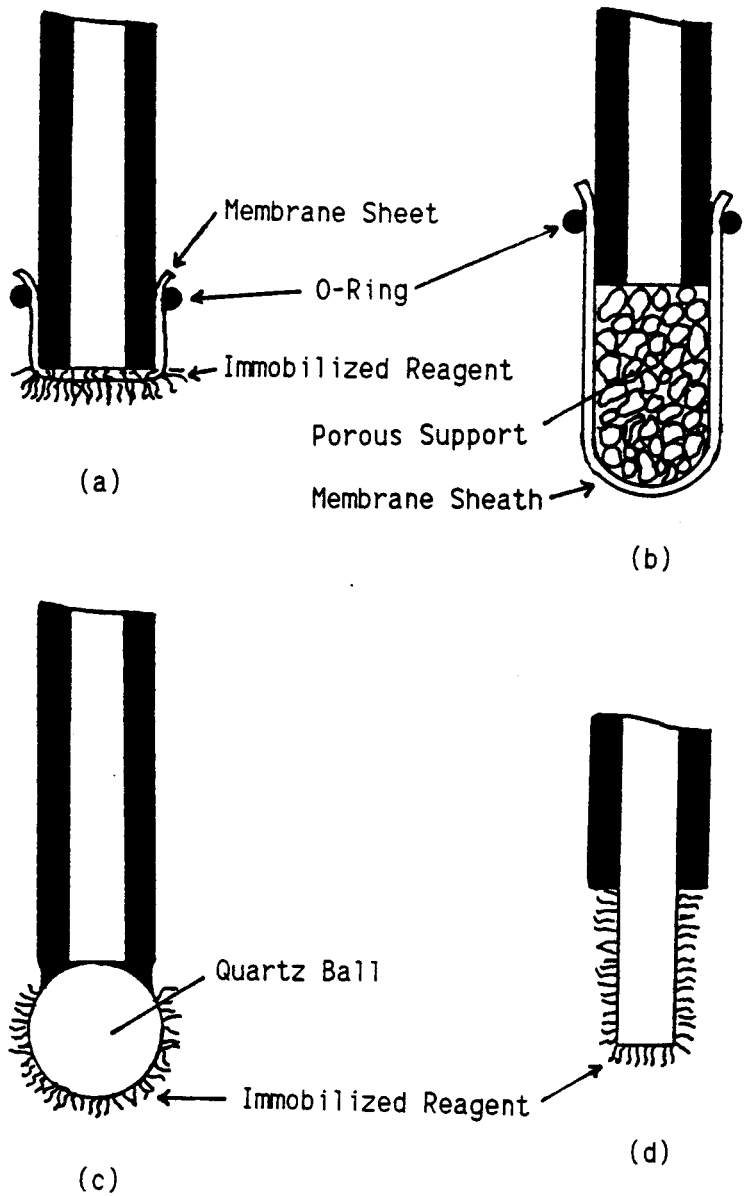

Figure 2.12. Some immobilized reagent FOCSs. The reagent immobilized on a membrane sheet (2.12a), the reagent immobilized on some porous support (e.g., silica gel) and held in view of the fiber optic with a membrane sheath (2.12b), the reagent immobilized on a quartz ball glued to the fiber termination (2.12c), and the reagent immobilized directly on the fiber optic (2.12d).

the products diffusing away from the fiber optic. The concentration of the product formed in view of the fiber optic is constant when the rate of product formation equals the rate of diffusion (of the product away from the fiber optic), resulting in a steady-state signal. If the immobilized reagent is an enzymatic substrate, the monitored product can be either bound or unbound; an unbound product gives a steady-state signal while a bound product can give either a steady-state or kinetic response, depending on whether the reaction is reversible (steady-state) or not (kinetic). When the immobilized reagent is either the ligand or binder in a reversible ligand-binder reaction (equilibrium based), the complexed analyte is in equilibrium with the analyte in the bulk sample and a steady-state signal is observed.

Sensors based on covalent or adsorptive immobilization cannot implement competitive-binding schemes because both the analyte and the competing ligand (or the analyte and the binder) must be mobile. Implementation of multi-reagent chemistries is not possible for the same reason. However, hybrid sensors, in which one reagent is immobilized on the membrane and the other is contained in a reservoir, are possible. Competitive-binding and/or multi-reagent systems are feasible for use in entrapment based sensors if the entrapped reagents retain any mobility within the polymer matrix; however, relatively long response times would result.

Comparing different reactor types for a given application requires consideration of the relative response times, sensitivities, and sizes of the resulting sensors. Sensors based on reagent immobilization (covalent bonding, adsorption, or entrapment) are

usually smaller than those employing a reservoir. However, the useful lifetime will most likely be less than that of a reservoir reactor when the chemical transducer is an irreversible chemical reaction; this is because the quantity of reagent available for reaction is limited by the surface area available for immobilization. The same factor can also limit calibration sensitivity; the volume probed by an immobilized reagent sensor is defined by the surface area of the reagent phase and, depending on the optical characteristics of the immobilization matrix, its thickness. A reservoir reactor monitors a volume of solution defined by the diameter and NA of the fiber optics and the size of the reservoir. If entrapment is used, the thickness of the polymer matrix can be made large enough to provide both increased sensor lifetime and calibration sensitivity (due to the increased quantity of reagent associated with the increased volume of the polymer matrix viewed) if the analyte can diffuse into the polymer and the matrix is transparent to the analytical wavelengths. However, this increases response times. Generally, probes based on covalent or adsorptive immobilization will exhibit shorter response times than those based on either a reagent reservoir or reagent entrapment.

Another consideration is the need to control the conditions under which the probe reaction occurs. Reservoir sensors gain selectivity by extracting analyte from the sample into a separate, well characterized, reagent phase; factors such as pH (through use of a buffer) can be controlled. This is also true, to a limited extent, for sensors utilizing reagent entrapment in polymer matrices. This is not the case with immobilized reagent (covalent or adsorptive

immobilization) sensors which, ideally, use the sample itself as the reaction solvent. Thus, the sample must be stable and well characterized in order to ensure a valid analysis. However, addition of a membrane to these sensors can improve selectivity, at the cost of response time.

A final consideration must be the effect of immobilization on the reactivity and selectivity of the reagent/indicator. Loss of enzyme activity due to immobilization is well known (115,122). This may be due to involvement of the active site in binding, restricted steric orientation on the substrate, or other microenvironment effects (122). These factors may affect any immobilized reagent system. In addition, the spacer groups used in covalent immobilization may contribute non-specific interactions to the observed response (124). Finally, immobilization may induce spectral shifts and affect the absorptivity or quantum efficiency of a bound reagent or indicator.

Active Fiber Optic Chemical Sensors

The principle of an active waveguide sensor was first presented in 1975 (125). Hardy et. al. coated a quartz rod with a 0.1% (w/w) solution of sodium picrate and allowed it to dry. The transmission of the rod was then measured and a known amount of CN^- applied to the rod (and allowed to dry). The reaction between the picrate and cyanide ions changed the optical properties of the coating resulting in a decrease in the transmission proportional to the amount of CN^- added. However, this device was not a true sensor as it could only operate in the batch mode.

In 1976, David and coworkers reported the first true active waveguide sensor (126). Using the same methodology as Hardy, they coated quartz rods with a polyvinyl alcohol solution of ninhydrin (triketohydrindene hydrate), and allowed the polymer to set. Exposing to NH_3 vapor gave a colored product and a time dependent loss in rod transmission (attenuated internal reflection). The rate of change of attenuation was shown to be linear with ammonia concentration. Although fiber optics were not used, this device operated in the continuous mode and was thus a true sensor. This sensor was used by Smock in 1979 for the vapor phase determination of blood ammonia (127). A similar ammonia sensor utilizing glass capillary tubes and a reversible colorimetric reaction with an oxazine per-chlorate dye was reported in 1983 (128).

The first true FOCS was a pH sensor reported in 1980 (129,130). Peterson's sensor consisted of a dual-path non-transmittive probe and an immobilized reagent reactor. Phenol red was covalently bound to polyacrylamide microspheres (5- to 10-μm diameter) encased in cellulosic dialysis tubing into which the fiber optics were inserted (see Figure 2.11b). By monitoring the relative absorbance (using a non-absorbed wavelength as a reference) of the base form of the indicator dye, pH values in the physiological range (7.0 to 7.4) were quantifiable to the nearest 0.01 pH unit. The probe was tested in vivo and shown to provide response times and accuracy comparable to that of a pH electrode. The data indicated that most of the measurable absorption occurs in the first few tenths of a millimeter of sample solution adjacent to the fiber optics (129,130). Independent in vivo (131) and in vitro (132) tests of

this probe have been reported and the initial studies validated.

Since this work, many FOCSs for a wide variety of analytes have been reported. In the interest of brevity, table 2.1 summarizes these reports and no attempt to describe each device in detail will be made; only those sensors clearly defining a common approach, or those representing a unique methodology, are discussed in any detail. The most basic factors differentiating one sensor from another (besides analyte) are probe configuration, the mode of chemical transduction, and the reactor configuration. These factors have already been discussed and are listed in table 2.1.

Inspection of table 2.1 reveals some general trends. First, the vast majority of reported FOCSs utilize either the single- or the dual-path non-transmittive probe configuration, and the remainder utilize dual- or single-path evanescent (transmittive) probes. Not one reported active FOCS utilizes a non-evanescent transmittive probe (see Figure 2.7). This is most likely due to the difficulties associated with maintaining the axial alignment of two fiber optics and miniaturizing this configuration. The non-transmittive configurations are of the most utility as they provide the greatest signal to size ratio (vide supra). Second, immobilized reagent reactors predominate over reagent reservoir reactors. Size is a factor here too. Third, sensors based on reversible chemistries far outnumber those based on irreversible chemistries. This is most likely due to the desire to maximize the useful lifetime of the sensor (vide supra). Finally, a large majority of the reported sensors utilize fluorescence methodology. The advantages afforded by fluorescence spectroscopy have been well documented and include both

Table 2.1 Summary of active FOCS literature.

ANALYTE	SIGNAL[a]	PROBE[b]	TRANSDUCER[c]	REFERENCES
pH	F	NT	I/E	140,142,144,151 155,163,176
pH	A/R	NT	I/E	143,146,147
NH_3	A/R	NT	I/E	138,171
NH_3	A/R	NT	R/E	136
O_2	F	NT	I/E	142,148,150,159 160,174,172
O_2	A/R	NT	I/E	178
Halothane	F	NT	I/E	172
CO_2	F	NT	I/E	142,156,174,177
SO_2	F	NT	I/E	173
F^-	A/R	NT	I/D	157
K^+	A/R	NT	I/E	134
Metal Cations	F	NT	I/E	137,164,165 166,175
Mg^{2+},Zn^{2+}	F	NT	R/D	149
Na^+	F	NT	I+R/CB	179
Ionic Strength	F	NT	R/E	139
Hydrocarbons	A/R	E	I/E	145
$CHCl_3$	F	NT	R/D	153,154
Polar Solvents	A/R	NT	I/E	161
H_2S	A/R	NT	I/D	158
Humidity	A/R	E	I/E	162

Glucose	F	NT	R/CB	152,167
Enzyme Substrates	F	NT	I/D	169
Enzyme Substrates	A/R	NT	I/D	135
Penicillin	F	NT	I/E	141
Ethanol	F	NT	R/D	168
Carboxylesterase	F	NT	I/D	170

[a]F = Fluorescence (including quenching).
A/R = Attenuated reflectance (absorbance).

[b]NT = Dual- or single-path non-transmittive.
E = Dual- or single path evanescent.

[c](Reactor configuration/Chemistry)
where reactor configuration is R (reagent reservoir)
or I (immobilized reagent) and chemistry is E
(reversible), D (irreversible), or CB
(competitive binding).

increased specificity and detectability relative to absorption based measurements (133). Overall, the vast majority of reported FOCSs utilize non-transmittive probes, immobilized reagent reactors, equilibrium based chemical transduction, and fluorometric monitoring.

The archetypical FOCS is adequately represented by Zhujun's pH FOCS (176). The trisodium salt of 8-hydroxyl-1,3,6-pyrene trisulfonic acid (HOPSA) was electrostatically immobilized onto an anion-exchange membrane which was held on the end of a bifurcated fiber optic (dual-path non-transmittive probe) with a piece of Tygon tubing (see Figure 2.11a). The acid and base forms of HOPSA can be selectively monitored as protonation results in a shift in excitation wavelength (176). Thus, the ratio of the fluorescence intensities of the acid and base forms of HOPSA was used to quantify pH values between 6 and 9. The response time of this sensor ranged from 70 to 120 s.

Jordan et. al. have reported a unique pH FOCS based on energy transfer between an immobilized fluorophore and a pH dependent absorber which exhibits response times of ca. 4 s. (144). Phenol red and eosin were co-immobilized directly onto the termination of a single-path, non-transmittive probe and the fluorescence of eosin was monitored. Over the pH range 6.0-8.0, the absorption band of phenol red shifts with pH (λ_{max} shifts to longer wavelengths with increasing pH) and overlaps the emission band of eosin to differing degrees. Thus, changes in the absorption of phenol red as a function of pH were detected fluorometrically. Comparing the response time of this sensor to that of Zhujun's sensor demonstrates the effect membranes can have on response times.

Another unique pH FOCS, employing controlled release methodology, was reported in 1989 (151). Luo and Walt entrapped two dyes, one pH sensitive and the other not, in a polymer matrix and constructed the sensor shown in figure 2.13. In aqueous solutions the rate of release of both dyes from the polymer was constant over a period of ca. 30 days. The ratio of fluorescence intensities from the two dyes provided a linear response for pH values between 5.5 and 8.0 with a precision of ca. 0.1 pH unit. The controlled (slow) release of the reagents ensures a useful lifetime for the sensor, but results in response times on the order of 60 min. per pH unit. The two dyes employed shared a common excitation wavelength and were differentiated via emission wavelength. Ratioing the two signals compensates for source fluctuations, and ideally, variations in the optical properties of the sample and the rate of release of the dyes (from the polymer matrix).

In order to maintain calibration stability, many sensors utilize ratioed measurement schemes. A reference signal obtained directly from the source (prior to source injection into the fiber optic) is not sufficient to ensure calibration validity for a FOCS; the reference signal must travel the same optical path as the analytical signal. For fluorescence measurements, a reference signal satisfying this requirement is scattered source radiation outside the absorption band of the indicator (130,131); Raman scattering of the excitation radiation by the fiber optics or the sample solvent (e.g. water) can also be used as a reference. When using conventional sources, these signals may be of limited intensity. In addition, this signal does not compensate reagent loss from the FOCS. The

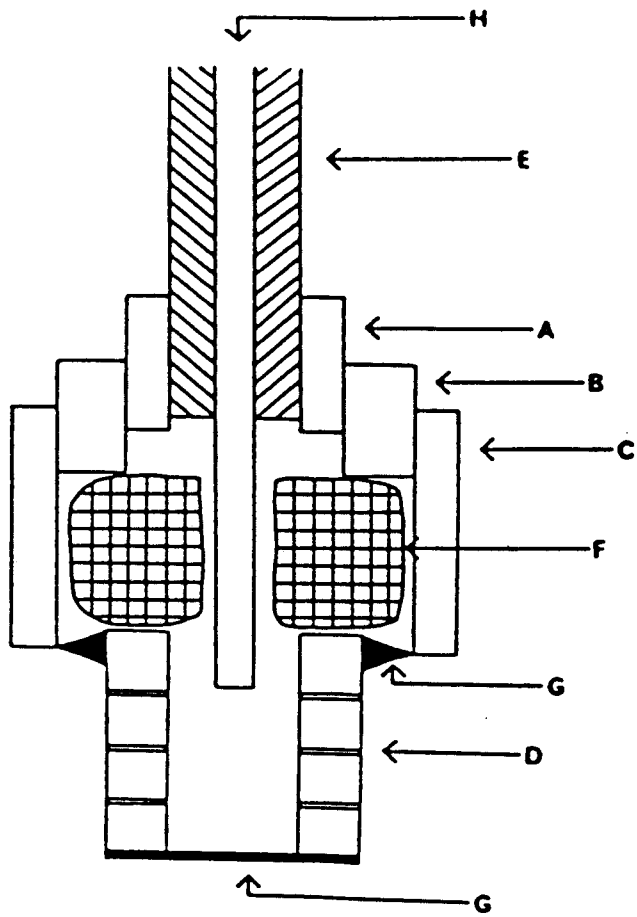

Figure 2.13. Cross section of Luo's pH FOCS (from ref. 151). (A) Teflon capillary tube; (B) Tygon tube; (C) Teflon tube; (D) Teflon tube with tiny holes; (E) plastic coating; (F) polymer matrix; (G) Parafilm; (H) fiber optic.

method employed by Luo and Walt performs this function only as long as the rate of loss (release) of the reference dye and the indicator dye remain equal (i.e., as long as the concentration ratio in view of the probe remains constant). This is a potential problem for any sensor utilizing a second, reference, indicator within the reagent phase (142).

The ideal reference signal is one derived directly from the indicator of a transducer. This case is represented by equation 25 and a practical example of this methodology is Zhujun's pH probe (176); other sensors based on reversible chemistry also utilize this methodology (148). Unfortunately, this approach is not feasible for sensors based on irreversible chemistry, for which a reference signal must be obtained from another source.

For sensors based on absorption, a reference signal can be obtained by monitoring the source signal at a wavelength where the monitored species does not absorb. If a reversible (equilibrium) chemical transducer is used, the ratio [P]/[R] can be monitored (eq. 25).

Lippitsch has reported an oxygen FOCS utilizing the fluorescence decay time as the signal (150). A fluorescent metal-chelate susceptible to oxygen quenching was entrapped in a silicone matrix at the end of a dual-path non-transmittive probe. As the concentration of oxygen increased, the fluorescence lifetime of the indicator decreased. Thus, the phase shift (relative to the modulated source) of the indicators fluorescence is related to oxygen concentration. This methodology results in an amplitude-independent signal which is stable with respect to both instrumental drifts and

indicator leaching.

In addition to response time and calibration stability, selectivity is an important parameter affecting the utility of a sensor for any given application. Generally, lack of selectivity still hampers the majority of the sensors listed in table 2.1.

Sensors for monitoring pH are the most well characterized FOCSs and, arguably, the most specific. All the pH FOCSs reported to date rely on a reversible equilibrium between an indicator dye and hydrogen ion. Like pH electrodes, these sensors are subject to errors introduced by temperature and ionic strength effects (129). Fluorescence-based transducers are also susceptible to quenching errors (140). Temperature, ionic strength, and quenching effects can be compensated with a ratioed measurement (176). Although the validity of relating concentration measurements to pH has been questioned (180,181), both in vivo and in vitro tests have shown that pH FOCSs can provide accuracy and precision comparable to pH electrodes over a range of ionic strengths and temperatures (129-132).

In general, the selectivity of a sensor is related directly to the selectivity of the chemical transducer employed. However, specificity can be altered through judicious use of membranes. By surrounding a pH sensor (FOCS) with a buffer solution contained within a gas-permeable membrane, a CO_2 FOCS can be constructed (142,156,174,177). Changes in the pH of the buffer solution caused by changing concentrations of CO_2 are monitored via the pH sensor. This methodology is subject to interferences from volatile species capable of affecting the pH of the internal buffer, and H_2S and

SO_2 have been identified as interferents (177). All reported ammonia FOCSs operate on exactly the same principle (136,138,171), and SO_2, N_2O, and CO_2 have been identified as interferents (171). Thus, these probes cannot be considered truly specific for the species as listed in table 2.1.

Chemical transducers based on dynamic quenching have been reported for monitoring O_2 and SO_2 (see Table 2.1). These sensors all utilize the same methodology; a natively fluorescent indicator is isolated from the bulk sample by a gas-permeable membrane, and decreases in the indicator fluorescence signal are related to analyte concentration via the Stern-Volmer relationship. All these sensors respond to both SO_2 and O_2 (173). Sensors tested for in vivo monitoring of blood oxygen levels (142,160) have been shown to be susceptible to interference from halogenated anesthetics (160,172). However, in the absence of these compounds, the sensors are capable of providing readings within a few tenths of a Torr of electrode readings (160). Wolfbeis has proposed the use of multi-probe systems to simultaneously monitor oxygen and anesthetics in vivo (172).

Sensors exhibiting specificity for individual metal cations have yet to be developed. Table 2.1 differentiates sensors reported for this application based solely on differences in external characteristics (e.g., probe configuration). All of these sensors are based on reversible complexation between a ligand and the metal ion. The sensors listed as responding to "metal cations" actually respond, to differing degrees, to many ions including Al^{3+}, Mg^{2+}, Zn^{2+}, Ca^{2+}, Cu^{2+}, Co^{2+}, Ni^{2+}, Be^{2+}, and others. In addition, all

the binding reactions show strong pH dependencies. It has been suggested that these sensors be utilized in arrays for the simultaneous monitoring of metal ions (137).

In an attempt to obtain Na^+ specific response, Zhujun et. al. have used a sodium-selective ionophore in a competitive-binding FOCS (179). This unique FOCS makes use of both an immobilized reagent and a reagent reservoir. The sodium-selective ionophore was electrostatically immobilized onto silica supported by cellophane tape and isolated from the external sample by a dialysis membrane. The volume defined by this membrane/tape barrier was filled with a reagent solution containing both a (fluorescent) ligand and the (quenching) competing binder. Sodium ions crossing the dialysis membrane form cationic complexes with the ionophore, resulting in the silica surface becoming cationic. The cationic silica surface competes with the quenching binder in solution and forms an ion-pair with some of the anionic fluorophore, destroying the quenched complex and increasing the observed fluorescence due to the anionic fluorophore. However, the sensor exhibited approximately equal responses to Na^+, K^+, and Ca^{2+}. Likewise, a sensor for the detection of K^+ exhibited response to Na^+ (134), the response for Ca^{2+} was not tested.

Many of the FOCSs listed in table 2.1 exhibit "group" specificity, as indicated by the generic analytes specified. The $CHCl_3$ sensor actually responds to a wide variety of gem-polyhalogenated hydrocarbons (153). However, Russell's humidity sensor provides a selective response based on monitoring the color change associated with exposure of cobalt(II) chloride to moisture (162).

Sensors utilizing enzymatic transducers are theoretically capable of a high degree of specificity. Arnold has demonstrated the feasibility of biosensors utilizing an immobilized enzyme providing response selective for the specific substrates (135,169). In addition, an FOCS utilizing immobilized enzyme substrates for the detection of esterase enzymes has been reported (170). Fuh et. al. added an immobilized penicillinase membrane to a pH FOCS and were able to monitor penicillin via the enzymatic production of penicilloic acid (141).

An enzyme-based FOCS for the detection of volatile alcohols has been reported by Walters et. al (168). A gas-permeable membrane separated the sample solution from a buffered solution of NAD^+ and alcohol dehydrogenase. Ethanol in the sample diffused through the membrane into the reagent phase where the enzyme catalyzed its oxidation, and the associated formation of NADH was monitored fluorometrically. The rate of NADH production was shown to be linear with ethanol concentrations over the range from 0.9 to 9 mM.

One of the more unique FOCSs reported to date is the gluose sensor of Meadows and Schultz (152). A reservoir defined by a dialysis membrane contains a buffered solution of fluorescein isothiocyanate (FITC) labeled dextran (FITC-dextran) and Concanavalin A labeled with Rhodamine (Rh-ConA); Conconavalin A is a bioreceptor selective for sugars and carbohydrates while FITC and Rhodamine are the donor and acceptor, respectively, of an energy transfer pair. Within the reagent reservoir, the labeled dextran and ConA bind. On binding, the distance between the two labels decreases and energy transfer between the acceptor/donor pair is at a maximum. Glucose

enters the reservoir, competes for the binding sites of the Rhod-ConA complex, displaces the FITC-dextran and decreases the net energy transfer from the donor complex (FITC-dextran) to the acceptor complex (Rhod-ConA). Thus, the presence of glucose results in a net increase in observed fluorescence due to the FITC-dextran complex.

Recently, a novel approach to (chemical) remote sensing with fiber optics has been reported. Utilizing the "Remote Reaction Chamber" (RRC) shown in figure 2.14, Waddle was able to implement complex, multi-step, chemistries at the distal termination of a fiber optic probe (182); applying a momentary vacuum draws a small aliquot of aqueous sample into the RRC, and a chemical analysis is initiated by injecting reagent(s). Although not a true sensor, this approach allows frequent analysis of remote samples with minimal sample handling. Furthermore, Waddle has demonstrated the ability to perform remote standard additions with the RRC (182). This is important as a standard addition analysis avoids the problems associated with maintaining the calibration of a true sensor once the device is placed in a remote sample (vide supra). Overall, the ability to implement both multi-step chemistries and standard addition methodology increases the range of analyses possible and the overall calibration stability achievable.

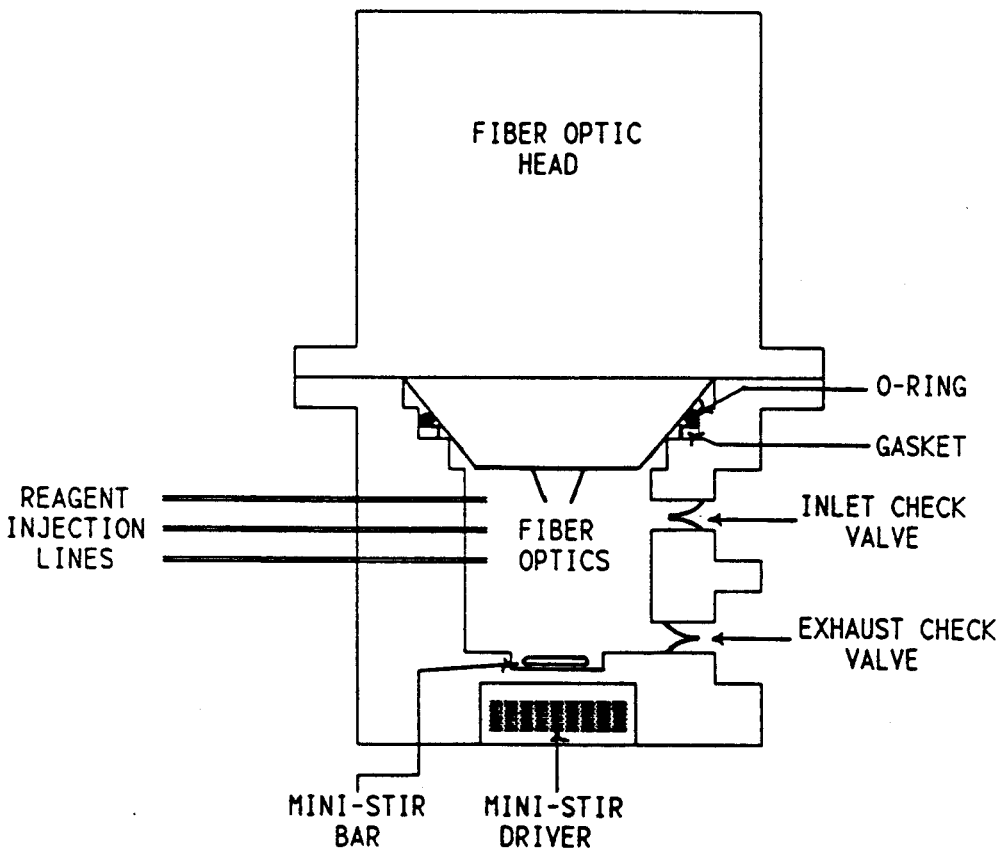

Figure 2.14. Schematic of Waddle's remote reaction chamber (from ref. 182).

REFERENCES

1. Yappert, C., Ph.D. Thesis, 1985, Oregon State University.

2. Ratzlaff, E.H.; Harfman, R.G.; Crouch, S.R. Anal. Chem. 1984, 56, 342-347.

3. Mitchell, D.G.; Garden, J.S.; Aldous, K.M. Anal. Chem. 1976, 48, 2275-2277.

4. Smith, R.M.; Jackson, K.W.; Aldous, K.M. Anal. Chem. 1977, 49, 2051-2053.

5. Reichert, W.M.; Ives, J.T.; Suci, P.A. Appl. Spec. 1987, 41, 1347-1350.

6. Dakin, J.P. SPIE Vol. 375, "Fiber Optics '83" (1983), 172-177.

7. Harmer, A.L. in Kersten, R.Th. and Kist, R., Editors, "Proc. of the 2nd Intl. Conf. on Optical Sensors", VDE-Verlag GmbH, Berlin, 1984, 17-22.

8. Wanser, K.H.; Wagoner, R.E. Photonics Spectra Oct. 1983, 61-66.

9. Daly, J.; Lakshmanasamy, S. in Basch, E.E., Editor, "Optical Fiber Transmission", H.W. Sams & Co., Indianapolis, 1987, 9-24.

10. Gallawa, R.L. Electro-opt. Sys. Des. April 1982, 46-54.

11. Snyder, A.W. and Love, J.D. "Optical Waveguide Theory", Chapman & Hall, London, 1983, 6-88.

12. Midwinter, J.E. "Optical Fibers for Transmission", John Wiley & Sons, N.Y., 1979, 87-90.

13. Snyder, A.W. and Love, J.D. "Optical Waveguide Theory", Chapman & Hall, London, 1983, 589-623.

14. Marcuse, D. "Principles of Optical Fiber Measurement", Academic Press, N.Y., 1981, 11-67.

15. Cheo, P.K. "Fiber Optics; Devices and Systems", Prentice-Hall, Englewood Cliffs, 1985, 63-88.

16. Suematsu, Y. and Iga, K. "Introduction to Optical Fiber Communications", John Wiley & Sons, N.Y., 1982, 141-150.

17. Culshaw, B. "Optical Fibre Sensing and Signal Processing", Peter Peregrinus Ltd., London, 1984, pp 15.

18. Basch, E.E.; Carnes, H.A. in Daly, J.C., Editor, "Fiber Optics", CRC Press, Boca Raton, 1984, 151-181.

19. Carnes, H.; Kearns, R.; Basch, E. in Basch, E.E., Editor, "Optical Fiber Transmission", H.W. Sams & Co., Indianapolis, 1987, pp 475.

20. Schulman, J.H.; Compton, W.P. "Color Centers in Solids", Pergamon Press, N.Y., 1962.

21. Midwinter, J.E. "Optical Fibers for Transmission", John Wiley & Sons, N.Y., 1979, 128-157.

22. Drexhage, M.G.; Moynihan, C.T. Scientific American Nov. 1988, 110-116.

23. Aggarwal, I.D. in Daly, J.C., Editor, "Fiber Optics", CRC Press, Boca Raton, 1984, 21-50.

24. Angel, S.M. Spectroscopy 1987, 2, 38-48.

25. Dahne, C.; Sutherland, R.M.; Place, J.F.; Ringrose, A.S. SPIE Vol. 514, "Conf. Proc. 2nd Intern. Conf. Opt. Fiber Sensors (1984); Stuttgart, FR Ger., 75-79.

26. Andrade, J.D.; Vanwagenen, R.A.; Gregonis, D.E.; Newby, K. Lin, J.N. IEEE Tans. Electron Devices 1985, ED-32, 1175-1179.

27. Snyder, A.W.; Love, J.D. "Optical Waveguide Theory", Chapman & Hall, London, 1983, 120-133.

28. Benner, R.E.; Chang, R.K. in Bendow, B. and Mitra, S.S., Editors, "Fiber Optics: Advances in Research and Development", Plenum Pree, N.Y., 1979, 625-640.

29. General Fiber Optics, Inc. product literature.

30. DuPont Fiber Optic Cable product literature.

31. Culshaw, B. "Optical Fibre Sensing and Signal Processing", Peter Peregrinus Ltd., London, 1984, 133-145.

32. Chabay, I. Anal. Chem. 1982, 54, 1071A-1080A.

33. Polanyi, M.L.; Hehir, R.M. Rev. Sci. Instrum. 1962, 33, 1050-1054.

34. Enson, Y.; Briscoe, W.A.; Polanyi, M.L.; Cournand, A. J. Appl. Physiol. 1962, 17, 552-558.

35. Gamble, W.J.; Hugenholtz, P.G.; Monroe, R.G.; Polyani, M.; Nadas, A.S Circulation 1965, 31, 328-343.

36. Hugenholtz, P.G.; Gamble, W.J.; Monroe, R.G.; Polyani, M. Circulation 1965, 31, 344-355.

37. McCarthy, B.; Hood, W.B.; Lown, B. J. Appl. Physiol. 1967, 23, 641-645.

38. Taylor, J.B.; Lown, B.; Polyani, M. J.A.M.A. 1972, 221, 667-673.

39. Kapany, N.S.; Silbertrust, N. Nature 1964, 204, 138-142.

40. Alder, J.F. Fresenius Z. Anal. Chem. 1986, 324, 372-375.

41. Boisde, R.E.; Blanc, F.; Perez, J. Talanta 1988, 35, 75-82.

42. Boisde, R.E.; Perez, J. in Kersten, R.Th. & Kist, R., Editors, "Proc. 2nd Intl. Conf. on Optical Sensors", VDE-Verlag GmbH, Berlin, 1984, 227-231.

43. Borman, S.A. Anal. Chem. 1981, 53, 1616A-1618A.

44. Brown, R.G.W. J. Phys. E: Sci. Instrum. 1987, 20, 1312-1320.

45. Harmer, A.L.; Narayanaswamy, R. in Edmonds, T.E., Editor, "Chemical Sensors", Chapman and Hall, N.Y., 1988, 275-294.

46. Hirschfeld, T.; Deaton, T.; Milanovich, F.; Klainer, S. Opt. Eng. 1983, 22, 527-531.

47. Hirschfeld, T. Fresenius Z. Anal. Chem. 1986, 324, 618-624.

48. Hirschfeld, T. InTech Feb. 1986, 45-50.

49. Krull, U.J.; Brown, S. in Measures, R.M., Editor, "Laser Remote Chemical Analysis", J. Wiley & Sons, N.Y., 1988, 505-532.

50. Maugh. T.H. Science 1982, 218, 875.

51. Milanovich, F.P.; Hirschfeld, T. InTech March 1984, 33-36.

52. Milanovich, F.P.; Hirschfeld, T. Adv. in Instrum. 1983, 38, 407-418.

53. Narayanaswamy, R.; Sevilla, F. J. Phys. E: Sci. Instrum. 1988, 21, 10-17.

54. Peterson, J.I.; Vurek, G.G. Science 1984, 102, 123-127.

55. Scheggi, A.M. in Kersten, R.Th. & Kist, R., Editors, "Proc. 2nd Intl. Conf. on Optical Sensors", VDE-Verlag GmbH, Berlin, 1984, 93-104.

56. Schirmer, R.E.; Gargus, A.G. Am. Lab. Dec. 1986, 30-39.

57. Seitz, W.R. Anal. Chem. 1984, 56, 16A-34A.

58. Snow, J.W. Sea Tech. July 1987, 10-13.

59. Wolfbeis, O.S. Fresenius Z. Anal. Chem. 1986, 325, 387-392.

60. Wolfbeis, O.S. Pure & Appl. Chem. 1987, 59, 663.

61. Janata, J.; Bezegh, A. Anal. Chem. 1988, 60, 62R-74R.

62. Freeman, J.E.; Childers, A.G.; Steele, A.W.; Hieftje, G.M. Anal. Chim. Acta 1985, 177, 121-128.

63. Milano, M.J.; Kim, K. Anal. Chem. 1977, 49, 555-559.

64. Beckman Instruments, Westbury, N.Y.

65. Guided Wave Inc., Rancho Cordova, Calif.

66. Oriel Corp., Stamford, Conn.

67. Harrick, N.J. "Internal Reflection Spectroscopy", Wiley, N.Y., 1968.

68. Tai, H.; Tanaka, H.; Yoshino, T. Opt. Lett. 1987, 12, 437-439.

69. Paul, P.H.; Kychakoff, G. Appl. Phys. Lett. 1987, 51, 12-14.

70. (Cited as Reference 76 in Reference 25)

71. (Cited as References 77-81 in Reference 25)

72. Simhony, S.; Katzir, A. Appl. Phys. Lett. 1986, 49, 252-254.

73. DeGrandpre, M.D.; Burgess, L.W. Anal. Chem. 1988, 60, 2582-2586.

74. Newby, K.; Reichert, W.M.; Andrade, J.D.; Benner, R.E. Appl. Optics. 1984, 23, 1812-1815.

75. Deaton, T., Ph.D. Thesis, 1984, Univ. of Calif. Davis.

76. Desiderio, R. Oregon State University, Personal Communication.

77. Schwab, S.D.; McCreery, R.L. Anal. Chem.1984, 56, 2199-2204.

78. Plaza, P.; Dao, N.Q.; Jouan, M.; Fevrier, H.; Saisse, H. Appl. Optics 1986, 25, 3448-3454.

79. Ingle, J.D.; Crouch, S.R. "Spectrochemical Analysis", Prentice Hall, Englewood Cliffs, 1988, pp 501.

80. Louch, J.R.; Ingle, J.D. Anal. Chem. 1988, 60, 2537-2540.

81. Dakin, J.P.; King, A.J. "IEE Conf. Publ. (Opt. Fibre Sens.)", 1983, 221, 195-199.

82. Dakin, J.P.; King, A.J. "IEE Colloquium on Optical Fibre Sensors", 1982, 1-3.

83. Chan, K.; Ito, H.; Inaba, H. Appl. Optics 1984, 23, 3415-3420.

84. Alarcon, M.C., Ito, H., Inaba, H. Appl. Phys. B 1987, 43, 79-83.

85. Inaba, H, Chan, K.; Ito, H. SPIE Vol. 514, Conf. Proc. 2nd Intern. Conf. Opt. Fiber Sensors (1984); Stuttgart, FR Ger., 211-214.

86. Saturday, K.A. Anal. Chem. 1983, 55, 2459-2460.

87. Kobayasi, T.; Hirama, M.; Inaba, H. Appl. Optics 1981, 20, 3279-3280.

88. Woldarczyk, M.T.; Vickers, D.J.; Kozaitis, S.P. SPIE Vol. 718, Fiber Optic and Laser Sensors IV (1986); Cambridge, MA., 192-196.

89. Mayevsky, A.; Chance, B. Science 1982, 217, 537-540.

90. Sepaniak, M.J.; Tromberg, B.J.; Eastham, J.F. Clin. Chem. 1983, 29, 1678-1682.

91. Tromberg, B.J.; Eastham, J.F.; Sepaniak, M.J. Appl. Spec. 1984, 38, 38-42.

92. Coleman, J.T.; Eastham, J.F.; Sepaniak, M.J. Anal. Chem. 1984, 2246-2249.

93. Lund, T. "IEE Conf. Publ. (Optical Fibre Sensors)", 1983, 221, 190-194.

94. Jorgensen, B.B.; Des Marais, D.J. Limnol. Oceanogr. 1988, 33, 99-113.

95. Kychakoff, G.; Kimball-Linne, M.; Hanson, R.K. Appl. Optics 1983, 22, 1426-1428.

96. Issacs, E.D.; Heiman, D. Rev. Sci. Instrum. 1987, 58, 1672-1674.

97. Wolfbeis, O.S. Fresenius Z. Anal. Chem. 1985, 320, 271-273.

98. Benaim, N.; Grattan, K.T.V.; Palmer, A.W. Analyst 1986, 111, 1095-1097.

99. Chudyk, W.A.; Carrabba, M.M.; Kenny, J.E. Anal. Chem. 1985, 1237-1242.

100. Chudyk, W.A.; Kenny, J.; Jarvis, G.; Pohlig, K. "Proc. of ISA (Advances in Instrumentation)", 1986, 41, 1237-1243.

101. Chudyk, W.A.; Kenny, J.; Jarvis, G.; Pohlig, K. InTech 1987, 53-57.

102. McCreery, R.L.; Fleishmann, M.; Hendra, P. Anal. Chem. 1983, 146-148.

103. Vickers, G.H.; Miller, R.M.; Hieftje, G.M. Anal. Chim. Acta 1987, 192, 145-153.

104. Mark, H.B., Jr. Talanta 1972, 19, 717-746.

105. Seitz, W.R CRC Crit. Rev. in Anal. Chem. 1980, 8 (4), 367-465.

106. Bartos, J.; Pesez, M. Talanta 1972, 19, 93-124.

107. Gomez-Hens, A.; Valcarcel, M. Analyst 1982, 1274, 465-494.

108. Feigl, F. "Spot Tests in Organic Analysis", Elsevier, N.Y., 1966.

109. Feigl, F. "Spot Tests in Inorganic Analysis", Elsevier, N.Y., 1972.

110. Snell, F.D.; Snell, C.T. "Colorimetric Methods of Analysis", Volumes I-IV, Van Norstrand Reinhold, N.Y., 1948-1970.

111. Allport, N.L.; Keyser, J.W. "Colorimetric Analysis", Chapman & Hall, London, 1957.

112. Thomas, L.C.; Chamberlin, G.S. "Colorimetric Chemical Analytical Methods", The Tintometer Ltd., Salisbury, 1953-1980.

113. Boltz, D.F.; Howell, J.A. "Colorimetric Determinations of Nonmetals", J. Wiley & Sons, N.Y., 1978.

114. Sternson, L.A. in Frei, R.W. & Lawrence, J.F., Editors, "Chemical Derivatization in Analytical Chemistry, Volume 1: Chromatography", Plenum Press, N.Y., 1981, 127-210.

115. Bowers, L.D.; Bostick, W.D. in Frei, R.W. & Lawrence, J.F., Editors, "Chemical Derivatization in Analytical Chemistry, Volume 2: Separation and Continuous Flow Techniques", Plenum Press, N.Y., 1982, 97-143.117. Lawrence, J.F. ibid, 191-242.

116. Ingle, J.D.; Crouch, S.R. "Spectrochemical Analysis", Prentice Hall, Englewood Cliffs, 1988, 343-344.

117. Seare, N.J. in Edmonds, T.E. "Chemical Sensors", Chapman & Hall, N.Y., 1988, 155-167.

118. Kricka, L.J. "Ligand-Binder Assays", Marcel Dekker, N.Y., 1985, 125-164.

119. Lonsdale, H.K. J. Memb. Sci. 1982, 10, 81-181.

120. Millipore Catalog 1986, Millipore Corp., Bedford MA.

121. Pratt, H.R.C. in Lo, T.C.; Baird, M.H.I.; Hanson, C. Editors "Handbook of Solvent Extraction", J. Wiley & Sons, N.Y., 1983, 91-123.

122. Carr, P.W.; Bowers, L.D. "Immobilized Enzymes in Analytical and Clinical Chemistry", J. Wiley & Sons, N.Y., 1980, 148-196.

123. Scouten, W.H. "Affinity Chromatography; Bioselective Adsorption on Inert Matrices", J. Wiley & Sons, N.Y., 1981, 20-85.

124. ibid, 85-102.

125. Hardy, E.E.; David, D.J.; Kapany, N.S.; Unterleitner, F.C. Nature 1975, 257, 666-667.

126. David, D.J.; Wilson, M.C.; Ruffin, D.S. Anal. Lett. 1976, 9, 389-404.

127. Smock, P.L.; Orofino, T.A.; Woooten, G.W.; Spencer, W.S. Anal. Chem. 1979, 51, 505-508.

128. Giuliani, J.F.; Wohltjen, H.; Jarvis, N.L. Optics Letters 1983, 8, 54-56.

129. Peterson, J.I.; Goldstein, S.R.; Fitzgerald, R.V.; Buckhold, D.K. Anal. Chem. 1980, 52, 864-869.

130. Goldstein, S.R.; Peterson, J.I.; Fitzgerald, R.V.; J. Biomech. Eng. 1980, 102, 141-146.

131. Tait, G.A.; Young, R.B.; Wilson, G.J.; Steward, D.J.; MacGregor, D.C. Am. J. Physiol. 1982, 243, H1027-1031.

132. Suidan, J.S.; Young, B.K.; Hetzel, F.W.; Seal, H.R. Clin. Chem. 1983, 29, 1566.

133. Hirschfeld, T. Appl. Spectrosc. 1977, 31 (3), 245.

134. Alder, J.F.; Ashworth, D.C.; Narayanaswamy, R.; Moss, R.E.; Sutherland, O. Analyst 1987, 112, 1191-1192.

135. Arnold, M.A. Anal. Chem. 1985, 57, 565-566.

136. Arnold, M.A.; Oster, T.J. Anal. Chem. 1986, 58, 1137-1140.

137. Bright, F.V.; Poirier, G.E.; Hieftje, G.M. Talanta 1988, 35, 113-118.

138. Caglar, P.; Narayanaswamy, R. Analyst 1987, 112, 1285-1288.

139. Christian, L.M.; Seitz, W.R. Talanta 1988, 35, 119-122.

140. Fuh, M.S.; Burgess, L.W.; Hirschfeld, T.; Christian, G.D.; Wang, F. Analyst 1987, 112, 1159-1163.

141. Fuh, M.S.; Burgess, L.; Christian, G.D. Anal. Chem. 1988, 60, 433-435.

142. Gehrich, J.L.; Lubbers, D.W.; Opitz, N.; Hansmann, D.R.; Miller, W.W.; Tusa, J.K.; Yafuso, M. IEEE Trans. Biomed. Eng. 1986, BME-33, 117-132.

143. Guthrie, A.J.; Narayanaswamy, R.; Russell, D.A. Analyst 1988, 113, 457-461.

144. Jordan, D.M.; Walt, D.R.; Milanovich, F.P. Anal. Chem. 1987, 59, 437-439.

145. Kawahara, F.K.; Fiutem, R.A.; Silvus, H.S.; Newman, F.M.; Frazar, J.H. Anal. Chim. Acta. 1983, 151, 315-327.

146. Kirkbright, G.F.; Narayanaswamy, R.; Welti, N.A. Analyst 1984, 109, 1025-1028.

147. Kirkbright, G.F.; Narayanaswamy, R.; Welti, N.A. Analyst 1984, 109, 15-17.

148. Lee, E.D.; Werner, T.C.; Seitz, W.R. Anal. Chem. 1987, 59, 279-283.

149. Lieberman, S.H.; Inman, S.M.; Stromvall, E.J. Proc. Electrochem. Soc. 1987,(Proc. Sym. Chem. Sens.), 464-475.

150. Lippitsch, M.E.; Pusterhufer, J.; Leiner, M.J.P.; Wolfbeis, O.S. Anal. Chim. Acta. 1988, 205, 1-6.

151. Luo, S.; Walt, D.R. Anal. Chem. 1989, 61, 174-177.

152. Meadows, D.; Schultz, J.S. Talanta 1988, 35, 145-150.

153. Milanovich, F.P. Environ. Sci. Technol. 1986, 20, 441-442.

154. Milanovich, F.P.; Daley, P.F.; Klainer, S.M.; Eccles, L. Anal. Inst. 1986, 15, 347-358.

155. Munkholm, C.; Milanovich, F.P.; Klainer, S.M. Anal. Chem. 1986, 58, 1427-1430.

156. Munkholm, C.; Walt, D.R.; Milanovich, F.P. Talanta 1988, 35, 109-112.

157. Narayanaswamy, R.; Russell, D.A.; Sevilla, F. Talanta 1988, 35, 83-88.

158. Narayanaswamy, R.; Sevilla, F. Analyst 1988, 113, 661-663.

159. Okazaki, T.; Imasaka, T.; Ishibashi, N. Anal. Chim. Acta. 1988, 209, 327-331.

160. Peterson, J.I.; Fitzgerald, R.V.; Buckhold, D.K. Anal. Chem. 1984, 56, 62-67.

161. Posch, H.E.; Wolfbeis, O.S.; Pusterhofer, J. Talanta 1988, 35, 89-94.

162. Russell, A.P.; Fletcher, K.S. Anal. Chim. Acta. 1985, 170, 209-216.

163. Saari, L.A.; Seitz, W.R. Anal. Chem. 1982, 54, 821-823.

164. Saari, L.A.; Seitz, W.R. Anal. Chem. 1983, 55, 667-670.

165. Saari, L.A.; Seitz, W.R. Analyst 1984, 109, 655-657.

166. Saari, L.A.; Seitz, W.R. Anal. Chem. 1984, 56, 810-813.

167. Schultz, J.S.; Sims, G. Biotech. Bioeng. Symp. 1979, 9, 65-71.

168. Walters, B.S.; Nielsen, T.J.; Arnold, M.A. Talanta 1988, 35, 151-155.

169. Wangsa, J.; Arnold, M.A. Anal. Chem. 1988, 60, 1080-1082.

170. Wolfbeis, O.S. Anal. Chem. 1986, 58, 2874-2876.

171. Wolfbeis, O.S.; Posch, H.E. Anal. Chim. Acta. 1986, 185, 321-327.

172. Wolfbeis, O.S.; Posch, H.E.; Kroneis, H.W. Anal. Chem. 1985, 57, 2556-2561.

173. Wolfbeis, O.S.; Sharma, A. Anal. Chim. Acta. 1988, 208, 53-58.

174. Wolfbeis, O.S.; Weis, L.J.; Leiner, M.; Ziegler, W.E. Anal. Chem. 1988, 60, 1028-2030.

175. Zhujun, Z.; Seitz., W.R. Anal. Chim. Acta. 1985, 171, 251-258.

176. Zhujun, Z.; Seitz, W.R. Anal. Chim. Acta. 1984, 160, 47-55.

177. Zhujun, Z.; Seitz, W.R. Anal. Chim. Acta. 1984, 160, 305-309.

178. Zhujun, Z.; Seitz, W.R. Anal. Chem. 1986, 58, 220-222.

179. Zhujun, Z.; Mullin, J.L.; Seitz, W.R. Anal. Chim. Acta. 1986 184, 251-258.

180. Janata, J. Anal. Chem. 1987, 59, 1351-1356.

181. Edmonds, T.E.; Flatters, N.J.; Jones, C.F.; Miller, J.N. Talanta 1988, 35, 103-107.

182. Waddle, R.D., Masters Thesis, 1989, Oregon State University.

CHAPTER 3

EXPERIMENTAL COMPARISON OF SINGLE- AND DOUBLE-FIBER CONFIGURATIONS FOR REMOTE FIBER OPTIC FLUORESCENCE SENSING

Jeff Louch and J. D. Ingle, Jr.

Department of Chemistry
Oregon State University
Gilbert Hall 153
Corvallis, OR 97331-4003

ABSTRACT

A simple experimental procedure for measurement of the relative fluorescence collection efficiencies of single- and double-fiber optrode (fiber optic chemical sensor, FOCS) configurations is presented. The fluorescence collection efficiency of the basic single-fiber configuration is shown to be approximately 50% greater than that of the basic double-fiber configuration. The implications of this finding on instrumental design and overall relative signal levels are discussed. Detection limits for HIDC Iodide dye for both single- and double-fiber configurations were evaluated. The single-fiber system was limited by background noise and yielded a detection limit of 0.2 ng/mL with a signal-to-background ratio (S/B) of 0.03 for a 0.5 ng/mL dye solution. The double-fiber system was limited by dark current noise and gave a detection limit of 0.04 ng/mL with a S/B of 10 at 0.5 ng/mL of dye.

INTRODUCTION

Interest in the application of fiber optics to chemical remote sensing is growing rapidly (1-7). Generally, fiber optics are utilized to guide radiation to and from a remote sample containing an analyte of interest. This species can then be quantitated using traditional spectroscopic methodologies such as absorption or fluorescence spectrometry. Many unique methodologies for detecting non-absorbing and non-fluorescing species have been reported (1-7). Most fiber optic chemical sensors (FOCS), or optrodes, for the detection of fluorescence employ either the single- or double-fiber probe configuration. To date, no quantitative comparison of the these two basic configurations has appeared. We are interested in remote fiber fluorometry (RFF) and in this work describe a simple experimental scheme for measuring the relative fluorescence collection efficiencies of single- and double-fiber probe systems. This ratio is important as it ultimately limits the relative signal levels obtainable from these systems.

A single-fiber optrode for fluorescence measurements uses the same fiber to transmit the excitation radiation to the sample and to guide the collected signal radiation (the wavelength-shifted luminescence) to the detection system. The detection system consists of an emission monochromator or filter (with appropriate entrance optics), photomultiplier tube (PMT), a signal processor, and a readout device. An optical interface or coupler capable of spatially

separating these two radiation components at the proximal end of the fiber optic is required.

Double-fiber optrodes for fluorescence measurements utilize one fiber to guide the excitation radiation to the sample, and a second fiber to collect and guide the emission radiation back to the detection system. It is also possible to use one excitation fiber and two or more emission fibers (8,9). Such systems are conceptually similar to the double-fiber configuration. Several researchers have also used bifurcated fiber optic bundles (10,11), in which half the fibers carry the excitation radiation while the other half return the emission radiation to the detection system. This approach may be prohibitively expensive for remote sensing over long distances. Also, it is difficult to optimize the angle between excitation and emission fibers.

A number of different optical interfaces for use with single-fiber systems have been reported (12,13). In addition, modifications to enhance the signal obtained with the single-fiber configuration (12,13) and the double-fiber configuration (8,14) have been presented. The optical efficiency of the single-fiber configuration (13) and double-fiber configurations (8,14) have been theoretically treated. Still lacking, however, is any quantitative comparison between the two configurations.

Factors which must be weighed when choosing the appropriate configuration include: cost, complexity, ruggedness, size (of the FOCS), and detectability. For fixed excitation conditions and a given type and size of fiber optics, the detectability for a specific analyte varies between optrode configurations due to differences in

the fluorescence emission collection efficiency, the magnitude of the background signal (and hence blank noise), and the efficiency of the single-fiber configuration optical coupler. Overall, the net signal obtained will be a function of both probe collection efficiency and the efficiency of this necessary optical coupler, which can be easily measured. By quantitating the relative collection efficiencies of the two basic probe configurations (single- and double-fiber), it is then possible to calculate the overall relative signal levels obtainable when using different couplers and sources.

EXPERIMENTAL

Instrumentation

The instrumental configuration used is shown in figure 3.1. The excitation source is a 2.5-mW Helium-Neon laser (Melles Griot, λ of 632 nm). The optical coupler is designed around a f/0.75 convex mirror (5.2-cm diameter) with a 3-mm hole in its center. Maxlight, PCS fiber optics (plastic clad silica fiber optic, core/cladding diameter of 860 μm with a 600-μm core, NA ≃ 0.33) were used throughout. The excitation mount for two fibers was constructed in-house utilizing two Newport, FPH-DJ fiber optic chucks and a Newport, LP-05-XY translator. This mount holds the two fibers at the same vertical height and allows for xyz translation as a pair. The distance between the center of two fibers was ≃ 5.7 mm. The excitation fiber (f.o. #2) was positioned two focal lengths (78 mm) from the mirror and the angle defined by f.o. #2, the mirror hole, and f.o. #3 was ≃ 4.2^{o}. The distal (sensing) ends of the fiber optics (the optrode) were stripped of cladding and held at a 20^{o} angle by a Teflon holder constructed in-house.

The detection system consists of a f/0.75 glass aspherical lens, a PTR Optics "Minichrome" monochromator (reciprocal linear dispersion of 20 nm/mm, set to 732 nm, effective aperture of f/4, 1-mm square emission and excitation slits), a 660-nm cutoff filter (located between the exit slit of the monochromator and the PMT), and an RCA 4840 PMT powered by a Keithley high voltage power supply

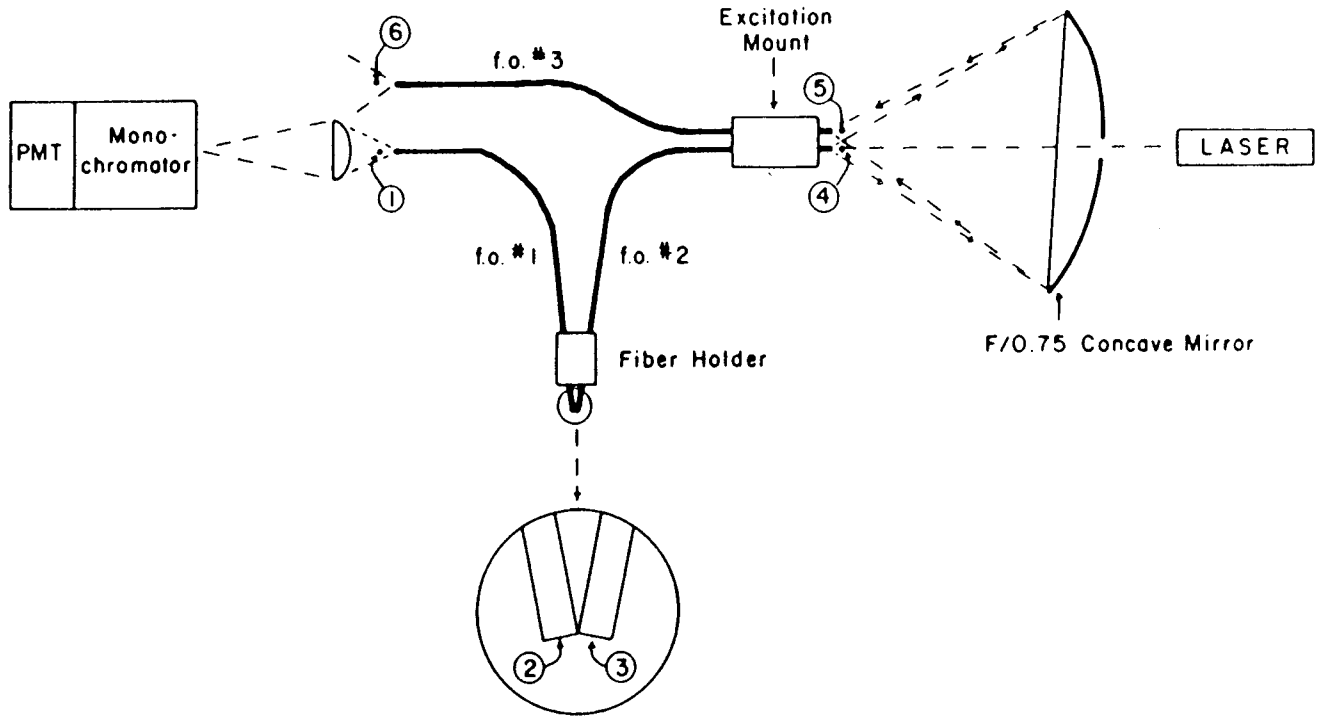

Figure 3.1. Schematic of the laser/fiber optic instrumentation. Fiber optics #1 and #2 are both 1 m in length and are stripped of all cladding at the probe tip.

(model 244). The PMT signal was monitored with a DVM after current to voltage conversion and amplification. The sample cell was a 10-mL beaker over which the fiber optic holder fit. This system provided a light-tight enclosure and reproducible optrode positioning in the sample solution at ca. 2.5 cm above the bottom of the beaker. At this depth, the sample volume was determined to be large enough so as to have no effect on signal levels.

Procedures

The efficiency of the optical interface for the single fiber configuration was evaluated as follows. The sensing end of fiber optic #2 was illuminated by green light from a tungsten lamp and bandpass filter combination. The radiant power exiting at point 4 (Φ_4) was then measured with a photodiode (PTR Minichrome Silicon Detector). The radiant power exiting fiber optic #3 at point 6 (Φ_6) was then maximized by optimizing the off-axis angle of the mirror (relative to fiber #3) and the vertical position of both fiber terminations. The efficiency E is defined as

$$E = \Phi_6/\Phi_4 \qquad (1)$$

For fluorescence measurements, the laser beam was first adjusted to pass through the hole in the mirror and directly impinge only on optical fiber #2 at point 4. Fluorescence measurements were then obtained from one dye solution (emission maximum at 732 nm) using both optrode configurations by simply switching fibers 1 and 3 at the input to the detection system. These measurements were then

repeated for a blank solution. The fluorescence signal ratio (R_f) is calculated as

$$R_f = S_6/S_1 \qquad (2)$$

where S_6 is the blank corrected fluorescence signal from the single-fiber optrode and S_1 is the blank corrected signal from the double-fiber configuration. From R_f and E, the corrected fluorescence ratio R_{cf} is calculated as

$$R_{cf} = R_f/E \qquad (3)$$

The corrected fluorescence ratio is a direct measurement of the relative fluorescence collection efficiencies of the two configurations.

Fibers 1 and 2 were then exchanged and another set of measurements taken (obtaining new values of E, R_f, and R_{cf}). This pairing of measurements helps compensate for any variations in the transmission characteristics of the two fiber optics (e.g., surface inhomogeneities). The paired fluorescence measurements were repeated twice, between which the fibers were repolished and reorientated in the holder. Performing these replicate measurements helps compensate for any bias due to variability in the orientation of the fibers (at the probe tip) in the final ratio.

Reagents

HIDC Iodide laser dye (1,1,3,3,3',3'-Hexamethyl-indodicarbo-

cyanine iodide) was obtained from Sigma and 1.96×10^{-7} M (100 ng/mL) and 9.80×10^{-10} M (500 pg/mL) solutions were prepared using reagent grade DMSO (Baker).

RESULTS AND DISCUSSION

Other experiments showed that an approximate 20^{o} angle between fibers gave the optimum S/B for the double-fiber configuration and this angle was used for all measurements. This is consistent with the model of Plaza et. al. (14).

Table 3.1 lists the experimental values obtained for E, R_f, and R_{cf}. Runs A and A' are paired as are runs B and B'. The mean values of R_{cf} for each paired run are 1.52 and 1.53 (A & B) and the mean of the two means is 1.52 with a relative standard deviation (RSD) of 0.7%. The RSD calculated from the four (unpaired) values is 36%. Before the paired measurement scheme was implemented, eleven unpaired experiments were conducted and yielde a mean value for R_{cf} of 1.40 (RSD = 34%), which is in good agreement with the value obtained from the paired measurement scheme.

The significant scatter in the values of E determined (RSD = 37%) is attributed to imprecision in adjusting the positions of the laser and mirror between measurements. An optical table was not used for the temporary optical setup employed nor were the laser or mirror mounted on micrometer-controlled translation stages. The scatter in the individual values of R_f is due to scatter in E and to the differences in transmission characteristics of the two fiber optics employed. By the division of each value of R_f by the corresponding value of E (eq. 2), the error introduced by the variability of E is compensated. Thus, the scatter of R_{cf} is due primarily to the

Table 3.1. Experimentally determined values of E, R_f, and R_{cf}[a].

Run	E	R_f	R_{cf}	R_{cf}(paired)
A	0.68	0.60	0.89	
A′	0.40	0.86	2.14	1.52
B	0.49	0.83	1.69	
B′	0.25	0.34	1.36	1.53

[a]Test solution: 100 ng/mL HIDC dye

differences (e.g., transmission characteristics) between the two fibers. With the two fibers switched, the measurements repeated, and the value of R_{cf} reported as the mean of these paired measurements (A & A', B & B'), this source of error is also minimized, as evidenced by the marked decrease in uncertainty (paired vs. unpaired). For example, if the fiber optic with better transmission characteristics is used as f.o. #1, the single value of R_{cf} obtained will be less than the true value (i.e., the value that would be obtained using equivalent fiber optics). Likewise, the experimental value of R_{cf} will be greater than the true value if f.o. #1 exhibits lower transmittance than f.o. #2 (the data for runs A & A' reflect this effect).

For the fiber used, the fluorescence collection efficiency of the basic single-fiber configuration is only about 50% greater than that of the basic double-fiber configuration. Thus, the efficiency of an optical coupler used with the single-fiber configuration must be ca. 70% to provide the same signal level as the double-fiber configuration. Single-fiber couplers are generally based either on dichroic beam splitters (12,13,15) or geometric couplers utilizing prisms and/or simple mirrors (12,13,16,17). The simplest geometric coupler consists of a planar mirror with a small hole in its center. Source radiation is focussed through the hole onto the fiber optic, while most of the radiation exiting the fiber is reflected to the detection system. When used with laser sources, these devices can be designed such that their efficiency is limited primarily by the reflectivity of the mirror and thus are theoretically capable of collecting ca. 90% of the radiation exiting the fiber optic. This

assumes that losses due to the hole (< 1% for a 2-mm hole in a 2.5-cm diameter mirror when the aperture defined by the mirror is filled) and aberrations are insignificant (i.e., all radiation reflected by the mirror is imaged into the detection system). When this type of coupler is used, the signal advantage afforded by the single-fiber configuration (over the double-fiber configuration) could be as high as ca 45%.

If a conventional source is used in place of a laser, the same throughputs cannot be achieved. This is due to fundamental limitations in the design which force a trade-off between the efficient coupling of excitation radiation through the hole in the mirror into the fiber optic and efficient collection of emission radiation exiting the fiber optic. For example, if the source radiation is focused through the hole onto the fiber optic at a large f/#, significant magnification of the source image results. An image magnification of two results in a factor of four decrease in the excitation irradiance at the fiber optic and a corresponding decrease in emission. On the other hand, if the source radiation is used at a lower f/#, a portion of the beam will be blocked by the mirror resulting, again, in the attenuation of the net fluorescence signal.

Couplers based on dichroic beam splitters do not require that source radiation be focused as a large f/# beam. These devices utilize the wavelength discriminating characteristics of the dichroic beam splitter, or edge filter (18), to direct the two radiation components (excitation and emission) along differing optical paths. Both the excitation and emission radiation are attenuated to a certain extent. As an example, Sepaniak and co-workers report (15)

on a system which reflects ca. 60% of the emission (to the detection system) while transmitting ca. 90% of the excitation (to the fiber optic). In this case, a single-fiber probe will provide only about 80% (1.52 x 0.90 x 0.60) of the signal of a double-fiber probe utilizing the same source without the coupler, regardless of the type of source employed.

To further characterize the two systems, single-point calibrations using 500 pg/mL dye and blank solutions were performed to determine the detection limits and S/B's. The detection limit is defined as the concentration yielding an analytical signal equal to twice the blank noise. The detection limit calculated for the single-fiber system was 0.2 ng/mL with a S/B of 0.03. For the double-fiber configuration, the detection limit was 0.04 ng/mL with a S/B of 10. Thus, the double-fiber configuration provides about a factor of 300 S/B advantage and an approximate factor of 5 detection limit advantage for the specific system studied. Because the calibration slopes are approximately equal, the detection limit for the single-fiber configuration is worse primarily due to higher blank noise. Spectral scans identified the dominant background signal to be due to fiber optic fluorescence, a common problem with single-fiber systems (13,15,19). Thus, noise in the background fluorescence signal limits detectability. The double-fiber measurements were limited by dark current noise.

CONCLUSIONS

To predict the relative signal levels obtainable using different fluorescence probe configurations, their relative collection efficiencies (R_{cf}), and the efficiency of the single-fiber coupler, must be determined. With the fiber optics tested, there is only about a 50% difference in the fluorescence collection efficiencies of single- and double-fiber probe configurations. For a single-fiber coupler efficiency of 70%, the two configurations would yield essentially equivalent signals. The collection efficiencies of the two basic probe configurations are expected to depend, to a degree, on the numerical apertures of the fiber optics employed. However, theoretical modeling (13,14) has shown that the collection efficiencies of both configurations are, as a first approximation, proportional to the fiber optic numerical aperture, and thus the ratio, R_{cf}, is not expected to change appreciably from the experimental value determined in this work. The experimental scheme presented in this work could be used to survey the relative collection efficiencies of probes constructed using a variety of fiber optics. As the fluorescence signals obtained with the basic single- and double-fiber configurations would be expected to differ by no more than a factor of 2 or 3, other factors (size, cost, ruggedness, or S/N) may be more important in choosing the configuration for a given application.

The single-fiber configuration is, in one sense, the simplest

as there are no alignment requirements at the distal end of the system. This configuration is also easily miniaturized. However, the complexity is increased and the overall optical efficiency reduced by the need for an optical interface. Also, the background signal is greater than that obtained with multiple fiber configurations because a single optical path is shared by the emission and excitation radiation. Hence, in addition to the requirements placed on the optical interface, the emission wavelength selector must have a high rejection ratio for stray radiation. However, background radiation from the fiber at wavelengths within the emission bandpass cannot be rejected except by time discrimination methods.

When high excitation powers and wide emission bandpasses are used to increase the fluorescence signal and improve the detection limit, the double-fiber configuration yields better detectability when background signal noise is limiting (i.e., greater than dark current noise). The S/B and S/N disadvantage of the single-fiber configuration will depend on the particular optical system, fiber optics, and analyte (i.e., excitation and emission wavelengths). Background fluorescence and Raman scattering from fibers are expected to increase in intensity when excitation wavelengths shorter than that used in this study are employed. Clearly, selection of low background fluorescence fibers is more critical for the single-fiber configuration.

REFERENCES

1. Seitz, W.R. Anal. Chem. 1984, 56, 16-34A.

2. Maugh, T.H. Science 1982, 218, 875-876.

3. Chabay, I. Anal. Chem. 1982, 54, 1071-1080A.

4. Wolfbeis, O.S. Pure & Appl. Chem. 1987, 59, 663-672.

5. Angel, S.M. Spectroscopy (Springfield, OR) 1987, 2 (4), 38-48.

6. Arnold, M.A. (Ed.) Talanta 1988, 35 (2).

7. Janata, J.; Bezegh, A. Anal. Chem. 1988, 60, 62-74R.

8. Schwab, P.; McCreery, R. L. Anal. Chem. 1984, 56, 2199-2204.

9. Lieberman, S.H.; Inman, S. M.; Stromvall, E. J. Proc. Electrochem. Soc. 1987, 87-9 (Proc. Symp. Chem. Sens.), 464-475.

10. Saari, L.A.; Seitz, W.R. Anal. Chem. 1982, 54, 821-823.

11. Kirkbright, G.F.; Narayanaswamy, R,; Welti, N. Analyst 1984, 109, 1025-1028.

12. Hirschfeld, T.; Deaton, T.; Milanovich, F.; Klainer, S.M. "The Feasibility of using Fiber Optics for Monitoring Groundwater Contaminants" 1983, U.C.I.D.-19774, Lawrence Livermore Laboratory.

13. Deaton, T. "Instrumentation and Methodology for Remote Fiber Fluorometry" 1984, Ph.D. Thesis, Univ. Calif. at Davis.

14. Plaza, P.; Dao, N.Q.; Jouan, M.; Feurier, H.; Saisse, H. Appl. Optics 1986, 25, 3448-3454.

15. Petrea, R.D.; Sepaniak, M.J.; Vo-Dinh, T. Talanta 1988, 35, 139-144.

16. Fuh, M.R.S.; Burgess, L.W.; Hirschfeld, T.; Christian, G.D.; Wang, F. Analyst 1987, 112, 1159-1163.

17. Tromberg, B.J.; Sepaniak, M.J.; Vo-Dinh, T; Griffin, G.D. Anal. Chem. 1987, 59, 1226-1230.

18. Ealing Electro Optics Guide 1986, 222.

19. Dakin, J.P.; King, A.J. "IEE Conf. Publ. (Opt. Fibre Sens.)" 1983, 221, 195-199.

CHAPTER 4

A FIBER OPTIC FLUOROMETER

Jeff Louch and J. D. Ingle, Jr.

Department of Chemistry
Oregon State University
Gilbert Hall 153
Corvallis, OR 97331-4003

ABSTRACT

A general discussion of the design factors affecting the performance of fiber optic fluorometers is presented and a fiber optic fluorometer is reported. The fiber optic fluorometer utilizes a dual-fiber optic probe constructed using 600-μm (core) PCS fiber optics. The absolute fluoresence signal and effective collection efficiency of the simple dual-fiber fiber optic probe is approximately one fifth that of a typical cuvette fluorometer. Experimental results agree with those predicted by theory. The effects of sample cell dimensions and color on the signal-to-background ratio are characterized and the viewing volume of the fiber optic probe is shown to be no greater than 0.04 mL. A quinine sulfate calibration curve obtained using the fiber optic fluorometer shows linearity from 10 pg/mL to 10 μg/mL. The detection limit for quinine sulfate is 10 pg/mL and is comparable to that of a conventional spectrofluorometer.

INTRODUCTION

By virtue of their small size and flexibility, fiber optics make possible increased versatility in both the design and application of spectrometric instrumentation. When fiber optics are used to guide radiation to and from a sample, instrumental design is no longer restricted by the need for fixed line-of-site optics viewing a well defined region of space (into which the sample is placed). Thus, a sample need not be placed in an instrument for measurement, but instead, a fiber optic probe can be placed in the sample. Many fiber optic probes, each optimized for a specific application, can be used with one spectrometer; it is even possible to have several probes multiplexed to a single spectrometer. In addition, fiber optic probes are central to the development of fiber optic chemical sensors (FOCS) for the selective (remote) detection of a wide range of chemical species (1,2).

By physically separating (with fiber optics) the radiation source, detector, and signal processing instrumentation from the sample, optical measurements can be obtained from samples not easily contained within an instrument, samples in remote or inaccessible locations, or samples in environments inhospitable to instrumentation. Thus, optical measurements have been obtained from samples suspended in high strength magnetic fields (3), samples held at low temperatures (3), and from combustion systems (4).

The small size of fiber optics also facilitates measurements on

very small sample volumes. Small volume fiber optic flow cells (5,6) and spectroelectrochemical probes (for monitoring electrode reactions at the electrode surface) have been reported (7). In addition, their small size also makes it possible to obtain more than one optically encoded signal from a single sample, even when the sample is contained in a cuvette (8).

Although the flexibility afforded by using fiber optics for spectrometric measurements is advantageous, it is desirable that detectability not be sacrificed. For fluorescence or Raman scattering measurements, the observed signal is proportional to the excitation radiant power incident on the sample, and thus, is dependent on the coupling efficiency (power into fiber optic/total source power) between the source and the fiber optic(s). Although fiber optics generally exhibit low f-numbers (f/n) (0.75-2), the aperture presented by a fiber optic is typically in the range 0.1-0.6 mm (diameter of the fiber optic core), or even smaller; the limiting aperture in a conventional spectrofluorometer (with a cuvette) is frequently the excitation monochromator slit(s), which typically have dimensions on the order of 1 X 5 mm. When laser sources are employed, the source irradiance is high, and the source image can generally be focussed to a size small enough that the small aperture presented by a fiber optic does not limit the coupling efficiency (between the source and the fiber optic). However, when conventional sources are used (for which the source image is usually larger than the cross section of the fiber optic), the aperture presented by a fiber optic can limit the source power collected and may degrade detectability.

Another factor which affects the detectabilities achievable with fiber optic probes configured for fluorescence or Raman measurements is their emission collection efficiency. The sample volume from which emission radiation is collected is often smaller with fiber optic probes than with conventional fluorometers. McCreery (9) has reported that a dual-fiber (two parallel fiber optics with a 200-μm core diamater,) Raman probe provided Raman signals ca. 13% (corrected for relative source power) of those obtained with a conventional 90° viewing geometry; a probe consisting of 1 excitation and 18 concentric collection fibers provided approximateley the same signals as the cuvette system (10).

Deaton (11) has derived a figure of merit, the effective pathlength, for single-fiber (fiber optic) probes which can be used to predict the net fluorescence signal. A numerical value for the effective collection efficiency of single-fiber probes can be estimated from the effective pathlength and the solid angle of collection of the (single) fiber optic (11). Deaton was able to predict signal levels to within 30% of the observed values. Plaza (12) has derived an analogous efficiency term for double-fiber (fiber optic) probes, but the validity of this model was not experimentally tested.

In this paper, we describe the design and characterization of a fiber optic fluorometer for use with dual-fiber fiber optic probes. The fluorescence collection efficiencies of a dual-fiber probe and a cuvette fluorometer are determined and compared. The effects of the materials of construction and the dimensions of the sample reservoir ("cuvette") for fiber optic measurements are evaluated, and the linearity and detection limit for quinine sulfate are assessed.

THEORY

For a conventional spectrofluorometer with a sample cell (cuvette), it is possible to predict the fluorescence signal observed from a solution of a given fluorophore if its concentration, molar absorptivity (at the excitation wavelength), quantum efficiency, and emission profile are known and the optical components are well characterized. For low concentrations of a fluorophore such that inner-filter effects are insignificant, and under conditions such that the molar absorptivity, emission profile, detector responsivity, and transmission or reflection efficiencies of the optical components can be considered constant over the excitation or emission bandpass, equation 1 applies (11,13,14).

$$E_F = \Phi_{ex} 2.303 a c [b^* (\Omega/4\pi)] Y_F T_C T_E (s/\Delta\lambda) T_f F_F m G R(\lambda) \qquad (1)$$

where

Φ_{ex} = total radiant power at sample (W)

a = absorptivity ($(\mu g/mL)^{-1}\ cm^{-1}$)

c = concentration ($\mu g/mL$)

b^* = pathlength of illumination and observation (cm)

Ω = solid angle of fluorescence collection (sr)

Y_F = fluorescence power yield

T_C = cell transmission

T_E = transmission of emission optics

s = spectral bandpass (half-width) of emission filter or monochromator (nm)

$\Delta\lambda$ = half-width of emission band (nm)

T_f = maximum transmission of emission filter or monochromator

F_F = relative emission intensity at monitored λ

m = PMT current gain

G = signal processor transfer function (V/A)

$R(\lambda)$ = PMT photocathodic responsivity at emission λ (A/W)

To use equation 1, the excitation radiant power incident on the sample must be measured or calculated.

Two critical instrumental parameters in equation 1 are b^* and Ω. For a conventional (cuvette) spectrometer, the values of these parameters can be independently estimated from the known characteristics of the emission optical components. The solid angle of collection for fluorescence (Ω) is normally determined by the diameter and object distance of the lens (or mirror) that collects the emission radiation and directs it to the emission monochromator or filter. As a first approximation, the excitation beam cross section is relatively constant across the cell; thus, the total volume element within which fluorescence is excited is the product of the cell pathlength b and the excitation beam cross sectional area. Normally, only the emission radiation from the central portion of this total volume element is collected and imaged onto the photodetector. The net pathlength b^* of illumination and observation is determined by the image magnification of the emission optics, any apertures or slits in the emission optical train, and in some cases, the active area of the photodetector. Overall, the value of b^* is typically 1-5 mm for spectrofluorometers with a 1-cm

pathlength cell.

Equation 1 is also applicable to fiber optic fluorometers where Φ_{ex} is the excitation radiant power exiting the excitation fiber optic. However, Ω and b^* cannot be uniquely determined and are not single valued. In this case, the excitation radiation (beam) diverges significantly as it leaves the fiber optic. Also, the solid angle of (emission) collection decreases as both the distance from the emission collection fiber optic and the radial distance (relative to the optical axis of the collection fiber) increase. Thus an accurate calculation of the product $b^*\Omega$, which is denoted the effective emission collection efficiency, is difficult (12). Conversely, an experimental determination of the same term, utilizing a rearranged form of equation 1, is relatively straightforward.

EXPERIMENTAL

Instrumentation

A block diagram of the fiber optic fluorometer is shown in figure 4.1. Radiation from a 75-W-compact Xenon arc lamp (or a 75-W Xe/Hg lamp) in a lamp housing equipped with an f/2.5 elliptical reflector (Model 02-A1000, Photon Technology International, Inc., Princeton, N.J.) is focused onto the termination of an entrance fiber optic (f.o. 1). Maxlight PCS fiber optics (plastic clad silica fiber optic, core/cladding diameter of 860 μm with a 600-μm core, NA ≃ 0.33) were used throughout. The termination of the excitation fiber at the lamp focal point is held in a Newport FPH-DJ fiber optic chuck and mounted in a Newport LP-05 XYZ translational stage to allow maximum flexibility in positioning; this termination is stripped of cladding (ca. 3 mm), and the bare core is inserted through a 0.024-in (ca. 600 μm) aperture drilled in a 1-in diameter aluminum disk so that ca. 0.12 in (ca. 3 mm) of the bare core is exposed to the focussed lamp radiation. This configuration protects the plastic cladding from the source radiation, preventing deterioration of the cladding and limiting the excitation of cladding modes.

The arc lamp is powered by a PTI model 02-LPS200 D.C. arc lamp power supply (set at 5.0 A and 14.5 V for either lamp), and the lamp current is modulated by a 400 Hz 1-V pp D.C. filtered sine wave (Heath Schlumberger function generator, model EU-81A) supplied to the optical feedback input of the power supply. A 0.8 μF capacitor (8 0.1 μF capacitors in parallel), in series with the output of the function generator, removes any D.C. component of the modulation

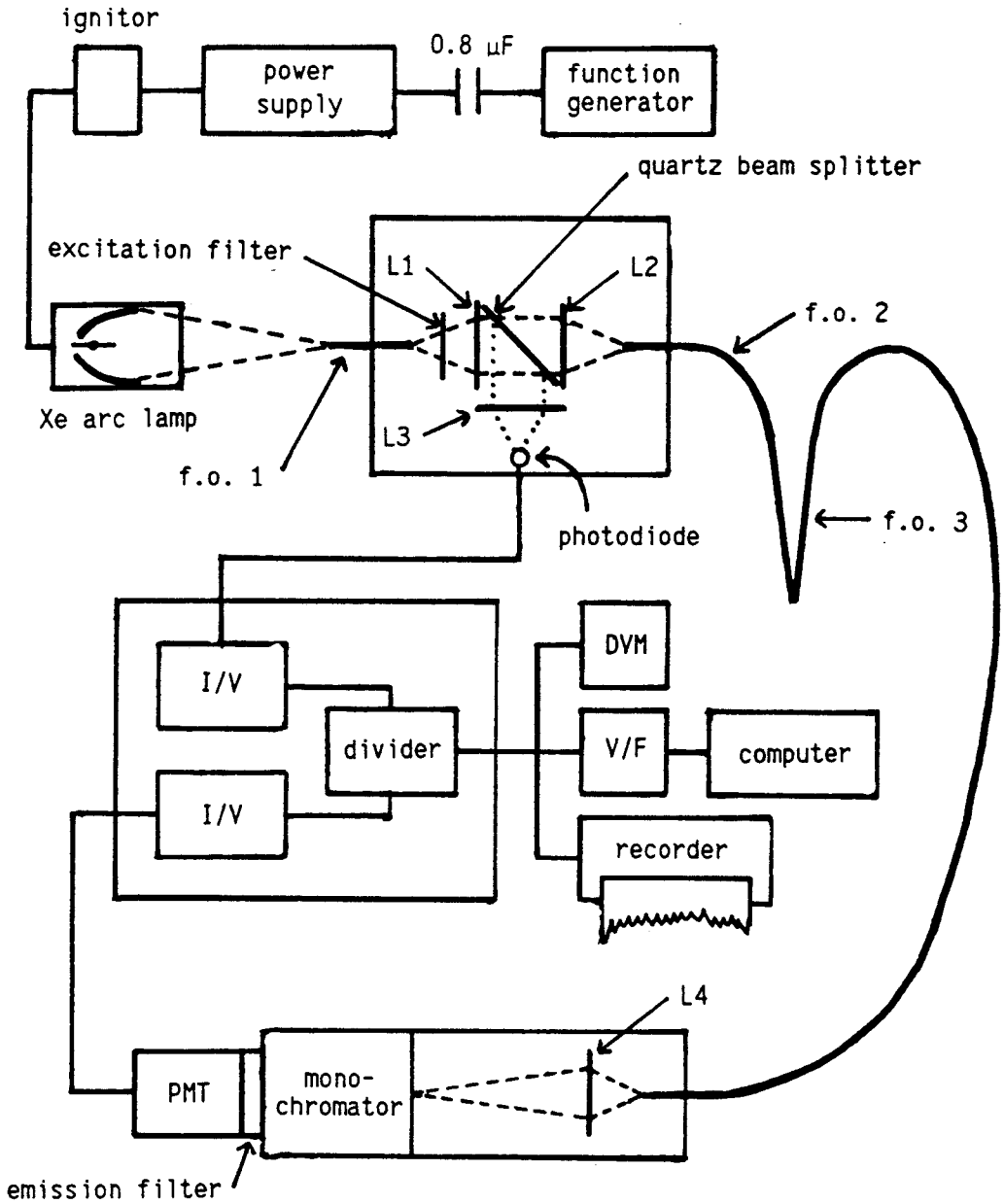

Figure 4.1. Block diagram of the fiber optic fluorometer.

signal. Modulation of the lamp is analogous to placing the arc in a varying magnetic field (13) and promotes even wear of the arc electrodes and reduces arc wander (15).

Source radiation exits the entrance fiber optic within a light-tight housing where it passes through an excitation filter and is collimated by an f/1 fused silica lens (L1, 1-in dia.). The collimated beam then passes through a quartz plate beam splitter which directs ca. 8% of the sorted source radiation to the f/1.5 (L3, 1-in dia.) focussing lens of the reference detector. A 0.197-in (5-mm) square photodiode from a PTI optical feedback unit (model 02-LPS002) is used as the reference detector. The image of the fiber optic face (f.o. 1) at the photodiode (focal point of L3) is ca. 0.035 in (900 μm) in diameter (magnified by a factor of 1.5), and the whole image is viewed by the photodiode. Excitation radiation passing through the beam splitter is refocussed onto the excitation fiber optic of the fiber optic probe (f.o. 2) with a second f/1 fused silica lens (L2, 1-in dia.). The excitation fiber optic is mounted in an XYZ translational stage (vide supra).

The excitation fiber optic (f.o. 2, 1-m) guides excitation radiation to the sample, and a portion of the resulting fluorescence is collected by a second (1-m) fiber optic (the emission fiber optic, f.o. 3). The radiation exiting the emission fiber optic is focussed by an f/0.75 glass aspherical lens (L4, 1-in dia.) either onto the entrance slit of a monochromator (the lens is positioned to match the f/n of the monochromator), or through an emission filter onto the photocathode of a photomultiplier tube (PMT).

For some single wavelength (quantitative) measurements, a PTR

Optics (Waltham, MA) "Mini-Chrom" monochromator (reciprocal linear dispersion of 20 nm/mm, effective aperture of f/4, 1-mm square entrance and exit ports) was used, with the sorted radiation exiting the monochromator impingent on a PMT. An emission filter can be inserted between the exit port and the PMT. For other quantitative measurements, the monochromator was removed from the optical train and the radiation exiting the emission fiber optic was focussed through an emission filter directly onto a PMT. Monochromator scans were performed utilizing another PTR monochromator (300-μm entrance and exit slits, reciprocal linear dispersion of 6 nm/mm, effective f/4 aperture), a PTR PMT unit (model PMT-1), and a PTR CB-1 monochromator stepper motor controller unit interfaced to an IBM compatible PC.

Both RCA 4840 and RCA 1P28A PMTs were used in this work and were powered by a Keithley high-voltage power supply (model 244). After current to voltage conversion and amplification, the PMT signal is ratioed to the reference signal with a divider. The source compensated fluorescence signal is monitored with a DVM, or for spectral scans, input sequentially into a voltage to frequency converter and a timer counter interface board (Metrabyte CTM-05) for computer data acquisition.

The dual-fiber probe constructed for this work is shown in figure 4.2. The probe housing holds the distal (sensing) ends of the fiber optics (f.o.s 2 and 3) at a 20° angle, and is constructed from Teflon with a black Delrin outer casing and two Newport FPH-DJ fiber optic chucks. The two fiber optics are stripped of cladding (ca. 15 mm), inserted into the fiber optic chucks, polished, and then

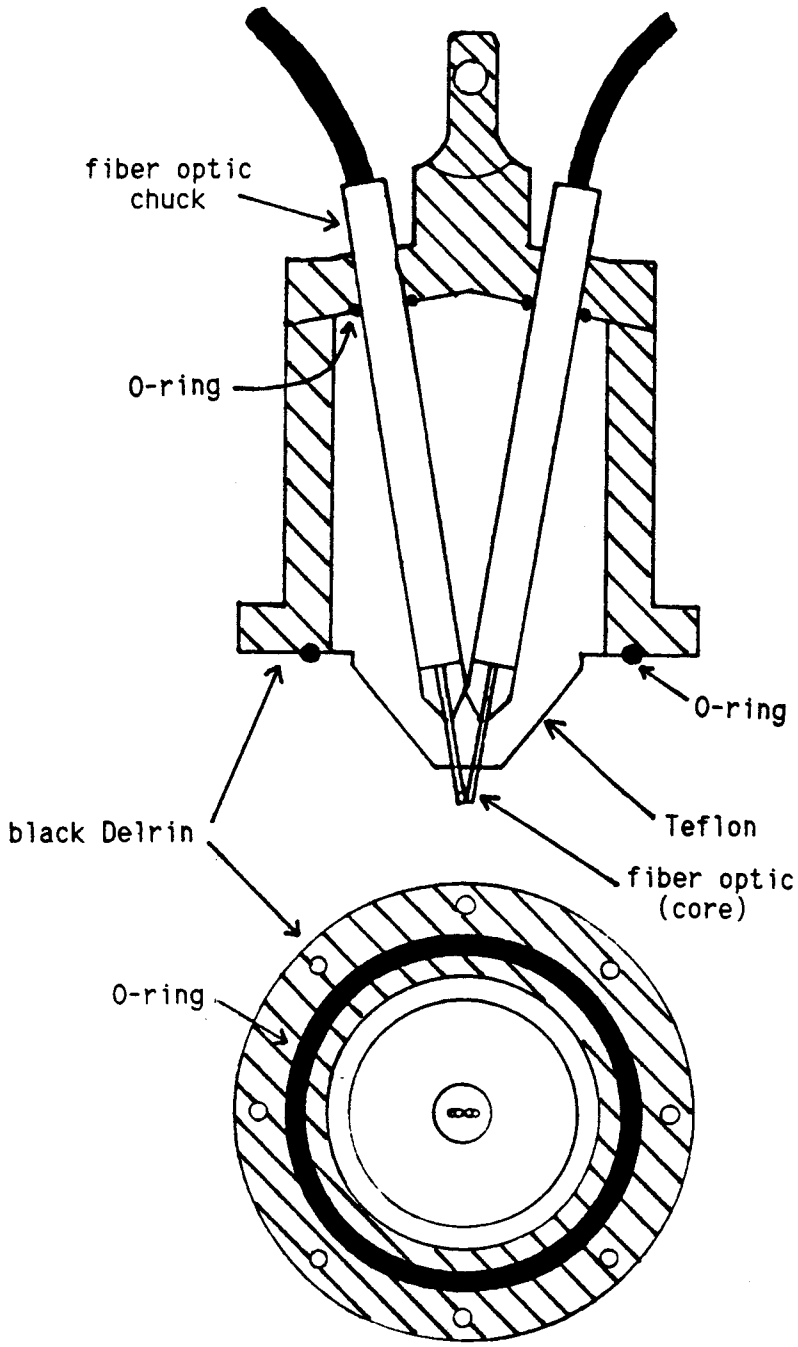

Figure 4.2. Cross-sectional and bottom views of the dual-fiber probe constructed for use with the fiber optic fluorometer.

inserted into the probe housing. When assembled, the two fiber optic tips just touch each other, and they protrude ca. 0.15 in (3.8 mm) beyond the probe housing.

The fiber optic probe is interfaced with an aqueous sample using the holder shown in figure 4.3. The "spacer" is friction fit into the upper black Delrin collar. To assemble, a sample reservoir is placed in the "reservoir holder" and enough solution is added to just fill the reservoir (depending on the dimensions of the reservoir itself). The upper collar is then placed over the reservoir, and the fiber optic probe is then placed on top of this piece. When assembled (figure 4.3b), this apparatus is light-tight and provides reproducible positioning of the fiber optic tips (of the probe) ca. 0.10 in below the surface of the sample solution. The sample reservoirs themselves are cylindrical wells milled into 2.00-in lengths of 1.50-in diameter black or white Delrin or Teflon, and the wells used in this work had diameters ranging from 0.1 to 0.5 in and depths ranging from 0.1 to 1.0 in.

The fluorometer used for comparison was constructed in-house by Wilson and has been described elsewhere (14). This cuvette instrument utilizes a 90° fluorescence viewing geometry, a 200-W Xe/Hg arc lamp, and an f/4.7 excitation monochromator. The emission optics were configured to collect emission radiation from the sample at f/2, and the emission radiation was focussed through an emission filter directly onto a PMT (vide infra).

Procedures

Determination of Effective Collection Efficiencies. To

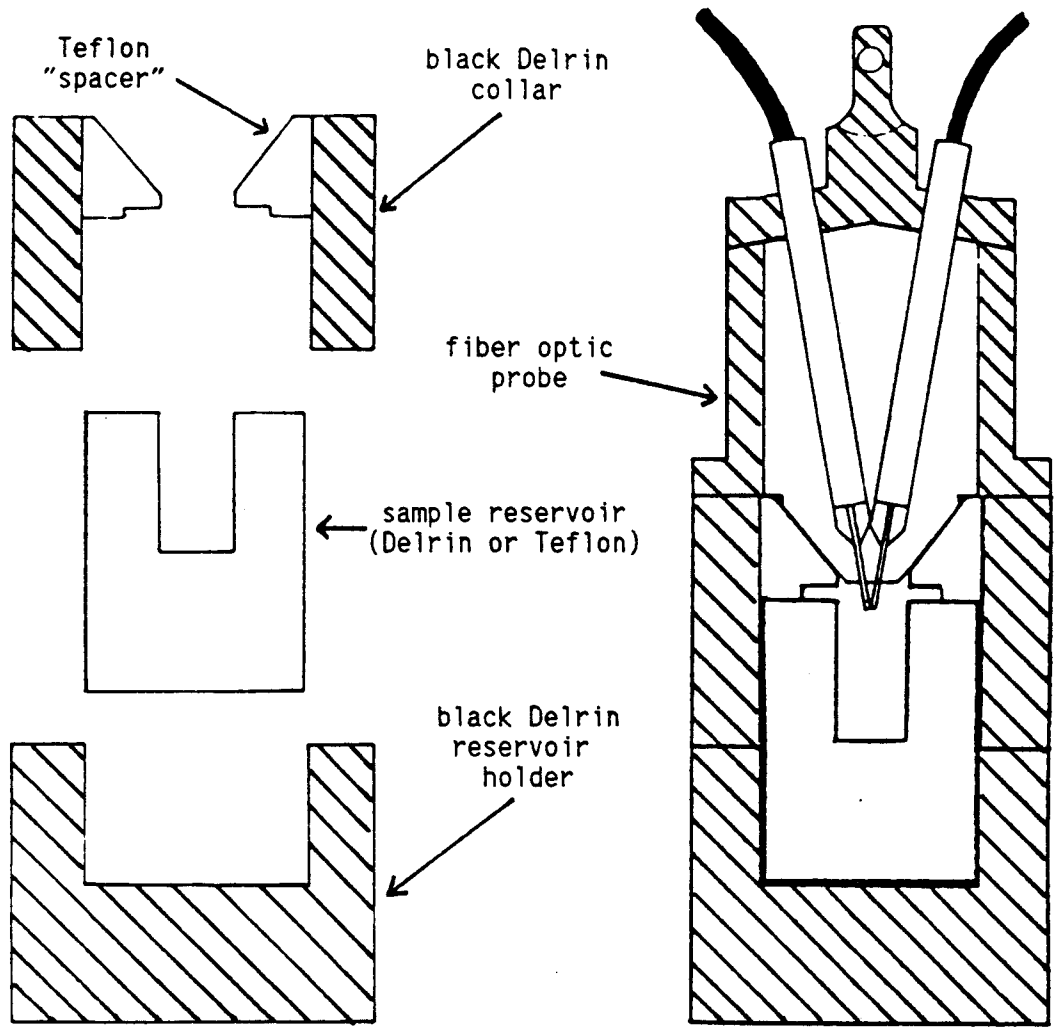

Figure 4.3. Cross-sectional view of the apparatus constructed for interfacing the fiber optic probe with aqueous samples.

compare the emission collection efficiencies the fiber optic and cuvette fluorometers, fluorescence signals from quinine sulfate (QS) solutions (over the range 1-100 ng/mL) were measured in both spectrometers. From equation 1, the measured values of E_F and Φ_{ex}, and estimates of analyte and instrumental parameters, $b^*\Omega$ was calculated. To ensure that conditions were as identical as possible, the same excitation wavelength (366 nm), emission filter (460-nm interference filter, 40% peak transmittance, 10-nm half-width), PMT (RCA 1P28), PMT bias voltage (-900 V), and signal processor gain ($G = 10^7$ V/A) were used. Hence in equation 1, a, c, Y_F, s, $\Delta\lambda$, F_F, m, G, and $R(\lambda)$ are identical for both sets of measurements.

For measurements with the conventional fluorometer, the excitation wavelength and spectral bandpass were 366 nm and 21.25 nm, respectively. For the fiber optic measurements, a 366-nm excitation interference filter was employed (peak transmittance of 25% and halfwidth of 10 nm) with the 75-W Xe arc lamp. For these measurements (for the determination of effective collection efficiency), the fluorescence signals were not ratioed with the source reference signal.

The excitation radiant power was determined using a modified photodiode detector (PTR Mini-Chrom Silicon Detector, model SDM-1); from the measured photodiode voltage, the excitation radiant power was calculated using the current-to-voltage transfer function (54.5×10^3 A/W) and the photodiode responsivity at 366 nm (0.16 A/W). For the cuvette fluorometer, the image of the excitation monochromator exit slit at the position corresponding to the center of the sample

cuvette (with the cuvette and the cuvette holder removed) was 5 X 10 mm, or twice the area of the photodiode. Thus, the radiant power at the cuvette was taken to be twice the power reading obtained. The power impingent on the sample was calculated by multiplying this measured power by the factors 0.96 (loss due to cell wall reflectance) and 0.4 (the aperture loss due to the 2 mm X 15 mm excitation slit placed at the cell). For the fiber optic system, the excitation fiber optic was placed close to the photodiode such that all the radiation was detected. The measured value was multiplied by a factor of 1.04 to account for the decreased reflective loss when the fiber optic is placed in an aqueous (sample) solution.

The current gain m of the PMT used was determined experimentally (16). The values of the other parameters in equation 1 were estimated from previous data (14), the Fresnel equation, or optical efficiency measurements.

For these experiments, the sample reservoir for the fiber optic fluorometer was a 0.5-in diameter, 1.0-in deep cylindrical well machined into black Teflon (vide supra); the sensing terminations of the fiber optics were ca. 0.1 in below the solutions surface and 0.9 in above the bottom of the cell.

Effect of Reservoir Characteristics on the Signal/Background. The fluorescence signal from a 0.100 μg/mL solution of QS and a blank were measured with the fiber optic fluorometer and black and white sample reservoirs of different depths and diameters. These measurements were performed using an Xe/Hg arc lamp, the RCA 4840 PMT, and the "Mini-Chrom" monochromator (only). The emission wavelength was 463 nm and the 366-nm excitation filter was used.

Quinine Sulfate Calibration. A calibration curve for QS over the range 0.01 ng/mL to 200 µg/mL was constructed from blank corrected fluorescence signals obtained using the Xe/Hg arc lamp, RCA 4840 PMT, 366-nm excitation interference filter, 460-nm emission filter (only), and a black Delrin sample reservoir having a diameter of 0.5 in and a depth of 1.0 in.

Reagents

All solutions were prepared with double deionized water obtained from a Millipore Milli-Q system fed by house-deionized water. QS was reagent grade (Baker) and all solutions were 0.1 N in sulfuric acid. All glassware was cleaned as previously described (14). Initial quinine sulfate solutions were made and allowed to equilibrate (for weeks) with the glassware. Fresh QS solutions were prepared using the dedicated glassware ca. 1 hour prior to measurement.

RESULTS AND DISCUSSION

Instrumental Design

A salient feature of the instrumental configuration shown by figure 4.1 is the use of a fiber optic as the initial source collection optic. The purpose of this is twofold: first, the small diameter fiber optic reduces the source power entering the optical interface so that heat filters are not necessary to protect the excitation filters, and second, the fiber optic spatially sorts the source image so that the reference detector views only that portion of the image which is (eventually) accepted by the excitation fiber optic. The use of an entrance fiber optic does not significantly reduce the amount of radiation input into the excitation fiber (f.o. 2) because the portion of the source image utilized is ultimately limited by the cross-sectional area of the (excitation) fiber optic core, which is identical to that of the entrance fiber optic. In addition, use of this entrance fiber optic simplifies construction of the interface box; the port through which the fiber optic enters the optical interface box is easily made light-tight, and alignment of this entrance port with the source image is not necessary as the termination of the fiber optic (at the source focal point) is held in an XYZ translational stage.

To maximize the coupling efficiency between the source and the "entrance" fiber optic, the source radiation should be focussed at a numerical aperture (NA) no greater than that of the fiber optic. Of the reflectors available (f/1, f/2.5, f/4.5), the f/2.5 reflector was

selected because it provides the maximum irradiance (minimum source magnification) at the fiber optic while not exceeding the NA of the fiber optics employed (ca. 0.33, or f/1.5).

Optical components exhibiting f/n's lower than the fiber optics (ca. f/1.5) are used for both the excitation and emission optical interfaces to prevent aperture loss. If f/2 lenses were used in the excitation optical train, the limiting aperture presented by the lens in the collimating configuration (object distance of one focal length) would result in an approximate 44% loss of power when used with the f/1.5 fiber optics. The use of f/1 lenses ensures that the lens aperture is underfilled in the collimating configuration, and only reflection losses need be considered. Note that an aperture loss of ca. 44% would result if a single f/1 lens was used for 1:1 imaging of the entrance fiber optic output onto the excitation fiber optic of the fiber optic probe. In addition, spherical aberration affects image quality to a greater extent in this configuration relative to the collimating configuration.

The optical efficiency (throughput) of the excitation interface was assessed by measuring the radiant power, using the photodiode (vide supra), at various points along the optical train. For these measurements, a halogen microscope illuminator was focussed through a 520-nm interference filter onto the input end of f.o. 1. The net throughput is defined as the ratio of the radiant power exiting the system (exiting f.o. 2) to that entering the optical interface (exiting f.o. 1 in the optical interface) and was determined to be ca. 42%. The calculated transmittance accountung for reflective losses (six 90° air-silica interfaces at 4.0% loss each and two 45°

air-silica interfaces at 4.6% each) is ca. 71%, and the remaining loss is attributed to image degradation resulting from spherical aberrations. The image of the entrance fiber optic (f.o. 1) face at the image focal point of the optical system (at f.o. 2) exhibited a noticeable halo. The spectral attenuation of the fiber optic is ca. 20 db/km at 520 nm (17) and thus the fiber optic contributes (only) ca. 1% to the observed attenuation.

With a 75-W Xe arc lamp, the (measured) net radiant power exiting f.o. 2 at 366 nm (366-nm interference filter) was 277 μW. With the same interference filter and a new 75-W Xe/Hg arc lamp, the measured radiant power was ca. 1 mW; using the Xe/Hg lamp, the measured radiant power at 545 nm (545-nm interference filter) was 1.5 mW.

Determination of Effective Collection Efficiency

The QS calibration curves obtained with both the cuvette and the fiber optic fluorometers (for the determination of effective collection efficiency) are shown in figure 4.4. The blank-corrected fluorescence signals obtained from a 0.1 μg/mL solution of QS were 0.53 V and 2.59 V for the fiber optic and the cuvette fluorometers, respectively. The corresponding values normalized for the source radiant power (at the sample) are 1.9 and 8.6 V/mW.

From the data for a 0.1 μg/mL solution of QS and estimates of the instrumental parameters, as presented by table 4.1, the calculated effective collection efficiencies ($b^*\Omega$) are 0.017 cm sr and 0.081 cm sr for the fiber optic and cuvette fluorometers, respectively. When the slopes of the two calibration curves are

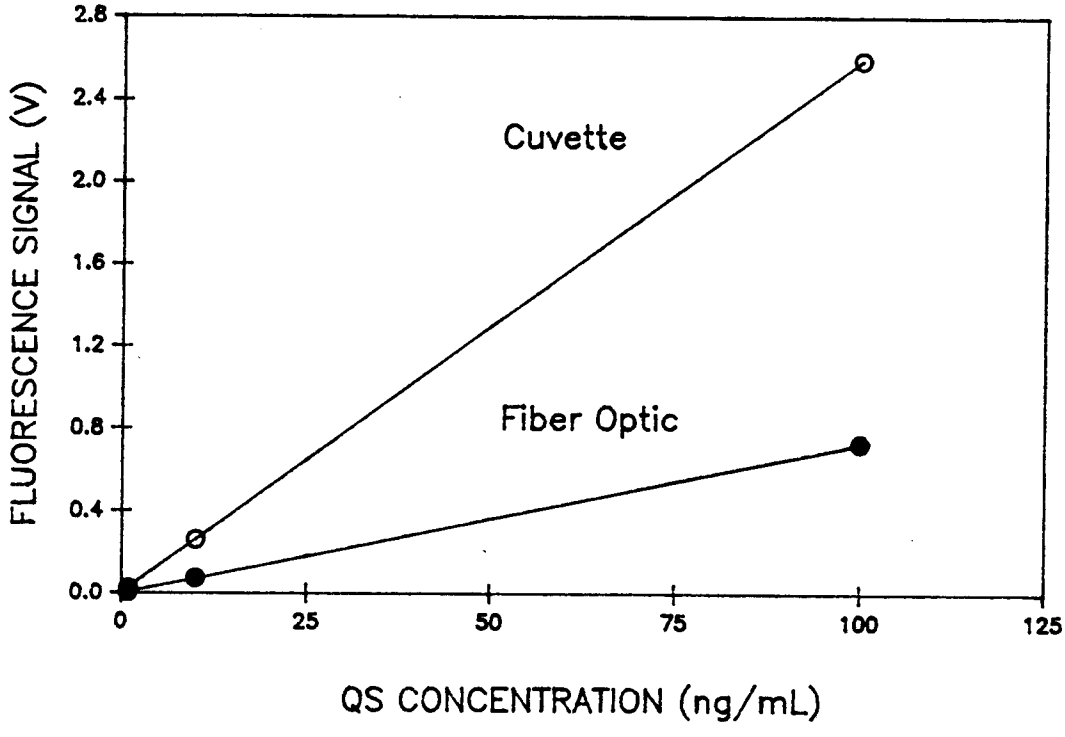

Figure 4.4. Calibration curves for quinine sulfate (1-100 ng/mL) obtained from a cuvette fluorometer and the fiber optic fluorometer using the same PMT and emission filter. The measured excitation powers at the sample were 301 μW and 277 μW for the cuvette and fiber optic fluorometers, respectively.

Table 4.1. Values used for calculating the effective collection efficiency (eq. 1) of both the cuvette and the fiber optic fluorometers.[a]

	Cuvette	Fiber Optic
Φ_{ex} (μW)	301	277
2.303ac (cm^{-1})	1.73×10^{-3}	1.73×10^{-3}
Y_F	0.44	0.44
T_C	0.96[b]	1.0[c]
T_E	0.85[d]	0.88[e]
$(s/\Delta\lambda)T_F F_F$	0.024	0.024
$mGR(\lambda)$ (V/W)	9.01×10^{10}	9.01×10^{10}
Observed E_F (V)	2.59	0.53
E_F/Φ_{ex} (V/mW)	8.6	1.9
$b^*\Omega$ (cm sr)[f]	0.081	0.017

[a]Constants from reference 14: $a = 7.5 \times 10^{-3}$ $(\mu g/mL)^{-1}$ cm^{-1}; $Y_F = \phi_F(\lambda_{ex}/\lambda_{em})$, where ϕ_F is the quantum efficiency of QS (0.55), λ_{ex} is the excitation wavelength (366 nm), and λ_{em} is the wavelength of maximum QS emission (455 nm); $\Delta\lambda$ = 170 nm. Instrumental parameters from this work: s = 10 nm; T_F = 0.4; F_F = 0.98 (18); $m = 2.65 \times 10^5$ (at -900 V); $G = 10^7$ V/A; $R(\lambda)$ = 34 mA/W (19).

[b]Assuming reflection loss of 4% at cell-air interfaces.

[c]No cell walls with fiber optics.

[d]Reflection loss of 4% at 4 lens-air interfaces.

[e]Reflection losses, 1 fiber-air (4%), 1 fiber-water (0.4%), and 2 lens-air interfaces (4%).

[f]Calculated using equation 1 and the values listed in table 4.1.

used instead, the same values are calculated. The experimentally observed value of the effective collection efficiency for the cuvette instrument is in good agreement with the specified value of 0.093 cm sr (14). Thus, the effective collection efficiency of this fiber optic probe is an approximate factor of 5 less than that of a typical cuvette (90° viewing geometry) fluorometer.

For a fiber optic probe similar to that employed in this work, the theory of Plaza predicts a collection efficiency of ca. 0.015 cm sr (see figure 12, ref. 12) which is within a factor of two of the experimental value of 0.017 cm sr. The theoretical value represents a lower limit as the specific probe modeled (by Plaza) employs fiber optics having a NA of 0.27, and the radii (315 μm) of the fibers includes the thickness of the cladding material (ca. 15 μm for each fiber). A probe assembled from fibers exhibiting larger NA's with the cladding removed (thus, the viewing volumes of the two fiber optics overlap to a greater extent) would be expected to exhibit a greater effective collection efficiency (12).

Previously, we reported that the net fluorescence collection efficiency of the dual-fiber probe used in this work is a factor of 1.52 less than that of a single-fiber probe constructed from the same fiber optic (20). The effective collection efficiency of a single-fiber probe can be calculated using the "effective" pathlength as defined by Deaton (11) and the corresponding solid angle of emission collection, which is dependent on the f/n of the fiber optic (11). After accounting for an arithmetic error found in Deaton's derivation (21) which changes the numerical value of the constant from 1.303 to 1.076, the predicted effective pathlength ($L_E = b^*$) for the

single fiber-probe in an aqueous solution is 0.126 cm, and the corresponding solid angle of collection is 0.197 sr. The predicted fluorescence collection efficiency for a single-fiber probe constructed from the fiber optic used in this work is then 0.025 cm sr. This leads to a predicted effective collection efficiency for the dual-fiber probe (single-fiber/1.52) of 0.016 cm sr.

The agreement between the experimentally determined effective collection efficiency and the predictions based on the models of Plaza and Deaton indicates that both models (Plaza's and Deaton's) are useful for predicting the performance of either single- or dual-fiber fiber optic probes to within a factor of 2. Numerical values for the effective collection efficiency of dual-fiber probes can be obtained by dividing the value predicted by Deaton (for a single-fiber probe) by the experimentally determined factor 1.52 (20). Conversely, analogous values for single-fiber probes can be obtained from Plaza's predicted values for dual-fiber probes by multiplying by the same factor.

Signal/Background Studies

Figure 4.5 shows the S/B for fluorescence measurements of a 100 ng/mL QS solution (blank-corrected) as a function of reservoir depth using black Delrin reservoirs of varying diameters. The S/B curves appear to approach an asymptotic maximum as the reservoir depth increases, and a S/B of 40 was obtained with a (black) reservoir having a diameter of 1.20 in and a depth of 1.25 in (not shown in the figure). The dependence of the S/B on reservoir diameter is minor.

Figure 4.6 is an analogous plot for reservoirs made from white

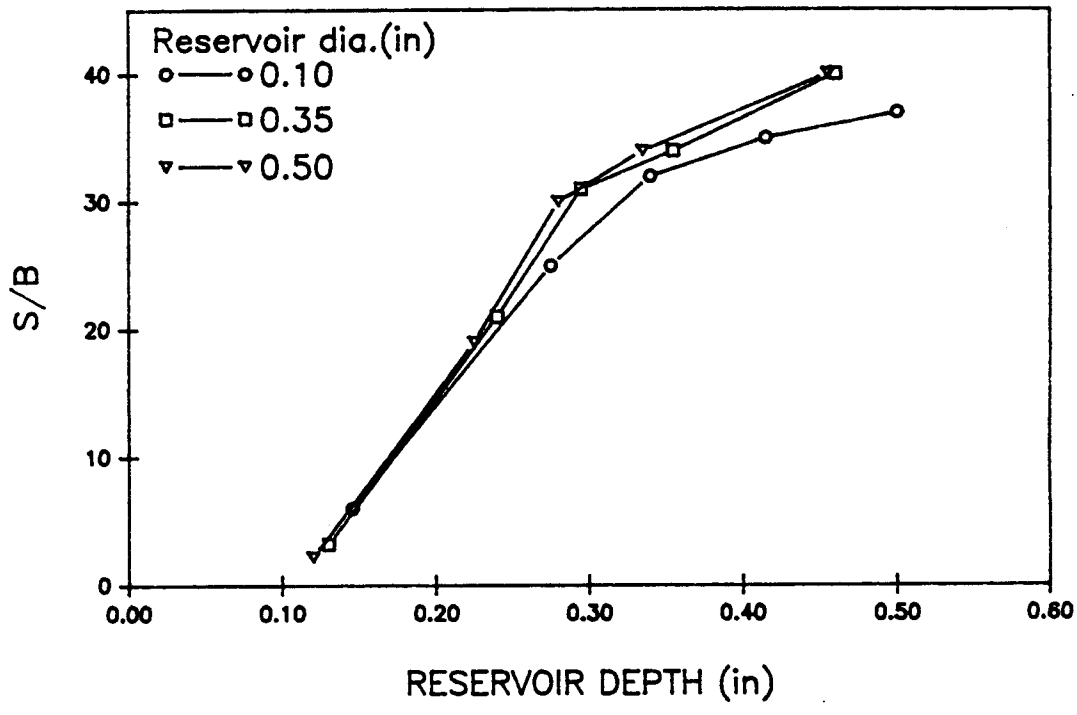

Figure 4.5. Dependence of the signal-to-background ratio on sample reservoir diameter and depth; reservoirs milled in black Delrin.

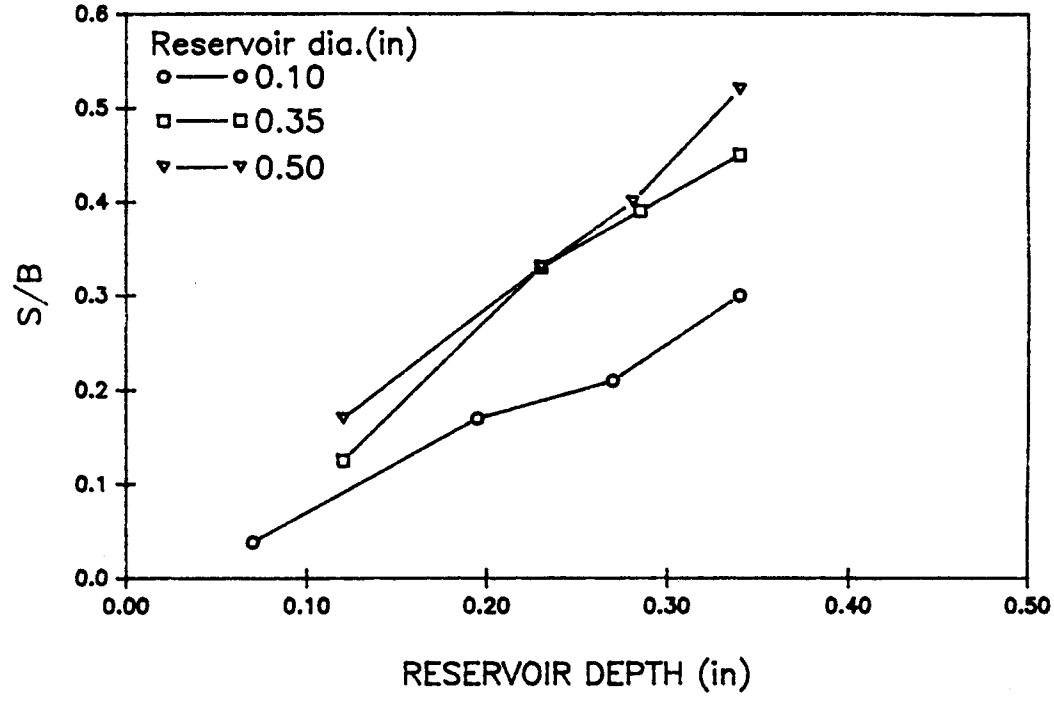

Figure 4.6. Dependence of the signal-to-background ratio on sample reservoir diameter and depth; reservoirs milled in white Delrin.

Delrin. In this case the S/B is much lower, and a maximum value of approximately 0.5 was observed with a reservoir depth of 0.35 in and a diameter of 0.50 in; for a given reservoir depth, the S/B improves by an ca. factor of two as the reservoir diameter increases from 0.10 to 0.50 in.

The data in figures 4.5 and 4.6 shows that reservoirs made from black material provide an ca. factor of 100 greater S/B than do comparable reservoirs made with white material. Obviously, the use of black reservoirs will provide better detection limits under background noise limited conditions.

Figure 4.7 shows the blank corrected fluorescence signal and blank signal (dark signal corrected) as a function of reservoir depth for the smallest (Figure 4.7a) and largest (Figure 4.7b) diameter black and white reservoirs. The S/B with the white reservoirs is much less than that with black reservoirs because the background signal is ca. 100 times greater. This large background signal is attributed to excitation radiation that is elastically scattered off the white surface and collected by the emission fiber. A portion of this radiation is passed by the emission monochromator as a stray radiation component (vide infra). In addition, the scattered excitation radiation collected by the emission fiber can excite fiber optic fluorescence, contributing further to the background signal (vide infra). Overall, the improvement in the S/B with increasing reservoir depth is due mostly to the decreasing blank signal, although the fluorescence signal also increases slightly with increasing reservoir depth (which results in a greater viewing volume from which the fiber optic probe can collect fluorescence).

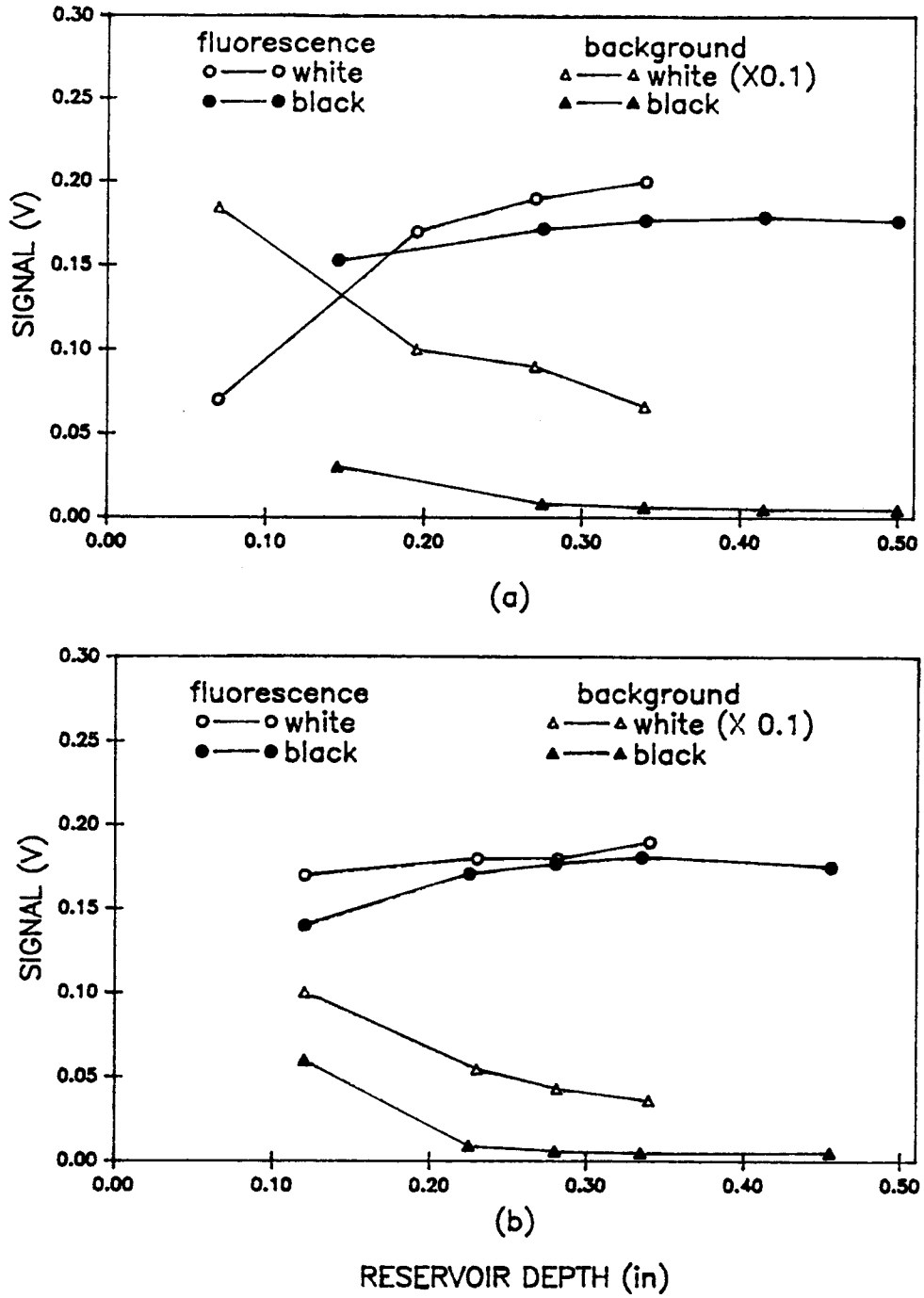

Figure 4.7. Blank corrected fluorescence signals and dark corrected background signals for 0.1-in (a) and 0.5-in (b) diameter sample reservoirs.

For a given size reservoir (diameter and depth), the fluorescence signal is slightly greater with the white reservoirs. This is probably due to reflected and scattered excitation radiation exciting additional fluorescence within the viewed volume of the sample solution. This mechanism is consistent with the observed dependence of the magnitude of the blank signal on reservoir dimensions (vide supra). The magnitude of this "excess" signal (above that observed with a black reservoir) decreases as the reservoir diameter and depth increases.

The plots in figure 4.7 show that ca. 90% of the maximum fluorescence signal is obtained from the first 0.3 in (ca. 8 mm) of solution in front of the fiber optic faces and, for a given reservoir depth, the magnitude of the blank-corrected fluorescence signals are essentially independent of well diameter. Thus, 90% of the observed fluorescence is obtained from a volume no greater than 0.04-mL (i.e., the volume of a 0.3-in deep, 0.1-in diameter reservoir).

Overall, the utility of white sample reservoirs is limited by high background signals. A white sample cell having a 0.1 in diameter and a depth of 0.3 in provides ca. 90% of the maximum obtainable signal but exhibits a S/B of ca. 0.25; a similar black reservoir provides essentially the same blank corrected fluorescence signal with a S/B of ca. 30. These considerations are especially important when designing small volume flow cells or fiber optic chemical sensors (FOCS) utilizing reagent reservoirs.

Performance Characteristics for Quinine Sulfate

A QS calibration curve obtained with the fiber optic

fluorometer is shown in figure 4.8. This curve is unique in that the linear dynamic range extends from 10 pg/mL to almost 10 µg/mL. Due to inner-filter effects, calibration curves for QS (obtained using a 1-cm pathlength cell and a 90° viewing geometry) usually exhibit an ca. 15% negative deviation from linearity at 10 µg/mL QS, and an ca. 80% negative deviation at 100 µg/mL (8); the corresponding values observed in this work were 3.6% at 10 µg/mL and 28% at 100 µg/mL, respectively. This improvement in linearity at higher QS concentrations is attributed to the front surface viewing geometry of the fiber optic probe. A front surface viewing configuration is known to be less susceptible to both primary and secondary inner-filter effects (13), and other workers have observed this effect with fiber optic probes (22).

Another interesting characteristic of the curve shown in figure 4.8 is the linearity exhibited all the way down to the detection limit. Non-linearity at lower concentrations is a common phenomenon often attributed to sorption equilibria between QS and the glass walls of both the solution flasks and the cell walls (8,14). At the time the data for the calibration curve were obtained, the dedicated glassware had held QS solutions for ca. 3 months. In addition, the blank (0.1 N H_2SO_4) was mixed in large volumes (9 L) and held in a dedicated Nalgene carboy for the same period of time. Measurements were obtained within one hour of preparing fresh solutions (QS and blank). The long pre-equilibration period may have eliminated errors due to sorption equilibria. Furthermore, the fact that the solutions are in contact with Delrin, rather than fused silica, during the measurement may also minimize this source of error.

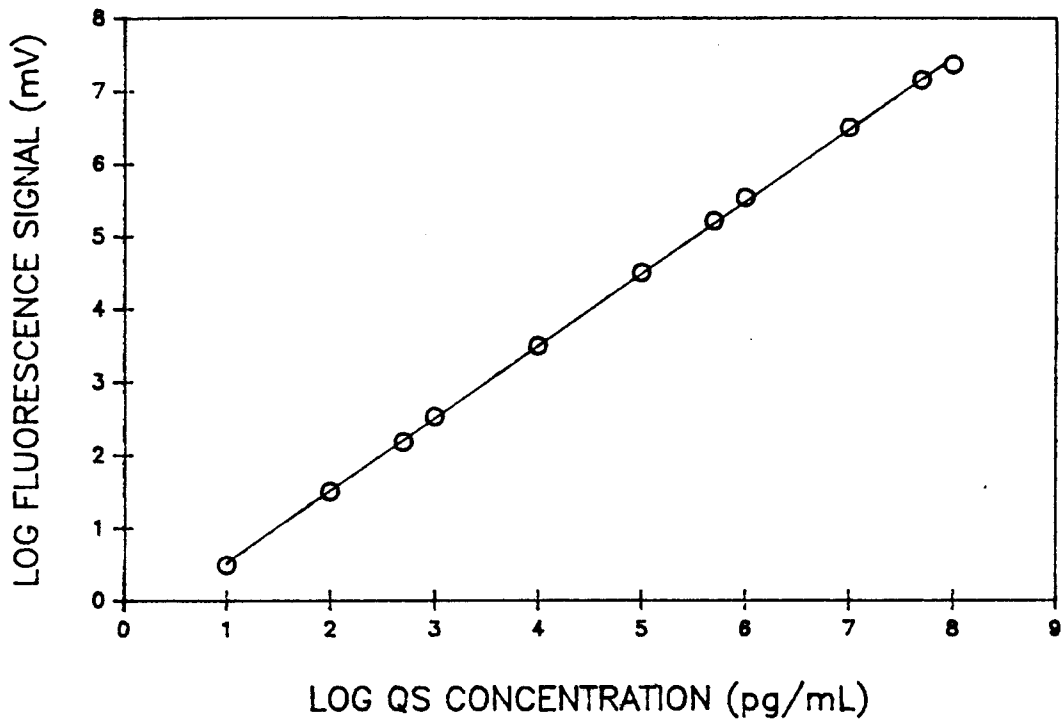

Figure 4.8. Calibration curve for quinine sulfate obtained using the fiber optic fluorometer. The slope of the log-log plot is 0.998 with a standard error of 0.004. Xe/Hg arc lamp, RCA 4840 PMT (-900 to -400 V), R_f (1-10 MΩ), 366-nm interference excitation filter, and 460-nm interference emission filter. All signals are normalized to an R_f of 10 MΩ and a PMT bias voltage of -900 V.

Table 4.2 compares the performance characteristics of the fiber optic fluorometer to those of a cuvette spectrofluorometer previously characterized (8) and the spectrofluorometer used to evaluate the effective collection efficiency . The detection limit for QS using the fiber fluorometer is 10 pg/mL and is comparable to that obtained with the cuvette fluorometers. At the detection limit, a combination of dark current noise and background signal noise are limiting.

The blank equivalent concentration (BEC) for the fiber optic fluorometer is slightly greater than that of the cuvette fluorometer using the same emission filter. A higher background is expected due to scattered source radiation and fiber optic fluorescence. The front surface viewing geometry of the fiber optic probe collects a greater fraction of the elastically scattered excitation radiation than the 90° viewing geometries of typical cuvette systems.

When a 400-nm cut-on filter is placed in front of the 460-nm interference filter in the emission optical train to further decrease scattered 366-nm radiation, the blank signal decreases by a factor of ca. 2. When a Mini-Chrom monochromator is used in place of the emission filter, the magnitude of the blank signal decreases by a factor of ca. 24. However, the net fluorescence signal also decreases by a factor of 12, and the net decrease in the blank signal (using the monochromator) is, again, a factor of ca. 2. Thus, filter fluorescence is not the dominant source of the observed blank signal. Fluorescence scans of the fiber optic showed that the fiber optics used in this work do fluoresce (when excited at 366 nm) over the region 450-600 nm.

Overall, the detection limit can be improved by increasing the

Table 4.2. Performance characteristics of the fiber optic fluorometer compared to two other fluorometers.[a]

	A[b]	B[c]	C[d]
Dark Signal	1	1	1
Blank Signal	7.2	0.2	1.6
QS Signal (0.10 μg/mL)	5.2×10^2	7.3×10^2	1.7×10^2
BEC[e] (pg/mL)	1385	27	835
DL[f] (pg/mL)	10	40	20

[a]All values normalized to a dark signal of 1 unit: for A = 60 mV, B = 50 mV , C = 15 mV.

[b]Fiber optic fluorometer: PMT (RCA 4840) bias voltage = -900 V($m = 4.73 \times 10^6$), R_f = 10 MΩ, C_f = 0.1 μF.

[c]Cuvette fluorometer with excitation and emission monochromators (8): PMT (RCA 1P28) bias voltage = -900 V ($m = 6.4 \times 10^6$), R_f = 100 MΩ.

[d]Cuvette fluorometer with excitation monochromator and emission filter: PMT (RCA 1P28) bias voltage = -900 V ($m = 2.65 \times 10^5$), R_f = 10 MΩ.

[e]BEC = blank equivalent concentration (concentration of QS yielding a fluorescence signal equal to the observed blank signal).

[f]Detection limit = $2s_{bk}/m$, (m = calibration sensitivity); $s_{bk} = 2.7 \times 10^{-2}$ dark units (10 measurements) for A, 0.15 dark units for B, and 1.7×10^{-2} dark units for C.

S/B. This can be accomplished by using a 400-nm cut-on filter in conjunction with the 460-nm interference filter and cooling the PMT to reduce dark current noise. The component of the background noise due to fiber optic or blank fluoresence cannot be discriminated by wavelength selection, and may ultimately be the limiting noise source.

CONCLUSIONS

The data reported here show that the absolute fluorescence signal and effective collection efficiency of a simple dual-fiber fiber optic probe (constructed from 600-μm core fiber optics having a NA of 0.33) are ca. one fifth that of a typical conventional cuvette fluorometer. Thus, a fiber optic fluorometer can achieve detection limits comparable to a conventional fluorometer when dark current noise or noise due to background luminescence (from species in the sample) is limiting. The data also indicate that the theories of both Plaza and Deaton are useful in predicting numerical values for the effective collection efficiencies of both single- and dual-fiber optic probes to within a factor of 2. In addition, the effects of sample cell dimensions and color on S/B have been demonstrated and the viewing volume of the probe used in this work shown to be no greater than 0.04 mL.

REFERENCES

1. Angel, S.M. Spectroscopy (Springfield, OR) 1987, 2 (4), 38-48.

2. Seitz, W.R. Anal. Chem. 1984, 56, 16A-34A.

3. Issacs, E.D.; Heiman, D. Rev. Sci. Instrum. 1987, 58, 1672-1674.

4. Kychakoff, G.; Kimball-Linne, M.; Hanson, R.K. Appl. Optics 1983, 22, 1426-1428.

5. Smith, R.M.; Jackson, K.W.; Aldous, K.M. Anal. Chem. 1977, 49, 2051-2053.

6. Ratzlaff, E.H.; Harfman, R.G.; Crouch, S.R. Anal. Chem. 1984, 56, 342-347.

7. Van Dyke, D.A.; Cheng, H.-Y. Anal. Chem. 1988, 60, 1256-1260.

8. Yappert, C.; Schuyler, M.W.; Ingle, Jr., J.D. Anal. Chem. 1989, 61, 593-600.

9. McCreery, R.L.; Fleishmann, M.; Hendra, P. Anal. Chem. 1983, 55, 146-148.

10. Schwab, S.D.; McCreery, R.L. Anal. Chem. 1984, 56, 2199-2204.

11. Deaton, T. "Instrumentation and Methodology for Remote Fiber Fluorometry" 1984, Ph.D. Thesis, Univ. Calif. at Davis.

12. Plaza, P.; Dao, N.Q.; Jouan, M.; Feurier, H.; Saisse, H. Appl. Optics 1986, 25, 3448-3454.

13. Ingle, J.D., Jr.; Crouch, S.R. "Spectrochemical Analysis", Prentice Hall, Englewood Cliffs, N.J., 1988, 438-493.

14. Wilson, R.L. "Design, Development and Optimization of a Fluorometric Reaction-Rate Instrument and Method of Analysis for Metal Ions" 1977, Ph.D. Thesis, Oregon State University.

15. Oldham, P.B.; Patonay, G.; Warner, I. Rev. Sci. Instrum. 1985, 56, 297-302.

16. Bower, N.W.; Ingle, J.D., Jr. Anal. Chem. 1975, 47, 2069-2072.

17. Raychem Corp. 1981, #H51157.

18. Miller, J.N. "Standards in Fluorescence Spectrometry", Chapman and Hall, London, 1981, p. 81.

19. RCA 1P28 Specification Sheet, Aug. 1975.

20. Louch, J.R.; Ingle, J.D., Jr. Anal. Chem. 1988, 60, 2537-2540.

21. Desiderio, R. Oregon State University, Personal Communication, 1989.

22. Mitchell, D.G.; Garden, J.S.; Aldous, K.M. Anal. Chem. 1976, 48, 2275-2277.

CHAPTER 5

INVESTIGATION OF THE FUJIWARA REACTION FOR THE SPECTROPHOTOMETRIC AND FLUOROMETRIC DETECTION OF CHLOROFORM WITH FIBER OPTIC CHEMICAL SENSORS

Jeff Louch and J. D. Ingle, Jr.

Department of Chemistry
Oregon State University
Gilbert Hall 153
Corvallis, OR 97331-4003

ABSTRACT

A discussion of sensor methodology for the monitoring of reaction intermediates is presented and a simple kinetic model for predicting the time dependent response of such a sensor is developed. Two possible mechanisms for the Fujiwara reaction with chloroform are discussed in terms of the kinetic model. The effect of pyridine, water, and base concentrations on reaction kinetics were evaluated to develop optimized single-phase Fujiwara reagent mixtures for both the fluorometric and spectrophotometric determination of chloroform. A unique "continuous-exposure" apparatus for the determination of volatile species with conventional cuvette-based spectrometers is presented. With this apparatus, the spectrophotometric detection limit for chloroform using the optimized spectrophotometric reagent is 11 ng/mL and the chloroform concentration in tap water was determined to be 33 ng/mL. An initial assessment of potential interferants in the continuous-exposure determination of chloroform in drinking water is presented which suggests that the average error due to interfering species in such a measurement would be on the order of 11%.

INTRODUCTION

Chemical transduction (1) is the process by which an active fiber optic chemical sensor (FOCS) extracts an optically encoded signal, related to analyte concentration, from a sample. Ideally, this signal reversibly tracks analyte concentration (i.e., the observed signal increases with increasing analyte concentration and decreases with decreasing concentration) when the sensor is exposed to a sample for extended periods of time. The development of chemistries capable of performing this function is central to the development of FOCSs. Generally, chemical reactions used in chemical transducers can be classified as being either reversible or irreversible (1).

Many FOCSs utilizing reversible chemistry for chemical transduction have been reported, the most common being pH sensors utilizing acid/base indicators (1). For these cases, the concentration of the monitored species shifts (either increasing or decreasing) in response to a change in sample pH, and a constant pH results in a static signal. When this type of equilibrium-based reaction is used, the lifetime of the sensor is not affected by reagent consumption and a continuous readout related to analyte concentration is obtained. In addition to acid/base indicators, metal-chelate reactions and dynamic quenching have also been used to develop FOCSs (1). The vast majority of FOCSs based on reversible chemical transduction respond to ionic species and low molecular weight, non-hydrocarbon, molecules (1). For many species

of interest, there are no reversible chemistries for use as a chemical transducer; in these cases, an irreversible reaction may be suitable.

A small number of FOCSs utilizing irreversible chemistries (i.e., derivatization reactions) for chemical transduction have been reported (1). Generally, the transducer consists of a reagent system (held in view of the fiber optic) which reacts with the analyte, and the monitored species is either a reagent or a stable reaction product. Thus, either a decreasing (monitoring reagent consumption) or increasing (monitoring product formation) signal is observed, and the rate of change in the observed signal is related to analyte concentration. A sensor utilizing this type of chemical transduction performs what is essentially a kinetic analysis and provides response to changing analyte concentrations in the form of changing reaction rates. These sensors are intrinsically integrating devices which cannot provide instantaneous readout (to assess the rate of change in the signal, it must be observed over time). In addition, the useful lifetime of this type of sensor is inversely related to calibration sensitivity (i.e., if the reaction rate is increased, reagent consumption also increases). However, the range of possible analytes is extremely wide with this type of chemistry, and through manipulation (of the chemistry) and proper sensor design, it should be possible to build sensors exhibiting both useful lifetimes and calibration sensitivites.

As a group, gem-polyhalogenated hydrocarbons (hydrocarbons with two or more halogens bonded to a single carbon) are important environmental contaminants for which new analytical methodology would

be useful. Specifically, the presence of trihalomethanes (THM) in finished drinking water is of concern (2,3). Presently, the maximum contaminant level (MCL) for these species (chloroform, bromodichloromethane, dibromochloromethane, and bromoform) in drinking water is set at 100 ng/mL (4). To demonstrate compliance, municipal water treatment facilities are required to perform quarterly analyses, using prescribed analytical methodology, to quantitate these species in their finished drinking water (5).

For the determination of THMs in drinking water the EPA has specified several gas chromatographic methods, all requiring an initial preconcentration step. The recommended methods utilize purge-and-trap GC with electrolytic conductivity detection (6, EPA 501.1), solvent extraction followed by direct injection GC with electron capture detection (7, EPA 501.2), or purge-and-trap GC with selective-ion mass spectroscopic detection (8, EPA 501.3). All these prescribed methods require a high degree of analyst skill and a large initial investment in instrumentation. For these reasons, most drinking water facilities contract these analyses to private laboratories. Due to the increasing concern over the presence of these compounds in drinking water, a simple method for quantitating trihalomethanes amenable to on-site implementation is desirable. Ideally, these compounds could be monitored on a continuous basis in finished drinking waters.

In 1914, Fujiwara reported the formation of a deep red color on reacting chloroform with alkaline pyridine (9). Since that time, the Fujiwara reaction has been used to determine gem-polyhalogenated hydrocarbons in a variety of samples (10-12). Although the procedure

has been modified by many workers, the basic method remains: an aqueous base solution, pyridine, and an aliquot of sample are mixed, the reaction is driven with heat, and the absorbance of the pyridine phase (after separation in most cases) is measured at a specific point in time. Time is critical as the red color is known to fade, indicating that the monitored species is unstable.

Workers at Lawrence Livermore National Laboratories have demonstrated that an organic base can be substituted for inorganic hydroxides (e.g., NaOH) to achieve a single-phase reaction mixture and have reported a FOCS utilizing this type of "Fujiwara reagent" coupled with fluorescence monitoring for the detection of chloroform (13-15). The initial response of this sensor approximated that of a true integrating sensor (i.e., a constant increase in the observed signal with time) only for short periods of time (ca. 1 hour), after which the signal decayed even with continued exposure to chloroform. From this work, it is not clear whether this turnover is due to the instability of the monitored species (thus representing a limitation of the chemistry), to reagent consumption, or to inner-filter effects.

In this paper, a general discussion of the factors affecting the utility of monitoring a chemical transducer reaction via an unstable species is presented, and optimization of single-phase Fujiwara reagent mixtures suitable for use with a FOCS chemical transducer are reported. The reported chemistry can be used for either the spectrophotometric or fluorometric determination of chloroform and possibly other gem-polyhalogenated hydrocarbons. In addition, a unique apparatus for vapor phase transport to a cuvette

in a bench-top spectrometer is presented. The utility of this apparatus for the bench-top determination of chloroform in chlorinated tap water at sub-µg/mL levels (using the optimized single-phase Fujiwara reagent) is demonstrated.

THEORY

In the simplest case, an irreversible reaction between an analyte A and reagent R to give a reaction intermediate I and a final product P is described by equations 5.1 and 5.2

$$A + R \rightarrow I \rightarrow P \qquad (5.1)$$

$$d[I]/dt = k_f[A][R] - k_d[I] \qquad (5.2)$$

where k_f and k_d are the rate constants for the formation and decomposition, respectively, of I. When the reagent R is in excess ($[R]_0 \gg [A]_0$), equation 5.2 can be rewritten

$$d[I]/dt = k_f''[A] - k_d[I] \qquad (5.3)$$

where $k_f'' = k_f[R]_0$. Initially, [I] equals zero, and equation 5.3 predicts the initial rate of formation of I is proportional to [A], allowing a kinetic determination of [A].

For a FOCS, we assume that the concentration of A in the sample and in the reagent phase is constant (1). Under these conditions, equation 5.2 becomes

$$d[I]/dt = k_f'[R]_0 - k_d[I] \qquad (5.4)$$

where $k_f' = k_f[A]$ (for this discussion, k_f encompasses all physical rate constants important for the sensing mechanism of the

FOCS, see chapter 6). From equation 5.4, the decomposition of I is a first-order reaction and the formation of I is a pseudo-first-order reaction. The solution (of equation 5.4 for [I]) for this case of two consecutive first-order reactions is given in many textbooks (16) and is repeated below

$$[I] = \frac{k_f'[R]_0 e^{-k_d t}}{k_d - k_f'}(e^{(k_d - k_f')t} - 1) \qquad (5.5)$$

As a first approximation, equation 5.5 can be used to model the response of a FOCS when the monitored species is a reaction intermediate. For specific values of $[R]_0$ and [A], the time dependence of [I] is determined by the values of the rate constants k_f and k_d.

The time dependence of [I] as a function of the relative values of k_d and k_f' (for a given value of $[R]_0$) is shown in figure 5.1. The period of time over which a useful (pseudo-zero-order) kinetic response is observed decreases as k_d increases. However, for values of k_d such that $k_f'/k_d \leq 1$, [I] reaches a steady-state concentration (see curve a, figure 5.1).

Figure 5.2 shows the time dependence of [I] for two different concentrations of A for two cases. In figure 5.2a, $k_f'/k_d \ll 1$ and the pseudo-steady-state concentration $[I]_{ss}$ is proportional to [A]. In figure 5.2b, $k_f'/k_d \geq 100$ and the initial rate of formation of I is proportional to [A]. Thus, it is possible to determine [A] via d[I]/dt, or when I is highly unstable (i.e., $k_d \gg k_f$), by $[I]_{ss}$.

From figure 5.2a, there is an initial "induction" period prior

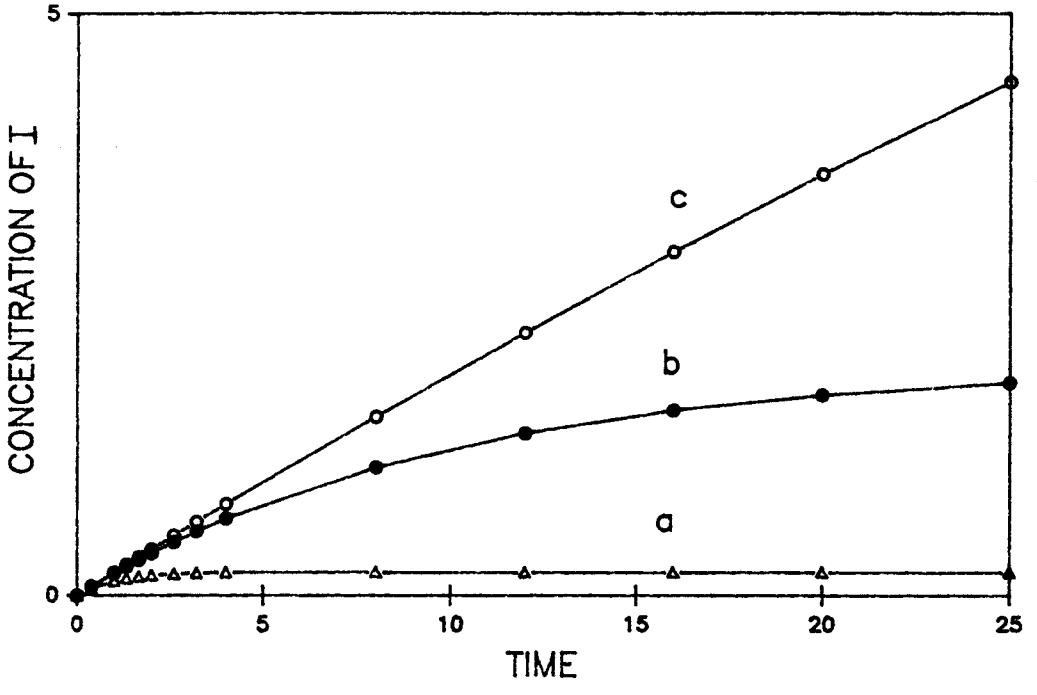

Figure 5.1. Time dependence of [I] as predicted by equation 5.5 for three values of k_f'/k_d; $k_f'/k_d = 1$ (a), $k_f'/k_d = 10$ (b), and $k_f'/k_d = 100$ (c). For all cases, $k_f' = 1$, [A] = 0.002, and $[R]_0 = 1000$. Both [I] and time are expressed in arbitrary units.

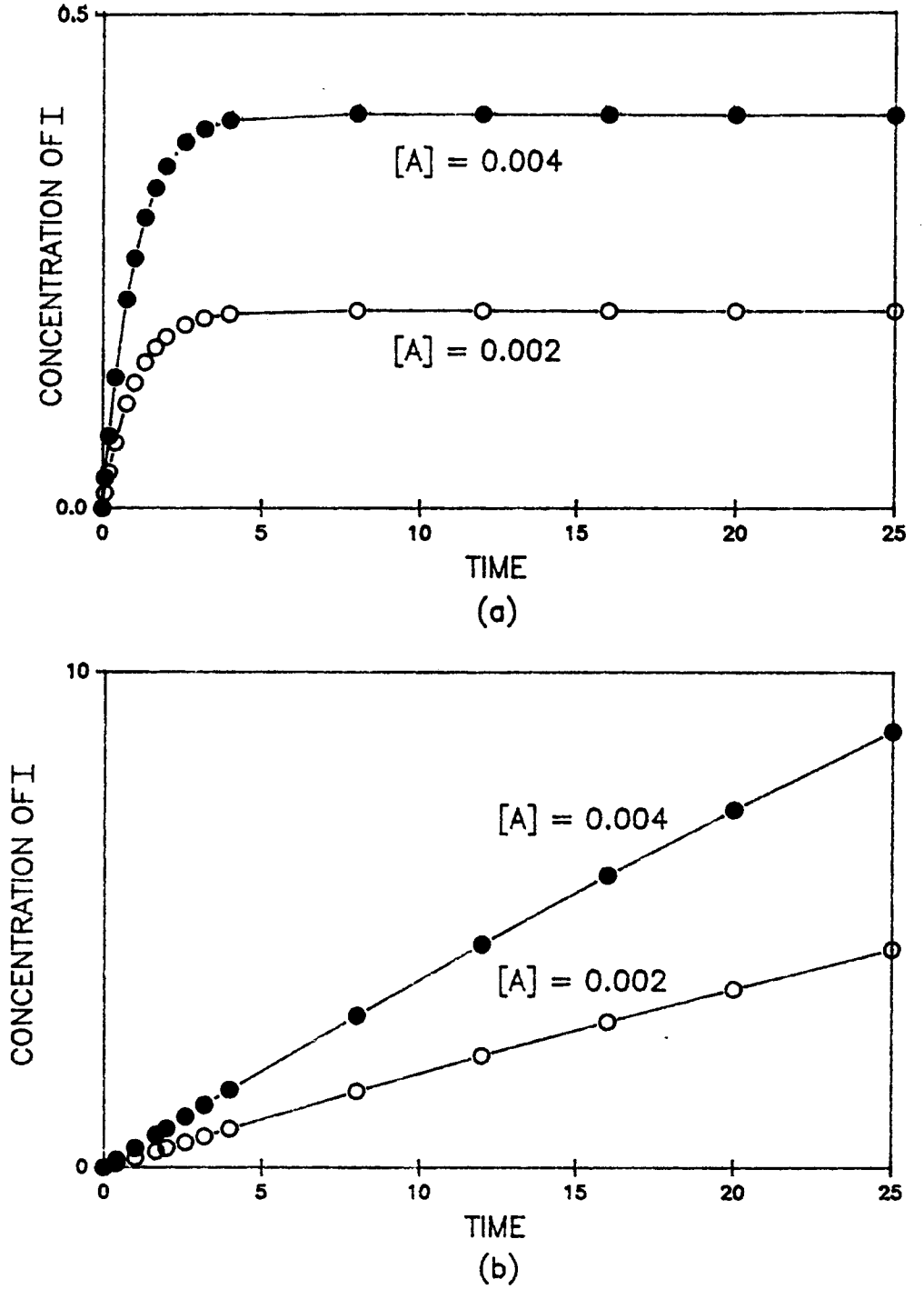

Figure 5.2. Time dependence of [I] as predicted by equation 5.5 for two values of [A] when $k_f'/k_d \ll 1$ (a), and when $k_f'/k_d \gg 100$ (b). For figure (a), $k_f = k_d = 1$; for figure (b), $k_f = 1$ and $k_d = 0.00001$. Both time and concentration(s) are expressed in arbitrary units.

to reaching $[I]_{ss}$. This induction period limits the response time of any FOCS utilizing the "pseudo-steady-state mode" of measurement; the "kinetic-mode" measurement (figure 5.2b) does not exhibit this drawback. In addition, note that the concentration of I formed under kinetic-mode conditions (figure 5.2b) is much greater than under pseudo-steady-state conditions (figure 5.2a) such that, as a first approximation, a better detection limit is expected for the kinetic measurement. For these reasons, this thesis work has focused on developing kinetic-mode chemistry.

Generally, the goals in developing chemistry for a FOCS are to obtain maximum (calibration) sensitivity and longevity of response; unfortunately, these criteria may be mutually exclusive when the monitored species is a reaction intermediate. Figure 5.3a shows the effects of varying k_f when monitoring over a longer period. When all other factors are constant, the calibration sensitivity (the initial rate of formation of I, or $[I]_{ss}$) increases proportional to k_f. However, increasing k_f also increases the rate of reagent consumption and thus reduces the period of time over which pseudo-zero-order kinetics (or a steady-state concentration $[I]_{ss}$) are observed. Thus, a trade-off is forced between calibration sensitivity and sensor lifetime.

In figure 5.3b, the effect of increasing $[R]_0$ is shown. If $[R]_0$ can be increased without affecting either k_f or k_d, an increase in calibration sensitivity can be achieved without sacrificing sensor lifetime.

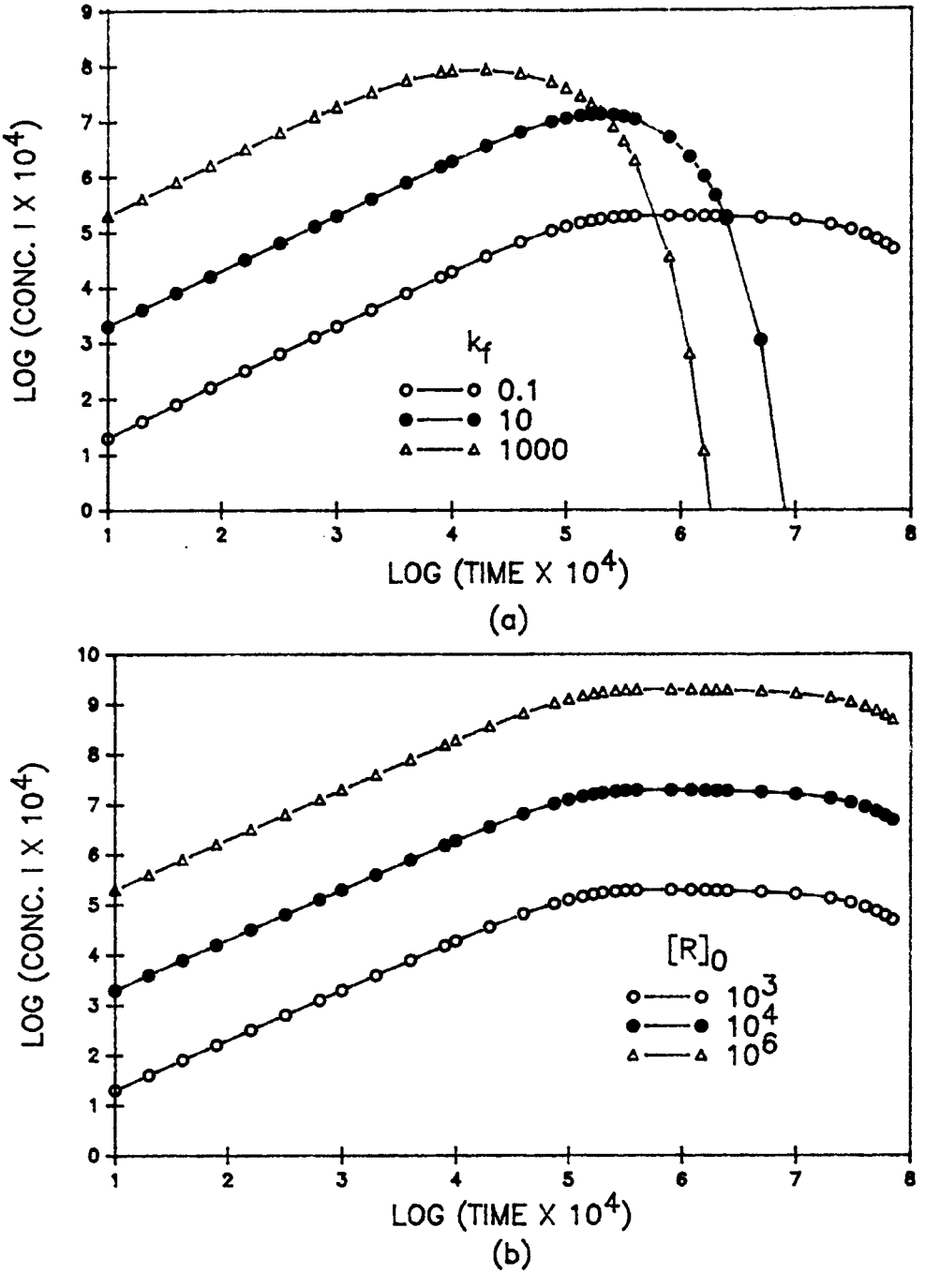

Figure 5.3. The effect on both calibration sensitivity and longevity of response (as predicted by equation 5.5) when either k_f' (a) or $[R]_0$ (b) is increased. For both figures, the default parameters are [A] = 0.02, $[R]_0$ = 1000, k_d = 1, and k_f = 0.1.

EXPERIMENTAL

Apparatus and Materials

Absorption measurements were obtained using an HP 8451A diode array spectrophotometer. This computerized spectrophotometer was programmed to measure and report absorbance at selected wavelengths (or wavelength windows) as a function of time; it was equipped to provide stirring of the solution held in the cuvette. Fluorescence scans were obtained using a cuvette spectrofluorometer constructed in-house (17); fluorescence measurements were conducted with a fiber optic fluorometer also constructed in-house (18).

The apparatus shown in figure 5.4 was assembled and used to expose reagent held in a cuvette (within the spectrophotometer) to the headspace above an analyte solution contained in a 50-mL three-neck reaction flask (14/20 taper). When assembled, the apparatus is gas-tight and is termed the "continuous-exposure" apparatus.

The continuous-exposure apparatus was designed to fit inside the sample compartment of the HP diode array spectrophotometer. The cuvette (Supracell RF-1010-I) was held in the unmodified cuvette holder, and the round bottom reaction flask was supported in a cork ring cut to fit within the sample compartment. A Helma Cuv-o-Stir (#333) unit was used to stir the analyte solution held within the reaction flask.

Procedures

Initial spectrophotometric studies comparing the suitability of

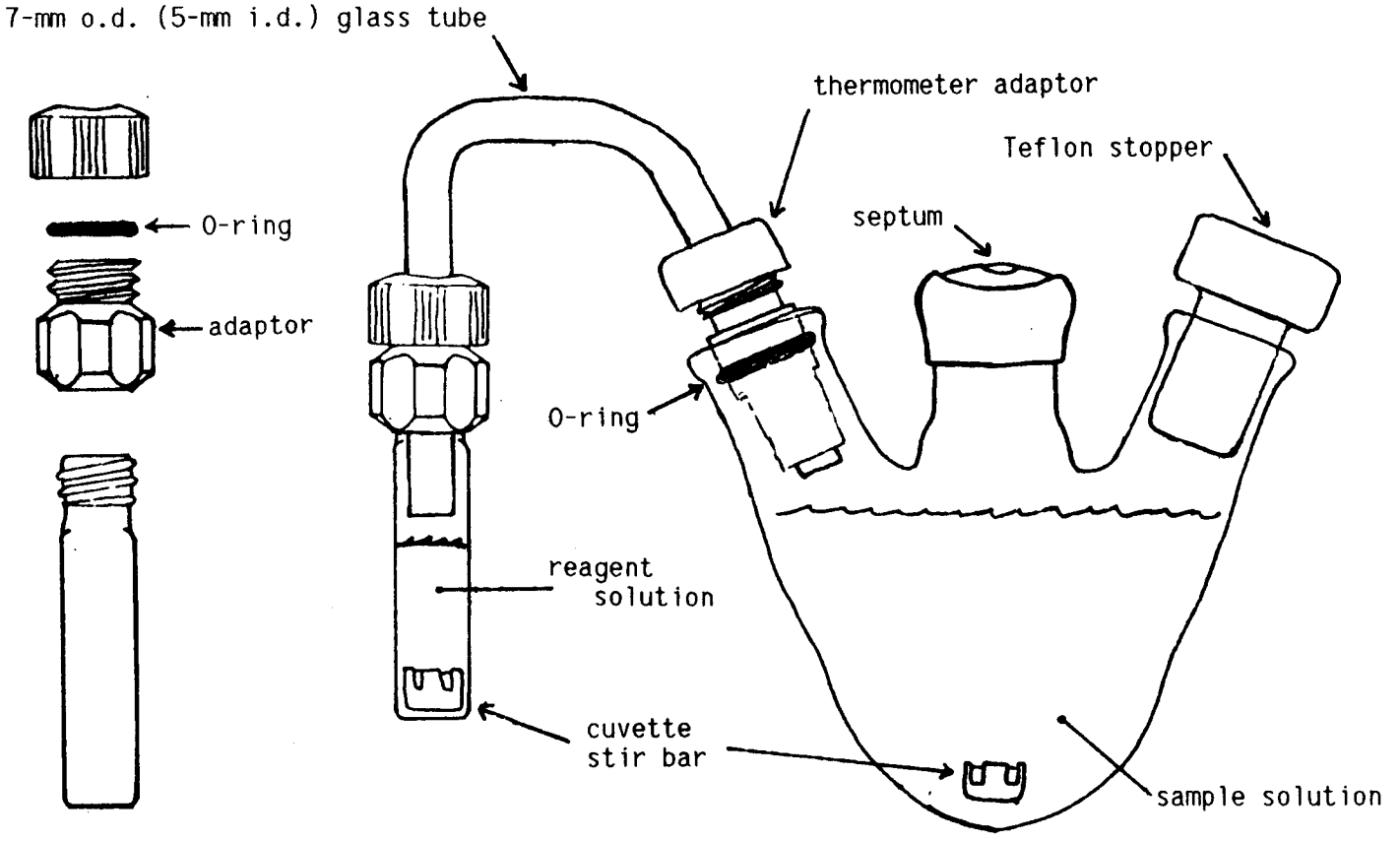

Figure 5.4. Continuous exposure apparatus for use in the HP diode array spectrophotometer. The gas phase analyte molecules diffuse into the cuvette and react with the reagent at the liquid surface (of the reagent). Stirring of the reagent ensures a homogeneous concentration of reaction products in the reagent phase, and stirring of the sample solution ensures a homogeneous concentration of the analyte in the sample solution (limiting diffusional effects).

various tetralkylammonium hydroxide bases for use in single-phase Fujiwara reagents were carried out by spiking 3.5 mL of stirred reagent mixture (in a cuvette) with 10 µL (Eppendorf pipet) of a 7.42 mg/mL chloroform solution (giving 21.1 µg/mL in the cuvette) and monitoring the absorbance (in time) of the reaction mixture (over the wavelength range 350-650 nm). The initial reaction rates (AU/min) were calculated as the best least-squares fit of the discrete absorbance values as a function of time (using an HP 15 calculator). The same procedure was also used for initial studies on the effect of the [pyridine]/[water] (of the single-phase Fujiwara reagents) on the reaction (with base concentration held constant). These experiments, referred to as batch-mode experiments, were performed at room temperature.

Initial optimization experiments with fluorescence detection were carried out in the batch-mode by spiking 1.25 mL of stirred reagent with 10 µL of a 148 µg/mL (ppm) aqueous chloroform standard (giving 1.17 µg/mL in the cuvette). The fluorescence of the reaction intermediate (vide infra) was monitored with the fiber optic fluorometer described previously (18), and the initial reaction rates were obtained from chart recorder tracings. In these experiments, the reagent mixture was placed in a 0.5-in. diameter, 0.75-in. deep well drilled into a white Teflon cylinder. The excitation source was a 75-W Xe arc lamp and the excitation wavelength was 545 nm as determined by an interference filter with an approximate 20-nm bandpass. The fluorescence was monitored at 610 nm as determined by a PTR "Mini-Chrom" monochromator (1-mm square entrance and exit ports, 20-nm bandpass); a 580-nm cut-on filter was placed at the exit

port of the monochromator and an RCA 4840 PMT was used.

Final optimization of the reagent mixture was performed (with the diode array spectrophotometer) using the apparatus shown in figure 5.4 as it more closely simulates the operation of the FOCS developed in this research. Stirred reagent mixture (2.5 mL) in the cuvette was connected to the headspace above 45 mL of blank water (Millipore Milli-Q) to obtain a blank rate. Then, 100 µL of a 740 mg/mL chloroform solution (in methanol) was injected into the stirred blank water (yielding a chloroform concentration of 164 µg/mL in the final 45.1 mL volume); these injections were performed using a Hamilton 100-µL syringe with the tip of the needle below the surface of the liquid. Any "blank" rate was subtracted from the observed analyte reaction rate, obtaining a blank-corrected rate. These experiments, referred to as continuous-exposure experiments, were also performed at room temperature.

Continuous-exposure calibration curves were obtained by making multiple 100-µL injections of selected analyte standards (1.48 X 10^3, 148, or 14.8 µg/mL) into a 45-mL volume of blank water. Again, blank corrected rates were obtained by subtracting any initial blank-rate observed prior to the injection of the chloroform standard from the analyte rates.

A standard additions analysis for the determination of chloroform in house tap water was performed by making two 100-µL injections of a 14.8 µg/mL chloroform standard into 45 mL of tap water. Thus, the added chloroform concentrations were 33 and 66 ng/mL. Prior to this analysis, the continuous-exposure apparatus was soaked in methanol overnight and baked to dryness (90° F). A

blank-rate measurement was obtained from this baked apparatus just prior to the tap water analysis (a fresh aliquot of reagent was used for the tap water analysis).

Reagents

The following reagents were purchased from Fluka: tetrabutylammonium hydroxide (40% in water), tetrapropylammonium hydroxide (20% in water), tetraethylammonium hydroxide (25% in water), and tetramethylammonium hydroxide (25% in water). Reagent grade pyridine and chloroform were obtained from EM Science; reagent grade methanol was obtained from Mallinckrodt. All chemicals were used as supplied, and all base solutions were refrigerated. All aqueous solutions were prepared with double deionized water obtained from a Millipore Milli-Q system fed by house-deionized water. All glassware was cleaned using a previously described proceedure (17).

Reagent solutions of pyridine, tetralkylammmonium hydroxides, and Millipore water were prepared gravimetrically in glass volumetric flasks and stored in a refrigerator. Typically, the mass of the specific base required to give the desired concentration was weighed into the tared volumetric flask. Next, the appropriate mass of water was added and the total mass recorded and the balance was re-tared; finally, pyridine was added to the volumetric mark, and the mass of pyridine recorded. For these solutions, the resulting molarity of water is calculated using the sum of the masses of the water added directly to the volumetric and the weight percent of water in the specific base (as supplied).

The primary chloroform standard (14.7 mg/mL) was prepared by

injecting 100 µL of reagent grade chloroform directly into 10 mL of methanol contained in a class A 10-mL volumetric flask. The contents of the flask were then transferred to a 4-mL borosilicate sample vial and capped with a Mininert valve such that there was no headspace in the capped vial; this primary standard was stored in a freezer. Working dilutions of the primary standard were made just prior to their use. For batch mode experiments, the 1:10 dilution was made by adding 1 mL of the primary standard to 10 mL of methanol; 1:100 and 1:1000 dilutions were made by spiking the appropriate volume of Millipore water with 100 µL of the primary standard. All standards for continuous-exposure experiments were made in methanol.

RESULTS AND DISCUSSION

For use in either a FOCS or a bench-top analysis, a single-phase Fujiwara-type reagent system providing a maximum kinetic response to chloroform was desired. For continuous monitoring (FOCS) applications, the response of the sensor should be related to analyte (chloroform) concentration for as long a period of time as possible. For a rapid bench-top analysis with a good detection limit, the amount of the monitored intermediate formed in 5 to 10 minutes should be maximized. To achieve these goals, the rate of formation (of the monitored species) should be maximized while the rate of decomposition should be minimized. To facilitate optimization of such a reagent mixture, a general mechanism for the Fujiwara reaction is helpful.

A proposed mechanism for the Fujiwara reaction with chloroform is shown in figure 5.5. This mechanism was formulated considering the experimental work of Uno et. al. (19,20) and general pyridine chemistry (21,22).

The reaction between pyridine and chloroform is postulated to begin with attack of the nucleophilic nitrogen of pyridine at the electron deficient carbon of chloroform (forming a), i.e., an S_N2 type displacement. The positive charge of the resulting adduct is localized on the α carbon of pyridine and constitutes a reactive site for the base-catalyzed cleavage of the pyridine ring (21). The "red" species d results from the reaction of two pyridine molecules with a single molecule of chloroform. Two possible pathways from a to d are shown: a sequence through b involving stepwise chloroform-pyridine

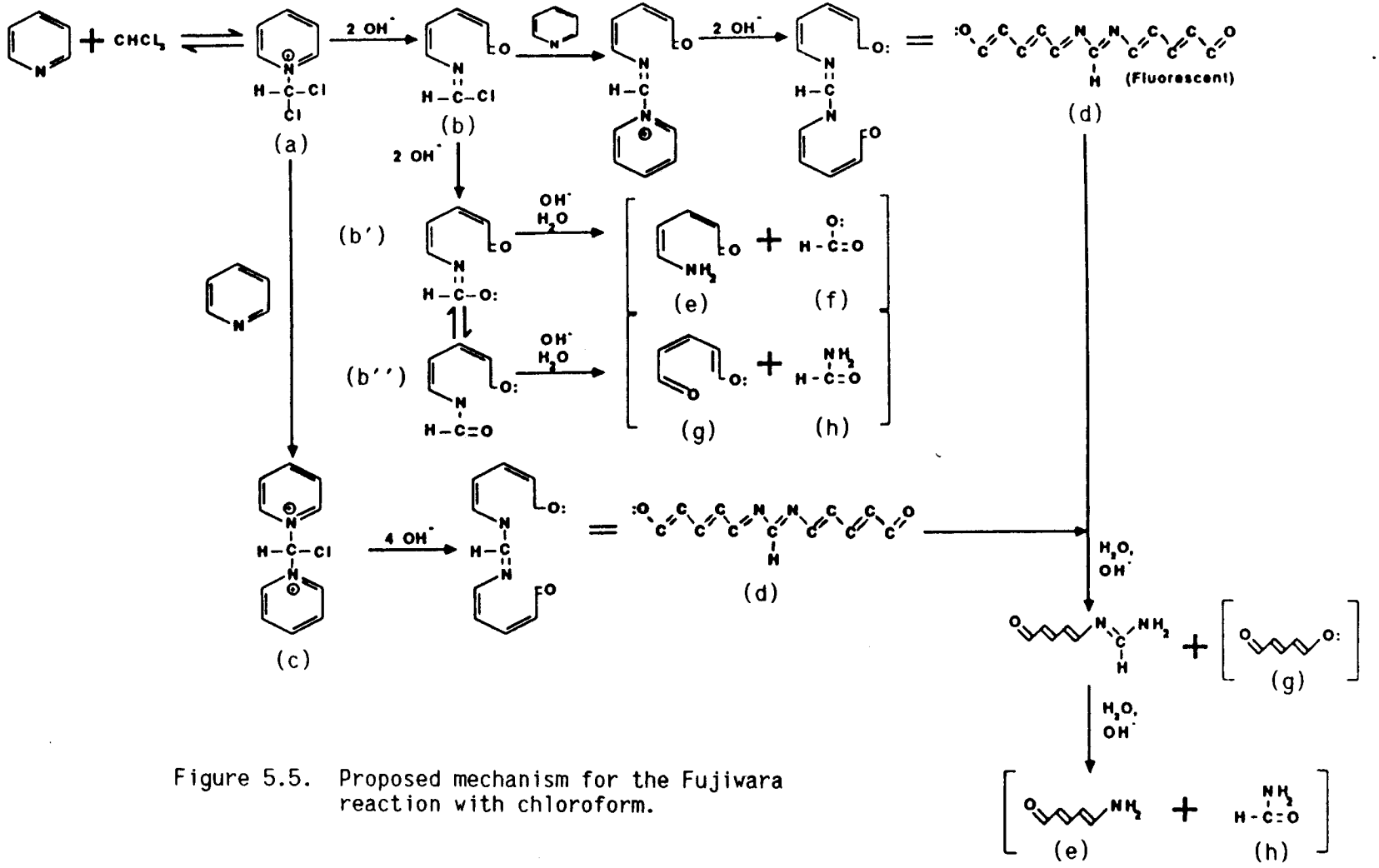

Figure 5.5. Proposed mechanism for the Fujiwara reaction with chloroform.

adduct formation and ring cleavage, and a sequence in which the di-pyridine adduct c is formed prior to hydrolysis of the pyridine rings.

The imine functional groups of b, c, and d (as well as b' and b'') are susceptible to base-catalyzed hydrolysis (22), giving the final products (e, f, g, and h). Note that the pathway through intermediates b' and b'' to products e, f, g, and h does not involve formation of intermediate d. The species labeled d, N^1,N^2-bis[(1E,3E)-4-formyl-1,3-butadien-1-yl] formamidine, has been isolated by Uno et. al. (20) and been shown to be responsible for the red color of the reaction mixture. Uno (20) has also studied the reaction with benzyltrichloride, and the analogs to species d, f (formic acid) and h (formamide) were isolated; glutaconaldehyde (g) has also been isolated (19,20). From the proposed mechanism, the traditionally monitored species d is a reaction intermediate.

An alternative mechanism for the formation of species a and c (figure 5.5) via conversion of chloroform to dichlorocarbene by hydroxide ion, as proposed by Angel et. al. (23), is shown in figure figure 5.6. Trichloromethyl anion r is generated from chloroform by action of hydroxide ion and is followed by alpha elimination to give dichlorocarbene s. The electrophilic dichlorocarbene formed reacts with pyridine to form the pyridinium ylide t. Protonation of the ylide t gives species a. This species is the same species as in the first mechanism and could further react by the pathway noted in figure 5.5, although this is considered unfavorable by Angel et. al. (23).

A second reaction pathway from t leads to c (the same species c

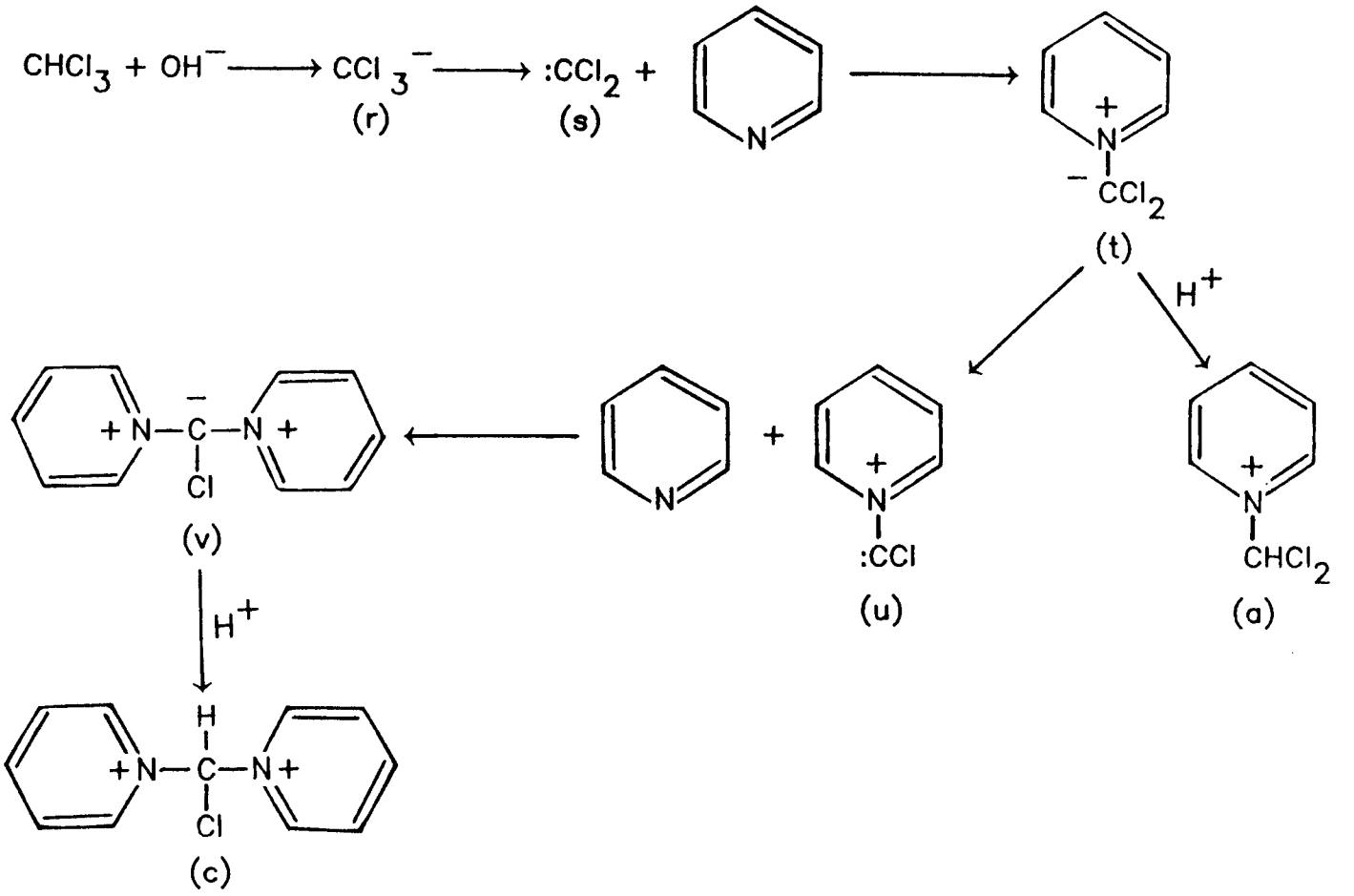

Figure 5.6. Alternative proposed mechanism for the Fujiwara reaction with chloroform (from ref. 23).

as shown in figure 5.5) via intermediates u and v. From species t, species u is postulated to result from the loss of a chlorine anion via solvolysis; the electron deficient pyridyl carbene u is then expected to form the dipyridyl anion v. Protonation of v gives c. From this point, the reaction is expected to follow the sequence outlined in figure 5.5, i.e, c goes to d, and then to the final decomposition products e, g, and h.

The feasibility of chloroform and pyridine forming species a via the S_N2 mechanism (figure 5.5) has been questioned (23). Studies of the base catalyzed hydrolysis of chloroform in aqueous systems have shown that this reaction proceeds through the dichlorocarbene route to the exclusion of an S_N2 pathway (24). In this case, both reactants (OH^- and $CHCl_3$) are sp^3 hybridized and the S_N2 route is considered to be sterically hindered (23). However, the nitrogen of pyridine is sp^2 hybridized ("flat"), which should reduce steric effects. Indeed, β-chlorination and β-bromination of pyridine by SO_2Cl_2 proceeds via an S_N2 pathway (21,25). Because the purpose of this work is the development of an optimized reagent mixture for use in the determination of chloroform, and not the elucidation of exact mechanistic pathways, no attempt has been made to gather evidence for either proposed mechanism.

Although the mechanisms for formation of d presented in figures 5.5 and 5.6 are substantially different, the reactants involved in the formation of the monitored species (d) are the same, i.e., hydroxide ion, chloroform, and pyridine. In addition, both proposed mechanistic pathways allow for the possibility of forming the final products without passing through intermediate d. Overall, there is

little difference between the net mechanisms. The decomposition of d is not addressed in the report by Angel et. al. (23). These facts allow a single discussion of the general factors affecting optimization of a single-phase Fujiwara reagent regardless of which (if either) mechanism is correct.

Generally, if the formation rate constant remains constant, the initial rate of formation of d is maximized without affecting the lifetime of the pseudo-zero-order kinetic response by increasing the concentration of the reagents (vide supra). However, for a single-phase reagent mixture, increasing the concentration of pyridine corresponds to decreasing the concentration of the other solvent, water. Thus, varying the pyridine concentration will affect the dielectric constant of a single-phase reagent via the concurrent change in water content and will affect the magnitudes of the formation rate constant(s). Any changes in the overall reaction kinetics resulting from this change in dielectric constant would depend on which mechanistic step is rate limiting and cannot be easily predicted.

One potential effect resulting from a decrease in the reagent dielectric constant is a decrease in the solubility of the hydroxide ion in the mixed phase (i.e., for a fixed concentration of base, the fraction in solution as ion-pairs is expected to increase). Under these conditions, increasing the concentration of pyridine in the reagent mixture will effectively increase the initial reaction rate only up to the point where the concurrent decrease in (effective) hydroxide ion concentration becomes the limiting kinetic factor. Overall, maximizing the rate of formation of d is complicated by the

effect of water on the stability of reaction intermediates and the effective hydroxide ion concentration. The water concentration may also effect the rate of formation and stability of carbenes if this pathway is operative.

Water also plays an important role in the decomposition of d; water both acts as a proton source in the base catalyzed hydrolysis of d and indirectly influences the effective hydroxide ion concentration (vide supra). Thus, the rate of decomposition of d might initially be predicted to decrease with reduced water content. However, the limiting step in the decomposition of d could also be affected by changes in the dielectric constant (brought about by changes in water content) and, again, this effect is dependent on which step is limiting and cannot be easily predicted. Also, the water concentration may affect the relative fraction of chloroform which reacts through pathways to form d.

By utilizing a solvent other than water, it is potentially feasible to achieve the optimum dielectric constant while simultaneously removing the proton source (water). Thus, it might be possible to maximize the rate of formation of d while limiting decomposition.

Visual scouting experiments testing the suitability of a few solvents were performed. These tests were carried out by dissolving small amounts of tetrabutulammonium hydroxide crystals in 2 mL of the selected solvent followed by 3 mL of pyridine and 1 drop (disposable pipet) of neat chloroform. Of the solvents tested (methanol, ethanol, dimethylsulfoxide, dimethylforamide, and acetonitrile), all dissolved the base with no apparent reaction except DMSO, which

turned yellow on addition of the base. On addition of pyridine and chloroform, no color formation was observed with the alcohols; the DMSO and DMF mixtures gave instant yellow/brown color while the acetonitrile mixture gave a dark red color instantly. Use of other solvent systems was not pursued further.

Traditionally, inorganic bases (i.e., NaOH) have been used for the Fujiwara reaction. In these cases, the charge density of the cation can limit the solubility of the salt (in a mixed pyridine-water phase). Through use of organic bases, such as tetrapropylammonium hydroxide, the effective concentration of hydroxide ion in lower dielectric solvent systems can be increased. Thus, the influence of water on the effective concentration of hydroxide ion in a single-phase reagent is reduced up to the point that the charge density of the hydroxide ion itself forces ion-pair formation (in the single-phase system).

Because of the multiple factors simultaneously affecting the rates of formation and decomposition of d, simple mono-variant optimization was not attempted. Instead, the approach taken was to first select an organic base for use in a mixed pyridine-water reagent, and to then map the response surface of the possible single-phase reagent compositions to find the reagent mixture giving the maximum initial rate of formation of d.

Spectrophotometric and Spectrofluorometric Monitoring

The progress of the reaction between chloroform and a single-phase Fujiwara reagent (pyridine, an organic base, and water) can be monitored spectrophotometrically via the absorbance of species

d (at 545 nm), or the absorbance of species g (at 368 nm). Figure 5.7 shows the time dependence of the absorption spectrum (over the wavelength range 320-620 nm).

The reaction can also be monitored fluorometrically, and figures 5.8 and 5.9 show the fluorescence emission and excitation spectra, respectively, of the same reaction mixture. When the reaction mixture is excited at 545 nm, an emission maximum is observed at 590 nm (the discrepancy between the fluorescence emission maximum from figure 5.8 and that reported earlier for the Mini-Chrome monochromator of the fiber optic fluorometer is attributed to inaccurate wavelength calibration of the Mini-Chrome).

Selection of an Organic Base

The initial rates of formation (of d) obtained with single-phase reaction mixtures made with equal concentrations of various tetraalkylammonium hydroxides, water, and pyridine were evaluated. Figure 5.10 shows that the initial reaction rate is dependent on the nature of the organic cation. These data suggest that the K_b's of these bases in the water-pyridine phase are dependent on the carbon content of the cation, and that those (bases) with greater organic character exhibit larger K_b's in the mixed pyridine-water system. Although the "propyl" and "butyl" bases gave equivalent initial rates for the specific pyridine-water system used in this experiment ([pyridine]/[water] $\simeq$ 0.9), the trend exhibited in figure 5.10 suggests that as the dielectric constant of the reagent mixture is decreased further (with increasing pyridine concentration), tetrabutylammonium hydroxide (TBAH) would provide a

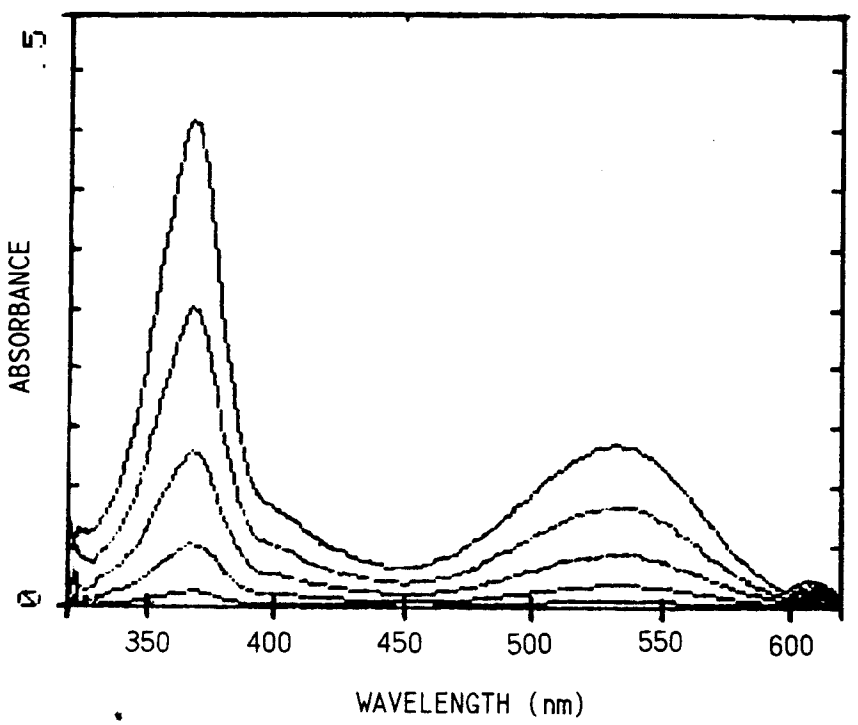

Figure 5.7. Absorption spectra (4 minute intervals) of reagent mixture (0.05 M tetrabutylammonium hydroxide, [pyridine]/[H_2O] = 2.5) when exposed to a 164 µg/mL chloroform solution using the continuous-exposure apparatus (figure 5.4).

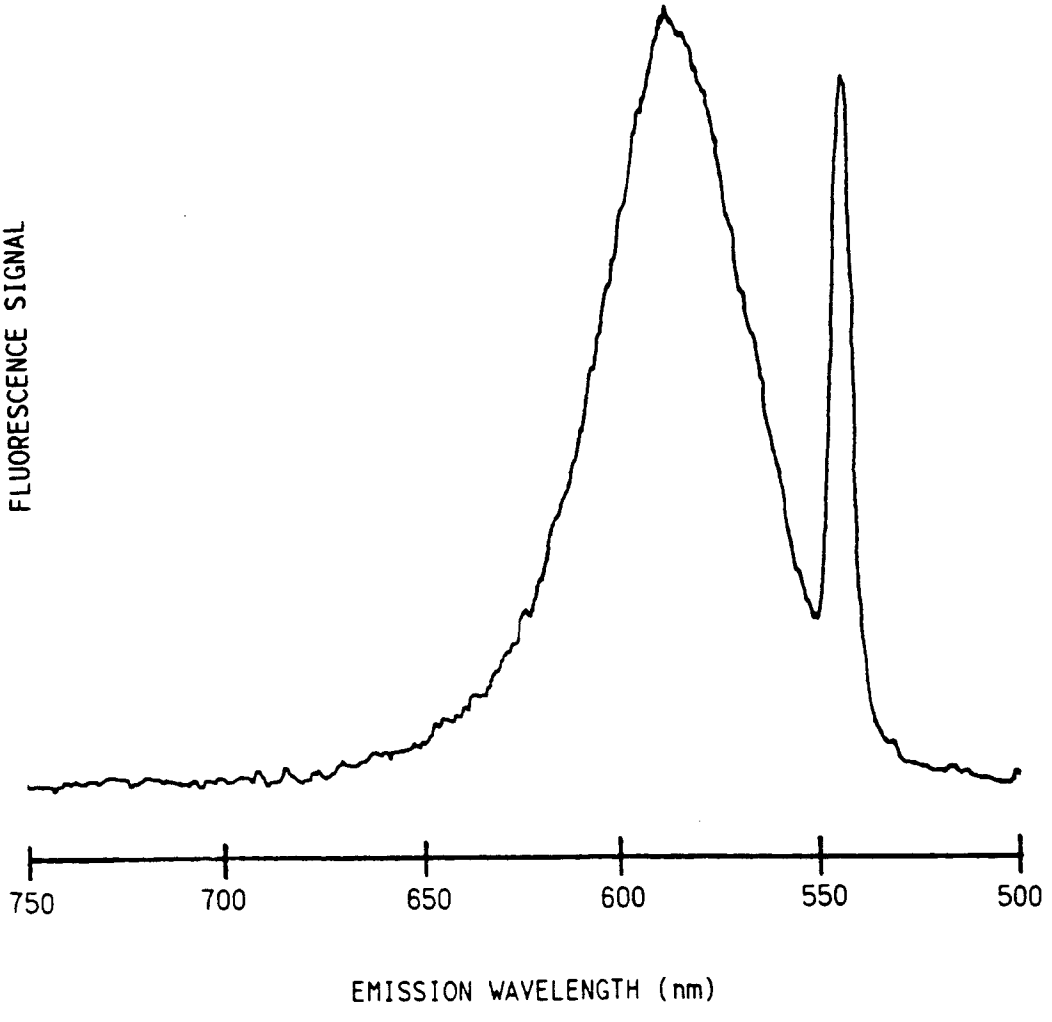

Figure 5.8. Fluorescence emission spectrum of the Fujiwara reagent mixture ([TBAH] = 0.05 M, [pyridine]/[water] = 2.5). Spectrum taken ca. 2 min after spiking 3.5 mL of stirred reagent with 10 µL of a 7.42 mg/mL chloroform solution; RCA 1P28 PMT at -900 V, R_f = 1 MΩ. The excitation wavelength was 545 nm.

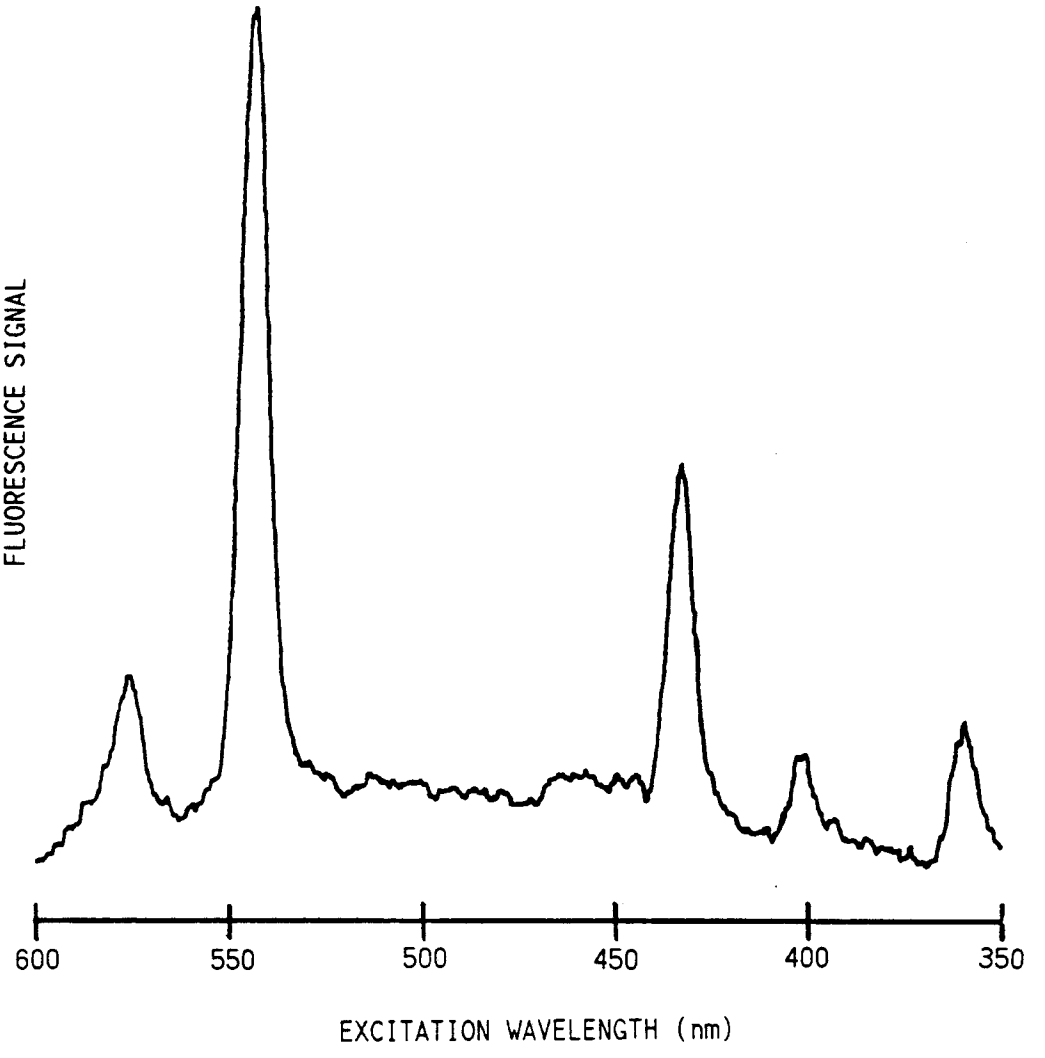

Figure 5.9. Fluorescence excitation spectrum of the reagent mixture. Experimental conditions the same as in figure 5.8. The emission wavelength was 590 nm.

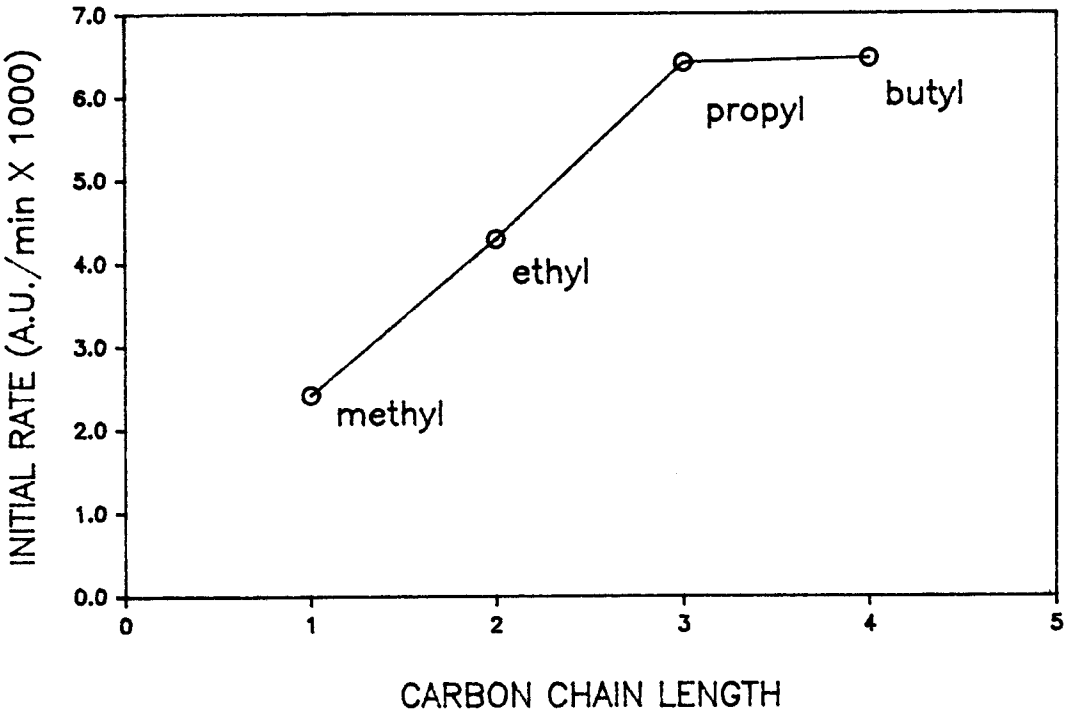

Figure 5.10. Initial reaction rate (absorption at 545 nm) as a function of alkyl chain length of tetraalkylammonium hydroxide bases. All solutions were 0.03 M in base with [pyridine]/[water] ≃ 0.9; 3.5 mL of reagent mixture was spiked with 10 µL of a 7.42 mg/mL chloroform solution.

greater initial rate than tetrapropylammonium hydroxide. In addition, the "tetrabutyl" base is available with less water than the "tetrapropyl" base, providing greater latitude in reagent compositions. For these reasons, TBAH was selected for use in all reagent optimization experiments.

Initial Survey Experiments

Some data from initial batch-mode experiments to assess the effect of varying the pyridine-to-water molar ratio ([P]/[W]) of single-phase Fujiwara reagent mixtures are shown in figure 5.11. It is apparent that [P]/[W] has a great effect on both the initial rate of formation (of d) and the overall shape of the reaction curves. The decay of the "red" Fujiwara product is obvious for [P]/[W] = 1.2, 1.8, 3.4, and 20. For lower values of [P]/[W], the reaction kinetics are quite slow.

Figure 5.12 shows how the initial reaction rate varies as a function of [P]/[W] when the absorbance is monitored at 545 nm (species d) and 368 nm (species g). For the specific base concentration used in these experiments (0.02 M), a maximum in both curves is observed at [P]/[W] = 3.4. This indicates the possibility of concurrent development of spectrophotometric methods based on monitoring species g (at 368 nm) or species d (at 545 nm), and a fluorometric method (545 nm is the excitation wavelength for species d). Because of the relatively low transmittance of even the best fiber optics at 368 nm, a spectrophotometric analysis at 368 nm is of limited use with a FOCS; however, such methodology would be amenable for use in cuvette-based instruments.

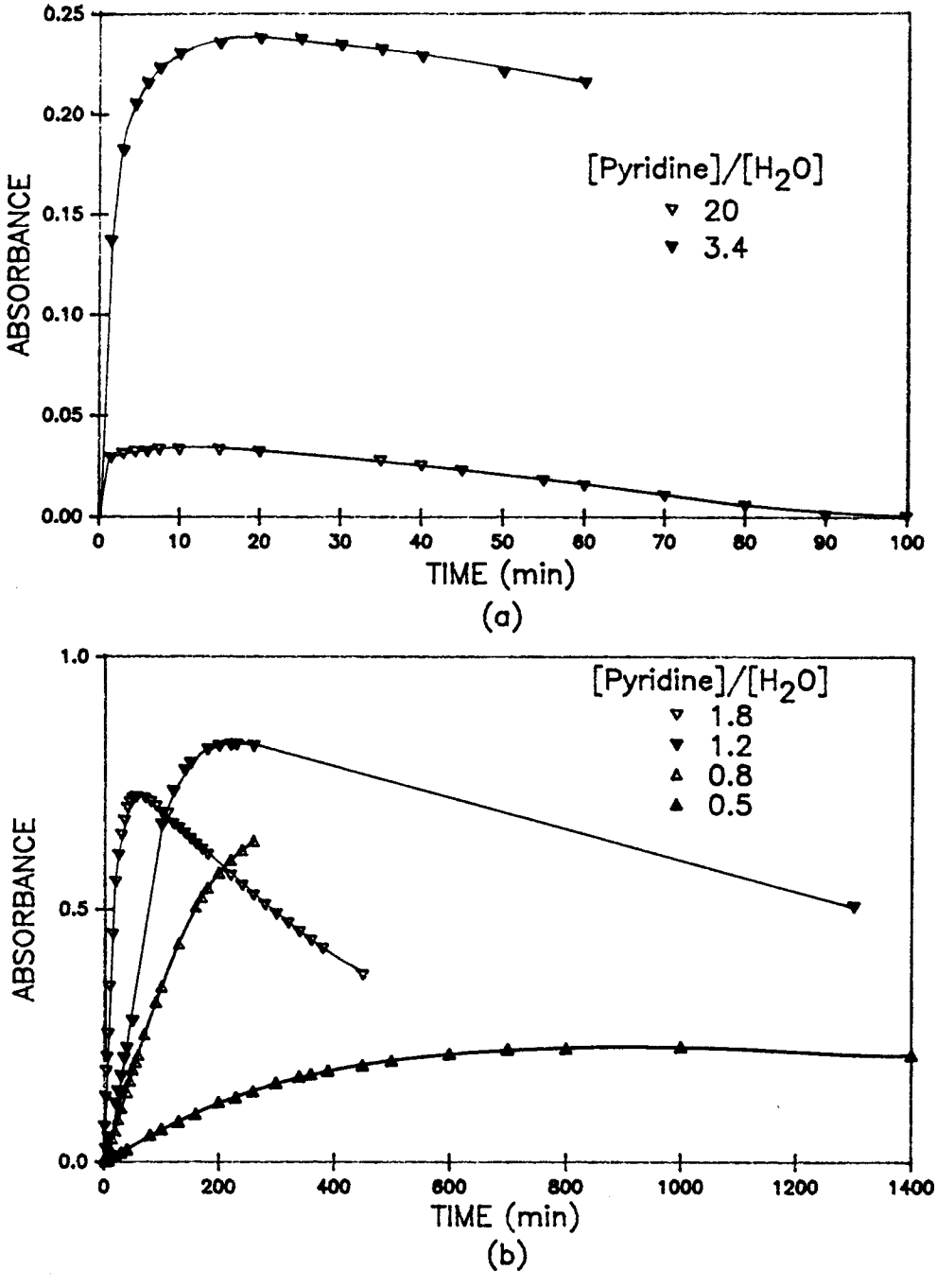

Figure 5.11. Reaction curves showing the effect of the pyridine to water molar ratio on batch-mode reaction kinetics. Species d monitored spectrophotometrically at 545 nm; 3.5 mL of reagent mixture spiked with 10 µL of 7.42 mg/mL chloroform to give 21 µg/mL in the cuvette; all reagents 0.02 M TBAH.

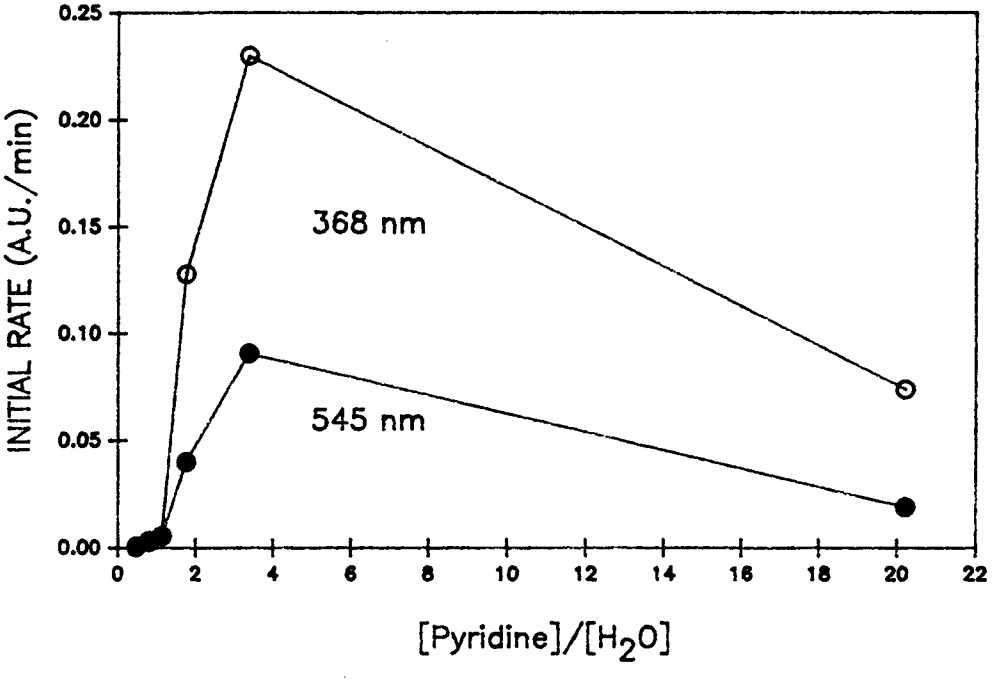

Figure 5.12. Initial rates of formation (of d) as a function of [P]/[W]. Data taken from the reaction curves shown in figure 5.11.

From figure 5.12, the rate of formation of d first increases to a maximum value as the water content in the reagent mixture is decreased, and then decreases from this maximum as the water content is decreased further. In addition, a negative rate is observed earlier for those reagent compositions exhibiting the greatest initial rates (for batch-mode experiments, this turnover is most likely due to consumption of the chloroform).

The observed initial rate increases by approximately a factor of 20 when [P]/[W] varies from 1.2 to 3.4; over this range, pyridine concentration increases from 10.3 to 11.5 M, while the water concentration decreases from 8.9 to 3.4 M. Because the rate would not be expected to change much with an ca. 12% increase in pyridine concentration, the change in water concentration is the dominant factor affecting the reaction kinetics.

Since water is not directly involved in the formation of d in the proposed mechanism, the means by which it so strongly affects the observed kinetics is not clear. Varying the water concentration may affect the fraction of the $CHCl_3$ that is converted to products via the proposed pathway not passing through the intermediate d. If the species responsible for the absorption band at 368 nm (g) was formed only via the decomposition of d then the rate monitored at 368 nm would be expected to increase slowly during the initial stages of the reaction. This initial "induction" period was not observed in any of the reaction curves obtained. Hence it may be that the relative importance of the routes to g (one through d and one through b' and b'') is dependent on water concentration.

It is also possible that decreasing the water content of the

reagent mixture increases the activity of the free hydroxide ions due to the decreased solvating ability of the reagent mixture (thus increasing the initial rate of formation). Note that this effect is separate from ion pair formation itself (26) and would also affect the rate of decomposition.

Overall, it is possible that reaction conditions are such that the rates of formation and decomposition are both important from initiation of the reaction. Thus, the experimentally observed reaction rates (for high [P]/[W] reagents) may be less than the true rates.

If the rate of decomposition of d is approximated by the maximum rate of decay (A.U./min) exhibited by the reaction curves shown in figure 5.11, then the relative rate ratio (formation/decomposition) can also be estimated; figure 5.13 is a plot of this apparent ratio F/D. Figure 5.13 shows a maximum for [P]/[W] = 3.4 (3.4 M water), corresponding to the reaction mixture giving the greatest initial rate of formation (see figure 5.12).

Although the data shown by figure 5.13 are from batch-mode experiments, the general shape of the continuous exposure response of a reagent mixture can be predicted. The reagent mixture yielding the largest F/D (rate of formation/rate of decomposition) in batch mode experiments is predicted to exhibit a pseudo zero-order rate of formation for the longest period of time in continuous-exposure experiments (vide supra). Figure 5.14 shows the continuous exposure response (to a 6 μg/mL chloroform solution) obtained using the reagent mixture exhibiting F/D = 130 ([P]/[W] = 3.4) and a reagent exhibiting F/D = 38 ([P]/[W] = 20) with the batch-mode experiments.

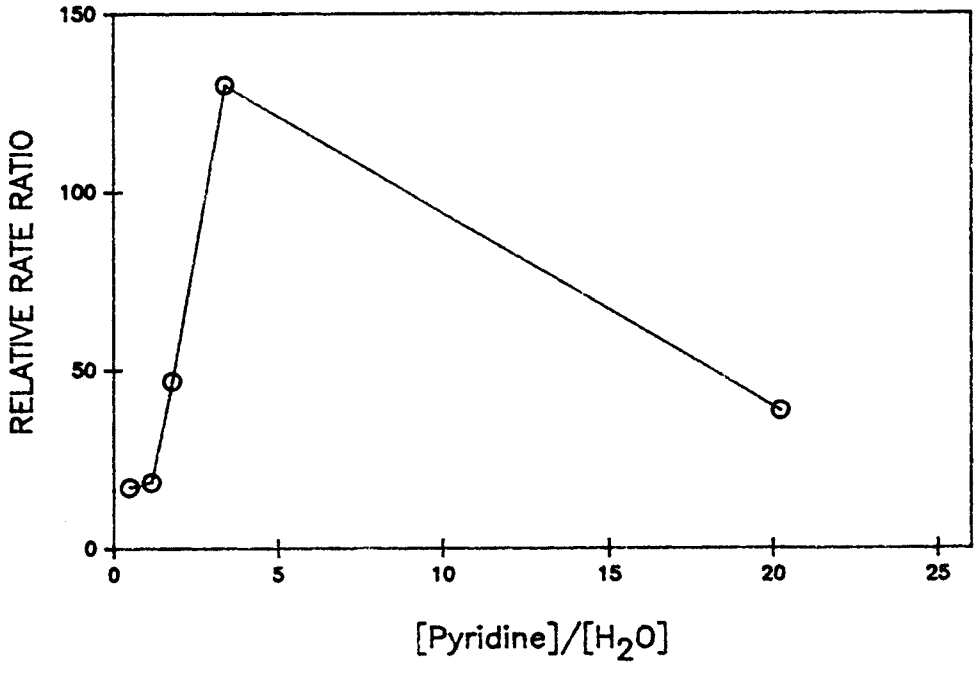

Figure 5.13. The dependence of the ratio of the rate of formation to the apparent rate of decomposition (of d) on [P]/[W]. Data taken from the reaction curves shown in figure 5.11.

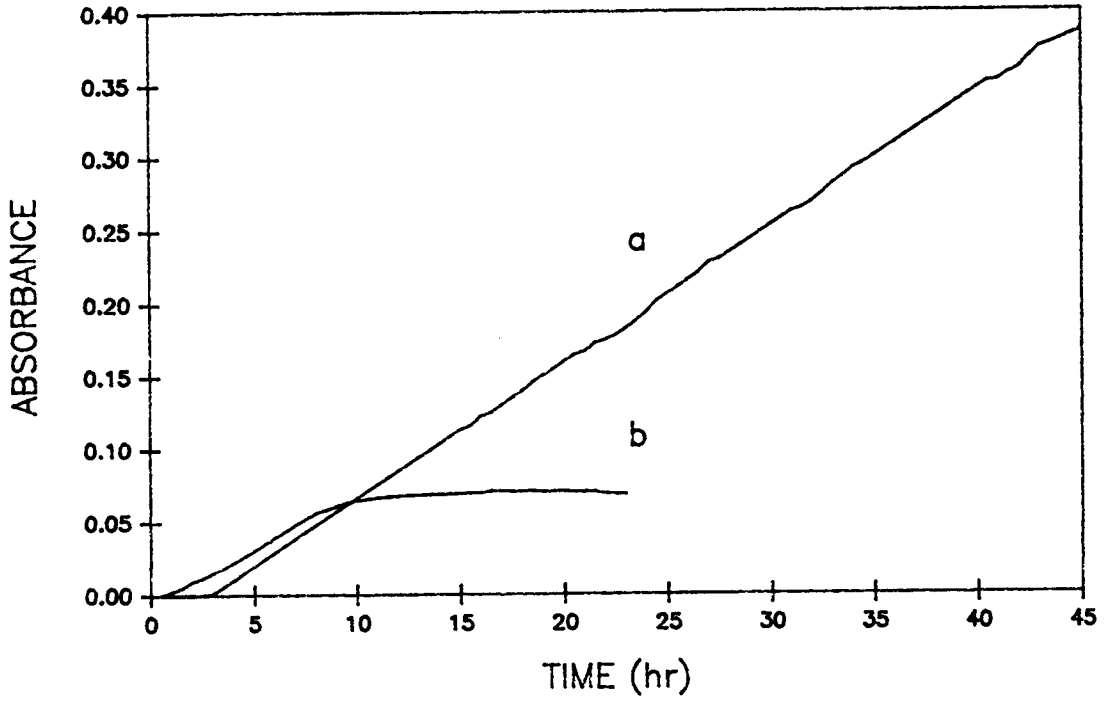

Figure 5.14. Continuous-exposure response (absorption of d at 545 nm) of two single-phase Fujiwara reagents exposed to a 6 µg/mL chloroform solution. (a) [P]/[W] = 3.4, (b) [P]/[W] = 20, [TBAH] = 0.02 M.

These experiments were performed with an apparatus similar to that shown in figure 5.4 except that the sample reservoir was 500 mL and the transfer tube was longer; the sample solution was replaced approximately once every 5 hours.

For the reagent mixture with [P]/[W] = 3.4 (curve a), a stable pseudo-zero-order kinetic response over an approximate 2-day period is demonstrated. This reagent mixture exhibited the largest apparent k_f'/k_d (figure 5.13) and corresponds to the situation predicted in figure 5.2b and curve c of figure 5.1. Note that the response time is relatively long.

For the reagent mixture with [P]/[W] = 20 (curve b), the apparent k_f'/k_d is approximately 4 times less than the value for curve a, and a steady state concentration of intermediate (as predicted in figure 5.2a and curve b of figure 5.1) is reached. Note that the response time exhibited by curve b (time to pseudo-steady-state intermediate concentration) is significantly longer than that for curve a.

The above experiments were also performed using a 12 μg/mL chloroform solution. The results of these experiments showed that (over the range tested) the responses with both reagent mixtures were proportional to chloroform concentration.

Overall, optimization of a reagent mixture for use in a kinetic, continuous-exposure (FOCS) analysis can be accomplished simply by maximizing the initial rate of formation; the data of figure 5.13 suggest that the resulting reagent composition will also provide the longest lived response (i.e., large k_f'/k_d).

Initial optimization experiments were performed in the

batch-mode with fluorescence monitoring (monitoring species d only). The purpose of these experiments was to characterize the general response (initial reaction rate) surface of the possible reagent mixtures over a wide range of both [P]/[W] and base concentration. The reagent mixtures tested are indicated in figure 5.15 by open circles. The range of reagent mixtures possible is limited by the water content of the base (60% by weight), as indicated by the curve in figure 5.15. Of the reagent mixtures tested, the maximum initial rate of formation (of d) in the batch-mode was obtained with a reagent mixture (marked by a half-darkened circle in figure 5.15) of 0.06 M TBAH, ca. 2.4 M H_2O, and ca. 11.6 M pyridine ([P]/[W] $\simeq$ 4.8).

As plotted in figure 5.15, the reagent compositions do not account for the effect of the water added with the chloroform solution spike. Spiking 1.25 mL of the reagent with 10 µL (0.01 g) of water reduces the concentrations of the base and pyridine very slightly; however, this added water increases the concentration of water in the resulting 1.26 mL volume enough to significantly decrease [P]/[W] for large values of [P]/[W]. Thus, the true optimum reagent mixture for use in continuous exposure applications will be shifted to a lower value of [P]/[W] and to a slightly lower base concentration (relative to the optimum mixture found using batch-mode experiments). To avoid this complication, final optimization of the reagent mixture was performed in the continuous-exposure mode.

Final Optimization and Calibration

Final optimization of a single-phase Fujiwaria reagent was

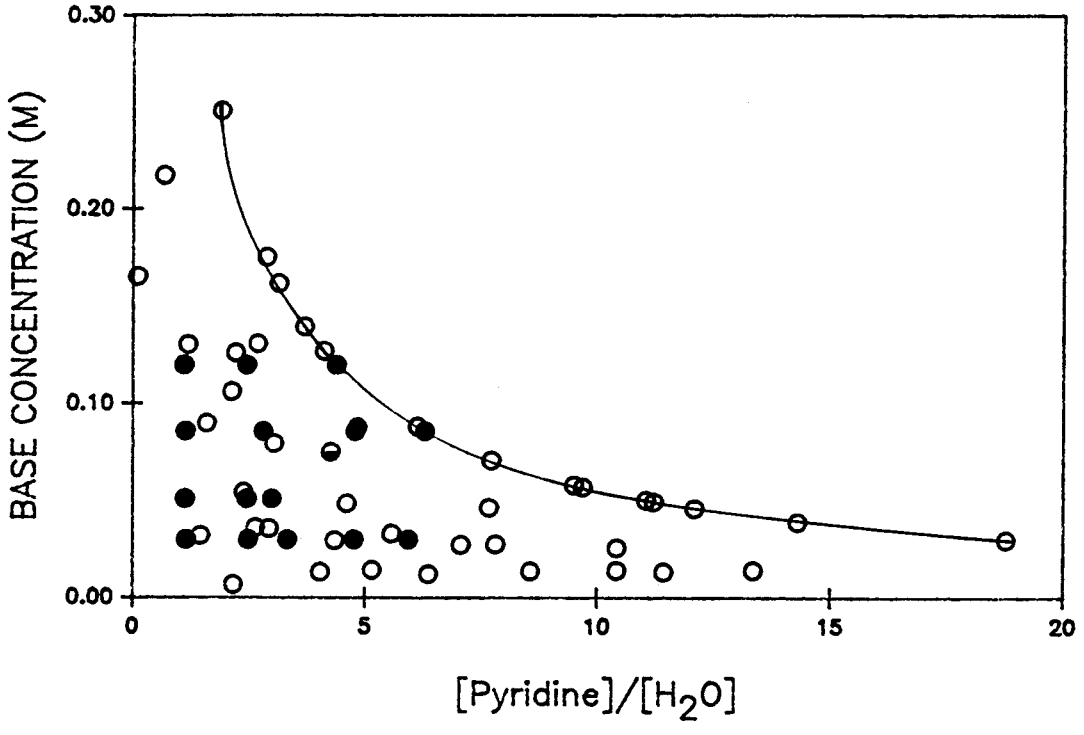

Figure 5.15. Reagent mixture compositions tested in the batch-mode optimization experiments (open circles) and in the final continuous-exposure optimization experiments (soild circles). The half-darkened circle indicates the reagent mixture yielding the greatest initial rate for the batch-mode (initial) optimization; the solid line represents the limit in reagent composition imposed by the water content of the TBAH (as supplied).

performed using the continuous- exposure apparatus (figure 5.4) and the HP spectrometer. Results of the batch-mode experiments narrowed the range of reagent mixtures tested to those indicated by the solid circles shown in figure 5.15.

The initial rates of formation of species d (545 nm) obtained from the mixtures tested are plotted in figure 5.16. These initial rates are the least-squares slope calculated from the discrete absorbance measurements obtained from the HP spectrophotometer. A clear maximum (initial rate) is observed for a reagent mixture consisting of 0.05 M TBAH, 4.5 M H_2O, and 11.2 M pyridine (i.e., a [P]/[W] $\simeq$ 2.5); this single-phase reagent mixture was selected for use in the FOCSs reported later in this thesis.

Figure 5.17 shows the initial rates of formation of species g (368 nm) obtained from the same reagent mixtures as plotted in figure 5.16. These plots show a maximum (initial rate) for a reagent mixture consisting of 0.086 M TBAH, 4.5 M H_2O, and 11.2 M pyridine (i.e., a [P]/[W] $\simeq$ 2.5). This single-phase Fujiwara reagent mixture was tested for use in a spectrophotometric determination of chloroform using the continuous-exposure apparatus.

From figures 5.16 and 5.17, the rates of formation pass through a maximum as a function of base concentration. The rate of formation decreases from this maximum as base concentration is either increased or decreased ([P]/[W] held constant). This may result from the effect of the expected increase in the rate of decomposition (with increasing base concentration) on the observed rate of formation, i.e., the apparent initial rate of formation may be decreased due to the effect of an increased rate of decomposition.

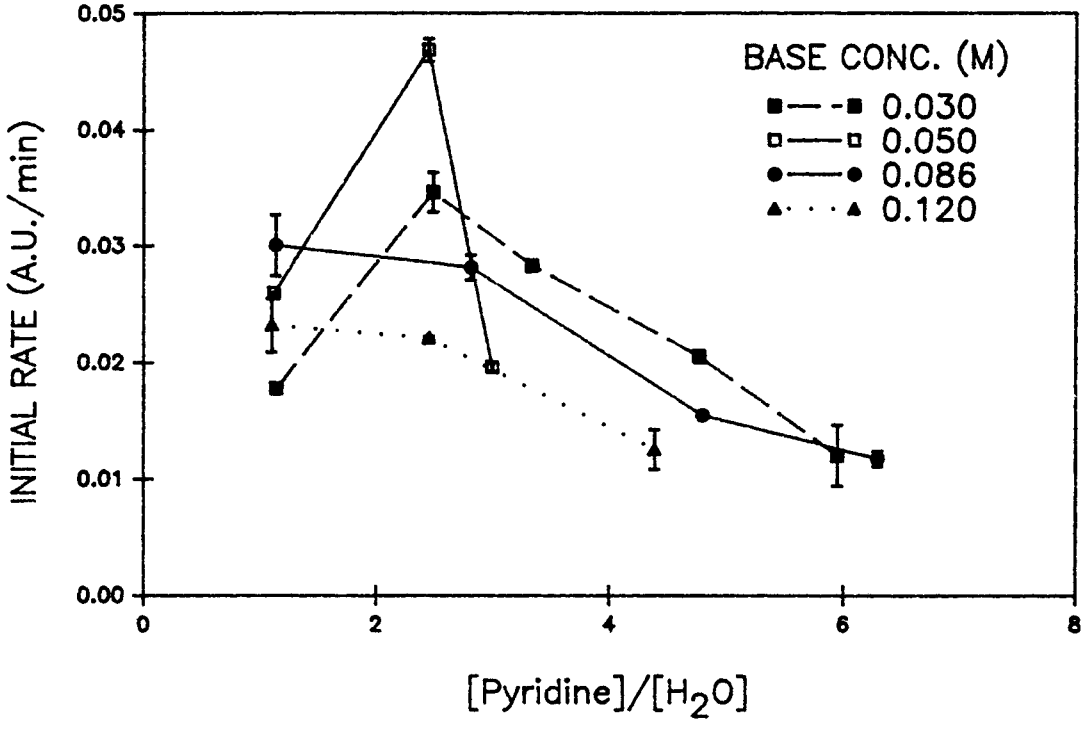

Figure 5.16. Dependence of the continuous-exposure initial rate of formation of d (545 nm) on both [P]/[W] and base concentration. The reaction mixtures were exposed to a 164 μg/mL chloroform solution. The error bars indicate ± one standard deviation (n = 2).

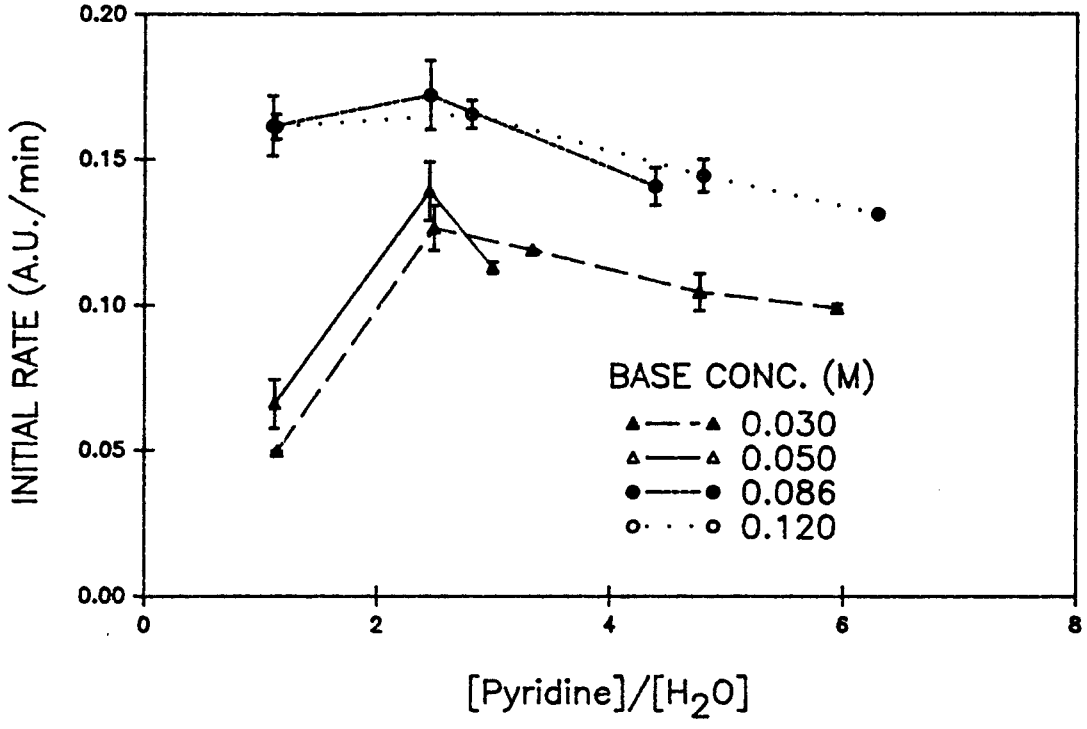

Figure 5.17. Dependence of the continuous-exposure initial rate of formation of g (368 nm) as a function of both [P]/[W] and base concentration. Reagent mixtures were exposed to 164 µg/mL chloroform. The error bars indicate ± one standard deviation (n = 2).

Figure 5.18 shows the continuous-exposure, blank-rate-corrected, initial rate of formation of species g (368 nm) as a function of chloroform concentrations over the range 32-640 ng/mL (ppb). The data for this calibration curve were obtained from three separate experiments, giving three blank rate measurements; the measured blank-rate was 8.0×10^{-5} A.U./min (absorbance units/min) with a standard deviation (s_{bk}) of 1.0×10^{-5} A.U./min. From the calculated slope of the calibration plot (m), the detection limit (DL) for chloroform is 11 ng/mL ($DL = 2s_{bk}/m$).

Figure 5.19 shows data for the continuous-exposure response obtained when multiple injections of a chloroform solution are made into 45 mL of blank water (held in the sample reservoir of the continuous exposure apparatus). The response time exhibited is ca. 10 min, i.e., it takes approximately 10 min for the observed rate (A.U./min) to stabilize after a change in analyte concentration; however, a period of ca. 40 min is required to obtain an accurate measurement of the rate using a chart recorder.

The significant blank-rate is attributed to run-to-run chloroform contamination associated with adsorption of chloroform onto the Delrin sample cell adaptor of the continuous-exposure apparatus. If the apparatus is soaked in methanol for ca. 24 hr and thoroughly dried, no blank-rate is observed. Utilization of more inert materials (i.e., glass or Teflon) in the construction of the apparatus should minimize this contamination problem and result in a reduction in the blank signal and an improvement in the method detection limit.

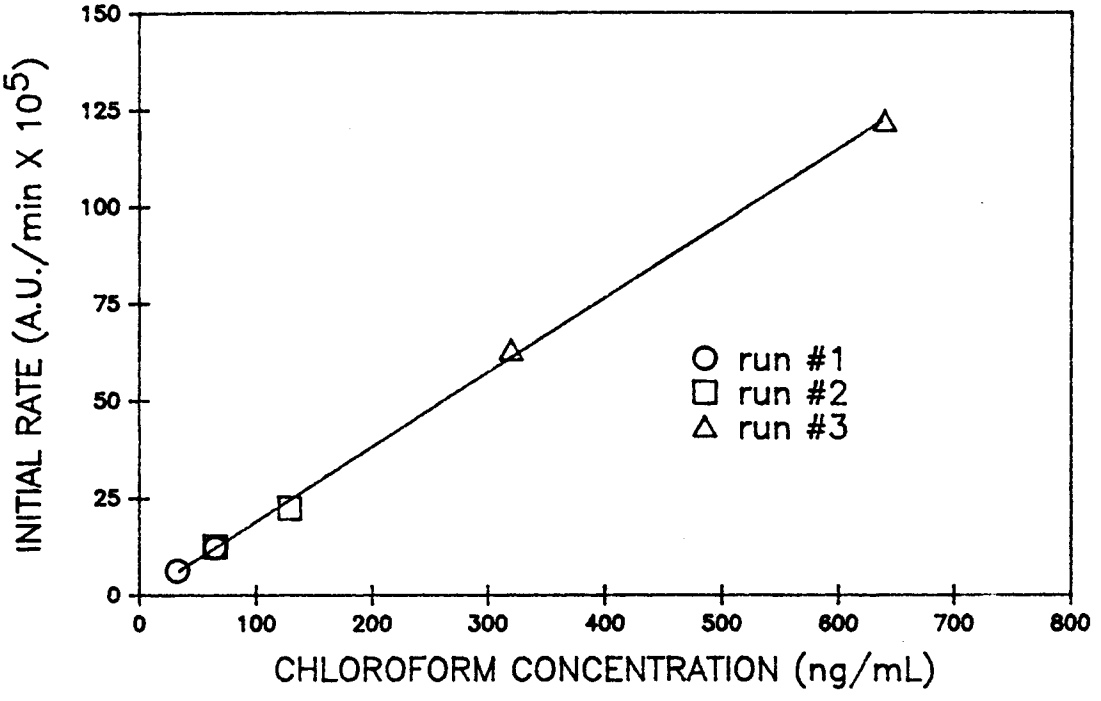

Figure 5.18. Spectrophotometric calibration curve for the determination of chloroform obtained using the continuous-exposure apparatus with the optimized single-phase Fujiwara reagent. The calculated least-squares slope is 1.93×10^{-6} A.U./min/(ng/mL chloroform) with a standard error of 4.30×10^{-8} A.U./min/(ng/mL $CHCl_3$).

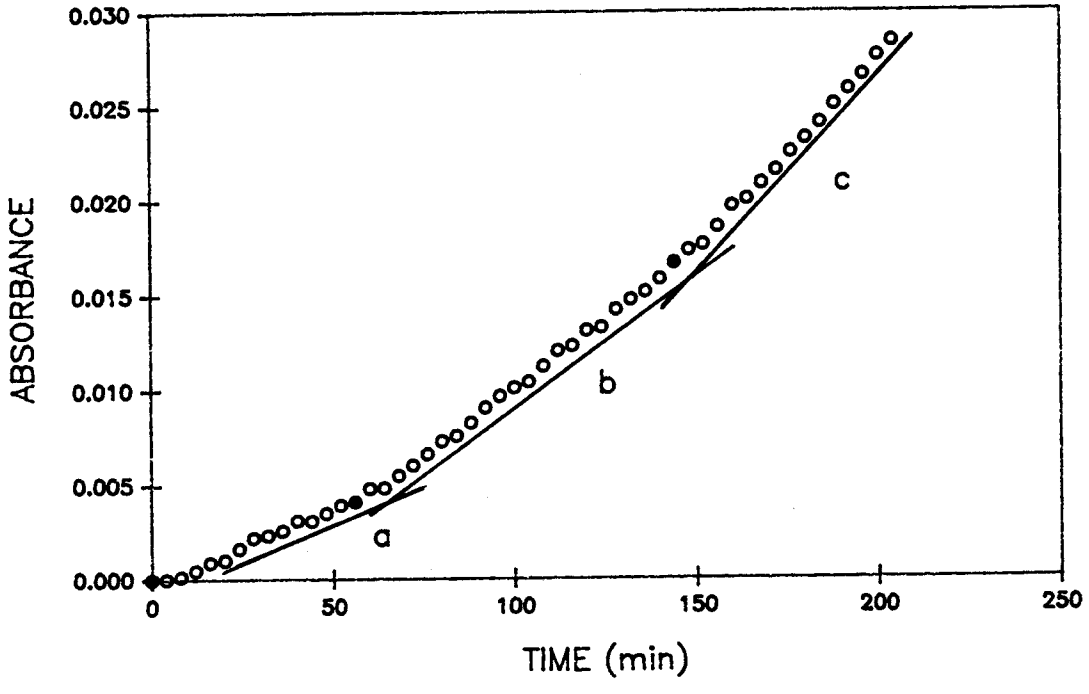

Figure 5.19. Continuous-exposure response showing the initial blank-rate (a) and the analytical rates for 33 (b) and 65 (c) ng/mL chloroform. The solid circles indicate the time of injection (to the blank water) to give the corresponding chloroform concentration.

Analysis of Tap Water for Chloroform

Figure 5.20 shows the results of a standard additions analysis of lab tap water for the determination of chloroform. No blank-rate was detected immediately prior to the tap water analysis (after rinsing and baking the continuous-exposure apparatus). Thus, the x-intercept of the least-squares fit of the data gives the concentration of chloroform in the tap water; the resulting chloroform concentration is 33 ng/mL.

The slope of the standard additions plot is 1.61×10^{-6} A.U./min/(ng/mL chloroform). This value compares favorably with the calibration sensitivity previously reported (1.93×10^{-6} A.U./min/(ng/mL chloroform)); the mean value and standard deviation are 1.77×10^{-6} and 0.23×10^{-6} A.U./min/(ng/mL chloroform), respectively. The relative standard deviation for these two calibration slopes (13%) is comparable to the precision limits (≤10% RSD) set by the EPA for the 500 series methods (6-8).

Although the precision of the continuous-exposure analysis is comparable to that obtained with the 500 series GC methods, the method is less selective and has a poorer detection limit. Still, the reported detection limit is adequate for detecting chloroform in most finished drinking waters; the National Organics Reconnaissance Survey for Halogenated Organics (NORS) reported a mean chloroform concentration of 44 ng/mL in finished drinking waters (27).

The batch-mode response of the single-phase reagent for some common gem-polyhalogenated species has been assessed by Siemion (28). For continuous-exposure determinations, the responses are also affected by the Henry's law constants. The continuous-exposure

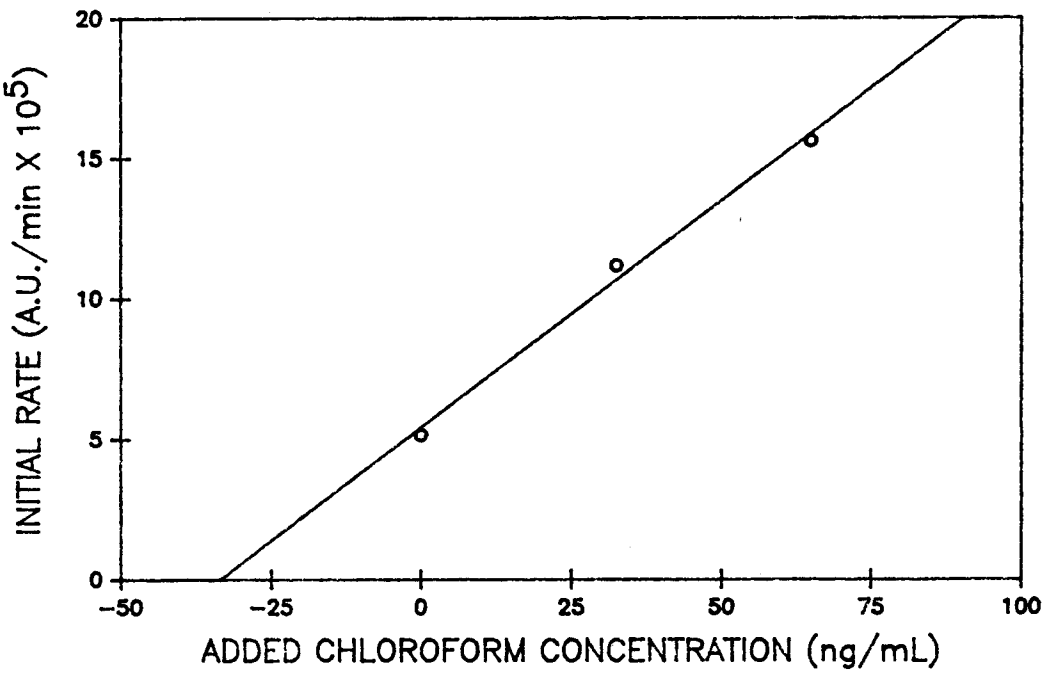

Figure 5.20. Standard additions plot for the determination of chloroform in tap water. The calculated least-squares slope is 1.61×10^{-6} A.U./min/(ng/mL chloroform) with a standard error of 1.38×10^{-7} A.U./min/(ng/mL $CHCl_3$).

response of the spectrophotometric (368 nm) single-phase reagent for these compounds is approximated by multiplying the 10-min absorbance found by Siemion (using batch-mode experiments) by the Henry's law constant. The predicted relative responses of bromodichloromethane, dibromochloromethane, bromoform, and trichloroethylene are listed in table 5.1.

For the determination of chloroform in tap-water, the major potential interferents are the other trihalomethanes; bromodichloromethane, dibromochloromethane, and bromoform. The median concentrations of the trihalomethanes in finished drinking water have been reported to be 21 ng/mL (chloroform), 6 ng/mL (bromodichloromethane), 1.2 ng/mL (dibromochloromethane), and < 5 ng/mL for bromoform (27). From the same study, the mean concentrations are 44, 14, 7, and < 5 ng/mL for chloroform, bromodichloromethane, dibromochloromethane, and bromoform, respectively (27). With the relative response values listed in table 5.1, the approximate error in the measured chloroform concentration due to the other trihalomethanes in "average" drinking water is predicted to be ca. 5 ng/mL (assuming a bromoform concentration 0.0-5.0 ng/mL). Thus, the average error incurred for chloroform quantitation in drinking water using the spectrophotometric reagent with the continuous-exposure apparatus is predicted to be ca. 11%.

Table 5.1. Relative response predicted for some common gem-polyhalogenated species using the single-phase spectrophotometric Fujiwara reagent (368 nm) with the continuous-exposure apparatus.

Compound	10 min Absorbance[a]	Relative Absorbance[b]	H[c]	H'[d]	RR[e]
$CHCl_3$	2.4	1	0.0029	1	1
$CHBrCl_2$	0.89	0.37	0.0024	0.83	0.31
$CHBr_2Cl$	0.49	0.20	0.00099	0.34	0.07
$CHBr_3$	0.36	0.15	0.00056	0.19	0.03
CCl_2CHCl	0.68	0.28	0.0091	3.1	0.86

[a]Absorbance at 368 nm 10 min after addition of test compound to reagent; all test compounds at 10 µg/mL; data from ref. 28.

[b]Absorbance of test compound/absorbance chloroform.

[c]Henry's law constant ($atm \cdot m^3/mol$), from ref. 29.

[d]Test compound H/choroform H.

[e]Test compound relative absorbance x test compound relative H.

CONCLUSIONS

A simple kinetic model for predicting the time-dependent concentration of the "red" Fujiwara reaction intermediate d was developed and shown to be a useful predictive tool in the development of reagent mixtures for use in fiber optic chemical sensors (FOCS). Generally, water concentration is the most critical factor determining response characteristics to chloroform for single-phase Fujiwara-type reagent mixtures used in the continuous-exposure-mode.

The optimum reagent mixture for use in a FOCS is one which provides the maximum response for the longest period of time. When monitoring a reaction intermediate, the relative reaction rate F/D (formation/decomposition) should be maximized. By monitoring for sufficient periods of time in batch-mode experiments, it is possible to observe "turnover" and obtain measurements of both the apparent rate of formation and the apparent rate of decomposition. Thus, a measure of the apparent F/D is obtained from batch-mode experiments. From this type of measurement, it is possible to predict the general response of the same reagent mixture in the continuous-exposure-mode. For determination of chloroform, single-phase Fujiwara reagent mixtures exhibiting batch-mode relative rate ratios (F/D) > 100 are capable of providing a useful kinetic response for up to 48 hours when monitored spectrophotometrically in the continuous-exposure-mode. This suggests that the decay of the FOCS fluorescence signal reported by workers at Lawrence Livermore is due to inner-filter effects (13-15).

The experimental data suggest that the reaction mixture

exhibiting the maximum rate of formation also provides the maximum F/D. Thus, optimization of a reagent mixture for use in a FOCS is achieved simply by maximizing the initial rate of formation of d.

The unique continous-exposure apparatus developed in this thesis is the first of its kind reported. The signal levels achieved using this apparatus for the spectrophotometric (species g, 368 nm) determination of chloroform in tap water are a function of the reagent mixture employed and the design of the apparatus itself. Considering that the single-phase reagent developed provides the maximum spectrophotometric response to chloroform, any increase in calibration sensitivity must result from optimization of the apparatus.

Two means of increasing calibration sensitivity are to increase the rate of analyte volatilization from the sample and to increase the rate of analyte transport from the sample to/into the reagent mixture. Increasing the surface area of the sample in the sample reservoir (30), heating the sample, adding salts to the sample ("salt out" the analyte), or increasing the stirring rate of the sample would all result in greater calibration sensitivity by increasing the rate of analyte volatilization. To increase the rate of transport of the analyte to/into the reagent the diameter of the transfer line could be increased while also shortening it's length.

Another way to increase the calibration sensitivity is to maximize the surface area to volume ratio (A_S/V) of the reagent (30). Although this could be accomplished by reducing the volume of reagent in the cuvette, the 2.5 mL volume used in this work is the minimum that can be used with the cell employed without underfilling

the cuvette-holder aperture (slits). The maximum A_s/V could be attained by employing a horizontal slit geometry for the spectrophotometer. With this slit geometry, the depth of the reagent in the cell could be reduced to the slit width and the total reagent volume could be viewed (without stirring).

The continuous-exposure apparatus could also be used with the reported fluorometric reagent to perform fluorescence based measurements (monitoring d). This might provide greater sensitivity than the absorption-based measurements even with the present apparatus. For fluorescence measurements, the horizontal slit geometry is capable of providing signal levels 3 to 50 times greater than that of the conventional vertical slit geometry (31). This, coupled with the potenial to greatly reduce the A_s/V of the reagent, suggests that the detection limit for chloroform might be pushed well below the reported 11 ng/mL for the spectrophotometric analysis.

Overall, consideration of how to optimize the geometry of the continuous-exposure apparatus to improve calibration sensitivity is complicated by the use of a cuvette. By performing the spectrometric measurements using a fiber optic spectrometer (18), the design of such an apparatus is not limited by the geometric restrictions imposed by a cuvette-based instrument. Thus, further optimization of the continuous-exposure apparatus leads to the development of a FOCS.

REFERENCES

1. Louch, J.L. "Fiber Optic Chemical Sensors for the Detection of Volatile gem-polyhalogenated Hydrocarbons" 1991, Ph.D. Thesis, Oregon State University, Chap. 1.

2. Rook, J.J. Water Treat. Exam. 1974, 23, 234-243.

3. Zierler, S.; Feingold, L.; Danley, R.A.; Craun, G. Int. Archives of Environ. Health 1988, 43 (2), 195-200.

4. National Interim Primary Drinking Water Regulations: Control of Trihalomethanes in Drinking Water; Final Rule Federal Register 1979, 44 (231), 68624-68683.

5. Drinking Water; Substitution of Contaminants and Drinking Water Priority List of Additional Substances Which may Require Regulation Under the Safe Drinking Water Act Federal Register 1988, 53 (14), 1892-1902.

6. Warner, B.J.; Cheng, S.C.; Friedman, C.S.; Mitrosky, S.; Snyder, A.D.; McMillin, C.R. "EPA Method Study 23A, Method 501.1, Trihalomethanes by Purge and Trap" 1984, EPA-600/4-84-020.

7. Warner, B.J.; Cheng, S.C.; Finke, J.M.; Friedman, C.S.; Mitrosky, S.; Snyder, A.D.; McMillin, C.R. "EPA Method Study 23B, Method 501.2, Trihalomethanes by Liquid/Liquid Extraction" 1984, EPA-600/4-84-021.

8. Measurement of Trihalomethanes in Drinking Water with Gas Chromatography/Mass spectrometry and Selected Ion Monitoring Method 501.3, EPA form 1320-4 (Rev. 3-76).

9. Fujiwara, K. Sitz. Nat. Ges. Rostock 1916, 6, 33.

10. Seto, T.A.; Schultze, M.O. Anal. Chem. 1956, 28, 1625-1629.

11. Lugg, G.A. Anal. Chem. 1966, 38, 1532-1536.

12. Reith, J.F.; van Ditmarsch, W.C.; Ruiter, T.H. Analyst 1974, 99, 652-656.

13. Milanovich, F.P. Environ. Sci. Technol. 1986, 20, 441-442.

14. Milanovich, F.P.; Daley, P.F.; Klainer, S.M.; Eccles, L. Anal. Instrum. 1986, 15, 347-358.

15. Herron, N.R.; Simon, S.J.; Eccles, L. Anal. Instrum. 1989, 18 (2), 107-126.

16. Bromberg, J.P. "Physical Chemistry", Allyn and Bacon, Boston, 1980, 814-815.

17. Wilson, R.L. "Design, Development and Optimization of a Fluorometric Reaction-Rate Instrument and Method of Analysis for Metal Ions" 1977, Ph.D. Thesis, Oregon State University.

18. Louch, J.L. "Fiber Optic Chemical Sensors for the Detection of Volatile gem-polyhalogenated Hydrocarbons" 1991, Ph.D. Thesis, Oregon State University, Chap. 4.

19. Uno, T.; Okumura, K.; Kuroda, Y. Chem. Pharm. Bull. 1982, 30, 1876-1879.

20. Uno, T.; Okumura, K.; Kurodo, Y. J. Org. Chem. 1981, 46, 3175-3178.

21. Abramovitch, R.A.; Singer, G.M. in Abramovitch, R.A., Editor, "Pyridine and its Derivatives", Interscience, N.Y., 1974, Chap. 1A.

22. Bruylants, A.; Feytmants-de Medicis, E. in Patai, S., Editor, "The Chemistry of the Carbon Nitrogen Double Bond", Interscience, N.Y., 1970, 465-502.

23. Angel, S.M.; Daley, P.F.; Langry, K.C.; Kulp, T.J.; Camins, I. "The Feasibility of Using Fiber Optics for Monitoring Groundwater Contaminants: VI. Mechanistic Evaluation of the Fujiwara Reaction for Detection of Organic Chlorides" 1987, EPA/600/X-87/467.

24. Hine, J. J. Amer. Chem. Soc. 1950, 72, 2438-2445.

25. Garcia, E.E.; Greco, C.V.; Hunsberger, I.M. J. Amer. Chem. Soc. 1960, 82, 4430-4431.

26. Lowry, T.H.; Richardson, K.S. "Mechanism and Theory in Organic Chemistry", Harper and Row, N.Y., 1981, 248-250.

27. Symons, J.M.; Bellar, T.A.; Carswell, J.K.; DeMarco, J.; Kropp, K.L.; Robeck, G.G.; Seeger, D.R.; Slocum, C.J.; Smith; B.L; Stevens, A.A. Jour. AWWA 1975, 67 (11), 634-647.

28. Siemion, E. Oregon State University, Personal communication, 1991.

29. Pankow, J.F.; Rosen, M.E. Environ. Sci. Technol. 1988, 22, 398-405.

30. Louch, J.L. "Fiber Optic Chemical Sensors for the Detection of Volatile gem-polyhalogenated Hydrocarbons" 1991, Ph.D. Thesis, Oregon State University, Chap. 6.

31. Ingle, Jr., J.D.; Crouch, S.R. "Spectrochemical Analysis", Prentice Hall, Englewood Cliffs, 1988, pp 455.

CHAPTER 6

FIBER OPTIC CHEMICAL SENSORS FOR THE DETECTION OF VOLATILE GEM-POLYHALOGENATED HYDROCARBONS

Jeff Louch and J. D. Ingle, Jr.

Department of Chemistry
Oregon State University
Gilbert Hall 153
Corvallis, OR 97331-4003

ABSTRACT

Two fiber optic chemical sensors (FOCS) for the detection of volatile gem-polyhalogenated hydrocarbons (GPHHC) are described and the factors affecting their performance are discussed. The sensors are based on an aliquot of a reagent solution held in contact with a double-fiber optic probe within a light-tight enclosure. When submerged in an aqueous sample the reagent is isolated from a bulk sample by a trapped headspace. One or more cavities in the bottom of the enclosures allow volatile species to migrate from the sample through the headspace to the surface of the reagent. The "reservoir" FOCS utilizes 1.3 mL of reagent held in a reservoir and the "drop" FOCS utilizes a 10-μL drop of reagent suspended on the sensing tips of the fiber optic probe. Volatile analytes react with the reagent to produce a fluorescent reaction product which is monitored at 600 nm. The rate of increase in the fluorescence signal is related to analyte concentration. The calculated detection limit for aqueous chloroform is 0.07 ng/mL for the reservoir FOCS and 0.08 ng/mL for the drop FOCS. The response times of the two sensors are comparable and the total measurement time (including the response time) is ca. 8 min at 2 ng/mL and ca. 4 min at 850 ng/mL (chloroform). The duration of the linear response is limited by inner-filter effects. The reservoir FOCS response to a number of volatile GPHHCs including the trihalomethanes are reported. With the reservoir FOCS, the chloroform concentration in tap water was determined with a standard addition procedure to be 23 ± 1.7 ng/mL ; duplicate GC/MS analysis gave 22 ± 0.9 ng/mL.

INTRODUCTION

The development of chemical sensors has been shown considerable interest over recent years. Generally, a chemical sensor is a transducer providing continuous information about the chemical composition of its environment (on a time scale appropriate to the application). Thus, sensors are capable of observing a sample in situ in dynamic environments and have found use in process control, clinicial, and environmental applications. Fiber optic chemical sensors (FOCS) are transducers that utilize fiber optics to guide optical radiation to and from a sample and transform chemical (concentration) information into the optical domain (1). The merits of optical sensing relative to other modes (of chemical transduction) have been discussed (1); of significant importance is the wide range of potential analytes possible with spectrometric methodology.

Gem-polyhalogenated hydrocarbons (GPHHC) are organic species having two or more halogen atoms bonded to a single carbon. Examples of such compounds are DDT, trichloroethylene, Eldrin, and the trihalomethanes (THM): chloroform, bromoform, bromodichloromethane, and dibromochloromethane. The THMs are important contaminants in chlorinated drinking water (2), while the pesticides and chlorinated solvents are important contaminants in ground waters (3).

As a group, GPHHCs are heavily regulated by the federal government (2-6). The Resource Conservation and Recovery Act (RCRA) requires that land-based waste disposal sites test underlying ground water at least twice yearly (6). The Safe Drinking Water Act (SDWA) requires that finished drinking water be tested on a quarterly basis

(4). The maximum contaminant level (MCL) for chloroform in finished drinking water is 70 ng/mL, while the total THM MCL is 100 ng/mL (2).

Presently, the EPA prescribed methodologies for quantitating these and other species in both drinking and ground waters are based on gas chromatography with a prior preconcentration step (7-10). Implementation of the prescribed analyses requires a high degree of operator skill and the EPA requires that each analyst must demonstrate the ability to "generate acceptable accuracy and precision", and has described a separate procedure for this purpose (10). This requirement, coupled with the high initial cost of the necessary instrumentation, results in most water treatment and waste disposal facilities contracting these analyses to private labs; these factors also limit the required frequency of analysis (11-12).

The ability to perform frequent analyses for determination of the GPHHCs is important for many reasons. By increasing the frequency of analyses, the potential for undetected contamination of either drinking water (due to fluctuating trihalomethane formation potential) or ground water (due to illegal waste discharge or landfill breakthrough) is reduced. In addition, a more complete data base allows for more accurate modeling of both the formation of THMs (in drinking water) and ground water transport phenomena.

Workers at Lawrence Livermore National Laboratories (LLL) and Lockheed have reported a FOCS for the detection of chloroform (13-15). The FOCS reported by LLL utilizes a single-phase reagent mixture derived from Fujiwara reaction chemistry (16) as a chemical transducer; the response obtained was a kinetic (reaction-rate) fluorescence signal.

The factors affecting the kinetic response of single-phase Fujiwara-type reagent mixtures to GPHHCs (specifically chloroform) have been discussed (17). Also, a single-phase reagent mixture providing a spectrophotometric signal related to chloroform concentration for a period of time up to two days has been developed (17). In addition, a single-phase reagent for the fluorometric detection of chloroform has also been developed (17).

In this paper, two FOCSs for the detection of volatile GPHHCs with the previously reported chemistry are reported. The fluorometric responses of the two sensors for detection of chloroform are characterized and the design factors affecting the relative (calibration) sensitivities of the two FOCSs are discussed. Some common volatile GPHHCs are tested using the "reservoir" FOCS and their FOCS calibration sensitivities are reported. The utility of the reservoir FOCS for the laboratory determination of chloroform in chlorinated drinking water is demonstrated.

EXPERIMENTAL

Apparatus and Materials

All fluorescence measurements were made using a fiber optic fluorometer constructed in house (18). The excitation wavelength was 545 nm as provided by a 545 nm bandpass filter (ca. 10 nm bandpass). The measured excitation power (75-W Hg/Xe compact arc lamp) at the distal termination of the excitation fiber optic ranged from ca. 1.5 to 2 mW. The emission wavelength as selected by a monochromator (linear reciprocal dispersion = 20 nm/mm, effective aperture = f/4, 1-mm square entrance and exit ports) was 600 nm; a 580-nm cut-on filter was also placed at the exit port of the monochromator. Two photomultiplier (detector) tubes were used in this work; an RCA 4840 was used for the initial reactor optimization studies, and a Hamamatsu 928 was used for all remaining experiments.

The FOCSs reported here were designed to interface with the fiber optic fluorometer. The fiber optic fluorometer utilizes a dual-fiber (20°) optic probe (600-μm core PCS fiber optics) assembly to guide radiation to and from a sample, and a FOCS is constructed by attaching a "reactor body" to this probe. Thus, a variety of reactor types can be utilized with the same fiber optic probe/fluorometer.

Figure 6.1 shows the components of one of the reactor bodies developed to perform head-space monitoring (for volatile species). This reactor was machined from an inner cylinder (core) of black Teflon pressed into a black Rulon sleeve. The reagent reservoir is a 0.50-in diameter by 0.50-in deep cylindrical well machined into the Teflon core of the reactor. A series of twelve 3/16 in (diameter)

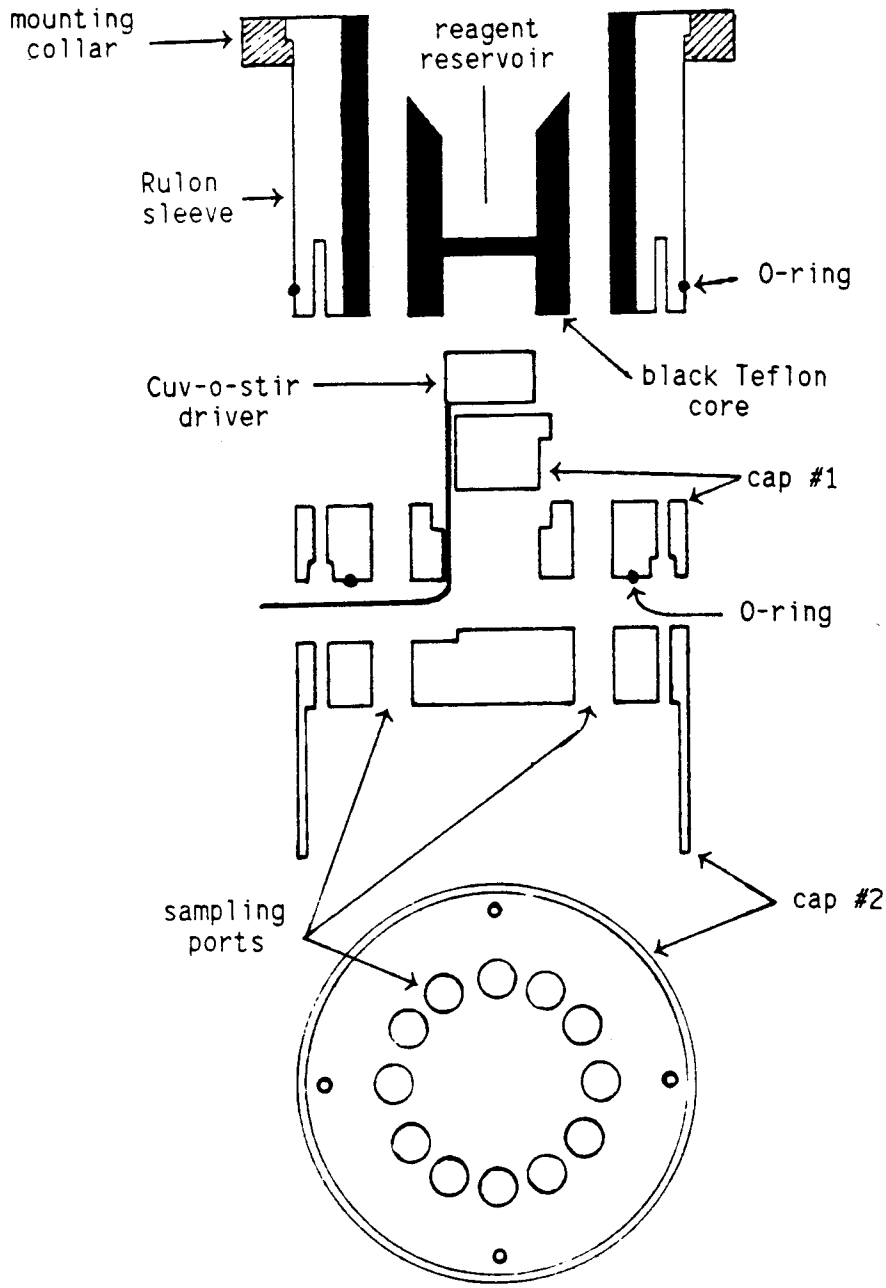

Figure 6.1. Exploded view of the reservoir FOCS reactor.

"sampling ports" surround the reagent reservoir and allow transport of gas phase analyte molecules (from outside the sensor body) to the surface of the reagent mixture. The bottom of the Teflon piece is machined to hold a Helma Cuv-o-Stir (model # 333) driver which spins a small stir bar within the reservoir (not shown). The Cuv-o-Stir driver is held in place by cap #1 (figure 6.1), which has a removable slotted plug machined into its center for the electrical lead of the Cuv-o-Stir driver. Otherwise, cap #1 is basically a disc with 12 holes around the circumference. Cap #1 was used during the initial experiments to characterize the effects of reactor design on the FOCS response. The second cap (cap #2, figure 6.1) was constructed as a consequence of these experiments and is essentially an inverted "cup"; the cup has an inner diameter of 5 cm, and is 2-cm deep. This cap was used in all remaining experiments. For convienence, cap #2 is attached to the FOCS reactor simply by removing the mounting screws for cap #1 and using longer screws to mount both caps.

To assemble the reservoir FOCS, the outer Rulon sleeve is attached to the fiber optic probe assembly using a stainless steel collar which bolts to the probe. When assembled (figure 6.2), the sensing (distal) ends of the fiber optics (of the fiber optic probe) are ca. 8.9 mm (≈0.35 in) above the bottom of the reactor reservoir. Thus, when the reservoir is loaded with 1.3-mL of reagent solution, the sensing (distal) terminations of the fiber optics are ca. 1.5 mm below the surface of the reagent. When submerged in a sample, the air-tight design traps a finite volume of air (the head-space) within the sensor, preventing the liquid sample from reaching the reagent mixture while allowing gas-phase transport of the analyte to the

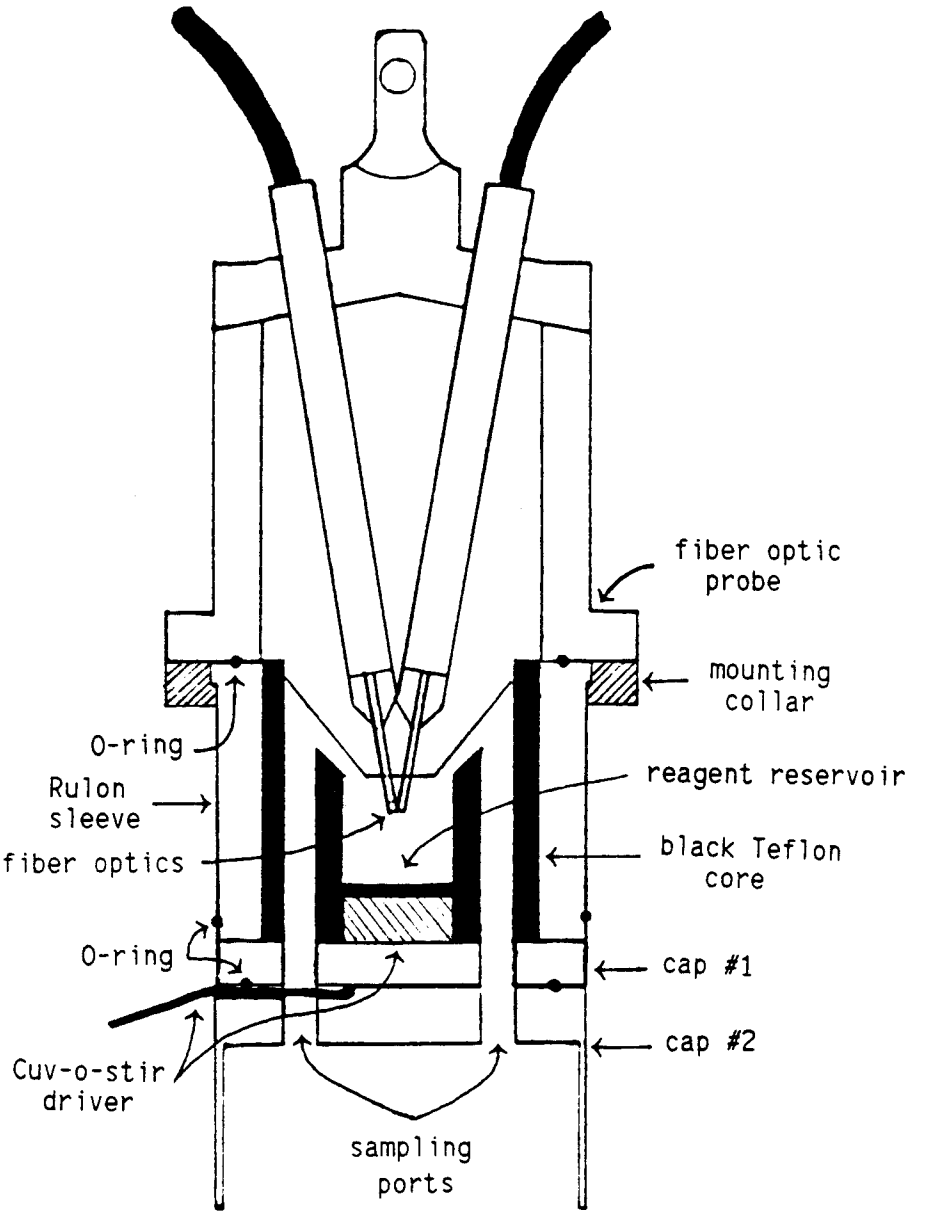

Figure 6.2. Assembled reservoir FOCS. The electrical lead of the Cuv-o-Stir driver (stir bar not shown) partially obstructs one of the 12 sampling ports.

FOCS reagent.

To test the performance of the FOCS with aqueous samples, the apparatus shown in figure 6.3 was constructed utilizing a 1 Qt. (ca. 946 mL) Kerr brand "Mason" canning jar and lid. The center plate of the jar's lid was replaced with the Teflon "stopper". The Teflon stopper is pressed into the jar's mouth and secured by screwing in the threaded ring of the lid, compressing the O-ring and forming a gas tight seal. The FOCS is then pressed into the hole in the center of the stopper (also sealed with an O-ring). Two small holes are drilled through the stopper: one for the electrical lead of the mini-stir driver (sealed with silicone) and the other to allow syringe injection of standards into the jar (this hole is threaded and is sealed with a machine screw). For a 800-mL aqueous sample, the syringe needle is below the liquid's surface during standard injection. To ensure mixing of the standard, the aqueous sample is stirred (2-in long X 1/4-in diameter) at a slow rate (no surface vortex).

A second reactor, designed to hold a single drop (10 µL) of the reagent mixture, is shown in figure 6.4. When attached to the conical fiber optic probe assembly, the two horizontal "support" fiber optics are positioned perpendicular to and below the probe fiber optics to create a "cage" which can support a single drop of liquid reagent (in view of the probe). The reactor (machined from a black Delrin rod) is simply a hollow "pipe". The support fiber optics are short lengths of PCS fiber optic (600 µm core), stripped of cladding material, press fit into two holes drilled through the rod (1.19 mm below the sensing tips of the fiber optic probe and

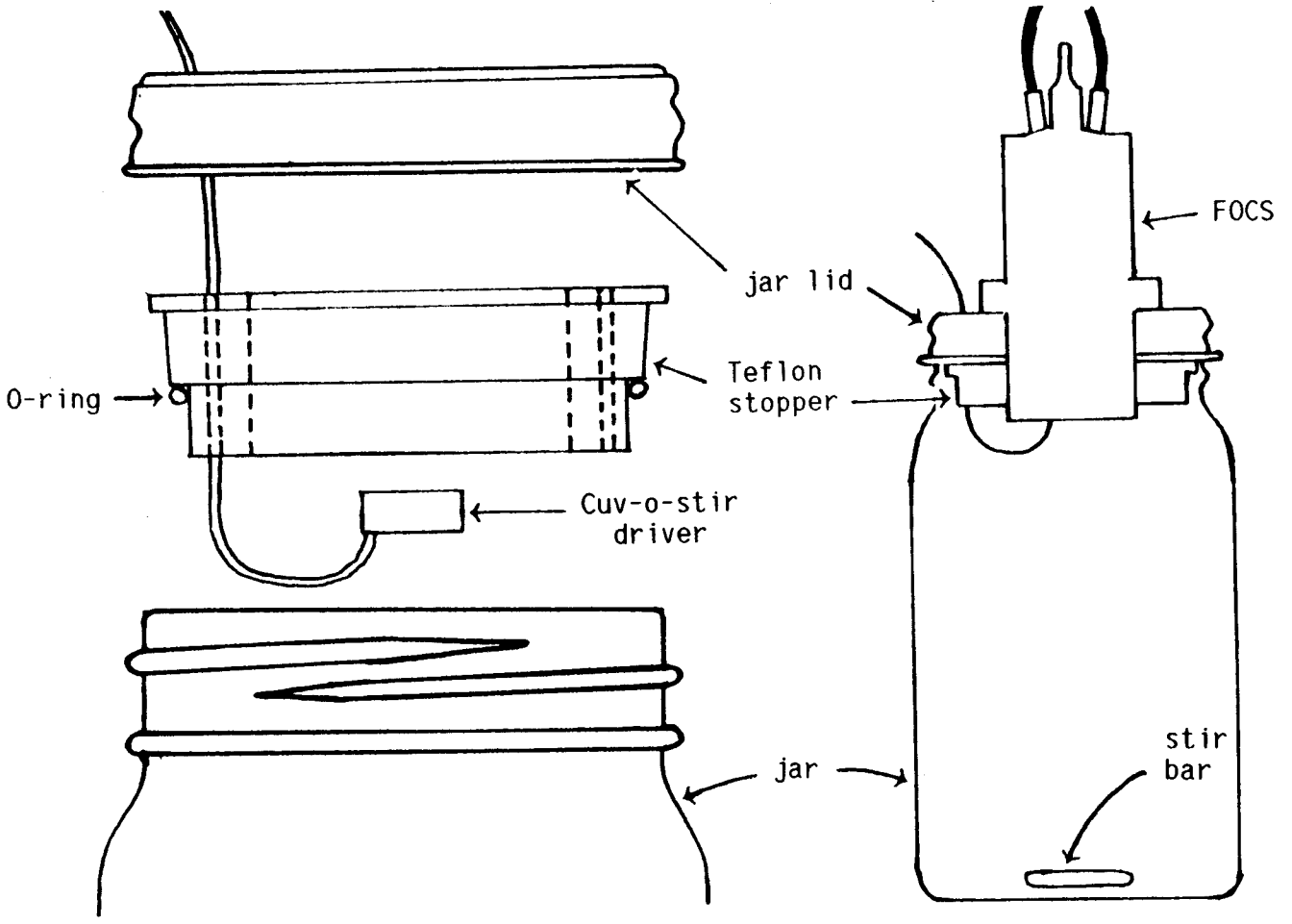

Figure 6.3. Apparatus for interfacing the two FOCSs with aqueous samples.

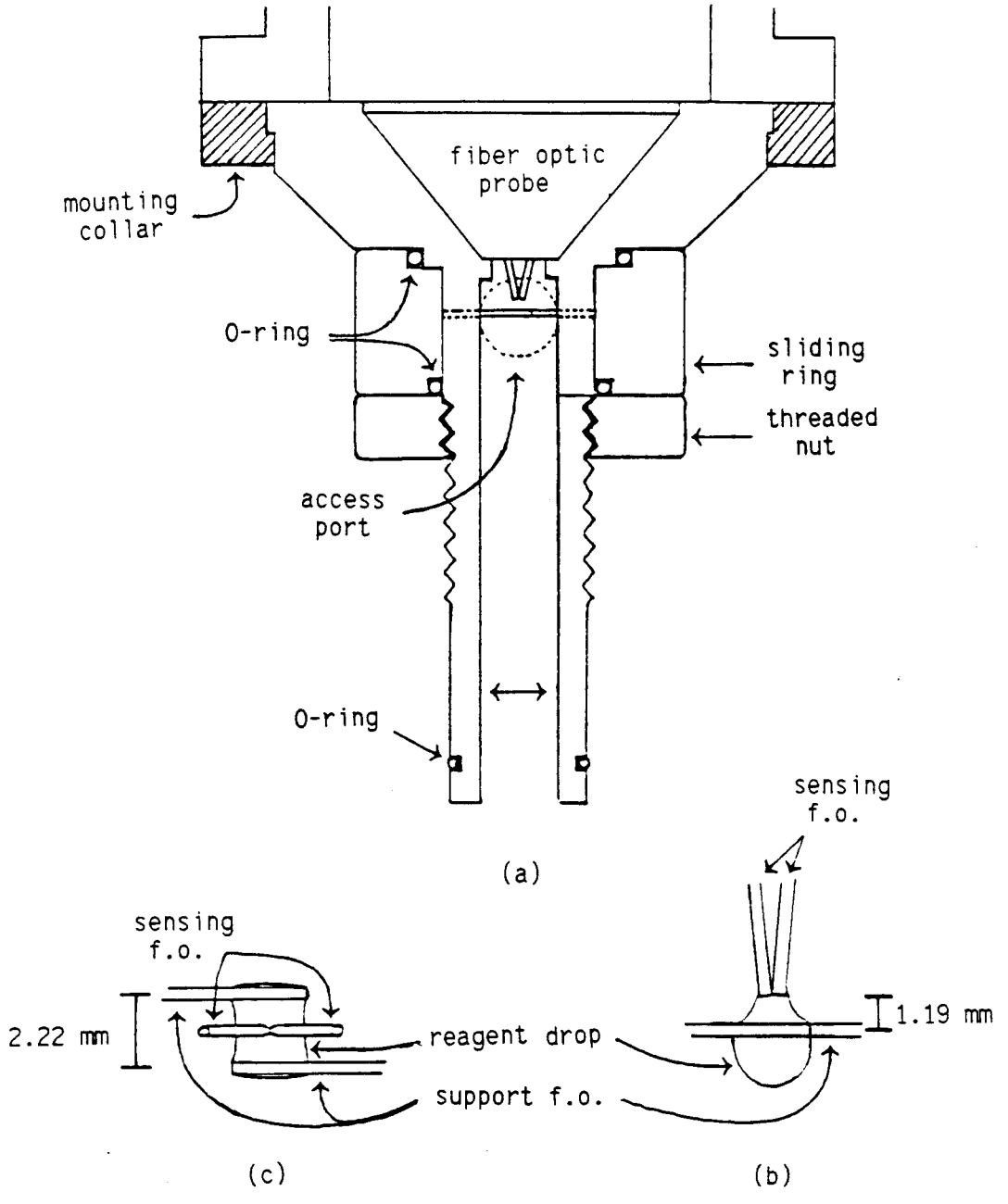

Figure 6.4. Assembled drop FOCS (a); (b) side and (c) "top" view of drop and fiber optics. The drop reactor is attached to the fiber opic probe using the mounting collar.

2.22 mm apart). Orthogonal to these support fiber optics, a small hole ("access port") provides a means to view or deposit reagent mixture into the fiber optic "cage" when the FOCS is assembled. With the threaded nut loosened, the O-rings relax and the "sliding ring" can be pushed down to allow placement of a drop of reagent into the "cage" (using a pipet). The access port is sealed by tightening the threaded nut against the ring, compressing the O-rings to form a gas-tight seal.

To interface this second FOCS with an aqueous sample, a modified version of the apparatus shown in figure 6.3 was used. The modification is simply a stopper with a reduced diameter center hole.

Absorption measurements were obtained using a Hewlett Packard 8451A diode-array spectrophotometer. The purge-and-trap GC/MS analysis of tap water for the trihalomethanes was performed using a CDS (#330) purge-and-trap unit (Supelco 624 trap) interfaced to a Hewlett Packard 5890/5970 GC/MSD system (30-m X 0.53 mm i.d. DB-624 wide-bore column, 3-μm film thickness, J&W Scientific).

Procedures

To study the effect of the sample surface area available for (analyte) volatilization on the observed (kinetic) signal, 850 mL of blank water was placed in the Mason jar. For this volume of water, the bottom of the reservoir FOCS (cap #1 only) was about 12 mm below the liquid surface when inserted through the Teflon stopper. Thus, the surface area available for analyte volatilization is determined by the summed cross sectional area of the ports. The initial experiment was performed with all twelve ports open. Successive

experiments were performed with an increasing number of ports blocked by pressing lengths of Delrin rod into the individual ports. For all measurements, a blank rate was first obtained prior to injection of the standard. For these experiments, 50 μL of a 14.4 mg/mL chloroform standard was injected (giving a chloroform concentration of 872 ng/mL in the Mason jar) and the reaction rate was monitored for ca. 20 min.

A similar set of experiments (same standards, etc.) was performed to study the effect of the cross sectional area available for vapor-phase transport between the sample surface and the FOCS reagent surface on the observed (kinetic) signal. For these experiments, 800 mL of water was used and the bottom of the FOCS was ca. 12 mm above the sample solution surface (in the Mason jar). Under these conditions, the surface area available for analyte volatilization is the total surface area of the water in the jar and is fixed. Thus, by plugging the sampling ports, only the area available for vapor-phase transport is varied.

To calibrate the optimized reservoir FOCS response for chloroform (figure 6.2 with cap #2), multiple injections of chloroform standards were made into 800 mL of blank water placed in the Mason jar. The FOCS was inserted such that the water level rose approximately halfway up into the cup defined by cap #2. Thus, the surface area for analyte volatilization is defined by the FOCS and not the Mason jar. For calculation of the method detection limit, 5 separate blank measurements were made, each with a new 1.3-mL aliquot of reagent, prior to the first standard injection. The low-level chloroform (< 20 ng/mL) calibration curve (including a blank

measurement) was obtained using a single 1.3-mL aliquot of reagent. At higher levels of chloroform, each measurement (corresponding to another injection of a chloroform standard) required a new aliquot of reagent.

The calibration of the drop FOCS (figure 6.4) response for chloroform was also performed by making multiple chloroform standard injections into an 800-mL sample of blank water held in the Mason jar. However, for the drop FOCS, the bottom of the sensor was above the water level (ca. 12 mm) in the Mason jar, and the surface area available for analyte volatilization is defined by the inner diameter of the jar. With the drop FOCS, each measurement requires a new drop of reagent, and each measurement was repeated 3 times (for the blank measurement, n = 5). The drops (10 µL) were placed using a 10-µL Eppendorf pipet with a glass capillary as the pipet tip.

To determine the impact of inner-filter effects on the observed fluorescence rate signal, the absorbance and the fluorescence signal of identical volumes of reagent during exposure to chloroform were monitored. A 800-mL sample of blank water was spiked with 15 µL of a 10.6 mg/mL chloroform standard to give a chloroform concentration of 198 ng/mL and the reservoir FOCS was used to monitor the fluorescence signal. At a measured time (t_0 = initial exposure time for the first aliquot of reagent), the 1.3 mL aliquot of reagent was removed with a disposable glass pipet and transferred to a spectrophotometer cell and its absorption at 545 nm (excitation wavelength) was measured. The combined time required for transfer and measurement was ca. 30 s. A fresh aliquot of reagent was added to the FOCS reservoir and the procedure was repeated except that the absorption

measurement time was increased ($t = t_0 + 1$ min). This cycle was repeated and the measured fluorescence signal and absorbance values were plotted as a function of time.

Experiments to determine the reservoir FOCS response to a variety of GPHHCs were carried out in a manner analogous to the chloroform calibrations. The Mason jar was loaded with 800 mL of blank water and the blank signal was monitored for ca. 10 min. Then, the blank water was spiked with ca. 2 μL of a 6.87 mg/mL chloroform standard (giving a nominal chloroform concentration of ca. 17 ng/mL) and the signal was monitored for ca. 10 min. After recording the signal due to chloroform, an aliquot of a GPHHC standard was injected and the reaction rate was monitored for a period of time sufficient to measure accurately the rate signal; this injection was followed by another of the same magnitude (doubling the analyte concentration). The FOCS calibration sensitivity for a given test compound was calculated as the average determined at the two concentration levels. The relative responsivity (to chloroform) was calculated using the paired chloroform response measured initially during the same run. The concentration levels tested for each compound were selected based on the results of preliminary experiments.

For the determination of chloroform in tap water, two 1-Qt. jars (figure 6.2) and two 40-mL VOA vials (I-Chem) were filled with tap water, capped (no headspace), and allowed to reach room temperature prior to analysis. These samples were taken from the laboratory tap next to the fume hood in Gilbert 254 after the water had run for ca. 10 min. The FOCS standard-additions analyses were performed within 2 hours; the confirmatory purge-and-trap GC/MS

analyses were performed after the FOCS analyses and within ca. 4 hours of taking the samples. The GC/MS samples were stored in a refrigerator while the FOCS analyses were being completed.

The standard-additions analyses of tap water for chloroform were performed using the reservoir FOCS (figure 6.2 with cap #2). One analysis was performed in a manner analogous to that of the low-level chloroform calibration (i.e., one aliquot of reagent); the other analysis was performed in a manner analogous to the high-level chloroform calibration (i.e., a fresh aliquot of reagent for each measurement). For both analyses, the initial procedure was the same: the reservoir FOCS was loaded with 1.3 mL of the reagent mixture and a blank rate was obtained from 800 mL of stirred blank water; the FOCS was removed from the sample jar, the blank water was discarded and the same sample jar was loaded with 800 mL of room temperature tap water; the FOCS was then replaced and the response to tap water was recorded. The standard additions consisted of multiple 2.5 µL (nominal) injections of a 6.87 mg/mL chloroform standard; thus, each addition corresponded to an added chloroform concentration of ca. 21.4 ng/mL (ppb).

Prior to GC/MS calibration or tap water analysis, the MSD was BFB (bromofluorobenzene) tuned to meet EPA criteria (9). For all standard and sample analyses, 5 mL of room temperature water (tap or blank) was spiked with 5 µL of 43.8 µg/mL bromochloromethane and 5 µL of 52.4 µg/mL bromofluorobenzene (as internal standards) to give final concentrations of 43.8 ng/mL and 52.4 ng/mL, respectively, in the purged sample volume. For trihalomethane (THM) calibration, the appropriate volumes of a 10 µg/mL THM standard were spiked into blank

water (along with the internal standards) to give 5, 10, 30, and 80 ng/mL standards. Samples and standards were purged for 11 min (fritted sparger) and desorbed from the trap at 200° C for 4 min. The temperature program consisted of a 5 min hold at 10° C followed by a 8° C/min ramp to 180° C. Trihalomethanes in the tap water samples were quantitated using the average response factor calculated from the four standard analyses; chloroform and bromodichloromethane were quantitated vs. bromochloromethane, while dibromochloromethane and bromoform were quantitated vs. bromofluorobenzene.

Reagents

Tetrabutylammonium hydroxide (40% in water) was obtained from Fluka; reagent grade pyridine was obtained from EM Scientific; reagent grade methanol was obtained from Mallinckrodt. Chloroform, bromoform, bromodichloromethane, dibromochloromethane, dichloromethane, 1,1-dichloroethane, 1,1,1-trichloroethane, and trichloroethylene were all acquired from Alltech. A 100-µg/mL trihalomethane standard (chloroform, bromoform, bromodichloromethane, dibromrochloromethane in methanol) was also obtained from Alltech. All chemicals were used as supplied. All aqueous solutions were prepared with double deionized water obtained from a Millipore Milli-Q system fed by house-deionized water.

Reagent mixtures of pyridine (11.2 M), tetrabutylammmonium hydroxide (0.05 M), and Millipore water (4.5 M) were prepared gravimetrically in glass volumetric flasks. Primary chloroform standards (10.6, 6.87, and 0.920 mg/mL) in methanol were prepared gravimetrically (in glass volumetric flasks) and were stored in 4-mL

vials capped with Mininert valves. All standards were stored in a freezer. Working dilutions (in methanol) of the primary standards were also stored in a freezer.

RESULTS AND DISCUSSION

For a fiber optic chemical sensor (FOCS), the process of chemical transduction is performed by some reagent system (interacting/reacting with the analyte) retained in view of a fiber optic probe. Thus, a FOCS consists of a fiber optic probe, a chemical reagent, and some type of "reactor" holding the reagent system in view of the (fiber optic) probe. Both the fiber optic probe (18) and the chemical reagent (17) used in the FOCSs reported here have been discussed; the development of different reactors that interface with these FOCS components is addressed here.

The purpose of a FOCS reactor is to retain a chemical reagent in the viewing volume (of a fiber optic probe) while simultaneously allowing analyte transport between this volume and a sample. A through review of the many methods of fulfilling this function has been presented (1). Generally, the reagent is held within a volume defined by some semipermeable barrier (allowing transport of the analyte but not the reagent). For the determination of volatile species, the semipermeable barrier can be a finite volume of headspace. In this case, the reagent must be physically held in view of the fiber optics by some type of "bucket" or reservoir (figure 6.1).

Figure 6.5 illustrates the sampling methodology employed by the FOCSs developed in this work. Conceptually, the measurement process can be considered as a series of discrete processes: volatilization of the analyte from the sample, diffusion of the gas phase molecules to/into the FOCS, solvation of the gas molecules at the reagent

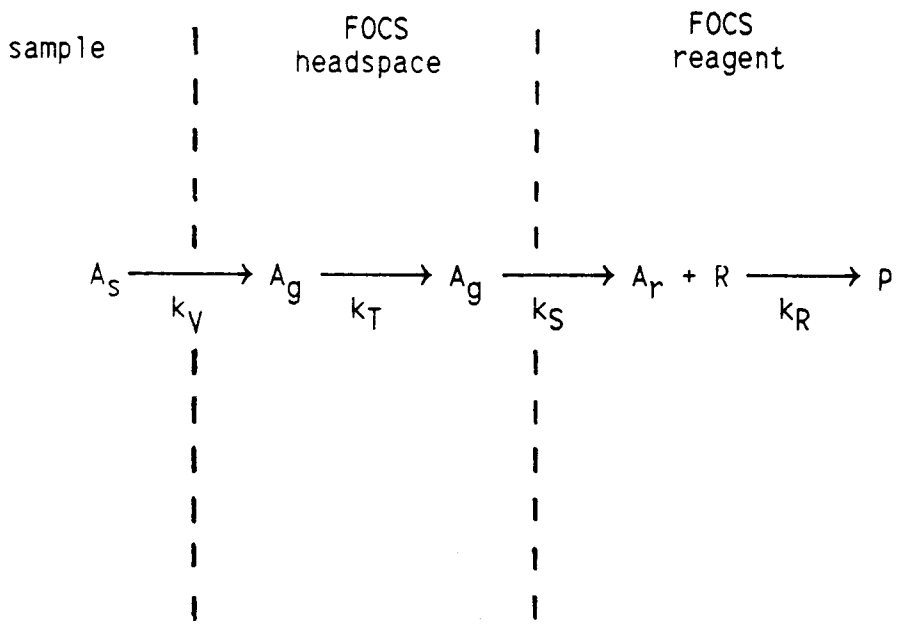

Figure 6.5. Schematic diagram depicting the sensing mechanism of the reported FOCSs. Each process has a characteristic rate constant: k_V = analyte volatilization; k_T = analyte transport; k_S = analyte solvation; k_R = analyte reaction with the FOCS reagent.

surface, and finally, reaction with the reagent. For a given concentration of analyte in a sample, the kinetic response observed can be affected by the rates at which all these independent processes proceed, although one or more process may be limiting. The rate of the chemical reaction between the analyte and the reagent is strictly a function of the chemistry and, for the reagent used in this work, has been discussed (17). The rate at which the other processes proceed can be maximized through proper design of the FOCS reactor.

Initial Studies

With the bottom of the reagent reservoir FOCS (cap #1 only) submerged below the surface of an aqueous sample, the surface area of the sample available for analyte volatilization was varied by selectively plugging the sampling ports of the FOCS. The cross-sectional area for vapor-phase transport is also simultaneously varied in this experiment. The data shown in figure 6.6a demonstrate a linear relationship between the observed reaction rate and the sample surface area. Generally, the rate of analyte volatilization and the observed reaction rate are predicted to increase with sampled surface area up to the point where either the rate of transport (to the reagent), the rate of solvation (of the gas-phase analyte in the reagent phase), or the rate of the chemical reaction becomes limiting.

The effect of reactor design on the rate of transport (of the gas-phase analyte) from the sample headspace to the FOCS reagent was studied by plugging the sampling ports when the bottom of the FOCS was held above a sample and observing the net reaction rate. Under

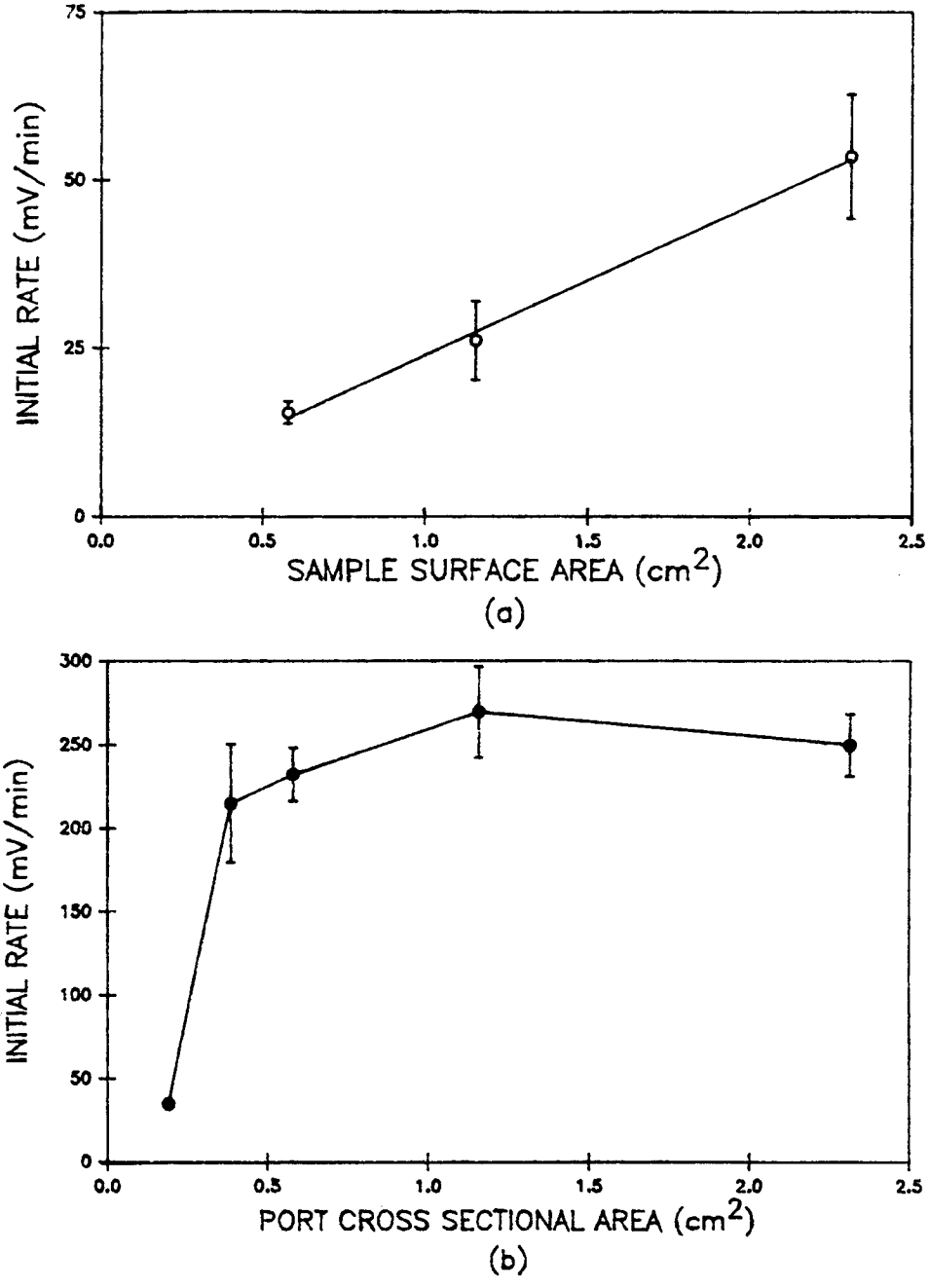

Figure 6.6. Effect of port cross-sectional area on the FOCS (rate) signal when the FOCS is submerged (a) and above the sample (b). The chloroform concentration was 872 ng/mL and the error bars denote ± one standard deviation. For 6.5a, n = 2, m = 22.2 with a standard error of 3.2 mV/min/(cm^2), b = 1.7 mV/min, r = 0.998; for 6.5b, n = 2 except for 1 port open n = 1.

these conditions the surface area sampled is constant, but the cross-sectional area for gas-phase transport is varied. The data from this experiment are shown in figure 6.6b. The observed reaction rate is independent of the port cross-sectional area above a value of ca. 0.5 cm^2. However, transport of analyte vapor could still be limiting as the cross-sectional area of the reagent well (1.27 cm^2) may become limiting when 6 or more ports are open (vide infra).

By extrapolating the least-squares fit of the data of figure 6.6a, the sample surface area giving the maximum rate in figure 6.6b is estimated to be ca. 12 cm^2. The Mason jar used in these experiments has an (inner) diameter of ca. 8.5 cm, and the sample surface area is ca. 56.7 cm^2 for the data presented in figure 6.6b. Thus, the kinetic response (figure 6.6b) is not limited by the sample surface area or the port cross-sectional area when 6 or more ports are open. For the "reservoir" FOCS tested in these experiments (with the FOCS held above the sample solution), the factor limiting the the rate of reaction is either the rate of analyte solvation in the FOCS reagent or the rate of the chemical reaction (or both).

The cross-sectional area of the cup defined by cap #2 (figures 6.1 and 6.2) is ca. 19.6 cm^2. Thus, when cap #2 is used, the FOCS rate response is not limited by the sample surface area or the port cross-sectional area even when the bottom of the FOCS is submerged.

The response time of the FOCS is the time between injecting a standard and the observance of a constant rate signal. With the FOCS above the sample surface, the response time with 12 ports and 1 port open was ca. 2 min and ca. 5 min, respectively. Because the volume of the trapped headspace affects the FOCS response time, the optimum

dimensions for the sampling port(s) are the minimum that provide the maximum observed reaction rate.

The kinetic signal obtained from the FOCS is related to the concentration of the analyte in the FOCS reagent phase and the rate constant of the transducer reaction. Generally, a constant rate signal is observed when a steady-state analyte (e.g., chloroform) concentration is reached where the rate (mol/min) of analyte entering the reagent is equal to the rate of consumption (in the reagent phase). If the rate constant (of the reaction) is relatively small, the concentration of analyte in the reagent will increase to a limiting value determined by the characteristic solubility of the analyte (in the specific reagent). Under these conditions, it is the chemistry which limits FOCS response. If the solubility limit is not reached, the FOCS response can be improved by increasing the steady-state concentration of the analyte in the FOCS reagent phase by increasing the rate of analyte solvation (in the reagent phase).

For a given reagent volume, the rate at which the analyte enters the reagent and the steady-state analyte concentration increase with the surface area of the reagent. Conversely, for a given surface area, the analyte steady-state concentration is increased by decreasing the volume of the reagent. Overall, the surface area determines the rate of transport (mol/min) into the reagent while the volume controls the dilution factor (mol/mL). Thus, the design parameter which is optimized to provide the maximum kinetic response is the surface area to volume ratio (A_S/V). This consideration led to the FOCS reactor shown in figure 6.4.

Reservoir FOCS Chloroform Calibration

Figure 6.7 shows the response of the reservoir FOCS (cap #2, excitation power ca. 2 mW) to chloroform over the range 0.66-17 ng/mL (ppb). The calibration sensitivity (m) for this FOCS is 2.2 mV/min per ng/mL (ppb). The measured blank response is 0.99 mV/min with a standard deviation (s_{bk}) of 0.08 mV/min (n = 5); the peak-to-peak noise in the blank signal and dark signal was ca. 3 mV and ca. 0.8 mV, respectively. From these data the calculated detection limit (DL = $2s_{bk}/m$) for chloroform is 0.07 ng/mL (ppb); the blank signal corresponds to a chloroform concentration of 0.45 ng/mL. For the experimental conditions used (Hamamatsu 928 PMT, PMT bias voltage = -900 V, R_f = 10 MΩ, C_f = 0.198 μF), the dark current signal was 20 mV and the initial background signal was 170 mV.

The data shown in figure 6.7 were obtained by making successive injections of chloroform standards into the initial 800 mL of blank water and monitoring the rate of change in the fluorescence signal (using a single 1.3-mL aliquot of reagent). Initially, the blank signal was monitored for ca. 30 min; after each chloroform injection, the reaction was monitored for ca. 20 min, and the response time was ca. 4 min. At ca. 120 min (near the end of the 20 min monitoring period for 17 ng/mL chloroform), the sensor's response was ca. 1.3 V and was becoming non-linear. The reagent mixture was replaced and a linear kinetic response was restored (at 17 ng/mL chloroform). This indicates that the concentration of chloroform in the water sample has not been significantly depleted. Subsequent chloroform injections (into the same water) to give 40 and 98 ng/mL chloroform both required fresh aliquots of reagent; at 98 ng/mL the sensor's

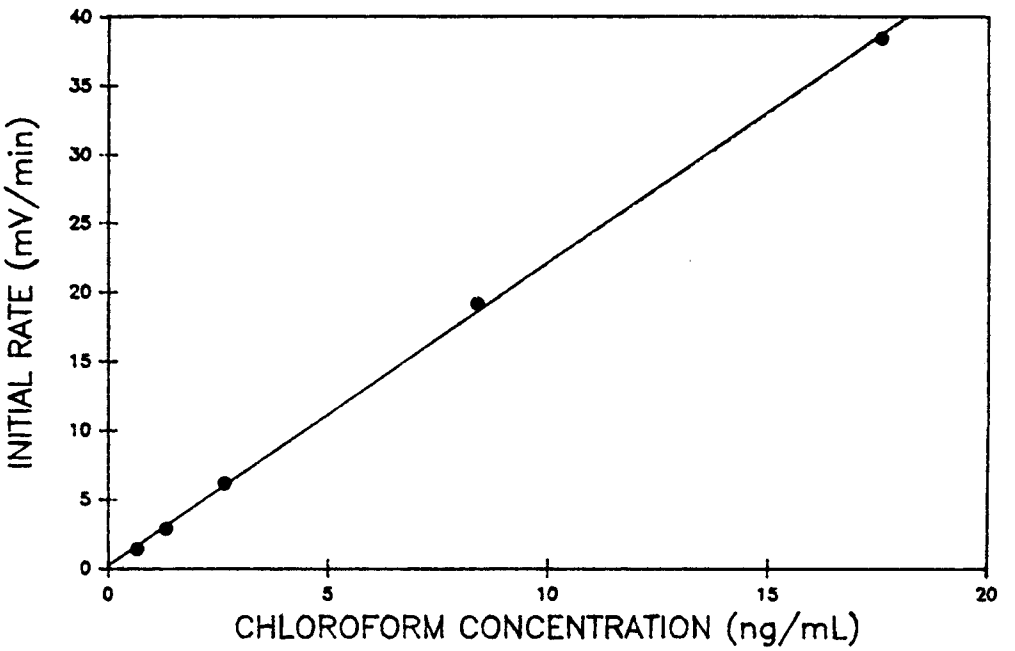

Figure 6.7. Low-level chloroform calibration curve for the reservoir FOCS; m = 2.2 mV/min/(ng/mL) with a standard error of 0.03 mV/min/(ng/mL), b = 0.2 mV/min.

response became non-linear within 6 min.

Previous experiments (17) using a different reagent mixture, which yields a slower initial rate in batch-mode experiments than thereagent mixture used in the FOCS, yielded a stable (rate) signal proportional to chloroform concentration at ug/mL levels for ca. 48 hr when the absorbance (at 545 nm) was monitored. In addition, another reagent mixture exhibiting approximately the same sensitivity to chloroform at 545 nm as the reagent mixture used in the FOCS did not show any decay after exposure to chloroform (30-60 ng/mL) for ca. 200 min (17). However, the rate of transport of chloroform (to the reagent mixture) was less with the apparatuses used in these experiments (relative to the FOCS). Still, the decay in the observed fluorescence (rate) signal within 10 min at 98 ng/mL chloroform was not suspected to be due to reagent consumption and was attributed to inner-filter effects.

Figure 6.8 compares the time dependence of both the absorption and fluorescence signals of the reagent mixture on exposure to chloroform. The absorption data indicate a constant rate signal over the time period monitored while the fluorescence data show a definite negative deviation. The ratio of absorption to fluorescence as a function of time in figure 6.9 clearly shows inner-filter effects beginning to attenuate the fluorescence signal from the FOCS at ca. 11 min. Approximating the optical pathlength of the reservoir FOCS to be 8.9 mm (the distance between the sensing terminations of the fiber optics in the reservoir and the bottom of reservoir), the absorbance at 11 min is ca. 3.6×10^{-2} A.U. (8.9 mm/1.0 cm) and the fluorescence signal is ca. 1 V. Primary absorption effects normally

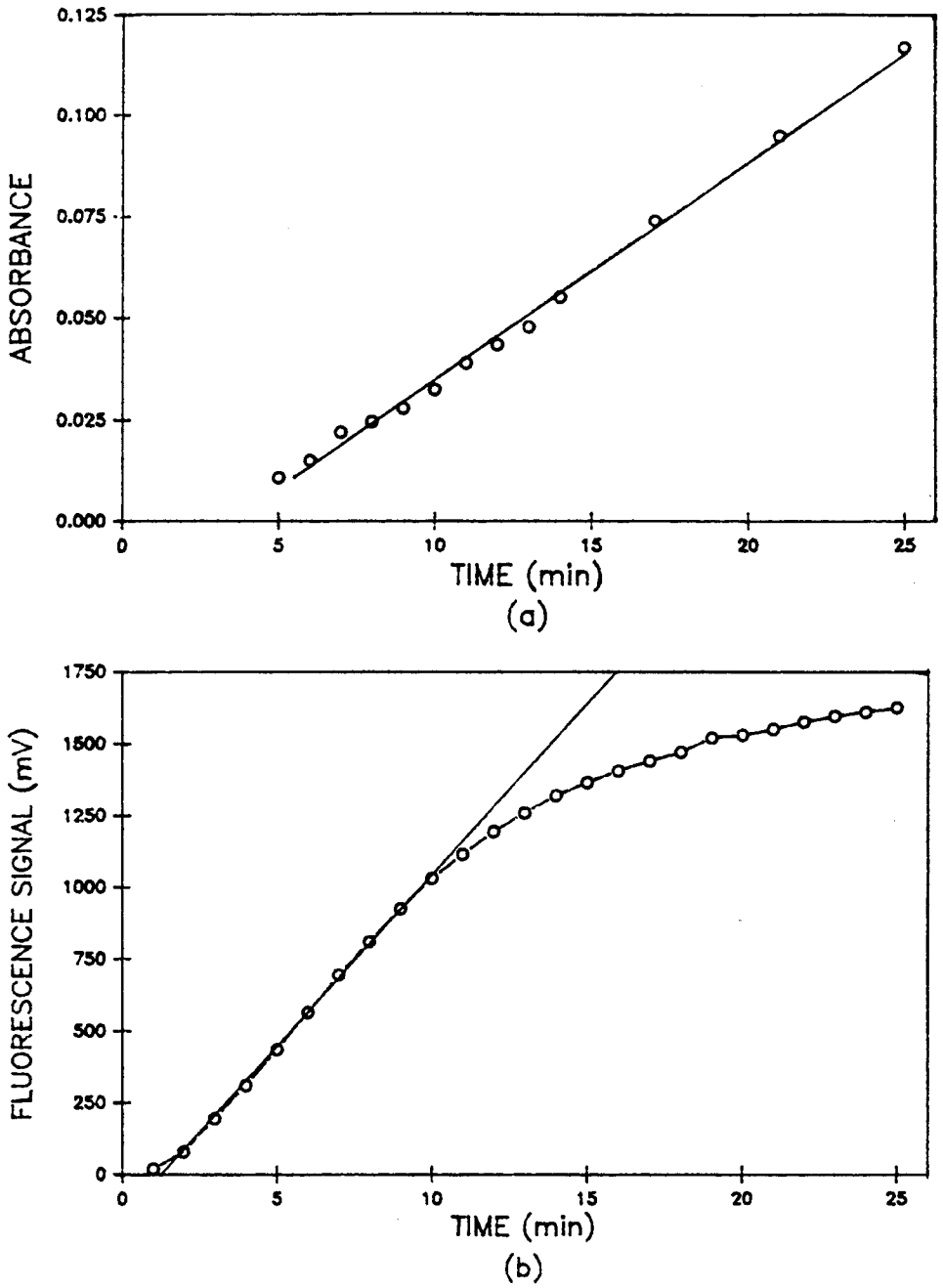

Figure 6.8. Time dependence of absorption (a) and fluorescence (b) response of the reservoir FOCS on exposure to 198 ng/mL chloroform. For (a), the initial slope is 5.4 X 10^{-3} A.U./min; for the linear portion of (b), the initial slope is 119 mV/min.

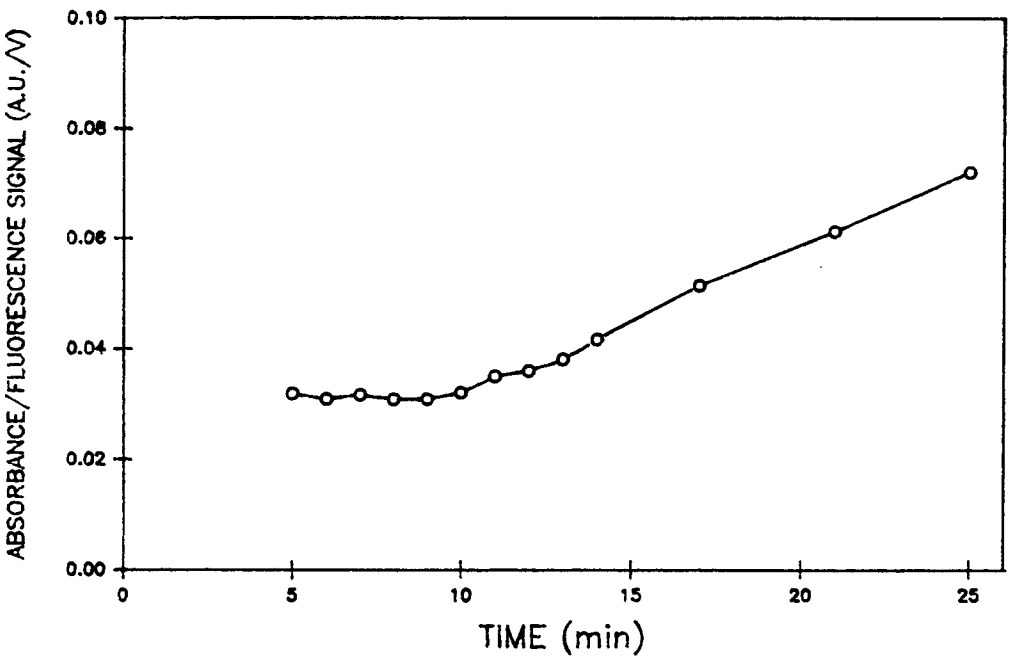

Figure 6.9. Time dependence of the ratio of absorbance to fluorescence signal (from figure 6.8).

cause nonlinearity when the absorbance is greater than 0.01 (19).

Figure 6.10 shows the response of the reservoir FOCS to chloroform over the range 30-1048 ng/mL (ppb); these data were obtained at a later date than that shown by figure 6.7 using a different reagent mixture and a re-assembled FOCS (after breakage of the fiber optics). For each chloroform concentration, a new 1.3 mL aliquot of reagent mixture was used. At 1048 ng/mL (ppb) chloroform, the response time (time to steady slope) was ca. 2 min. and the slope was constant for an additional 2 min; thus, the total measurement time was ca. 4 min.

The calibration sensitivity obtained from the data of figure 6.10 is 0.53 mV/min/(ng/mL chloroform) with an excitation radiant power of 1.5 mW; this value is an approximate factor of 4 less than that reported for the data of figure 6.7. The relative responsivity of the two different reagents used was determined (at two chloroform concentrations) to be 1.4 (fig. 6.7/fig. 6.10). The differences in reagent responsivity and excitation radiant power account for ca. 50% of the observed difference in the calibration sensitivities.

The run-to-run variation in calibration sensitivity may also be due to the condition and orientation of the fiber optics. The quality of the sensing tips of the fiber optics and the exact orientation between the excitation and emission fibers can affect the distribution pattern of the excitation radiation and the collection efficiency of the emission fiber. Thus, every time the probe is dismantled, the fibers repolished, and the probe re-assembled, differences in calibration sensitivity are expected (20).

Variability in the calibration sensitivity may also result from

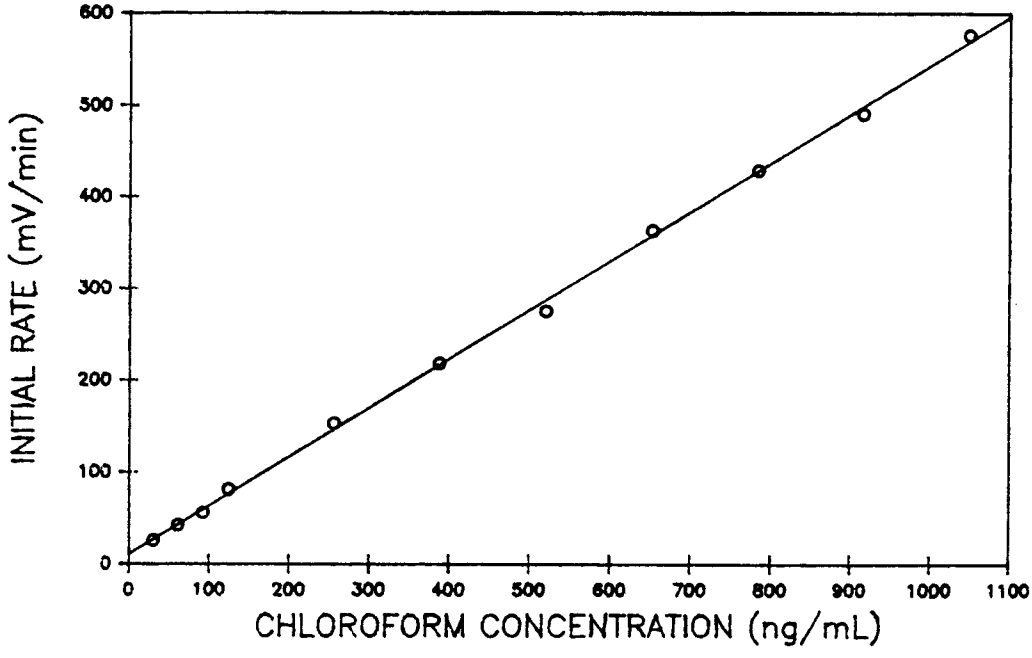

Figure 6.10. Higher-level chloroform calibration curve for the reservoir FOCS. From the linear least-squares fit m = 0.53 mV/min/(ng/mL) with a standard error of 0.06 mV/min/(ng/mL), b = 10.7 mV/min.

variability in the stirring rate of the water (the observed reaction rate generally decreases by an approximate factor of two when the water is not stirred). Although factors such as excitation power, reagent responsivity, stirring, and the optical alignment and condition of the fiber optics can affect the long-term stability of the FOCS calibration sensitivity, consecutive measurements using the same FOCS (i.e., same fiber optics) routinely exhibit RSDs under 20% (vide infra).

Overall, figures 6.7 and 6.10 show that the reservoir FOCS has a linear dynamic range for chloroform spanning ca. 3 orders of magnitude (0.08-1000 ng/mL). However, the utility of the sensor for remote monitoring applications is limited by inner-filter effects, i.e., even at concentrations as low as 20 ng/mL (ppb) chloroform, the sensor can provide a (rate) signal proportional to chloroform concentration for only about 1 hr (1 V/(20 mV/min)).

Direct comparison of the reservoir FOCS to the LLL FOCS (15) is difficult because of differences in instrumentation. The LLL fiber optic fluorometer utilizes an unspecified incandescent radiation source and an unspecified photodiode detector; thus, instrumental parameters such as excitation power, detector responsivity, and signal gain are unknown. Also, a detection limit is not reported.

The LLL chloroform FOCS utilizes a single-fiber fiber optic probe (320 μm silica clad low fluorescence fiber optic) and a single-phase Fujiwarwa reagent made with tetrapropylammonium hydroxide; the exact composition of the reagent is not specified. The FOCS reactor consists of a 1.1 mm (inner) diameter glass capillary which is open at one end and has the fiber optic epoxied

into the other end. The reactor is loaded with 2 μL of the reagent, and when the FOCS is immersed in an aqueous sample an air bubble is trapped in the capillary. The distance between the tip of the fiber optic and the reagent/air interface is ca. 1.4 mm.

The reported calibration sensitivity for the LLL FOCS for gas-phase chloroform is 1.8 mV/min/(ng/mL); using Dilling's value of 0.13 for the Henry's Law distribution coefficient (21), this corresponds to an aqueous chloroform calibration sensitivity of ca. 0.23 mV/min/(ng/mL). At 12 ng/mL gas-phase chloroform (ca. 92 ng/mL in the aqueous phase), the average (n = 3) response was 12 mV/min with a standard deviation of 2 mV/min. Thus, the gas-phase detection limit for chloroform is estimated to be ca. 4 ng/mL; the corresponding detection limit for aqueous chloroform is ca. 30 ng/mL. At 12 ng/mL (gas-phase) chloroform, the response time (time to a constant rate) is ca. 4 min, and the rate signal began to decay within 14 min, somewhat faster than with the reservoir FOCS.

Overall, the time-dependent response characteristics of the LLL FOCS are similar to the reservoir FOCS. Although not discussed by LLL, it is expected that sensor lifetime is limited by inner-filter effects just as with the reservoir FOCS. However, reagent consumption is also a possible cause of signal decay because the reagent volume is about a factor of 650 less than that of the FOCS.

The detection limit (for chloroform) of the LLL FOCS is somewhat worse than that exhibited by the reservoir FOCS. Although differences in reagent chemistry may be an important factor, there are no data allowing any direct comparison on this level. In addition, instrumental factors such as excitation power, etc. cannot

be discussed due to lack of data on the LLL FOCS (vide supra). However, from the viewpoint of FOCS design, there are some important differences which may affect the relative sensitivities of the two sensors.

Although the A_s/V ratio for the LLL FOCS (ca 4.75 cm^{-1}) is an approximate factor of 5 greater than that of the reservoir FOCS (0.97 cm^{-1}, vide infra), the absolute surface area of the sample monitored (9.5 X 10^{-3} cm^2) is about a factor of 2000 less (relative to the reservoir FOCS with cap #2). In addition, the optical pathlength of the LLL FOCS (ca. 1.4 mm) is substantially less than that of the reservoir FOCS (ca. 8.9 mm). The reduced pathlength and sampled (sample) surface area may limit the sensitivity of the LLL FOCS (relative to the reservoir FOCS). Another critical difference is the stirring provided by the reservoir FOCS which distributes the chloroform throughout the reagent mixture. With the LLL FOCS, the red product tends to form at the air-reagent interface as diffusion limits the movement of chloroform and the red product into the reagent mixture. Furthermore, single-fiber probes exhibit greater background signals, and thus background noise, than double-fiber probes (20) resulting in worse detection limits. Moreover, the use of a photodiode instead of a photomultiplier for detection may degrade detection limits because of the higher relative detector (dark) noise of photodiodes.

Drop FOCS Chloroform Calibration

Figure 6.11 is a low level calibration curve for the "drop" FOCS showing detection of 340 pg/mL chloroform. The calibration

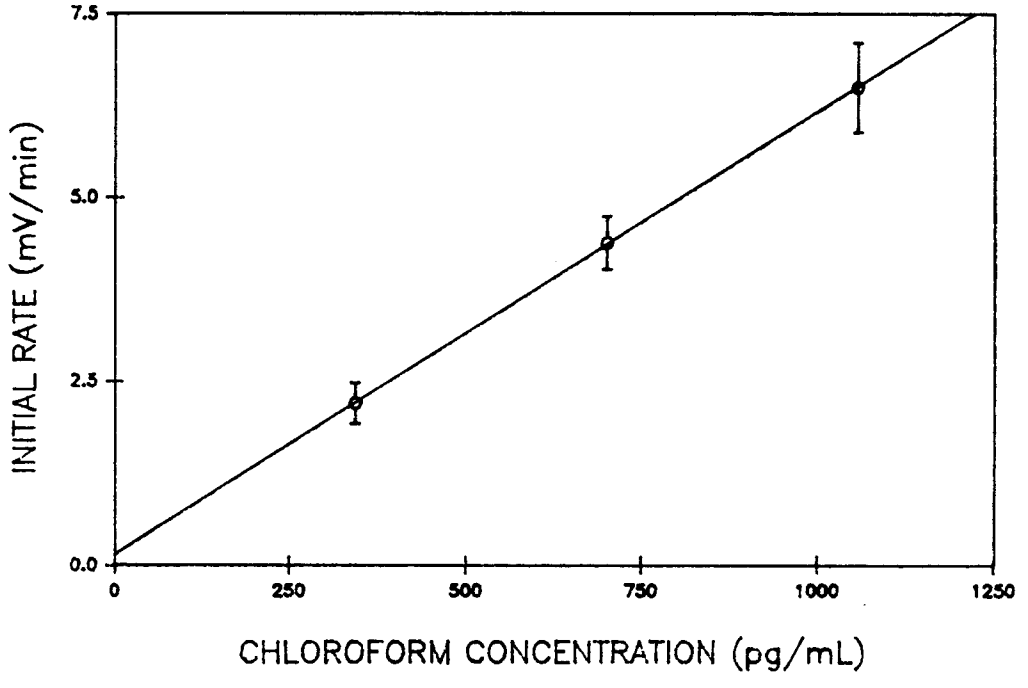

Figure 6.11. Low-level chloroform calibration curve for the drop FOCS. Each point represents the average of three measurements (error bars denote ± one standard deviation); m = 6.0 mV/min/(ng/mL) with a standard error of 0.38 mV/min/(ng/mL), b = 0.1 mV.

sensitivity is 6.0 mV/min/(ng/mL) chloroform. The measured blank signal was 1.8 mV/min with a standard deviation of 0.24 mV/min, giving a calculated detection limit for chloroform of 0.08 ng/mL; the blank signal corresponds to a chloroform concentration of 0.30 ng/mL.

Figure 6.12 shows the response of the drop FOCS to chloroform over the range 1-900 ng/mL; at 1600 ng/mL chloroform, the linear portion of the fluorescence vs. time chart recording was too short to accurately measure the slope. The calibration slope is 2.4 mV/min/(ng/mL) chloroform, a factor of ca. 3 less than that of the curve shown in figure 6.11. This discrepancy is attributed to the same factors as discussed for the reservoir FOCS (vide supra). Overall, the combined data from figures 6.11 and 6.12 demonstrate a linear dynamic range (for chloroform) of ca. 3 orders of magnitude for the drop FOCS.

As a first approximation, the sensitivity of the drop FOCS relative to the reservoir FOCS is related to both the relative A_s/V of the reagent (vide supra) and the relative optical pathlength. With the assumption that the 10 uL reagent "drop" is a sphere, A_s = 0.22 cm^2 and A_s/V = 22 cm^{-1}. For the reservoir FOCS, the radius of the reservoir is 0.25 in, A_s = 1.27 cm^2 and A_s/V = 0.97 cm^{-1}. Considering only the relative A_s/V, the drop FOCS should provide a signal level ca. 23 times that of the reservoir FOCS.

Although the optical pathlengths of the two sensors are uncharacterized, the maximum optical pathlengths correspond to the distance between the fiber optic terminations (in the reagent) and the bottom of the cell for the reservoir FOCS or the diameter of the

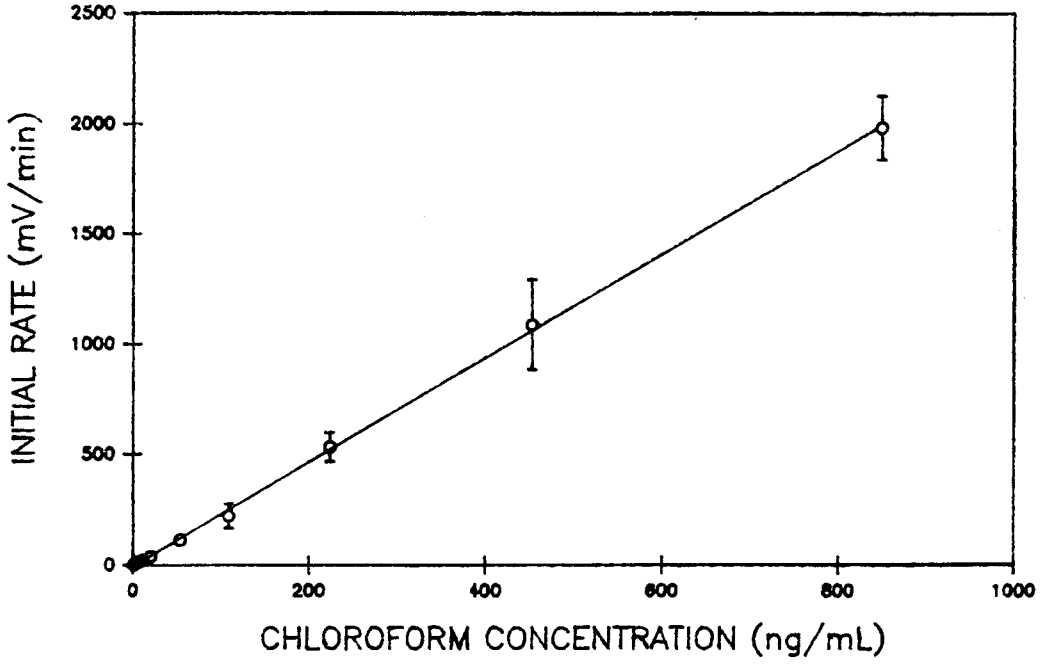

Figure 6.12. High-level chloroform calibration curve for the drop FOCS. Each point represents the average of three measurements (error bars denote ± one standard deviation); m = 2.4 mV/min/(ng/mL) with a standard error of 0.04 mV/min/(ng/mL), b = -0.5 mV.

drop for the drop FOCS. Thus, the maximum optical pathlength is 8.9 mm for the reservoir FOCS and ca. 2.7 mm for the drop FOCS. In addition, the diameter of the "samplig-port" of the drop FOCS (0.3") defines a cross-sectional area of ca. 0.46 cm^2. This value is ca. 60% less than the optimum value of 0.75 cm^2 (figure 6.6b), and restricts gas-phase transport between the sample and the reagent. Overall, these additional considerations, in conjunction with the relative A_s/V of the two FOCSs, predicts that the overall sensitivity of the drop FOCS should be approximately 4 times that of the reservoir FOCS. Differences in the fiber optic alignment, etc. will also affect this comparison (vide supra), and the observed factor of 3 greater calibration sensitivity for the drop FOCS (relative to the reservoir FOCS) is reasonable.

Although the drop FOCS provides a factor of ca. 3 more signal than the reservoir FOCS, the background signal and noise are greater. This is attributed to increased scattering of excitation radiation within the drop (or from the supports) and results in no net improvement in the detection limit (for the drop FOCS) relative to that of the reservoir FOCS (for chloroform).

The response time (time to observed steady rate) for the drop FOCS is ca. 2 mins. Overall, the net measurement time (including response time) ranged between 8 min (at 2 ng/mL) and 4 min (850 ng/mL).

Interference Study

Some volatile gem-polyhalogenated hydrocarbons were tested to characterize their response with the reservoir FOCS. The results of

these experiments are shown in table 6.1.

From table 6.1, with the exception of trichloroethylene, only those compounds with 3 or more halogens bonded to a single carbon give a response with the reservoir FOCS when utilizing the excitation and emission wavelength maxima determined for chloroform (545 nm and 600 nm, respectively). These observations are consistent with literature reports by other workers.

The literature contains many reports listing the responses of a wide range of compounds to a number of Fujiwara related chemistries (22-24). Generally, only gem-trihalogenated compounds provide response at 540 nm. An exception to this statement is 1,1,1-trichloroethane, which is reported to give little or no response at 540 nm (22,23). Although Lugg (23) reported that carbon tetrachloride provided ca. 50% of the response of chloroform (absorbance at ca. 540 nm) using his (two-phase) reagent mixture, other workers have observed much smaller levels of response and the response to CCl_4 has been attributed to chloroform contamination (22). In this thesis work, the response from CCl_4 was only 7% of that of chloroform. Among gem-dihalogenated compounds, only trichloroethylene and tribromoethylene have been observed to give a positive response at ca. 540 nm (22-24). Initial experiments have shown that methylene chloride gives absorption maxima at ca. 360 nm and ca. 450 nm when reacted with the FOCS Fujiwara reagent, and excitation at 450 nm results in fluorescence emission at ca. 520 nm.

Generally, the responsivity of the FOCS for a specific compound is dependent on its solubility (in the reagent mixture), volatility, and reactivity. The calibration sensitivities, in terms of molarity,

Table 6.1. Reservoir FOCS calibration sensitivities (slope) for some volatile gem-polyhalogenated hydrocarbons.[a]

Compound	TC conc. / m_{TC}	TC conc. / m_{TC}	$CHCl_3$ conc. / m_{CHCl_3}	m_{TC}[b] / m_{CHCl_3}
$CHBrCl_2$	48 / 0.21	109 / 0.21	20 / 0.42	0.50
$CHBr_2Cl$	68 / 0.24	136 / 0.26	21 / 0.55	0.45
$CHBr_3$	424 / 0.03	847 / 0.03	19 / 0.53	0.06
CCl_4	110 / 0.04	330 / 0.03	26 / 0.51	0.07
CH_2Cl_2	439 / NR	957 / NR	17 / 0.51	NR[c]
$CHCl_2CH_3$	467 / NR	958 / NR	15 / 0.53	NR
CCl_3CH_3	235 / NR	767 / NR	16 / 0.52	NR
CCl_2CHCl	259 / 0.06	459 / 0.05	20 / 0.56	0.10

[a]All test compound (TC) and chloroform concentrations in ng/mL: m_{TC} = test compound calibration sensitivity = (mV/min) per ng/mL (ppb) of test compound; the value used for comparison to chloroform is the average of the values determined at two different concentrations; m_{CHCl_3} = calibration sensitivity for $CHCl_3$ in mV/min/(ng/mL).

[b]The relative calibration sensitivities are calculated using the paired values for chloroform, which are also listed in the table.

[c]NR = no rate (reaction) observed.

and Henry's law constants for those compounds giving a positive FOCS response are listed by table 6.2. For CCl_4 and CCl_2CHCl, which have Henry's law constants considerably greater than that of chloroform, the relatively low calibration sensitivities are attributed to a combination of solubility and reactivity effects. For the other three compounds (all THMs), it appears that the relative responses observed are a function of all three factors.

For the determination of chloroform in tap-water with the FOCS, the major potential interferents are the other trihalomethanes; bromodichloromethane, dibromochloromethane, and bromoform. Since the FOCS responds to all four of the THMs, the suitability of an FOCS determination for chloroform is dependent on the relative levels of these compounds in the drinking water. The median concentrations of these compounds in finished drinking water have been reported to be 21 ng/mL (chloroform), 6 ng/mL (bromodichloromethane), 1.2 ng/mL (dibromochloromethane), and < 5 ng/mL for bromoform (26). From the same study, the mean values are 44 ng/mL (chloroform), 14 ng/mL (bromodichloromethane), 7 ng/mL (dibromochloromethane), and 2 ng/mL (bromoform). Thus, 50% of all drinking water facilities could quantitate chloroform to within ca. 17% (assuming 1 ng/mL bromoform) of the true value, while the "average" error incurred would be on the order of 23% (calculated using the relative response values listed in table 6.1). Still, the FOCS response might be useful as a "total THM" (surrogate) water quality indicator even for those waters exhibiting high levels for all the THMs.

Table 6.2. Relative molar response and Henry's Law constants for compounds giving positive FOCS response.

Compound	m[a]	m'[b]	H[c]	H'[d]
$CHCl_3$	62	1.0	0.0029	1.0
$CHBrCl_2$	34	0.55	0.0024	0.83
$CHBr_2Cl$	52	0.84	0.00099	0.34
$CHBr_3$	7.6	0.12	0.00056	0.19
CCl_4	5.4	0.09	0.023	7.9
CCl_2CHCl	7.2	0.12	0.0091	3.1

[a]Calibration sensitivity = mV/min/(μmol/L). Calculated using the average calibration sensitivities in table 6.1.

[b]Calibration sensitivity relative to chloroform calibration sensitivity.

[c]Henry's law constant ($atm \cdot m^3/mol$), from ref. 25.

[d]Henry's law constant relative to chloroform Henry's law constant.

Analysis of Tap Water for Chloroform

Figure 6.13 shows the results of two standard additions analyses of tap-water for the determination of chloroform. The measured chloroform concentration is 23 ± 2 ng/mL (ppb). Analyses of duplicate samples by GC/MS gave 22 ± 0.9 ng/mL (ppb). Table 6.3 summarizes the results of the replicate analyses.

From the GC/MS analyses, bromodichloromethane was detected at 2.34 ng/mL ± 0.01 ng/mL, dibromochloromethane at 0.12 ng/mL ± 0.09 ng/mL, and bromoform was not detected (although no assessment of the detection limit was made, typical values range from 1-5 ng/mL). Thus, the presence of $CHBrCl_2$ and $CHBr_2Cl$ are predicted to give an apparent chloroform concentration ca. 1.2 ng/mL (ppb) higher than the true value (utilizing the relative calibration sensitivities listed in table 6.1) for the FOCS analysis. At these concentration levels, the error (for chloroform) due to these compounds is on the order of the imprecision in the FOCS or GC/MS measurements themselves. Overall, the agreement between the two methods is very good.

The ability to perform the standard additions analysis using a single 1.3 mL aliquot of reagent is demonstrated by comparing curves 6.13a and 6.13b; the average (calibration) slope for the two measurements is 1.04 mV/min/(ng/mL chloroform) with a RSD of 6%.

Figure 6.14 shows the strip-chart recorder tracing of the reservoir FOCS response obtained for the standard additions determination of chloroform performed using a single 1.3 mL aliquot of reagent (6.13a). The total measurement time was 30 min (including the blank measurement); the first chloroform injection was at ca. 11

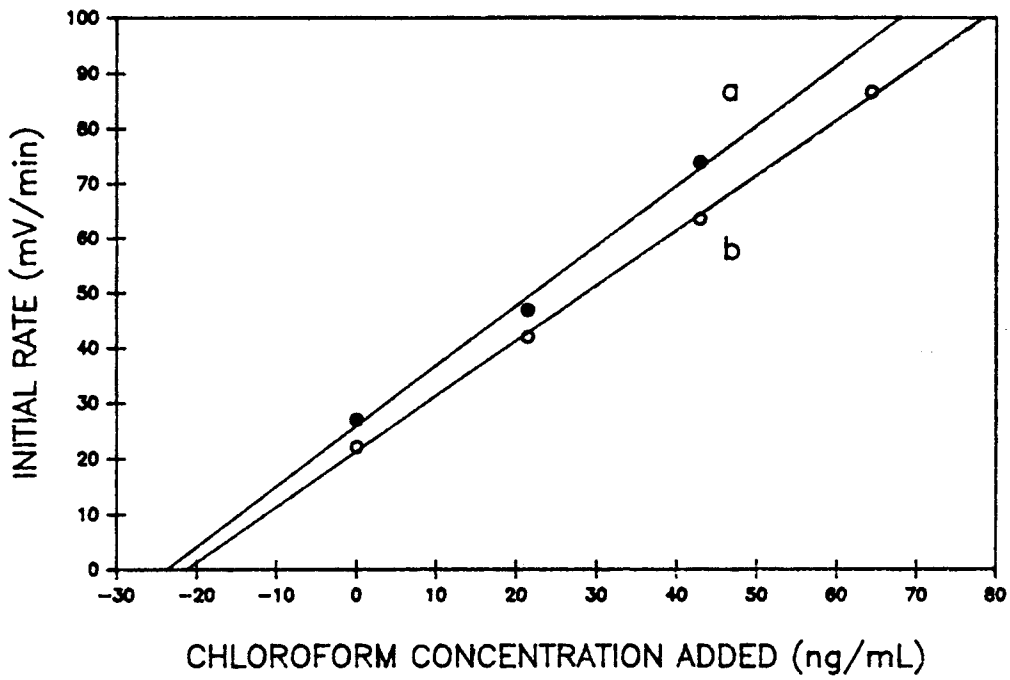

Figure 6.13. Standard addition analysis of laboratory tap-water for chloroform; (a) utilizing a single 1.3 mL volume of reagent (m = 1.09 mV/min/(ng/mL) with a standard error of 0.09 mV/min/(ng/mL)), (b) utilizing a new 1.3 mL aliquot of reagent for each point (m = 1.00 mV/min/(ng/mL) with a standard error of 0.02 mV/min/(ng/mL)).

Table 6.3. Summary of replicate THM analyses.

Compound	Concentration (ng/mL)			
	FOCS 1	FOCS 2	GC/MS 1	GC/MS 2
$CHCl_3$	21.4	23.8	21.5	22.8
$CHBrCl_2$	NA[a]	NA	2.33	2.35
$CHBr_2Cl$	NA	NA	0.19	0.06
$CHBr_3$	NA	NA	ND	ND

[a]Not analyzed.

[b]Not detected.

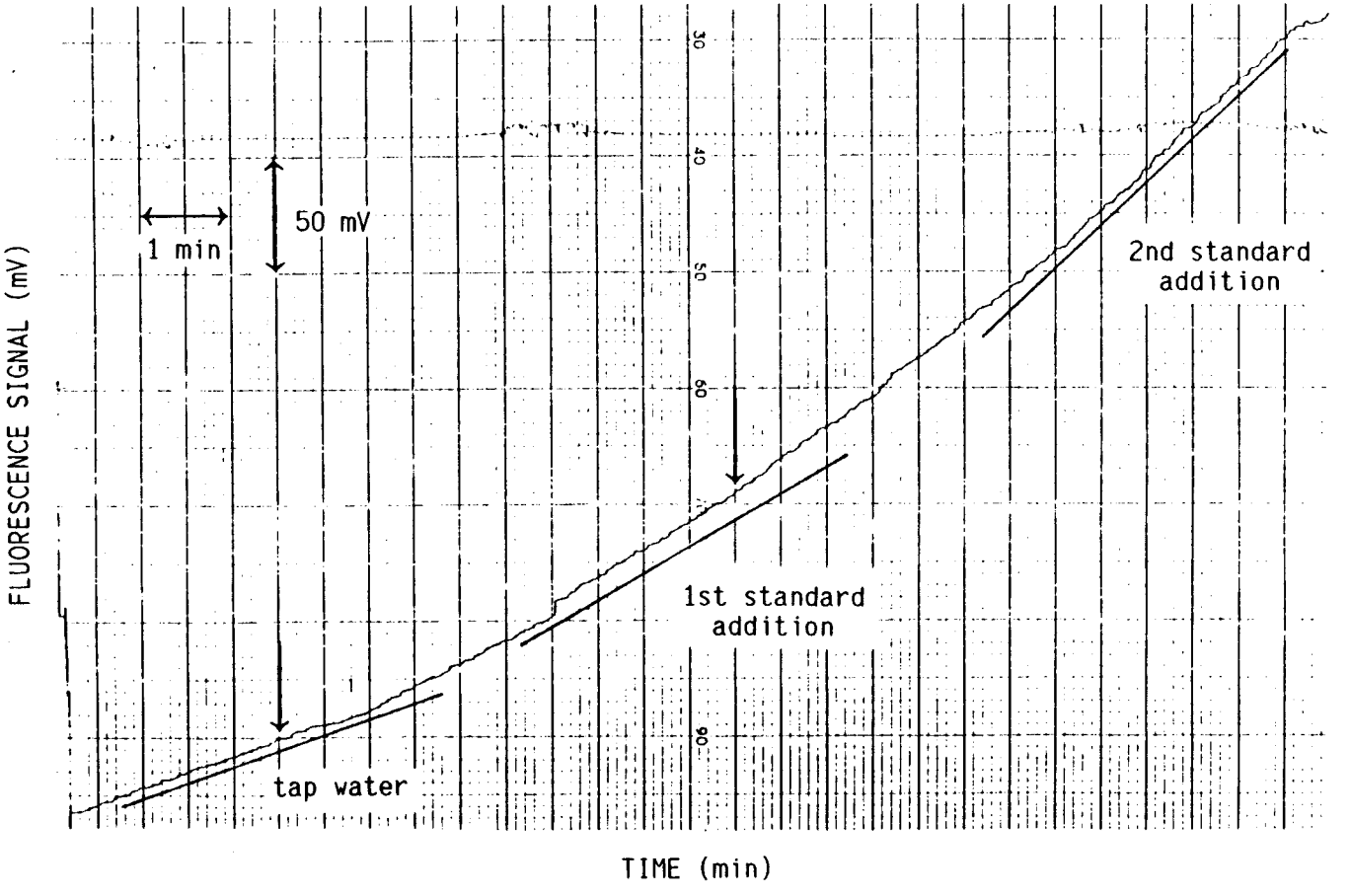

Figure 6.14. Strip-chart tracing of reservoir FOCS standard-additions analysis of tap water for the determination of chloroform. The arrows mark the two standard injections at $t \simeq 11$ min and $t \simeq 16$ min (the first ca. 9 min of the tracing are not shown).

min into the run and the second was at ca. 16 min. For both injections, the response time (time to observed steady rate) was ca. 3 min. At a chart speed of 2 cm/min, 2 min was a sufficient time period over which to measure accurately the reaction rate (mV/min); thus, total measurement time for each standard addition was ca. 5 min. The total time (purge time plus chromatographic program time) required for a single GC/MS analysis was ca. 45 min; the time required for the initial calibration was ca. 3 hr (4 analyses at 45 min each).

CONCLUSIONS

The two FOCSs developed in this research have been shown capable of detecting chloroform at sub-ppb (ng/mL) levels in laboratory experiments using stirred samples. In addition, the general utility of FOCS methodology for laboratory analyses has been demonstrated. The FOCS analysis of tap water for chloroform was carried out with minimal sample manipulation and no sample preconcentration. Overall, the (standard additions) FOCS determination of chloroform in drinking water was shown to be a viable alternative to more complex and costly GC and GC/MS methods (depending on the concentration levels of the other THMs).

The run-to-run reproducibility of the FOCS measurements on a given day with a given batch of reagent is reasonably good. This is clearly shown by the calibration sensitivities for chloroform listed in table 6.1, which exhibit an RSD of ca. 9% (0.52 ± 0.05 mV/min/(ng/mL chloroform)). The day-to-day reproducibility is affected by variability in the reagents responsivity (batch-to-batch), excitation power, optical alignment and condition of the fiber optics in the probe, and the rate of sample stirring. The standard addition procedure used compensates for most of these effects.

True remote-sensing applications require that a sensor be able to maintain an external calibration for extended periods of time. To increase long-term stability, the analytical signal should be ratioed to a reference signal to compensate for drifts in source power. For a FOCS, an ideal reference signal would also compensate for

fluctuations in fiber transmission (due to micro-bending, etc.) and coupling efficiency (source-to-fiber optic). To perform all these functions, the reference signal must be monitored at the detector end of the optical train. Potentially useful reference signals include the fiber optic Raman scatter of the excitation radiation and the transmission of a non-absorbed wavelength from the optical source.

A major problem associated with the probe used in this work is breakage of the fiber optics. The long-term reproducibility of FOCS measurements is adversely affected by the variability in the optical alignment of the fiber optics each time the probe is reassembled. Since, over time, breakage of the fiber optics is unavoidable, a more rugged probe configuration would improve long-term reproducibility. Although a single-fiber fiber optic probe would solve alignment problems, S/N and S/B considerations would most likely result in higher practical detection limits (20). A potentially useful probe might consist of two parallel fiber optics enclosed in a rigid tube. Although the signal levels obtained from such a probe would be ca. 50% less than those obtained from the 20° probe (28), it would be more rugged and allow for greater miniaturization of the total FOCS (without suffering from the drawbacks of a single-fiber probe). Properly designed multi-fiber fiber optic probes or probes utilizing fiber optic bundles should be able to provide signal levels at least as great as the probe used in this work (28,29) while also limiting alignment problems, and may be the optimum for use in FOCSs.

A factor limiting the utility of the reservoir FOCS for long-term monitoring is the relatively brief period of time over which a linear kinetic response is obtained (ca. 1 hr. for 10 ng/mL

chloroform). With the present design, the useful lifetime of sensor response can only be increased by sacrificing calibration sensitivity (17). This could be accomplished by decreasing the sampled surface area, by restricting analyte transport into the FOCS (by reducing the number or diameter of the sampling ports or incorporating a membrane), by changing the composition of the reagent mixture to reduce the reaction rate, or by using an excitation wavelength offset from the absorption maximum of the monitored species (d). Possibly the most attractive solution to this problem is to use the FOCSs as reported but monitoring absorbance and not fluorescence.

The feasibility of an absorbance-based FOCS determination of chloroform is demonstrated by figure 6.8a. From figure 6.8a, the calibration slope obtainable using the FOCS to monitor absorbance at 545 nm is on the order of 3×10^{-5} A.U./min/(ng/mL chloroform). This value is approximately 100 times greater than the calibration slope determined using the same reagent mixture, the same cuvette, and the same spectrophotometer with the cuvette-based continuous-exposure apparatus reported previously (see figure 5.16, ref 17). This increase in calibration slope is due solely to the increased rate of transfer of chloroform into the FOCS relative to the continuous-exposure apparatus.

Using a reagent mixture optimized for the spectrophotometric determination of chloroform at 368 nm, the detection limit for chloroform using the continuous-exposure apparatus is 11 ng/mL (17). Considering that the absorbance-based determination at 368 nm is ca. 4 times as sensitive as the absorbance-based determination at 545 nm (see figures 5.16 and 5.17, ref. 17), an FOCS absorbance-based (545

nm) determination of chloroform at sub ng/mL levels appears feasible.

Overall, the drop FOCS may be more useful for fluorescence based remote-sensing simply because it limits reagent consumption and is more amenable to remote reagent replacement. Utilizing a typical atomic absorption auto sampler it should be possible to precisely deliver 10 µL of reagent from a large reservoir to the remote sensor. The spent drop could be removed via a vacuum line.

Generally, the utility of the reported FOCSs for remote-sensing is limited by sample matrix variability, i.e., any parameter affecting sensor response (other than analyte concentration) must not fluctuate over the monitoring period in order to obtain accurate analyte quantitation. This fact is not unique to these sensors but is equally applicable to the vast majority of FOCSs reported to date.

For in-situ (remote-sensing) analyses the rate of sample mixing will be dependent on the nature of the sample itself. Generally, the mixing rates for ground water will be of less consequence than for surface waters or process streams. Although the data presented in this work were obtained using stirred samples, the stirring rate employed provided only an approximate factor of 2 increase in signal over non-stirred samples. Thus, the reported detection limits are within a factor of two of those which should be achievable without stirring.

An additional factor to consider for remote-sensing applications is sample temperature. For accurate quantitation, the FOCS must be calibrated at the temperature of the matrix to be tested, which itself must remain constant over the time period monitored.

REFERENCES

1. Louch, J.L. "Fiber Optic Chemical Sensors for the Detection of Volatile Gem-Polyhalogenated Hydrocarbons" 1991, Ph.D. Thesis, Oregon State University, Chap. 2.

2. National Interim Primary Drinking Water Regulations: Control of Trihalomethanes in Drinking Water Federal Register 1979, 44 (231), 68624-68683.

3. List (Phase 1) of Hazardous Constituents for Ground-Water Monitoring Federal Register 1987, 52 (131), 25942-25953.

4. Drinking Water; Substitution of Contaminants and Drinking Water Priority List of Additional SUbstances Which may Require Regulation Under the Safe Drinking Water Act Federal Resister 1988, 53 (14), 1892-1902.

5. Notice of the First Priority List of Hazardous Substances That Will Be the Subject of Toxicological Profiles Federal Register 1987, 52 (74), 12865-12874.

6. Hazardous Waste Management Systems; Permitting Requirements for Land Disposal Facilities Federal Register 1982, 47 (143), 32273-32388.

7. Warner, B.J.; Cheng, S.C.; Friedman, C.S.; Mitrosky, S.; Snyder, A.D.; McMillin, C.R. "EPA Method Study 23A, Method 501.1, Trihalomethanes by Purge and Trap" 1984, EPA-600/4-84-020.

8. Warner, B.J.; Cheng, S.C.; Finke, J.M.; Friedman, C.S.; Mitrosky, S.; Snyder, A.D.; McMillin, C.R. "EPA Method Study 23B, Method 501.2, Trihalomethanes by Liquid/Liquid Extraction" 1984, EPA-600/4-84-021.

9. Measurement of Trihalomethanes in Drinking Water with Gas Chromatography/Mass Spectrometry and Selected Ion Monitoring Method 501.3, EPA form 1320-4 (Rev. 3-76).

10. Guidlines Establishing Test Procedures for the Analysis of Pollutants Under the Clean Water Act; Final Rule and Interim Final Rule and Proposed Rule Federal Register 1984, 49 (209), 43233-43436.

11. Early, J.D. J. Environ. Health 1987, 50, 33-34.

12. Miller, K.J. WATER/ Engrg. and Management Feb. 1988, 30-32.

13. Milanovich, F.P. Environ. Sci. Technol. 1986, 20 (5), 441-442.

14. Milanovich, F.P.; Daley, P.F.; Klainer, S.M. Anal. Instrum. 1986, 15 (4), 347-358.

15. Herron, N.R.; Simon, S.J.; Eccles, L. Anal. Instrum. 1989, 18 (2), 107-126.

16. Fujiwara, K. Sitz. Nat. Ges. Rostock 1916, 6, 33.

17. Louch, J.L. "Fiber Optic Chemical Sensors for the Detection of Volatile Gem-Polyhalogenated Hydrocarbons" 1991, Ph.D. Thesis, Oregon State University, Chap. 5.

18. ibid, Chap. 4.

19. Ingle, Jr.; Crouch, S.R. "Spectrochemical Analysis", Prentice Hall, Englewood Cliffs, 1988, 438-493.

20. Louch, J.L. "Fiber Optic Chemical Sensors for the Detection of Volatile Gem-Polyhalogenated Hydrocarbons" 1991, Ph.D. Thesis, Oregon State University, Chap. 3.

21. Dilling, W.L. Environ. Sci. Technol. 1977, 11 (4), 405-409.

22. Reith, J.F.; Van Ditmarsch, W.C.; De Ruiter, Th. Analyst 1974, 99, 652-658.

23. Lugg, G.A. Anal. Chem. 1966, 38 (11), 1532-1536.

24. Leibman, K.C.; Hindman, J.D. Anal. Chem. 1963, 35 (9), 348-351.

25. Pankow, J.F. and Rosen, M.E. Environ. Sci. Technol. 1988, 22 (4), 398-405.

26. Symons, J.M.; Bellar, T.A.; Carswell, J.K.; DeMarco, J.; Kropp, K.L.; Robeck, G.G.; Seeger, D.R.; Slocum, C.J.; Smith, B.L.; Stevens, A.A. Jour. AWWA 1975, 67 (11), 634-647.

27. Louch, J.L. "Fiber Optic Chemical Sensors for the Detection of Volatile Gem-Polyhalogenated Hydrocarbons" 1991, Ph.D. Thesis, Oregon State University, Appendix I.

28. Plaza, P.; Dao, N.Q.; Jouan, M.; Feurier, H.; Saisse, H. Appl. Optics 1986, 25, 3448-3454.

29. McCreery, R.L.; Fleishmann, M.; Hendra, P. Anal. Chem. 1983, 146-148.

CHAPTER 7

FINAL CONCLUSIONS

The development and implementation of methodology for spectrometric remote-sensing with fiber optics is a complex endeavour. The work reported in this thesis comprises studies of the basic instrumental and chemical aspects of such methodology and forms the basis for a long-term research program for the development and field deployment of fiber optic chemical sensors (FOCS).

The fluorescence collection efficiency of the basic single- and double-fiber optic probe configurations have been characterized. Although the single-fiber probe can provide a signal level ca. 50% greater than the double-fiber probe, attenuation resulting from the necessary coupling optics associated with the single-fiber configuration and the decreased S/B (relative to the double-fiber probe) result in no net improvement in detection limits over double-fiber probes. In fact, when high excitation powers and wide emission bandpasses are used to increase fluorescence signal levels and improve detection limits, the double-fiber configuration yields better detectability when background noise is limiting.

The absolute fluorescence signal and the relative fluorescence collection efficiency of a simple double-fiber probe is shown to be approximately one fifth that of a typical right-angle cuvette fluorometer. In addition, the predictive capabilities of the theories of both Deaton (1) and Plaza (2) for the estimation of numerical values of the effective fluorescence collection

efficiencies for both single- and double-fiber probes (to within a factor of two) is demonstrated.

The overall detectability of a fiber optic fluorometer using a simple double-fiber probe is shown to be comparable to that of a cuvette-based fluorometer. From the theory of Plaza (2), further optimization of the probe is predicted to provide a further increase in effective fluorescence collection efficiency (relative to the simple double-fiber probe) resulting in detection limits lower than those achievable with traditional cuvette-based fluorometers or spectrofluorometers. Overall, the use of fiber optics in place of traditional line-of-sight optical trains does not adversely affect calibration sensitivity and results in increased flexibility in instrumental design.

The proposed mechanistic pathways for the Fujiwara reaction with chloroform provide a framework for understanding the optimization of Fujiwara-type reagent mixtures, and the single-phase Fujiwara reagent mixtures optimized for both spectrophotometric and fluorometric detection of gem-polyhalogenated hydrocarbons were shown to yield good analytical performance characteristics. In addition, the model for continuous-monitoring via detection of a transient species developed using first-order kinetics should be generally useful for the continued development of FOCSs.

A unique apparatus for the spectrophotometric detection of volatile species using cuvette-based spectrophotometers was constructed. With the single-phase spectrophotometric reagent mixture the spectrophotometric detection limit for chloroform is 11 ng/mL. The feasibility of quantitating chloroform in finished

drinking water using this methodology is demonstrated. Optimization of the continuous-exposure apparatus to improve detection limits is limited by constraints resulting from use of a cuvette.

Two FOCSs have been developed for the fluorometric detection of chloroform using the single-phase, fluorometric Fujiwara reagent. Both sensors are capable of detecting chloroform at sub-ng/mL levels. Studies show that FOCS reactor design factors such as the sample surface area, the cross-sectional area for vapor phase transport, and the reagent A_S/V strongly affect the resulting calibration sensitivity. All these factors make optimization of a cuvette-based reactor complex and demonstrate the increased flexibility in instrumental design afforded by use of fiber optics. Evaluation of the "reservoir" FOCS with a number of volatile gem-polyhalogenated hydrocarbons showed that the primary interferences are other trihalomethanes and trichloroethylene. With the same FOCS, the concentration of chloroform in laboratory drinking water was determined to be 23 ± 1.7 ng/mL; confirmatory analysis by GC/MS gave 22 ± 0.9 ng/mL. For this specific sample, the error in the reported chloroform concentration due to the presence of the other trihalomethanes is on the order of the imprecision in the analytical measurements and does not significantly affect quantitation.

As a result of the work presented in this thesis, a number of future studies are suggested. An integral component of the reported FOCSs is the double-fiber probe of the fiber optic fluorometer. Two characteristics of the probe which might be further optimized are the fluorescence collection efficiency (to improve calibration

sensitivity) and the ruggedness (to limit breakage). Studies to compare the fluorescence collection efficiencies of fiber optic probes with a wide range of different geometries could be carried out as per the procedures outlined in chapter 3 or chapter 4. For the initial study, the excitation fiber should be the same in all experiments while the number, orientation, and f-number of the collection fibers are varied. This ensures that the excitation power reaching the sample remains constant and that any variability in the observed fluorescence signal is due solely to changes in the collection efficiency. A parallel study would be optimization of probe geometries for absorption measurements; because of their simplicity and the potential for unlimited pathlength, this study should include single-path evanescent probe geometries.

The feasibility of absorption-based FOCS monitoring should be explored thoroughly. The main advantages of this approach over fluorescence-based monitoring are freedom from inner-filter effects which presently limit the dynamic range and a reduced dependency of calibration sensitivity on source intensity at the sample. This second fact might allow absorption-based monitoring at 368 nm even considering the increased fiber optic attenuation at this wavelength (relative to 545 nm). Because single-phase Fujiwara reagents suitable for spectrophotometric detection of chloroform (and other gem-polyhalogenated hydrocarbons) at 368 and 545 nm have been developed, this work would focus on modifying the instrumental electronics for absorption measurements and finding the optimum probe geometry (providing the maximum pathlength).

As a compliment to the above studies, the performance of the

cuvette-based continuous-exposure apparatus could be more thoroughly characterized. The level of error in a spectrophotometric (at 368 nm) determination of chloroform in tap water resulting from the presence of bromodichloromethane, dibromochloromethane, and bromoform should be determined experimentally. In addition, the apparatus could be used with the reported fluorometric reagent in a cuvette-based spectrofluorometer for the fluorometric detection of chloroform. Using Wilson's spectrofluorometer (3), the excitation and emission monochromators could be rotated to give a horizontal slit geometry. This would allow a reduction in reagent volume (in the cuvette) and a corresponding increase in the reagent volume A_s/V. This, coupled with the increased efficiency of the horizontal slit geometry (relative to a vertical slit arrangement) should provide better detection limits for chloroform.

Fully interfacing the fiber optic instrumentation with a computer would be useful. QuickBASIC code has already been written for computer control of the emission monochromator and data acquisition. Further software development allowing rate calculations from the raw data stored by the computer would likely improve overall precision relative to the present method of drawing a tangent to a chart recorder tracing. Furthermore, computer control would facilitate the used of multi-channel detection schemes, i.e., diode array (or intensified diode array), multiple emission filter-wheel, etc. These types of detection schemes are advantageous as they facilitate multi-wavelength measurements for the purpose of signal ratioing (reference signal) or multi-parametric analysis (i.e., monitoring more than one species at multiple wavelengths).

Further studies to characterize the specificity of the Fujiwara reagent for different compounds should be performed. Initial studies would focus on characterizing the response of the reported reagent mixtures to all the volatile compounds listed in table 1.1. These experiments could be carried out in a manner analogous to those reported in chapter 6. A more detailed mechanistic investigation of the Fujiwara reaction may be necessary to understand more fully how to improve selectivity for specific species. It might be possible to improve selectivity through modification of the reagent mixture composition. A more complete kinetic model of the reaction with chloroform (including the competing reaction pathways shown in figures 5.5 and 5.6) would be of use in further understanding the effects of factors such as solvent dielectric, etc., on the observed reaction rates.

The reported FOCSs have not been tested in true remote-sensing applications. In order to do this, field-deployable instrumentation has to be constructed. For long-term on-site continuous-monitoring applications, a gas-powered portable electric generator would allow field use of the instrumentation as reported in this thesis. However, the current requirements of the arc-lamp radiation source may limit the utility of this instrumentation in a truly portable instrument. The reduced need for high-intensity radiation sources for absorption-based measurements should simplify construction of portable, field-deployable instrumentation.

The ability of the FOCS to hold an external calibration has to be improved. Probably the most critical factor in this respect is the selection of a reference signal which accurately reflects source

power and fiber optic attenuation. The ability to simultaneously monitor more than one wavelength at the detection end of the optical train is desirable for this purpose. The reference signal monitored could be a non-absorbed wavelength component of the source radiation (generated by use of an excitation filter wheel for example) or the fiber optic Raman scattering of the source radiation.

Although the initial purpose of this work was to develop FOCSs for use in remote-sensing applications, it is apparent that sensor methodology is also quite useful in the laboratory. This is demonstrated by the reported analysis of tap water for the determination of chloroform. The detection limits obtained for chloroform using both the reported FOCSs are comparable with those achievable with more complex and costly GC and GC/MS analyses. The ability to optimize the design of the FOCS reactors (to maximize calibration sensitivity) is a direct result of the use of fiber optics.

REFERENCES

1. Deaton, T. "Instrumentation and Methodology for Remote Fiber Fluorometry" 1984, Ph.D. Thesis, Univ. Calif. Davis.

2. Plaza, P; Dao, N.Q.; Jouan, M.; Feurier, H.; Saisse, H. Appl. Optics 1986, 25, 3448-3454.

3. Wilson, R.L. "Design, Development and Optimization of a Fluorometric Reaction-Rate Instrument and Method of Analysis for Metal Ions" 1977, Ph.D. Thesis, Oregon State University.

BIBLIOGRAPHY

Abramovitch, R.A.; Singer, G.M. in Abramovitch, R.A., Editor, "Pyridine and its Derivatives", Interscience, N.Y., 1974, Chapt. 1A.

Aggarwal, I.D. in Daly, J.C., Editor, "Fiber Optics", CRC Press, Boca Raton, 1984, 21-50.

Alarcon, M.C., Ito, H., Inaba, H. Appl. Phys. B 1987, 43, 79-83.

Alder, J.F. Fresenius Z. Anal. Chem. 1986, 324, 372-375.

Alder, J.F.; Ashworth, D.C.; Narayanaswamy, R.; Moss, R.E.; Sutherland, O. Analyst 1987, 112, 1191-1192.

Allport, N.L.; Keyser, J.W. "Colorimetric Analysis", Chapman and Hall, London, 1957.

Andrade, J.D.; Vanwagenen, R.A.; Gregonis, D.E.; Newby, K. Lin, J.N. IEEE Tans. Electron Devices 1985, ED-32, 1175-1179.

Angel, S.M. Spectroscopy (Springfield, OR) 1987, 2 (4), 38-48.

Angel, S.M.; Daley, P.F.; Langry, K.C.; Kulp, T.J.; Camins, I. "The Feasibility of Using Fiber Optics for Monitoring Groundwater Contaminants: VI. Mechanistic Evaluation of the Fujiwara Reaction for the Detection of Organic Chlorides" 1987, EPA/600/X-87/467.

Arnold, M.A. Anal. Chem. 1985, 57, 565-566.

Arnold, M.A.; Oster, T.J. Anal. Chem. 1986, 58, 1137-1140.

Arnold, M.A. (Ed.) Talanta 1988, 35 (2).

Bartos, J.; Pesez, M. Talanta 1972, 19, 93-124.

Basch, E.E.; Carnes, H.A. in Daly, J.C., Editor, "Fiber Optics", CRC Press, Boca Raton, 1984, 151-181.

Benaim, N.; Grattan, K.T.V.; Palmer, A.W. Analyst 1986, 111, 1095-1097.

Benner, R.E.; Chang, R.K. in Bendow, B. and Mitra, S.S., Editors, "Fiber Optics: Advances in Research and Development", Plenum Pree, N.Y., 1979, 625-640.

Boisde, R.E.; Blanc, F.; Perez, J. Talanta 1988, 35, 75-82.

Boisde, R.E.; Perez, J. in Kersten, R.Th. & Kist, R., Editors, "Proc. 2nd Intl. Conf. on Optical Sensors", VDE-Verlag GmbH, Berlin, 1984, 227-231.

Boltz, D.F.; Howell, J.A. "Colorimetric Determinations of Nonmetals", J. Wiley & Sons, N.Y., 1978.

Borman, S.A. Anal. Chem. 1981, 53, 1616A-1618A.

Bower, N.W.; Ingle, Jr., J.D. Anal. Chem. 1975, 47, 2069-2072.

Bowers, L.D.; Bostick, W.D. in Frei, R.W. and Lawrence, J.F., Editors, "Chemical Derivatization in Analytical Chemistry, Volume 2: Separation and Continuous Flow Techniques", Plenum Press, N.Y., 1982, 97-143.117. Lawrence, J.F. ibid, 191-242.

Bright, F.V.; Poirier, G.E.; Hieftje, G.M. Talanta 1988, 35, 113-118.

Bromberg, J.P. "Physical Chemistry", Allyn and Bacon, Boston, 1980, 814-815.

Brown, R.G.W. J. Phys. E: Sci. Instrum. 1987, 20, 1312-1320.

Bruylants, A.; Feytmants-de Medicis, E. in Pati, S., Editor, "The Chemistry of the Carbon Nitrogen Double Bond", Interscience, N.Y., 1970, 465-502.

Caglar, P.; Narayanaswamy, R. Analyst 1987, 112, 1285-1288.

Carnes, H.; Kearns, R.; Basch, E. in Basch, E.E., Editor, "Optical Fiber Transmission", H.W. Sams & Co., Indianapolis, 1987, pp 475.

Carr, P.W.; Bowers, L.D. "Immobilized Enzymes in Analytical and Clinical Chemistry", J. Wiley & Sons, N.Y., 1980, 148-196.

Chabay, I. Anal. Chem. 1982, 54, 1071A-1080A.

Chan, K.; Ito, H.; Inaba, H. Appl. Optics 1984, 23, 3415-3420.

Cheo, P.K. "Fiber Optics; Devices and Systems", Prentice-Hall, Englewood Cliffs, 1985, 63-88.

Christian, L.M.; Seitz, W.R. Talanta 1988, 35, 119-122.

Chudyk, W.A.; Carrabba, M.M.; Kenny, J.E. Anal. Chem. 1985, 1237-1242.

Chudyk, W.A.; Kenny, J.; Jarvis, G.; Pohlig, K. "Proc. of ISA (Advances in Instrumentation)", 1986, 41, 1237-1243.

Chudyk, W.A.; Kenny, J.; Jarvis, G.; Pohlig, K. InTech 1987, 53-57.

Coleman, J.T.; Eastham, J.F.; Sepaniak, M.J. Anal. Chem. 1984, 2246-2249.

Culshaw, B. "Optical Fibre Sensing and Signal Processing", Peter Peregrinus Ltd., London, 1984, pp 15.

Culshaw, B. "Optical Fibre Sensing and Signal Processing", Peter Peregrinus Ltd., London, 1984, 133-145.

Dahne, C.; Sutherland, R.M.; Place, J.F.; Ringrose, A.S. SPIE Vol. 514, "Conf. Proc. 2nd Intern. Conf. Opt. Fiber Sensors (1984); Stuttgart, FR Ger., 75-79.

Dakin, J.P. SPIE Vol. 375, "Fiber Optics '83" (1983), 172-177.

Dakin, J.P.; King, A.J. "IEE Conf. Publ. (Opt. Fibre Sens.)", 1983, 221, 195-199.

Dakin, J.P.; King, A.J. "IEE Colloquium on Optical Fibre Sensors", 1982, 1-3.

Daly, J.; Lakshmanasamy, S. in Basch, E.E., Editor, "Optical Fiber Transmission", H.W. Sams and Co., Indianapolis, 1987, 9-24.

David, D.J.; Wilson, M.C.; Ruffin, D.S. Anal. Lett. 1976, 9, 389-404.

Deaton, T., "Instrumentation and Methodology for Remote Fiber Fluorometry" 1984, Ph.D. Thesis, Univ. of Calif. Davis.

DeGrandpre, M.D.; Burgess, L.W. Anal. Chem. 1988, 60, 2582-2586.

Desiderio, R. Oregon State University, Personal Communication, 1989.

Dilling, W.L. Environ. Sci. Technol. 1977, 11 (4), 405-409.

Drexhage, M.G.; Moynihan, C.T. Scientific American Nov. 1988, 110-116.

Drinking Water; Substitution of Contaminants and Drinking Water Priority List of Additional Substances Which May Require Regulation Under the Safe Drinking Water Act Federal Register 1987, 52 (130), 25720-25734.

Drinking Water; Substitution of Contaminants and Drinking Water Priority List of Additional Substances Which May Require Regulation Under the Safe Drinking Water Act Federal Register 1988, 53 (14), 1892-1902.

Ealing Electro Optics Guide 1986, 222.

Earley, J.D. J. Environ. Health 1987, 50, 33-34.

Edmonds, T.E.; Flatters, N.J.; Jones, C.F.; Miller, J.N. Talanta 1988, 35, 103-107.

Enson, Y.; Briscoe, W.A.; Polanyi, M.L.; Cournand, A. J. Appl. Physiol. 1962, 17, 552-558.

Feigl, F. "Spot Tests in Organic Analysis", Elsevier, N.Y., 1966.

Feigl, F. "Spot Tests in Inorganic Analysis", Elsevier, N.Y., 1972.

Freeman, J.E.; Childers, A.G.; Steele, A.W.; Hieftje, G.M. Anal. Chim. Acta 1985, 177, 121-128.

Fuh, M.S.; Burgess, L.W.; Hirschfeld, T.; Christian, G.D.; Wang, F. Analyst 1987, 112, 1159-1163.

Fuh, M.S.; Burgess, L.; Christian, G.D. Anal. Chem. 1988, 60, 433-435.

Fujiwara, K. Sitz. Nat. Ges. Rostock 1916, 6, 33.

Gallawa, R.L. Electro-opt. Sys. Des. April 1982, 46-54.

Gamble, W.J.; Hugenholtz, P.G.; Monroe, R.G.; Polyani, M.; Nadas, A.S Circulation 1965, 31, 328-343.

Garcia, E.E.; Greco, C.V.; Hunsberger, I.M. J. Amer. Chem. Soc. 1960, 82, 4430-4431.

Gehrich, J.L.; Lubbers, D.W.; Opitz, N.; Hansmann, D.R.; Miller, W.W.; Tusa, J.K.; Yafuso, M. IEEE Trans. Biomed. Eng. 1986, BME-33, 117-132.

Giuliani, J.F.; Wohltjen, H.; Jarvis, N.L. Optics Letters 1983, 8, 54-56.

Goldstein, S.R.; Peterson, J.I.; Fitzgerald, R.V.; J. Biomech. Eng. 1980, 102, 141-146.

Gomez-Hens, A.; Valcarcel, M. Analyst 1982, 1274, 465-494.

Guidelines Establishing Test Procedures for the Analysis of Pollutants Under the Clean Water Act; Final Rule and Interim FInal Rule and Proposed Rule Federal Register 1984, 49 (209), 43233-43436.

Guthrie, A.J.; Narayanaswamy, R.; Russell, D.A. Analyst 1988, 113, 457-461.

Hardy, E.E.; David, D.J.; Kapany, N.S.; Unterleitner, F.C. Nature 1975, 257, 666-667.

Harmer, A.L. in Kersten, R.Th. and Kist, R., Editors, "Proc. of

the 2nd Intl. Conf. on Optical Sensors", VDE-Verlag GmbH, Berlin, 1984, 17-22.

Harmer, A.L.; Narayanaswamy, R. in Edmonds, T.E., Editor, "Chemical Sensors", Chapman and Hall, N.Y., 1988, 275-294.

Harrick, N.J. "Internal Reflection Spectroscopy", Wiley, N.Y., 1968.

Hazardous Waste Management Systems; Permitting Requirements for Land Disposal Facilities Federal Register 1982, 47 (143), 32273-32388.

Herron, N.R.; Simon, S.J.; Eccles, L. Anal. Instrum. 1989, 18 (2), 107-126.

Hertz, H.S.; May, W.E.; Wise, S.A.; Chesler, S.N. Anal. Chem. 1978, 50, 428A-436A.

Hine, J. J. Amer. Chem. Soc. 1950, 72, 2438-2445.

Hirschfeld, T. Appl. Spectrosc. 1977, 31 (3), 245.

Hirschfeld, T.; Deaton, T.; Milanovich, F.; Klainer, S. Opt. Eng. 1983, 22, 527-531.

Hirschfeld, T.; Deaton, T.; Milanovich, F.; Klainer, S.M. "The Feasibility of Using Fiber Optics for Monitoring Groundwater Contaminants" 1983, U.C.I.D.-19774, Lawrence Livermore Laboratory.

Hirschfeld, T. Fresenius Z. Anal. Chem. 1986, 324, 618-624.

Hirschfeld, T. InTech Feb. 1986, 45-50.

Hugenholtz, P.G.; Gamble, W.J.; Monroe, R.G.; Polyani, M. Circulation 1965, 31, 344-355.

Inaba, H, Chan, K.; Ito, H. SPIE Vol. 514, Conf. Proc. 2nd Intern. Conf. Opt. Fiber Sensors (1984); Stuttgart, FR Ger., 211-214.

Ingle, Jr., J.D.; Crouch, S.R. "Spectrochemical Analysis", Prentice Hall, Englewood Cliffs, 1988.

Issacs, E.D.; Heiman, D. Rev. Sci. Instrum. 1987, 58, 1672-1674.

Janata, J. Anal. Chem. 1987, 59, 1351-1356.

Janata, J.; Bezegh, A. Anal. Chem. 1988, 60, 62R-74R.

Jordan, D.M.; Walt, D.R.; Milanovich, F.P. Anal. Chem. 1987, 59, 437-439.

Jorgensen, B.B.; Des Marais, D.J. Limnol. Oceanogr. 1988, 33, 99-113.

Kapany, N.S.; Silbertrust, N. Nature 1964, 204, 138-142.

Kawahara, F.K.; Fiutem, R.A.; Silvus, H.S.; Newman, F.M.; Frazar, J.H. Anal. Chim. Acta. 1983, 151, 315-327.

Kirkbright, G.F.; Narayanaswamy, R.; Welti, N.A. Analyst 1984, 109, 1025-1028.

Kirkbright, G.F.; Narayanaswamy, R.; Welti, N.A. Analyst 1984, 109, 15-17.

Kobayasi, T.; Hirama, M.; Inaba, H. Appl. Optics 1981, 20, 3279-3280.

Kricka, L.J. "Ligand-Binder Assays", Marcel Dekker, N.Y., 1985, 125-164.

Krull, U.J.; Brown, S. in Measures, R.M., Editor, "Laser Remote Chemical Analysis", J. Wiley and Sons, N.Y., 1988, 505-532.

Kychakoff, G.; Kimball-Linne, M.; Hanson, R.K. Appl. Optics 1983, 22, 1426-1428.

Lee, E.D.; Werner, T.C.; Seitz, W.R. Anal. Chem. 1987, 59, 279-283.

Leenheer, J.A. in Minear, R.A. and Keith, L.H., Editors, "Water Analysis; Vol. 3, Organic species", Academic Press, N.Y., 1984, 83-158.

Leibman, K.C.; Hindman, J.D. Anal. Chem. 1963, 35 (9), 348-351.

Lieberman, S.H.; Inman, S.M.; Stromvall, E.J. Proc. Electrochem. Soc. 1987,(Proc. Sym. Chem. Sens.), 464-475.

Lippitsch, M.E.; Pusterhufer, J.; Leiner, M.J.P.; Wolfbeis, O.S. Anal. Chim. Acta. 1988, 205, 1-6.

List (Phase 1) of Hazardous Constituents for Ground-Water Monitoring Federal Register 1987, 52 (131), 25942-25953.

Lonsdale, H.K. J. Memb. Sci. 1982, 10, 81-181.

Louch, J.R.; Ingle, Jr., J.D. Anal. Chem. 1988, 60, 2537-2540.

Lowry, T.H.; Richardson, K.S. "Mechanism and Theory in Organic Chemistry", Harper and Row, N.Y., 1981, 248-250.

Lugg, G.A. Anal. Chem. 1966, 38, 1532-1536.

Lund, T. "IEE Conf. Publ. (Optical Fibre Sensors)", 1983, 221, 190-194.

Luo, S.; Walt, D.R. Anal. Chem. 1989, 61, 174-177.

Marcuse, D. "Principles of Optical Fiber Measurement", Academic Press, N.Y., 1981, 11-67.

Mark, H.B., Jr. Talanta 1972, 19, 717-746.

Marr, I.L.; Cresser, M.S. "Environmental Chemical Analysis", Chapman and Hall, N.Y., 1983, 24-33.

Maugh. T.H. Science 1982, 218, p. 875.

Mayevsky, A.; Chance, B. Science 1982, 217, 537-540.

McCarthy, B.; Hood, W.B.; Lown, B. J. Appl. Physiol. 1967, 23, 641-645.

McCreery, R.L.; Fleishmann, M.; Hendra, P. Anal. Chem. 1983, 55, 146-148.

Meadows, D.; Schultz, J.S. Talanta 1988, 35, 145-150.

Measurement of Trihalomethanes in Drinking Water with Gas Chromatography/Mass Spectrometry and Selected Ion Monitoring, Method 501.3, EPA form 1320-4 (Rev. 3-76).

Midwinter, J.E. "Optical Fibers for Transmission", John Wiley and Sons, N.Y., 1979, 87-90.

Midwinter, J.E. "Optical Fibers for Transmission", John Wiley and Sons, N.Y., 1979, 128-157.

Milano, M.J.; Kim, K. Anal. Chem. 1977, 49, 555-559.

Milanovich, F.P. Environ. Sci. Technol. 1986, 20 (5), 441-442.

Milanovich, F.P.; Daley, P.F.; Klainer, S.M.; Eccles, L. Anal. Instrum. 1986, 15 (4), 347-358.

Milanovich, F.P.; Hirschfeld, T. InTech March 1984, 33-36.

Milanovich, F.P.; Hirschfeld, T. Adv. in Instrum. 1983, 38, 407-418.

Miller, J.N. "Standards in Fluorescence Spectrometry", Chapman and Hall, London, 1981, p. 81.

Miller, K.J. WATER/Engrg. and Management Feb. 1988, 30-32.

Mitchell, D.G.; Garden, J.S.; Aldous, K.M. Anal. Chem. 1976, 48, 2275-2277.

Munkholm, C.; Milanovich, F.P.; Klainer, S.M. Anal. Chem. 1986, 58, 1427-1430.

Munkholm, C.; Walt, D.R.; Milanovich, F.P. Talanta 1988, 35, 109-112.

Narayanaswamy, R.; Russell, D.A.; Sevilla, F. Talanta 1988, 35, 83-88.

Narayanaswamy, R.; Sevilla, F. J. Phys. E: Sci. Instrum. 1988, 21, 10-17.

Narayanaswamy, R.; Sevilla, F. Analyst 1988, 113, 661-663.

National Interim Primary Drinking Water Regulations: Control of Trihalomethanes in Drinking Water; Final Rule Federal Register 1979, 44 (231), 68624-68683.

Newby, K.; Reichert, W.M.; Andrade, J.D.; Benner, R.E. Appl. Optics. 1984, 23, 1812-1815.

Notice of the First Priority List of Hazardous Substances That Will Be the Subjecty of Toxicological Profiles Federal Register 1987, 52 (74), 12865-12874.

Okazaki, T.; Imasaka, T.; Ishibashi, N. Anal. Chim. Acta. 1988, 209, 327-331.

Oldham, P.B.; Patonay, G.; Warner, I. Rev. Sci. Instrum. 1985, 56, 297-302.

Pankow, J.F.; Rosen, M.E. Environ. Sci. Technol. 1988, 22, 398-405.

Paul, P.H.; Kychakoff, G. Appl. Phys. Lett. 1987, 51, 12-14.

Peterson, J.I.; Fitzgerald, R.V.; Buckhold, D.K. Anal. Chem. 1984, 56, 62-67.

Peterson, J.I.; Goldstein, S.R.; Fitzgerald, R.V.; Buckhold, D.K. Anal. Chem. 1980, 52, 864-869.

Peterson, J.I.; Vurek, G.G. Science 1984, 102, 123-127.

Petrea, R.D.; Sepaniak, M.J.; Vo-Dinh, T. Talanta 1988, 35, 139-144.

Plaza, P.; Dao, N.Q.; Jouan, M.; Fevrier, H.; Saisse, H. Appl. Optics 1986, 25, 3448-3454.

Polanyi, M.L.; Hehir, R.M. Rev. Sci. Instrum. 1962, 33, 1050-1054.

Posch, H.E.; Wolfbeis, O.S.; Pusterhofer, J. Talanta 1988, 35, 89-94.

Pratt, H.R.C. in Lo, T.C.; Baird, M.H.I.; Hanson, C. Editors "Handbook of Solvent Extraction", J. Wiley & Sons, N.Y., 1983, 91-123.

Ratzlaff, E.H.; Harfman, R.G.; Crouch, S.R. Anal. Chem. 1984, 56, 342-347.

Raychem Corp. 1981, #H51157.

RCA 1P28 Specification Sheet, AUg. 1975.

Reichert, W.M.; Ives, J.T.; Suci, P.A. Appl. Spec. 1987, 41, 1347-1350.

Reith, J.F.; van Ditmarsch, W.C.; Ruiter, T.H. Analyst 1974, 99, 652-656.

Rook, J.J. Water Treat. Exam. 1974, 23, 234-243.

Russell, A.P.; Fletcher, K.S. Anal. Chim. Acta. 1985, 170, 209-216.

Saari, L.A.; Seitz, W.R. Anal. Chem. 1982, 54, 821-823.

Saari, L.A.; Seitz, W.R. Anal. Chem. 1983, 55, 667-670.

Saari, L.A.; Seitz, W.R. Analyst 1984, 109, 655-657.

Saari, L.A.; Seitz, W.R. Anal. Chem. 1984, 56, 810-813.

Saturday, K.A. Anal. Chem. 1983, 55, 2459-2460.

Scheggi, A.M. in Kersten, R.Th. & Kist, R., Editors, "Proc. 2nd Intl. Conf. on Optical Sensors", VDE-Verlag GmbH, Berlin, 1984, 93-104.

Schirmer, R.E.; Gargus, A.G. Am. Lab. Dec. 1986, 30-39.

Schulman, J.H.; Compton, W.P. "Color Centers in Solids", Pergamon Press, N.Y., 1962.

Schultz, J.S.; Sims, G. Biotech. Bioeng. Symp. 1979, 9, 65-71.

Schwab, S.D.; McCreery, R.L. Anal. Chem. 1984, 56, 2199-2204.

Scouten, W.H. "Affinity Chromatography; Bioselective Adsorption on Inert Matrices", J. Wiley and Sons, N.Y., 1981, 20-85.

Seare, N.J. in Edmonds, T.E. "Chemical Sensors", Chapman and Hall, N.Y., 1988, 155-167.

Seitz, W.R. CRC Crit. Rev. in Anal. Chem. 1980, 8 (4), 367-465.

Seitz, W.R. Anal. Chem. 1984, 56, 16A-34A.

Sepaniak, M.J.; Tromberg, B.J.; Eastham, J.F. Clin. Chem. 1983, 29, 1678-1682.

Seto, T.A.; Schultze, M.O. Anal. Chem. 1956, 28, 1625-1629.

Siemion, E. Oregon State University, Personal Communication, 1991.

Simhony, S.; Katzir, A. Appl. Phys. Lett. 1986, 49, 252-254.

Smith, R.M.; Jackson, K.W.; Aldous, K.M. Anal. Chem. 1977, 49, 2051-2053.

Smock, P.L.; Orofino, T.A.; Woooten, G.W.; Spencer, W.S. Anal. Chem. 1979, 51, 505-508.

Snell, F.D.; Snell, C.T. "Colorimetric Methods of Analysis", Volumes I-IV, Van Norstrand Reinhold, N.Y., 1948-1970.

Snow, J.W. Sea Tech. July 1987, 10-13.

Snyder, A.W. and Love, J.D. "Optical Waveguide Theory", Chapman and Hall, London, 1983, 6-88.

Snyder, A.W. and Love, J.D. "Optical Waveguide Theory", Chapman and Hall, London, 1983, 589-623.

Snyder, A.W.; Love, J.D. "Optical Waveguide Theory", Chapman and Hall, London, 1983, 120-133.

Sternson, L.A. in Frei, R.W. & Lawrence, J.F., Editors, "Chemical Derivatization in Analytical Chemistry, Volume 1: Chromatography", Plenum Press, N.Y., 1981, 127-210.

Suematsu, Y. and Iga, K. "Introduction to Optical Fiber Communications", John Wiley and Sons, N.Y., 1982, 141-150.

Suidan, J.S.; Young, B.K.; Hetzel, F.W.; Seal, H.R. Clin. Chem. 1983, 29, 1566.

Symons, J.M.; Bellar, T.A.; Carswell, J.K.; DeMarco, J.; Kropp, K.L.; Robeck, G.G.; Seeger, D.R.; Slocum, C.J.; Smith, B.L.; Stevens, A.A. Jour. AWWA 1975, 65 (11), 634-647.

Tai, H.; Tanaka, H.; Yoshino, T. Opt. Lett. 1987, 12, 437-439.

Tait, G.A.; Young, R.B.; Wilson, G.J.; Steward, D.J.; MacGregor, D.C. Am. J. Physiol. 1982, 243, H1027-1031.

Taylor, J.B.; Lown, B.; Polyani, M. J.A.M.A. 1972, 221, 667-673.

The Random House Dictionary, Ballantine Books, New York, 1980.

Thomas, L.C.; Chamberlin, G.S. "Colorimetric Chemical Analytical Methods", The Tintometer Ltd., Salisbury, 1953-1980.

Tromberg, B.J.; Eastham, J.F.; Sepaniak, M.J. Appl. Spec. 1984, 38, 38-42.

Tromberg, B.J.; Sepaniak, M.J.; Vo-Dinh, T.; Griffin, G.D. Anal. Chem. 1987, 59, 1226-1230.

Uno, T.; Okumura, K.; Kuroda, Y. Chem. Pharm. Bull. 1982, 30, 1876-1879.

Uno, T.; Okumura, K.; Kuroda, Y. J. Org. Chem. 1981, 46, 3175-3178.

Van Dyke, D.A.; Cheng, H.-Y. Anal. Chem. 1988, 60, 1256-1260.

Vickers, G.H.; Miller, R.M.; Hieftje, G.M. Anal. Chim. Acta 1987, 192, 145-153.

Waddle, R.D., Masters Thesis, 1989, Oregon State University.

Walters, B.S.; Nielsen, T.J.; Arnold, M.A. Talanta 1988, 35, 151-155.

Wangsa, J.; Arnold, M.A. Anal. Chem. 1988, 60, 1080-1082.

Wanser, K.H.; Wagoner, R.E. Photonics Spectra Oct. 1983, 61-66.

Warner, B.J.; Cheng, S.C.; Friedman, C.S.; Mitrosky, S.; Snyder, A.D.; McMillin, C.R. "EPA Method Study 23A, Method 501.1, Trihalomethanes by Purge and Trap" 1984, EPA-600/4-84-020.

Warner, B.J.; Cheng, S.C.; Finke, J.M.; Friedman, C.S.; Mitrosky, S.; Snyder, A.D.; McMillin, C.R. "EPA Method Study 23B, Method 501.2, Trihalomethanes by Liquid/Liquid Extraction" 1984, EPA-600/4-84-021.

Wilson, R.L. "Design, Development and optimization of a Fluorometric Reaction-Rate Instrument and Method of Analysis for Metal Ions" 1977, Ph.D. Thesis, Oregon State University.

Woldarczyk, M.T.; Vickers, D.J.; Kozaitis, S.P. SPIE Vol. 718, Fiber Optic and Laser Sensors IV (1986); Cambridge, MA., 192-196.

Wolfbeis, O.S. Fresenius Z. Anal. Chem. 1985, 320, 271-273.

Wolfbeis, O.S. Fresenius Z. Anal. Chem. 1986, 325, 387-392.

Wolfbeis, O.S. Pure & Appl. Chem. 1987, 59, 663-672.

Wolfbeis, O.S. Anal. Chem. 1986, 58, 2874-2876.

Wolfbeis, O.S.; Posch, H.E. Anal. Chim. Acta. 1986, 185, 321-327.

Wolfbeis, O.S.; Posch, H.E.; Kroneis, H.W. Anal. Chem. 1985, 57, 2556-2561.

Wolfbeis, O.S.; Sharma, A. Anal. Chim. Acta. 1988, 208, 53-58.

Wolfbeis, O.S.; Weis, L.J.; Leiner, M.; Ziegler, W.E. Anal. Chem. 1988, 60, 1028-2030.

Yappert, C., Ph.D. Thesis, 1985, Oregon State University.

Yappert, C.; Schuyler, M.W.; Ingle, Jr., J.D. Anal. Chem. 1989, 61, 593-600.

Zhujun, Z.; Seitz., W.R. Anal. Chim. Acta. 1985, 171, 251-258.

Zhujun, Z.; Seitz, W.R. Anal. Chim. Acta. 1984, 160, 47-55.

Zhujun, Z.; Seitz, W.R. Anal. Chim. Acta. 1984, 160, 305-309.

Zhujun, Z.; Seitz, W.R. Anal. Chem. 1986, 58, 220-222.

Zhujun, Z.; Mullin, J.L.; Seitz, W.R. Anal. Chim. Acta. 1986 184, 251-258.

Zierler, S.; Feingold, L.; Danley, R.A.; Craun, G. Int. Archives of Environ. Health 1988, 43 (2), 195-200.

APPENDICES

APPENDIX I

INSTRUMENTAL SUPPLEMENT

OPTICAL SYSTEMS OF THE FIBER OPTIC FLUOROMETER

Figure 4.1 of this thesis is a block diagram showing the general layout of the fiber optic fluorometer constructed for use in this thesis research, and the instrumentation section of chapter four gives a detailed list of the components used. This section of appendix I presents a detailed discussion of the optical systems comprising the excitation and emission optical interfaces of the fiber optic fluorometer.

The excitation source and associated optics are shown in figure I.1 (see chapter 4 for a listing of components). The optics are contained in a light-tight black Plexiglass box which encloses a 10.75-in length of an optical rail (and is 10.25-in wide and 9.25-in high). The fiber optics and the photodiode signal cable are fed through 0.5-in diameter "ports" drilled in the sides of the interface box. These ports are made light-tight with putty.

All components within the optical interface box are mounted on separate carts held on the 30-in long optical rail; the optical axis is 2.00 in (50.8 mm) above the top surfaces of the carts, and is centered on the optical rail (see figures I.1 and I.2). As examples, the carts holding the (two) XYZ translation stages and the beam splitter/reference detector assembly are shown in figures I.2 and I.3, respectively. The assemblies holding the two lenses (L1 and L2, figure I.1), the excitation filter, and the "entrance" fiber optic (f.o. 1) are not shown as they are simply aluminum plates mounted on the carts with the appropriate sized holes drilled and centered on

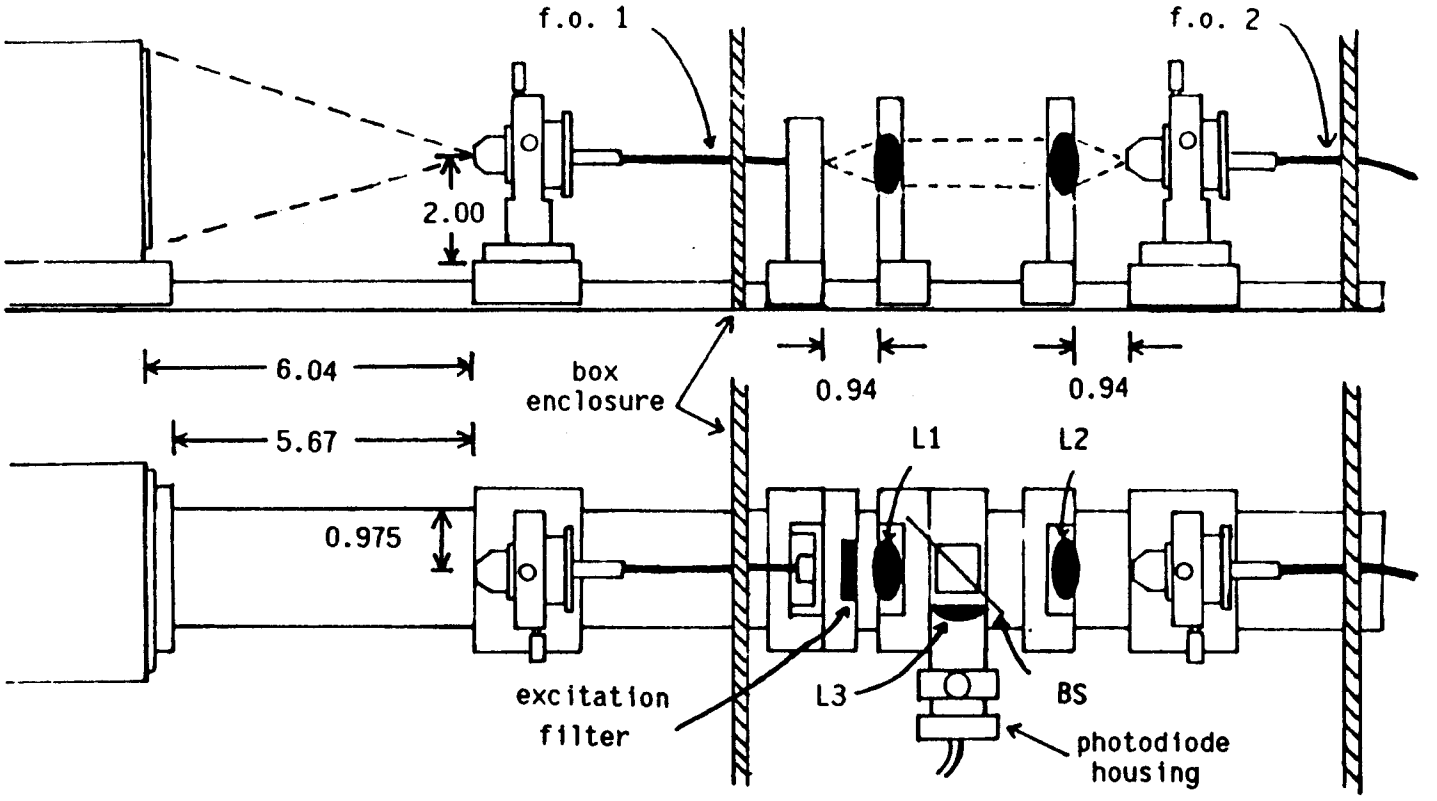

Figure I.1. Layout of the excitation interface of the fiber optic fluorometer. All dimensions are in inches.

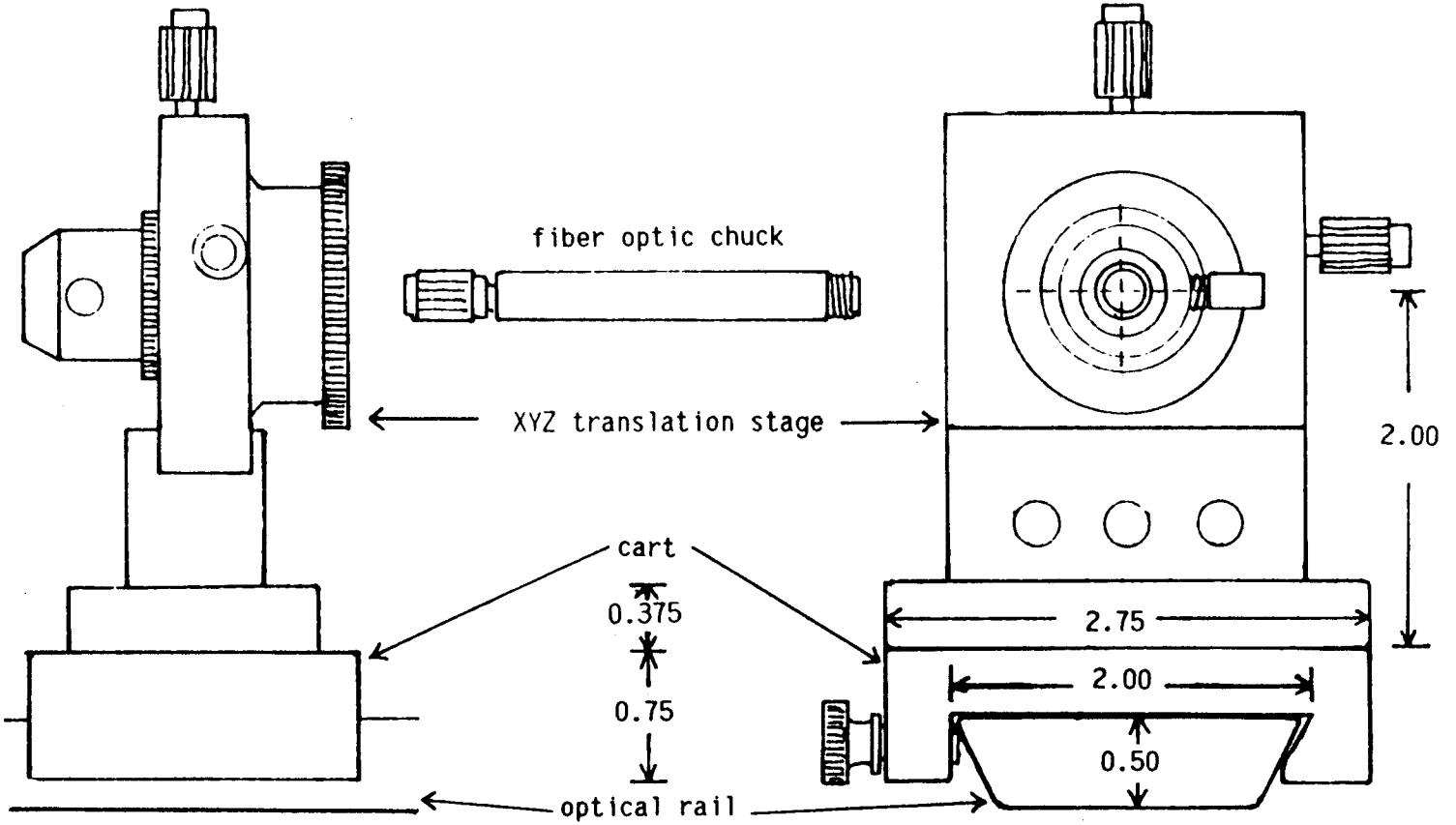

Figure I.2. Detailed diagram showing the dimensions of the optical cart(s) (and the optical rail) holding the Newport LP-05 XYZ translational stages. All dimensions are in inches.

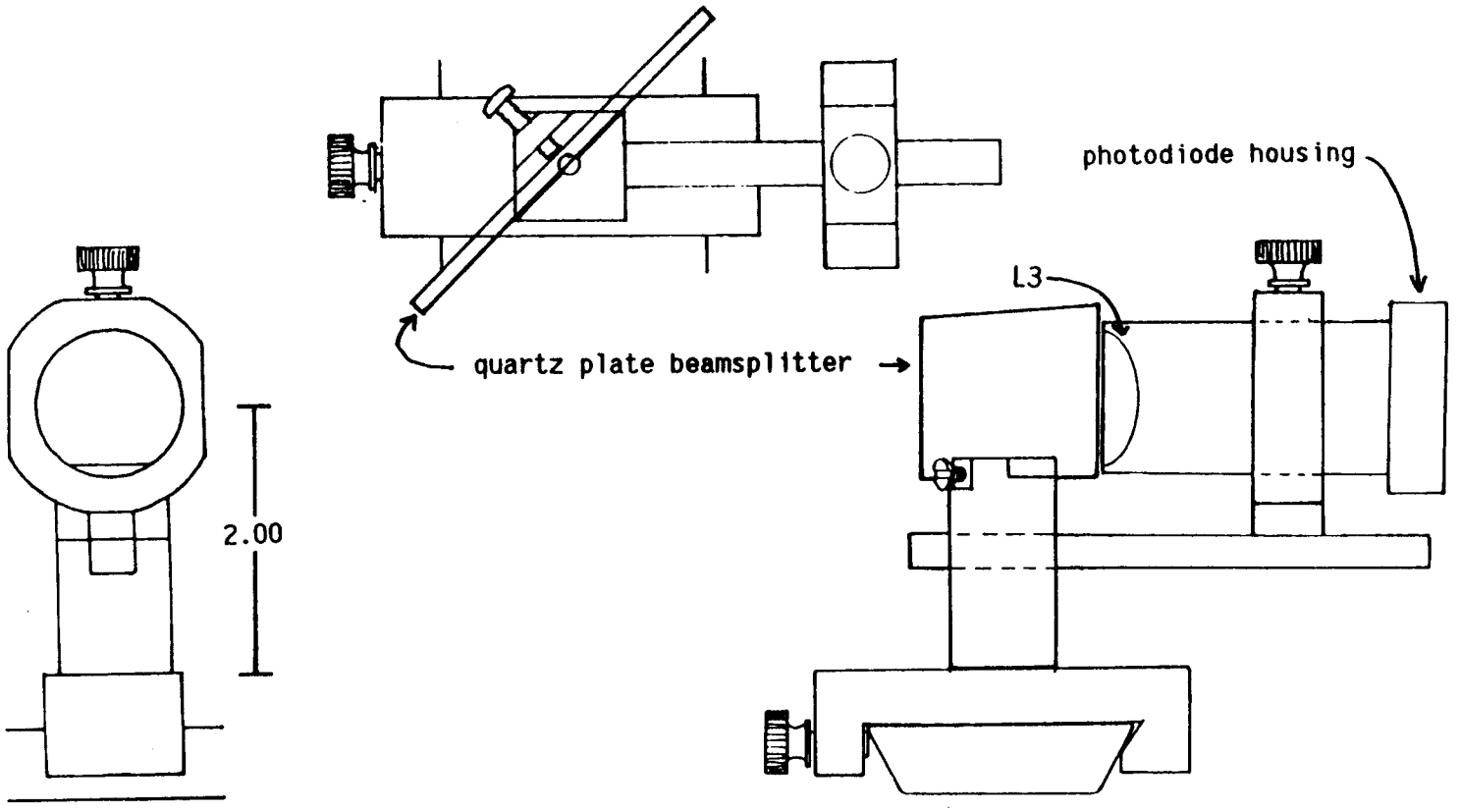

Figure I.3. Detailed drawing showing the optical cart holding the reference detector housing and the quartz plate beamsplitter. All dimensions are in inchs.

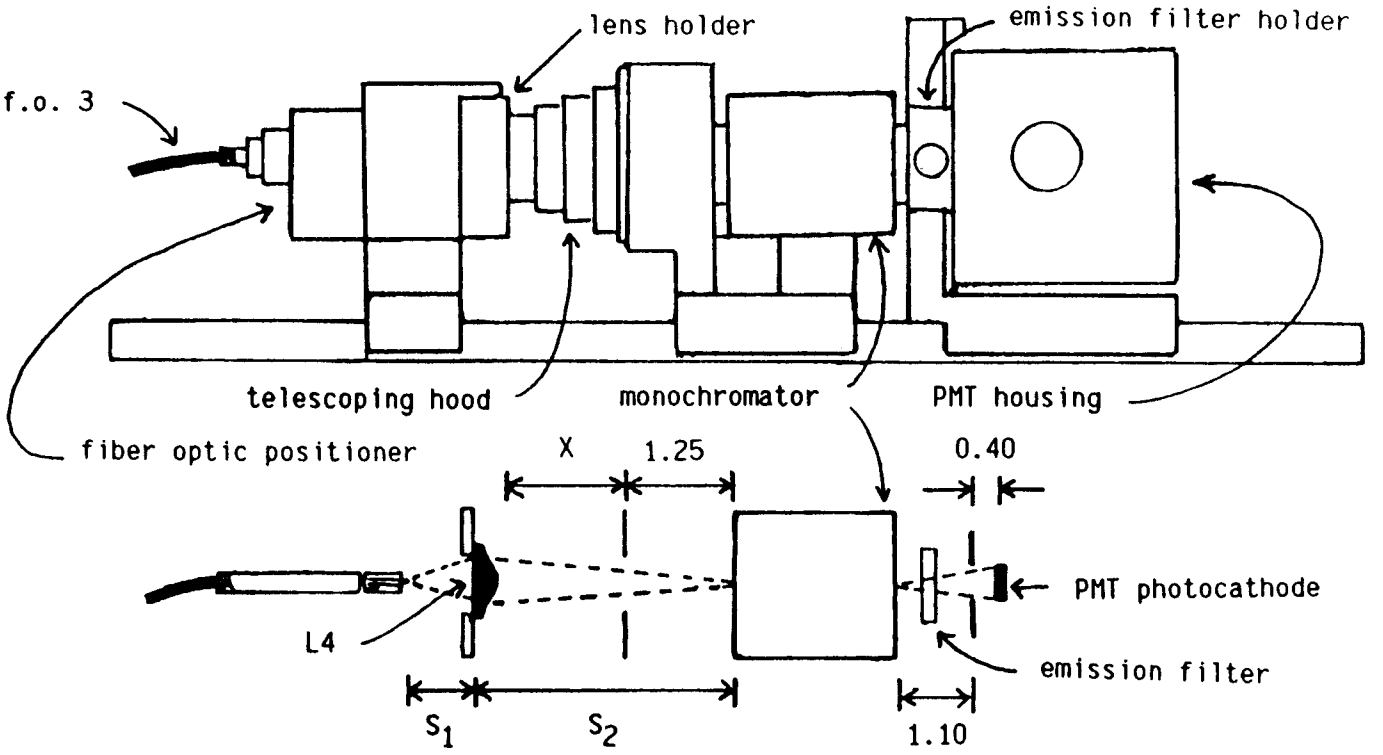

Figure 1.4. Layout of the emission interface of the fiber optic fluorometer (all dimensions are in inches). The distance X can be varied between 0.375 in and 1.500 in as determined by the maximum compression or extension of the telescoping hood. Thus, the range for S_2 is 1.625-2.75 in.

the optical axis.

The emission (detection) optical train is shown in figure I.4. This system is similar to the excitation optics in that all components are mounted on carts held on a single (16 in) section of optical rail. The optical train consists of a PMT housing (Heath model EU-701-93) mounted to an emission filter holder (which is fit to the exit slit of a Mini-Chrom monochromator), the monochromator, a telescoping hood which provides a variable focal length, light-tight, optical path interfacing the entrance slit of the monochromator to a lens holder, and a variable focal length fiber optic positioner which is also attached to the lens holder. The optical axis of this optical system is 1.75 in above the top surface of the carts (and is centered on the optical rail).

The emission monochromator (Mini-Chrom) is fitted with a wavelength dial which reads 100 units per 360° rotation. The monochromator is configured such that one full (360°) rotation of the wavelength selector shaft corresponds to 150 nm. Thus, when the wavelength dial reads 400, the wavelength setting is 600 nm. Conversely, to set the output wavelength of this monochromator to 610 nm, the dial should be set at 406.7 ((610/150) X 100 = 406.7).

From figure I.4, the distances S_1 and S_2 are variable. As drawn, S_1 and S_2 are measured from the optical center of the aspherical lens (L4), which is ca. 6.6 mm from the plano surface of the lens (1). The object focal length S_1 can be varied between 16 and 29 mm by adjusting the position of f.o. 3 relative to L4 with a thumbwheel positioner. The image focal length S_2 can be varied between 43 and 73 mm by moving the carrier (cart) holding the fiber

positioner and lens holder. Thus, when using f/1.5 fiber optics, monochromator f/n's in the approximate range 3.0-6.5 can be matched.

The cart holding the monochromator can be removed, and the "telescoping hood" can be attached directly to the PMT housing (cart), which also holds an emission filter. In this configuration, the object distance S_1 can still be varied between 16 and 29 mm, and the image distance S_2 (as measured from the PMT photocathode to the focussing lens L4) can now be varied over the range 50-78 mm.

ELECTRONICS

All the signal processing electronics for the fiber optic fluorometer are contained within a single component box, and all circuitry is assembled on a Vector board with a 44-pin edge-connector; table I.1 lists the "pin-out" for the Vector board. The signal processing electronics consists of three independent circuits: the PMT current-to-voltage converter (figure I.5), the reference (photodiode) detector current-to-voltage converter (figure I.6), a divider circuit (figure I.7), and the associated power supply (Sierracin, model A15D).

A PTI optical feedback detector unit (model 02-LPS002) was modified for use as the reference detector; this unit consisted of a photodiode detector and a current-to-voltage converter contained within a cylindrical housing equipped with an f/1.5 fused silica lens (see figure I.3). The current-to-voltage converter operational amplifier was removed from the housing circuit board and a jumper was placed on the housing circuit board to connect the photodiode to the

Table I.1. Vector board pin assignments for the signal processing electronics of the fiber optic fluorometer.

pin	description
5	-input from reference detector (pin #2, figure I.6)
6	P.S. common to P.S. decouple capacitors (figure I.6)
7	+input from reference detector (pin #3, figure I.6)
8	output of reference circuit (to case as V_x)
9	P.S. common to PMT I/V converter (pin #3, figure I.5)
10	common from PMT (case) input (pin #3, figure I.5)
11	P.S. common to P.S. decouple capacitors (figure I.5)
12	PMT signal (case) from R_{in} switch (pin #2, figure I.5) (also tied to C_f and R_f wafer switch on case)
13	PMT I/V converter null to case null pot (pin #1, figure I.5)
14	-15 V (from -15 V bus on board) to null pot
15	PMT I/V converter null to case null pot (pin #5, figure I.5)
16	PMT I/V converter output to case (and divider coupler switch on case)
17	C_f (pin #6, figure I.5)
18	R_f (pin #6, figure I.5)
21	P.S. -15 V to Vector board bus
A	P.S. +15 V to Vector board bus
C	P.S. common to Vector board bus
H	P.S. common for main (bus) decoupler capacitors
R	V_y (pin #4, figure I.7) to case output
S	P.S. common (pin #13, figure I.7)
T	V_y (pin #4, figure I.7) to R_1 on case
U	wiper of R_1 (on case, to pin #5, figure I.7)
V	V_o (pin #8, figure I.7) to case output
W	PMT signal (pin #6 figure I.5) from case couple switch
X	P.S. common to Vector board bus
Y	P.S. common to P.S. decouple capacitors (figure I.7)

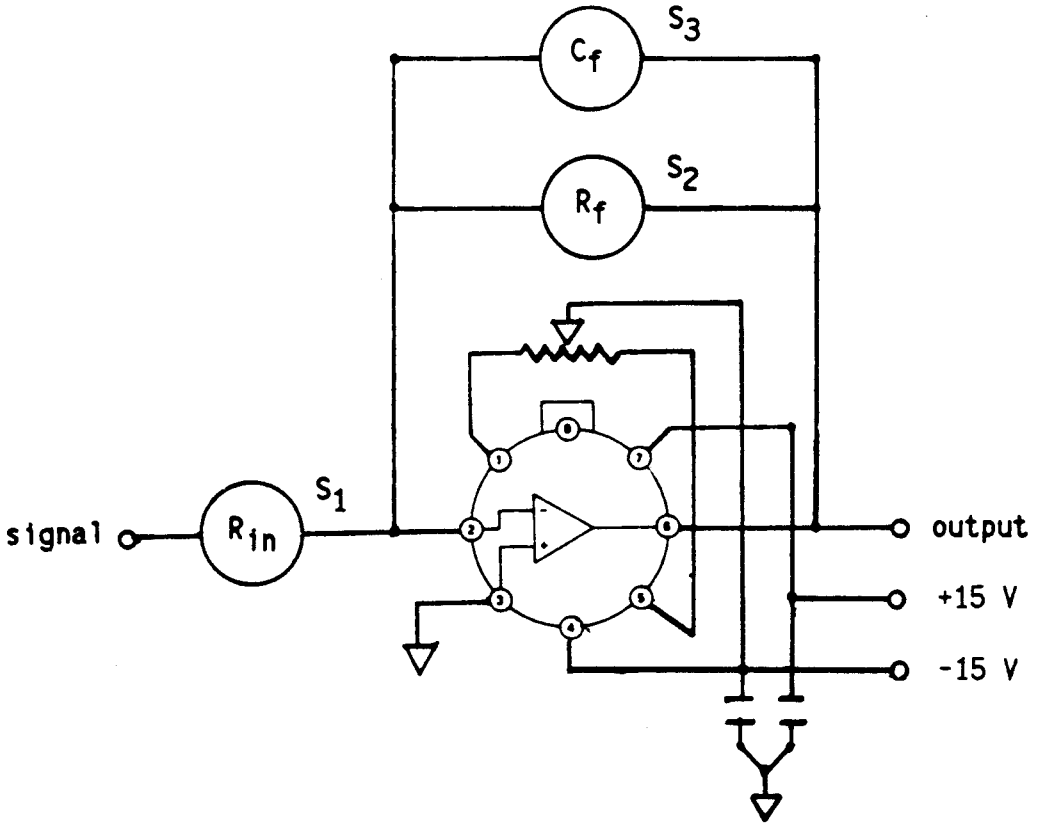

Figure I.5. Circuit diagram the PMT current-to-voltage converter (amplifier). The op-amp is a AD542 (Analog Devices); the null pot (20 kΩ) is located on the front face of the component case as are the three wafer switches S_1 (R_{in}), S_2 (R_f), and S_3 (C_f). The available component values are: R_{in}, 0 (I/V), 1 kΩ, 10 kΩ, 100 kΩ, and 1 MΩ; R_f, ∞ (NC), 10 kΩ, 100 kΩ, 1 MΩ, 2.5 MΩ, 5 MΩ, 7.5 MΩ, 10 MΩ, 50 MΩ, and 100 MΩ; C_f, 100 pF, 0.001 μF, 0.01 μF, 0.02 μF, 0.1 μF, 0.135 μF, 0.198 μF, and 1.0 μF. The power supply decoupler capacitors are 1 μF.

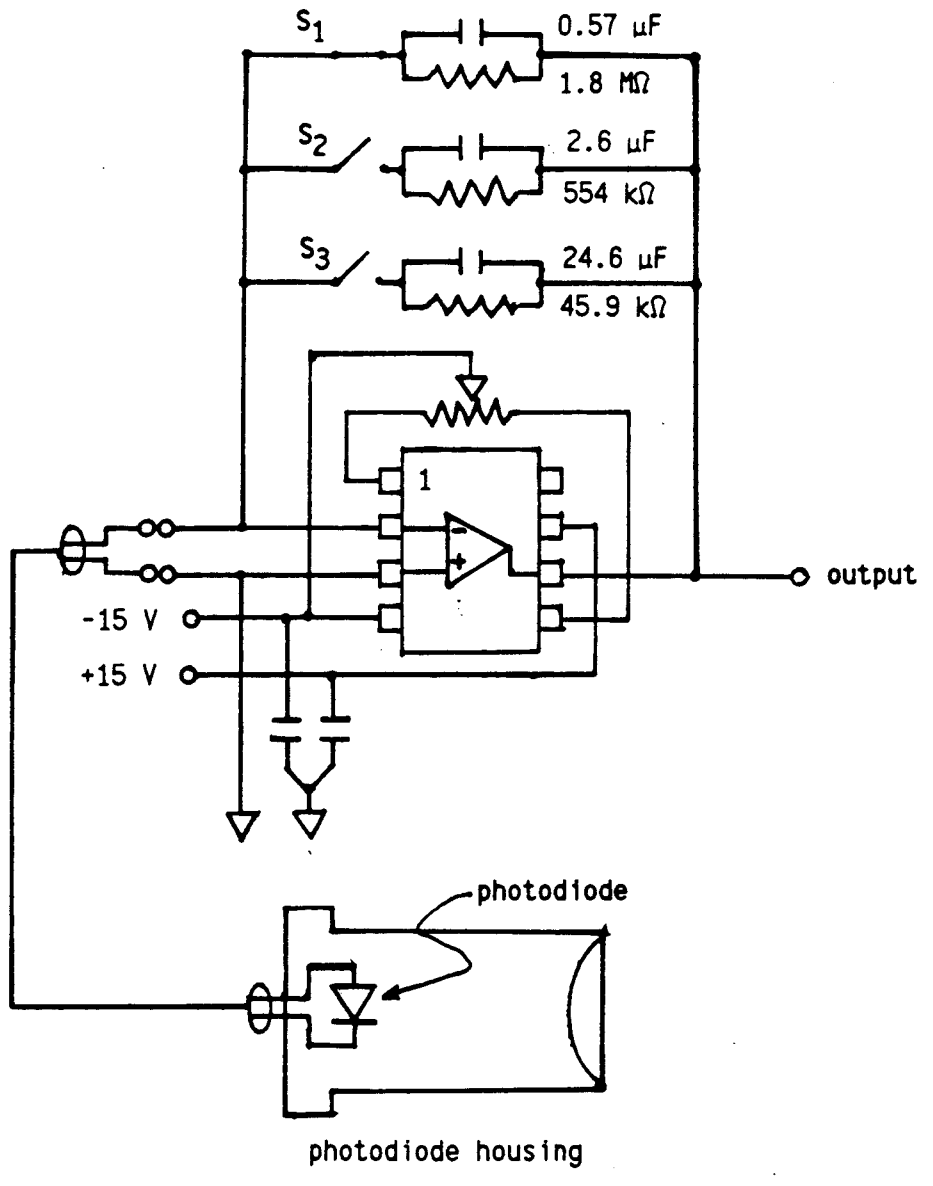

Figure I.6. Circuit diagram of the reference detector current-to-voltage converter. The operational amplifier is a TL081CP (Texas Instruments). The null pot (20 kΩ) is located on the Vector board, as is the DIP switch for selecting the gain for this circuit; the power supply decoupling capacitors are 1 µF.

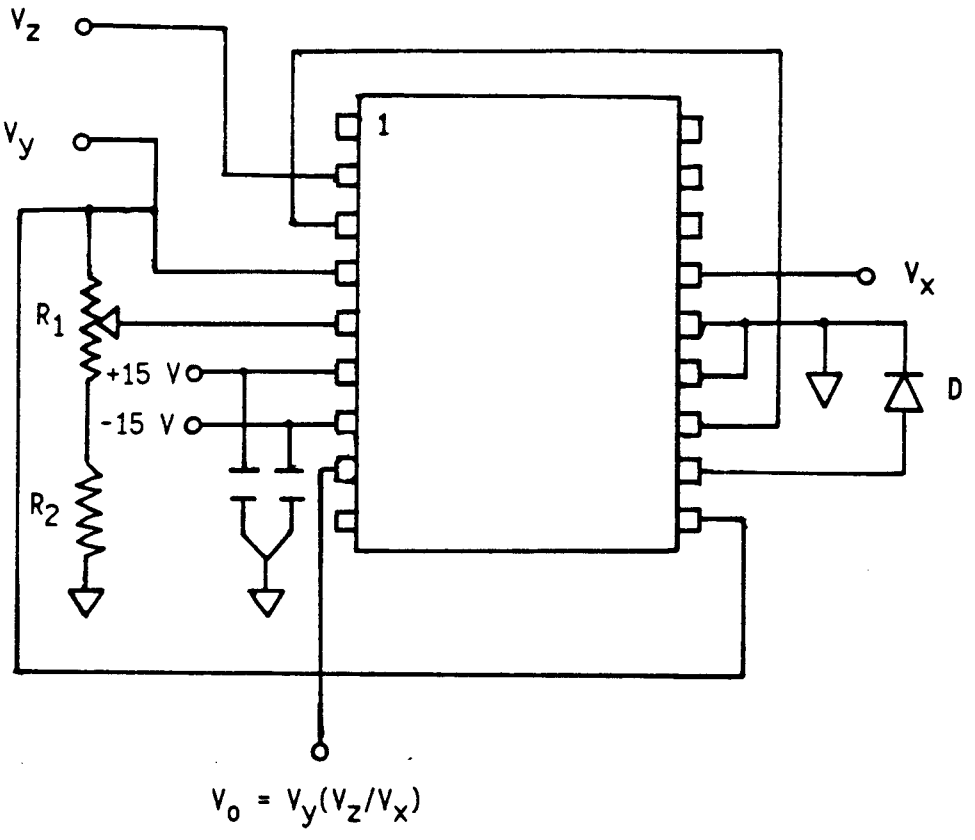

Figure I.7. Circuit diagram of the divider circuit. The divider is an AD538 (Analog Devices) I.C.. V_x (the reference photodiode signal) and V_z (the PMT signal) are connected (internally) to the outputs of the appropriate current-to-voltage converters. The pot R_1 (50 KΩ) is located on the front face of the component case and is used to adjust the value of V_y between 2.01 and 10.20 V. The power supply decoupling capacitors are 1 μF, D is a 1N4148 diode, and R_2 is 12 kΩ.

original output line. The photodiode current is brought to a current-to-voltage converter within the component box by a shielded cable.

A voltage-to-frequency converter was mounted in a separate box to allow data acquisition with a PC using a Metrabyte CTM-05 counter/timer board. Figure I.8 is a schematic of the V/F converter. An instrumentation amplifier configured for a gain of one is used to ensure a true differential input to the V/F converter. The V/F circuitry is powered by a AD904 (Analog Devices) power supply contained within the V/F box.

The computer program providing computer control of the PTR monochromator and synchronized data acquisition was developed using Quick BASIC 4.5. The program is designed specifically for use with the PTR CB-1 monochromator controller unit (via the RS-232 serial port of a PC) and a Metrabyte CTM-05 counter-timer board. A thoroughly commented listing of this program is given in appendix II of this thesis.

OPERATION OF THE FIBER OPTIC FLUOROMETER

To start the lamp, the power supply is first turned on (with the lamp current adjusted to read 5.0 A for either the Xe and the Xe/Hg lamp) and allowed to warm up for ca. 10-15 minutes. The cooling water is then turned on, and the ignitor (start) button is momentarily depressed. The lamp invariably starts on the first or second attempt. To prevent damage to the electronic circuitry, the power to all peripheral electronics should be off at this point.

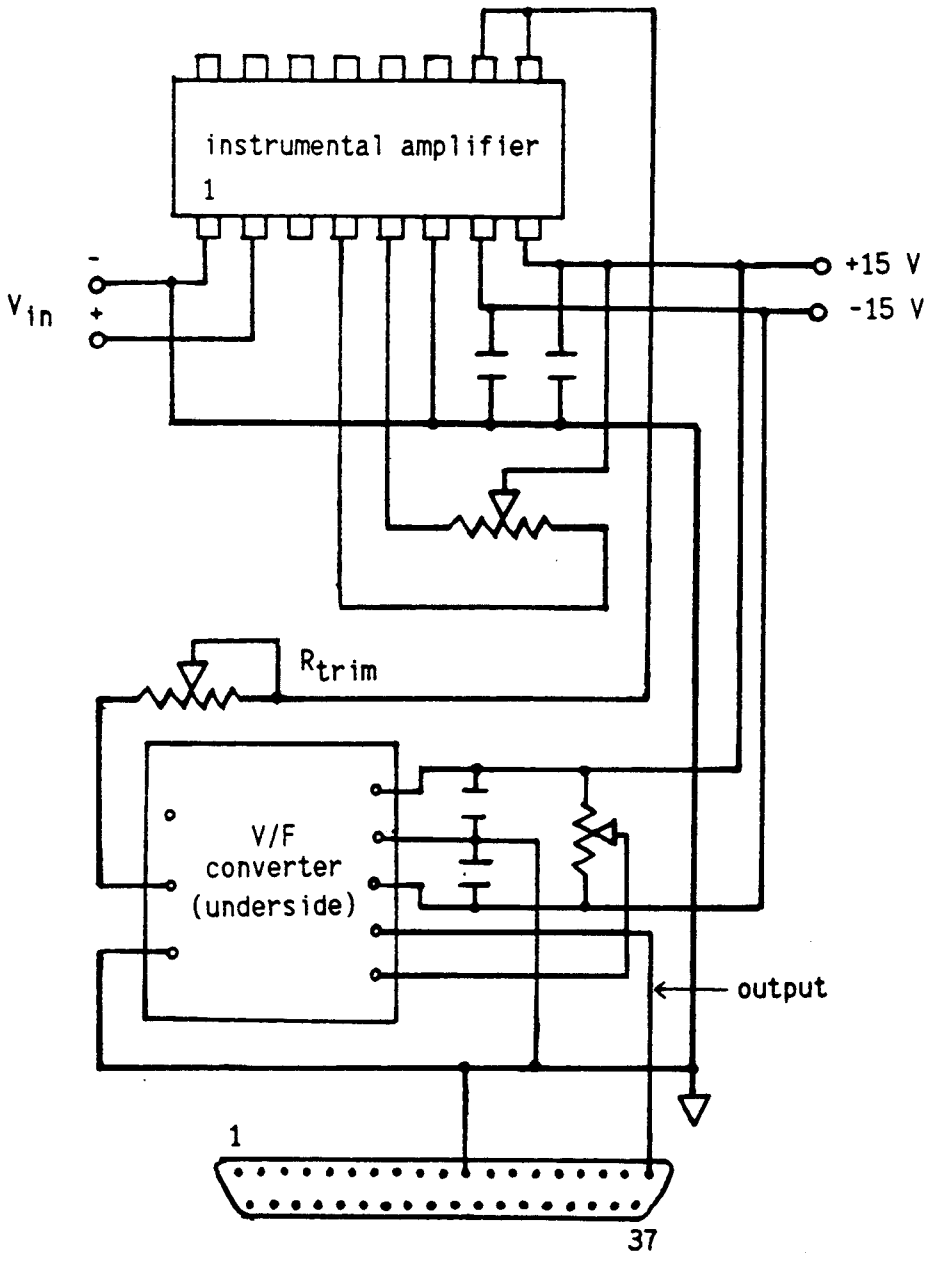

Figure I.8. Circuit diagram of the voltage-to-frequency converter. The instrumentation amplifier is an AD524 (Analog Devices) and the V/F converter is a (Teledyne Philbrick) 4705. The pin-out for the associated ribbon cable which carries the output of this circuit to the CTM-05 counter/timer board is also shown. The null pots are 20 kΩ, the V/F full scale trim pot (R_{trim}) is 200 Ω, and the power supply decoupling capacitors are 1 μF.

Once the lamp is on, the (D.C. filtered) modulation signal is applied immediately to the reference detector input of the lamps power supply.

The procedure for focussing the lamp (arc) image onto the termination of the entrance fiber optic (f.o. 1) is as follows: 1) the fiber optic is placed at the theoretical focal point of the housing (6.04 in in front of the housing for the f/2.5 reflector, and 2.00 in above the cart top), 2) the lamp adjustment screws are all screwed in to their limits, 3) the lamp is turned on and the adjustment screws are backed off 1 (full) turn at a time (symmetrically) while monitoring the power exiting f.o. 2 with a photodiode, 4) as the image size becomes smaller, the screws are adjusted independently to give a circular image centered on the fiber optic, 5) the screws are again backed off symmetrically, using smaller increments as the focus is approached. The source is focussed when a relative maximum in power is observed. Note, the alignment of the optical system within the optical interface itself does not affect this relative measurement.

The procedure for focussing the lamp image onto the entrance fiber optic can also be performed by maximizing the signal seen by the detection system. In this case, the monitored signal is the source radiation scattered by an empty sample reservoir (collected by f.o. 2).

Once the lamp is properly focussed, only slight adjustment of the position of f.o. 1 is necessary for routine use. The XYZ position of f.o. 1 is optimized using the XYZ translational stage by maximizing the output of the reference detector or of the PMT

(monitoring scattered, filtered source radiation). When using the 75-W Xe/Hg lamp, the reference signal at 545 nm (545-nm bandpass filter) is typically around 4.7 V (R_f = 45.9 kΩ) when the system is optimized; the reference signal at 366 nm (366-nm interference filter) is typically around 3.3 V (R_f = 554 kΩ). For measurements, the multiplier voltage of the divider circuit V_y is adjusted to equal the reference voltage V_x. Thus, the divider output equals the output of the PMT current-to-voltage converter.

The coupling between fiber optics 1 and 2 should also be reoptimized routinely. In this case, the XYZ position of f.o. 2 is optimized by maximizing the PMT output (monitoring scattered, or reflected, source radiation). Note that when the excitation wavelength is changed, reoptimization is necessary because of the effects of chromic aberrations on the image focal length.

A simple procedure for optimizing the coupling efficiency between the emission fiber optic (f.o. 3) and either a monochromator or a PMT directly (filter only) is as follows: the image focal length is set to the minimum value and the object focal length is optimized by maximizing the observed signal (scattered or reflected source radiation), the image focal length is then increased slightly and the object focal length reoptimized. After a few iterations of this procedure, a relative maximum in the observed signal will be apparent.

When interfacing the emission fiber optic (f.o. 3) to the f/4 Mini-Chrom monochromators, the optimum values are $S_1 \simeq 25.5$ mm and $S_2 \simeq 61.2$ mm, and the image of the fiber optic on the entrance slit of the monochromator is magnified by a factor of ca. 2.4 (giving a

spot ca. 1.44 mm in diameter). The beam diameter at the plano surface of L4 is ca. 12.6 mm (25.5 - 6.6 ÷ 1.5). For interfacing to either of the PMT housings (RCA 1P28 or RCA 4840), the optimum values are $S_1 \simeq 28$ and $S_2 \simeq 50$ (mm). Because of the relatively large size of the PMT photocathode (0.5 X 1.0 in), image magnification is not a problem.

FIBER OPTIC PREPARATION

Each length of fiber optic (f.o.s 1, 2, and 3) has to be cut and polished manually. Rough lengths of fiber optic are cut using either a pair of scissors or a razor blade. A cleaner cut is then obtained by stripping the fiber optic of the buffer and cladding material (with a sharp razor blade) and using a (sharpened) sapphire cleaving crystal. This is somewhat of an art and practice is required in order to obtain a "clean cleave"; a more uniform surface is obtained by polishing the fiber optic after cleavage.

For polishing, the fiber optics are stripped of the outer buffer and mounted in a fiber optic chuck (Newport, model FPH-DJ) with a length of fiber optic (stripped of the cladding material) extending beyond the chuck collet itself. This length (extending beyond the fiber optic chuck) varies depending on the position in the optical system. Figure I.9 shows the two general polishing configurations. Figure I.9a shows the approximate dimensions for the termination of fiber optic 1 at the source focal point and the terminations of fiber optics 2 and 3 at the optical interfaces (the non-sensing terminations). Figure I.9b shows the "polishing

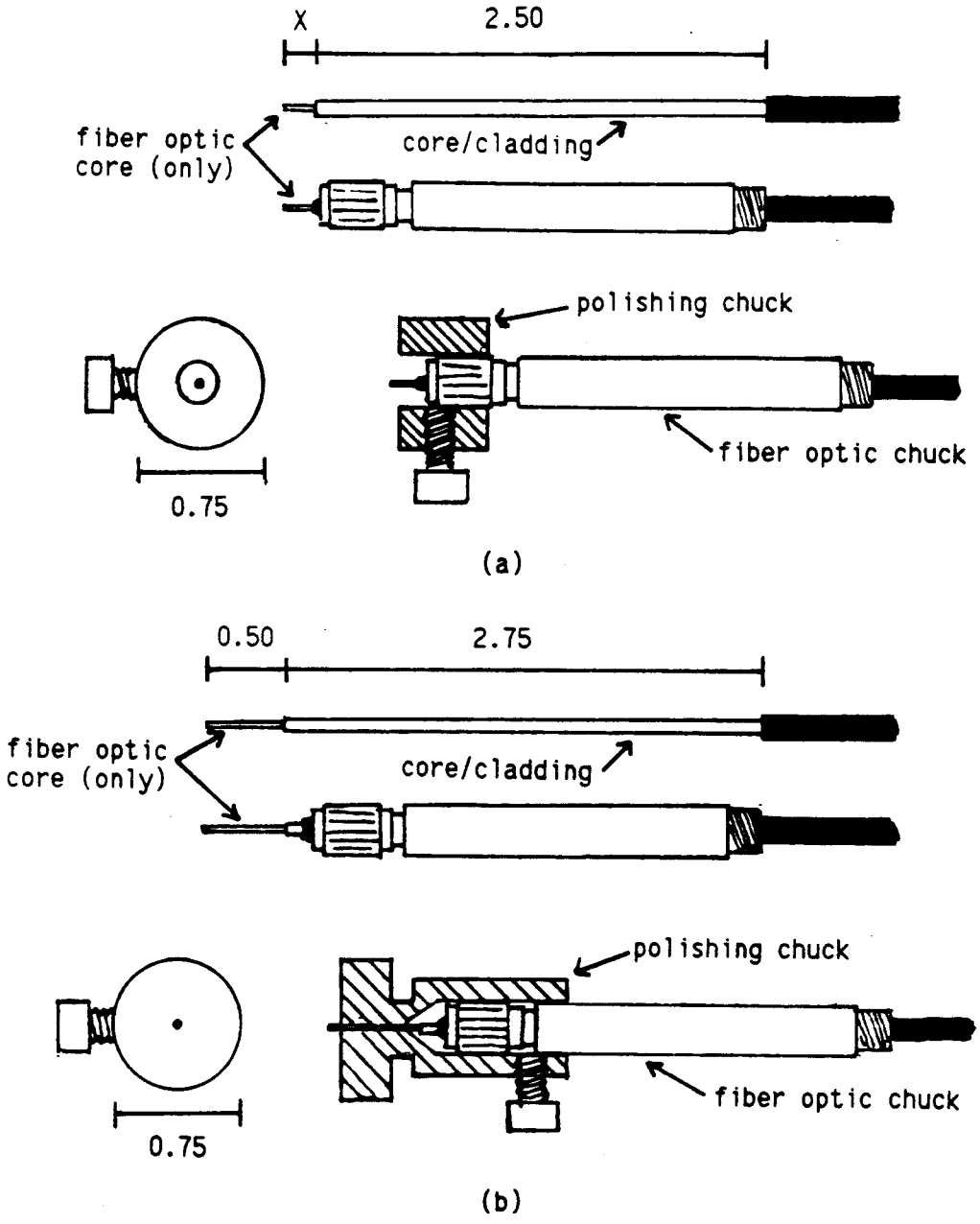

Figure I.9. Dimensions and apparatus for polishing the fiber optics. The configuration shown by I.9a is used for fiber optic terminations other than those of the sensor itself, and I.9b shows the configuration for polishing the sensor fiber optics. All dimensions are inchs.

dimensions" for the two sensing terminations of fiber optics 2 and 3 (mounted in the fiber optic probe).

From figure I.9a, the distance X is ca. 5 mm for f.o. 1 and 3 mm or less for f.o.'s 2 and 3. The greater length (X) for f.o. 1 is necessary as this termination must extend through the aluminum aperture disk placed at the source focal point. These fiber optics are polished by mounting the fiber optic chuck (holding the fiber optic) in a donut-shaped piece of aluminum (figure I.9a) so that a short length of the fiber optic core extends beyond the aluminum "polishing chuck". The fiber is then polished by drawing the fiber face across successively finer lapping films using a circular or figure-8 motion. The lapping films (Mark V Labs, East Granby, Conn.) range in grit size from 50-0.3 μm, and are taped onto glass plates for use. Typically, a "cleaved" fiber is polished with 50-μm lapping film just until a flat, "burr free" (circular) termination is achieved (as viewed under a microscope); the fiber is then polished briefly with each successively finer grit film, finishing with 0.3-μm grit film. Polishing is complete when inspection of the fiber optic face with the microscope reveals no surface imperfections (indicated by an obviously smooth glassy appearance under the microscope). The fiber optic chucks are then mounted in the fiber optic fluorometer at the appropriate locations.

Figure I.9b shows the polishing configuration for the two sensing terminations of fiber optics 2 and 3. Because these terminations are mounted in the fiber optic probe, a much greater length of fiber optic must extend beyond the chuck. This is problematic in that this increased (unsupported) length is prone to

breakage in the polishing process. For this reason, another polishing chuck is used to polish these terminations (figure I.9b).

The termination of f.o. 1 mounted at the object focal point of the excitation optical interface is mounted and polished in an Amp Inc. (530530-5) fiber optic connector.

OPTICAL POWER MEASUREMENTS

The optical power measurements reported in this work were obtained using a modified PTR Mini-Chrom Silicon (photodiode) Detector (model SDM-1). The feedback resistance of the detectors dedicated current-to-voltage converter was modified (a 54.8 kΩ resistor was added, in parallel, to the original 10.0 MΩ feedback resistor) to be 54.5 kΩ. The radiant power W incident on the detector (Φ) is calculated using the relationship

$$\Phi = V/(R_f \times R(\lambda)) \qquad (1)$$

where V is the output voltage of the current-to-voltage converter (volts), R_f is the gain (V/A) of the current-to-voltage converter (which is equal to the value of the feedback resistor in ohms), and $R(\lambda)$ is the absolute spectral responsivity of the photodiode (A/W); the value of $R(\lambda)$ at 366 nm is ca. 0.16 A/W, and ca. 0.30 A/W at 545 nm (2). For all power measurements, the source radiation is filtered and the value of $R(\lambda)$ is assumed to be a constant over the (ca. 10-nm) bandpass of the interference filters.

When the radiant power approachs 1 mW, the use of a neutral

density filter is necessary to perform measurements with the photodiode. This is required when a 75-W Xe/Hg arc lamp is used as the radiation source. For determination of the spectral radiant power exiting f.o. 2 (see figure 4.1), the (characterized) neutral density filter is placed at L1 (held in place with putty).

To obtain accurate measurements of the excitation radiant power when using excitation filters not well blocked in the red (i.e., the 366-nm and 545-nm interference filters used in this work), it is necessary to take measurements with a high-pass cut-on filter added to the excitation train at the same position as the excitation filter (held in place with putty). The radiant power at the excitation wavelength (only) is calculated using the difference between the net photodiode signal (excitation filter only) and the photodiode signal due to the longer wavelengths (excitation and high-pass cut-on filter), and equation 1.

FIBER OPTIC FLUORESCENCE

Fiber optic fluorescence spectra were obtained by connecting the excitation fiber optic (f.o. 2) directly to the detection system. An ca. 30-m length of fiber optic, on a spool, was used. For these scans, the emission end of the fiber optic was interfaced to a Mini-Chrom monochromator (300-μm slits, reciprocal linear dispersion of 6 nm/mm, effective f/4 aperture) equipped with a PTR PMT unit (model PMT-1). The scanning of the monochromator was controlled using a PTR CB-1 monochromator stepper motor controller unit, interfaced to a Corona PC via. the RS-232 serial port, and the

software listed in Appendix II. This software also controls the acquisition of the PMT signal by the voltage-to-frequency converter and the Metrabyte CTM-05 counter/timer board.

The fluorescence scans of the Maxlight PCS fiber optic used in this thesis are shown in figures I.10-I.14. For scans I.10-I.13, a 75-W Xe arc lamp was used as the excitation source (set at 5 A), the PMT voltage was -450 V, the scan rate was 100 nm/min, and the gate period on the counter was 0.6 s. Thus, 1 mV gives a count value of 60 and the rate of data acquisition corresponds to 1 point/nm. A single emission spectrum (figure I.14) was also obtained using a 2.5-mW Helium Neon laser (Melles Groit, λ_{max} of 632 nm) as the excitation source (and the same instrumental settings as listed above).

In figure I.10 (313-nm excitation), the sharp band observed at 364 nm is attributed to Raman scattering by the fiber optic. The Raman shift of 51 nm corresponds to 4476 cm^{-1}. The second order excitation and its Raman band are also apparent. The corresponding Stokes lines are seen in the emission spectra when the excitation wavelength is 422 nm (520 nm, see figure I.12) or 545 nm (721 nm, see figure I.13).

Of particular interest are the emission spectra obtained when exciting at 366 nm and 545 nm, the excitation wavelengths used for quinine sulfate and the Fujiwara reaction, respectively. From figure I.11, the fiber optics exhibit spectral features over the range 450-600 nm when excited at 366 nm. The predicted Raman (Stokes) line for 366-nm excitation should appear at ca. 438 nm, and a slight shoulder on the tail of the transmitted excitation band is apparent

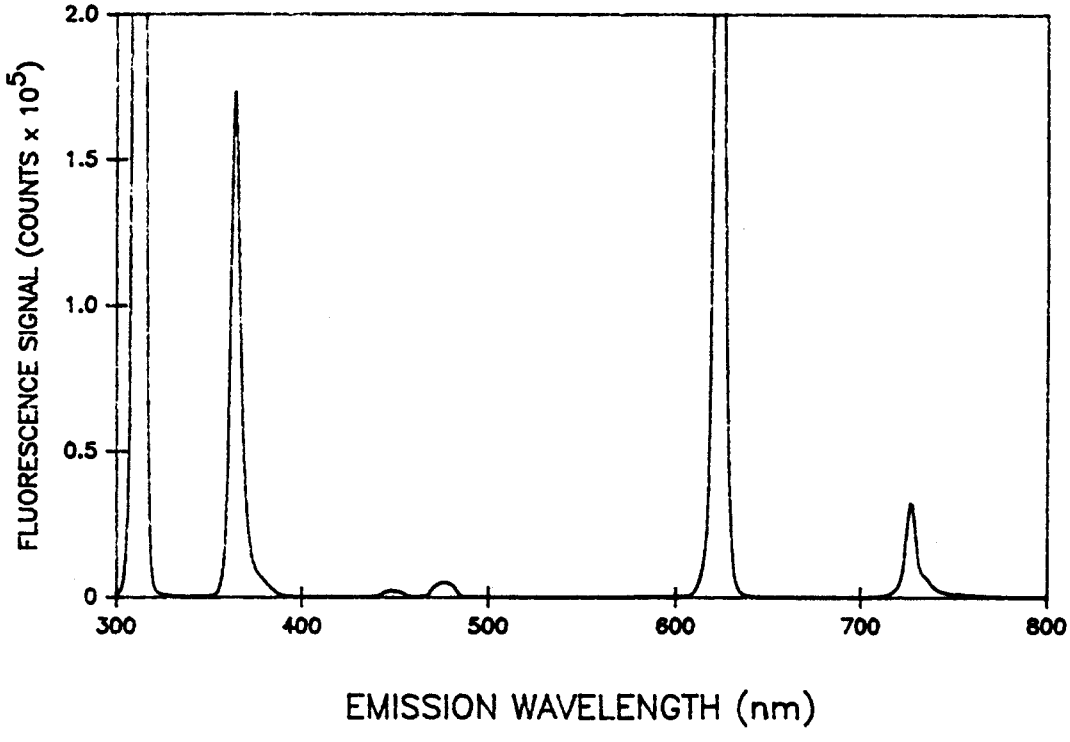

Figure I.10. Fluorescence emission spectrum of Maxlight PCS fiber optic when excited at 313 nm (313-nm bandpass excitation filter).

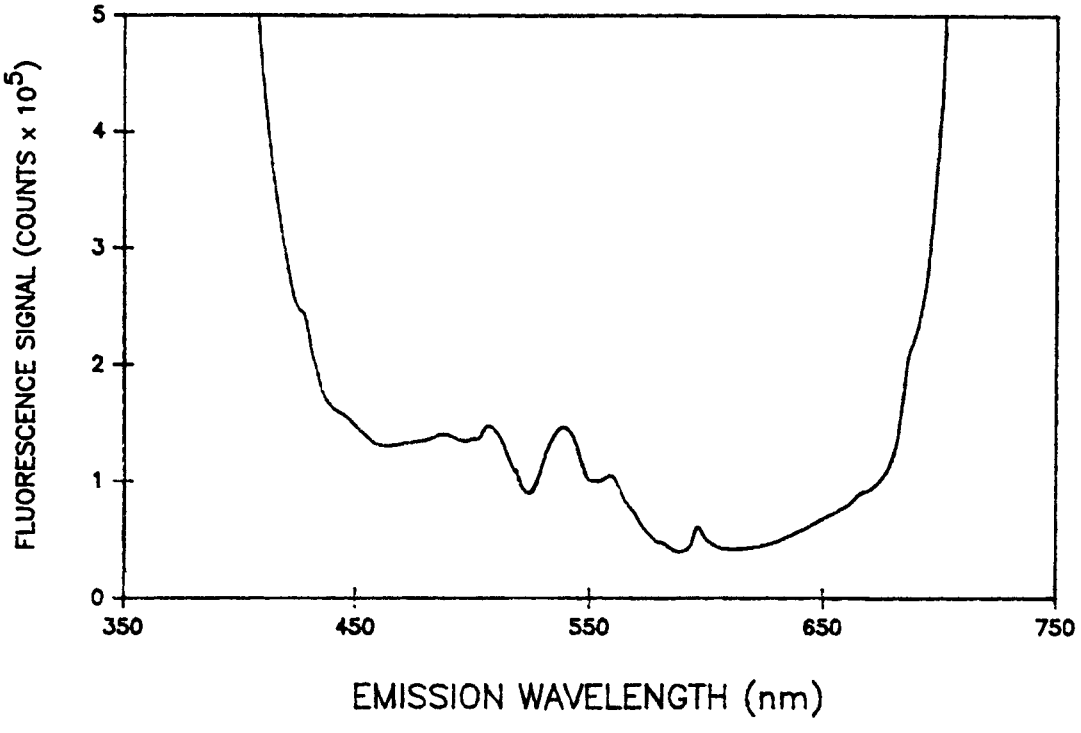

Figure I.11. Fluorescence emission spectrum of Maxlight PCS fiber optic when excited at 366 nm (366-nm bandpass excitation filter).

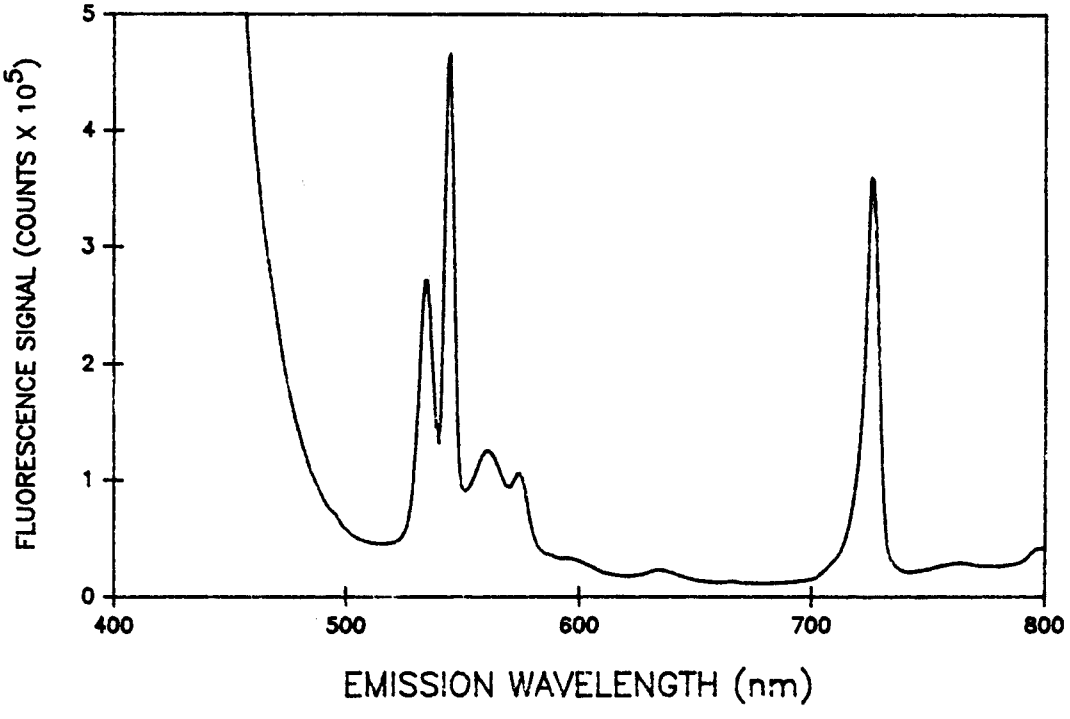

Figure I.12. Fluorescence emission spectrum of Maxlight PCS fiber optic when excited at 422 nm (422-nm bandpass excitation filter).

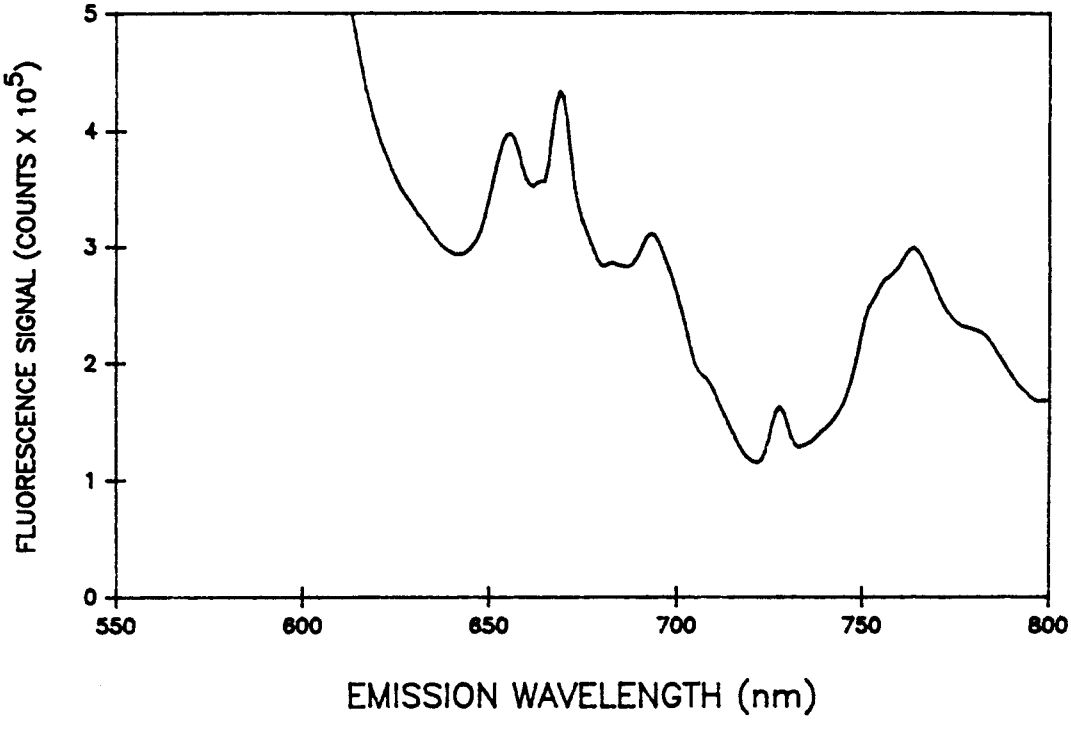

Figure I.13. Fluorescence emission spectrum of Maxlight PCS fiber optic when excited at 545 nm (545-nm bandpass excitation filter).

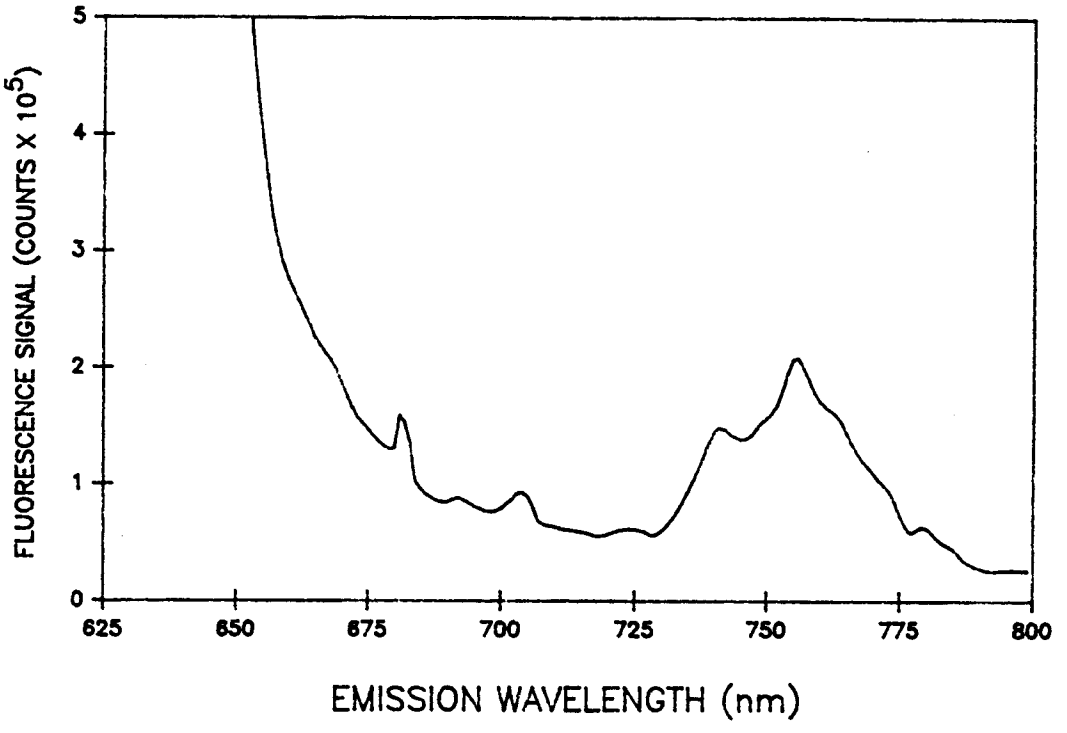

Figure I.14. Fluorescence emission spectrum of Maxlight PCS fiber optic when excited at 632 nm (Helium Neon laser).

at this wavelength. The large background signal in the 450-600 nm range is attributed to monochromator stray light and/or fiber optic fluorescence. Note that a significant background signal is detectable at 460 nm even though the holographic grating of the monochromator used exhibits a minimum in grating efficiency over the range from 400-500 nm (centered at ca. 450 nm). Thus, fiber optic fluorescence can contribute to the background signal when quinine sulfate fluorescence is excited at 366 nm and monitored at 460 nm.

The emission spectrum of the fiber optic when excited at 545 nm (figure I.13) shows structure from 640 nm to the limit of the scan at 800 nm. The spectrum also shows a significant background signal in the region of 610 nm (the emission wavelength used to monitor the Fujiwara reaction), which is likely due to some small finite transmittance of the excitation filter in this region (3).

PHOTOMULTIPLIER CALIBRATION

The experimental procedure of Bower (4) was used to determine the current gain m of the RCA 1P28 and the RCA 4840 PMTs used in this work. To summarize, the method of Bower utilizes a "PMT bias box" which allows a PMT tube to be operated as either a phototube or a photomultiplier. The bias box has a switch with two positions: in position one, the PMT is operated as a photomultiplier, and in position two, the cathode is biased at one tenth of the PMT bias voltage (the same cathode-first dynode potential as when operated as a PMT) and all the dynodes and the anode are connected to the measurement circuit (i.e., the PMT is configured at a PT). Thus, the

current gain of a PMT can be obtained from the ratio of the two signals (PMT/PT).

The PMT tubes were mounted in Bower's bias box which was then substituted for the normal PMT housing of the fiber optic fluorometer (Mini-Chrom monochromator, 20-nm spectral bandpass). A 460-nm interference filter (40% peak transmittance, 10-nm halfwidth) was used to filter the source radiation from a 75-W Xe arc lamp, and the monitored signal was the scattered (filtered) source radiation (from an empty 0.5-in dia., 0.5-in deep white Teflon sample reservoir) collected by the fiber optic probe.

The current gain m for the RCA 4840 PMT at a PMT bias voltage of -440 V, and a current amplification of 100 MΩ (a large gain was necessary to see the PT signal), was determined to be 1.39 ± 0.23 (X 10^4) (5 measurements). Then, the radiant power reaching the detector was reduced by a factor of ca. 10 (by moving f.o. 2 slightly off the focal point in the excitation optical interface), the feedback resistor in the amplification circuit was reduced to 1 MΩ, and the PMT signals measured for a range of PMT bias voltages. Since the photocathodic current is constant over all these measurements, the PMT current gains at the various bias voltages can be calculated by simply multiplying the relative (to the signal observed for V = -440 V with the 1 MΩ feedback resistor) PMT signal by the experimentally determined value of m at V = -440 V (1.39 X 10^4). The dark current voltages were subtracted from all measurements.

The current gain for the RCA 1P28 PMT at V = -900 V was determined for use in the determination of the effective collection efficiency of the fiber optic probe (see table 4.1). A value was

also obtained for V = -600 V in order to approximate the dependence of m on the PMT bias voltage.

Table I.2 lists the experimentally determined values of m, at various bias voltages, for the two PMTs studied, and figure I.15 shows a log-log plot of the current gains as a function of bias voltage. For the RCA 1P28 PMT, the manufacturer's "typical" current gains at -600 and -900 V are ca. 9×10^4 and 1.5×10^6, respectively (5). For the RCA 4840 PMT, RCA lists typical current gains at -600 and -900 V as 8×10^6 and 1.5×10^7, respectively (6). For both PMTs, the experimentally determined values are approximately a factor of 5 less than specified. Bower (4) has shown that gains of individual tubes can vary up to an order of magnitude from typical values.

OPTIMIZATION OF THE ANGLE BETWEEN THE FIBER OPTICS OF THE FIBER OPTIC PROBE

The effect of the angle between the two fiber optics of a dual-fiber probe on the net fluorescence collection efficiency and the signal-to-background ratio (S/B) was studied. Fluorescence and blank signals from a 10 µg/mL quinine sulfate (QS) solution (and a blank) were obtained using dual-fiber probes having different angles between the two fibers. The apparatus constructed for use in this experiment is shown in figure I.16. The sample solutions were contained in separate 500-mL beakers and the probe was suspended in the solution(s) such that the fiber optic terminations were just below the surface of the solution. The beaker was then covered with

Table I.2. Experimentally determined photomultiplier current gains (m).

PMT bias voltage (V)	m	
	RCA 4840	RCA 1P28
-400	6.64×10^3	--------
-440	1.39×10^4	--------
-500	3.96×10^4	--------
-600	1.75×10^5	1.8×10^4
-700	6.15×10^5	--------
-800	1.83×10^6	--------
-900	4.73×10^6	2.65×10^5

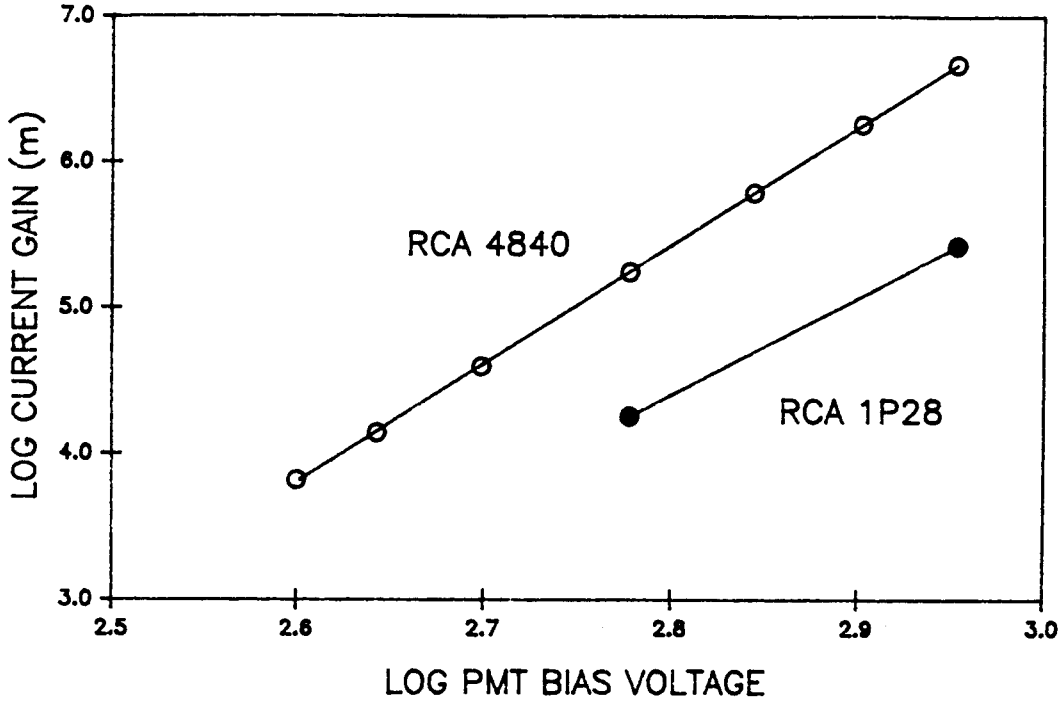

Figure I.15. Log-log plots of the experimentally determined PMT current gain vs. PMT bias voltage for the RCA 4840 and the RCA 1P28 PMTs used in this work.

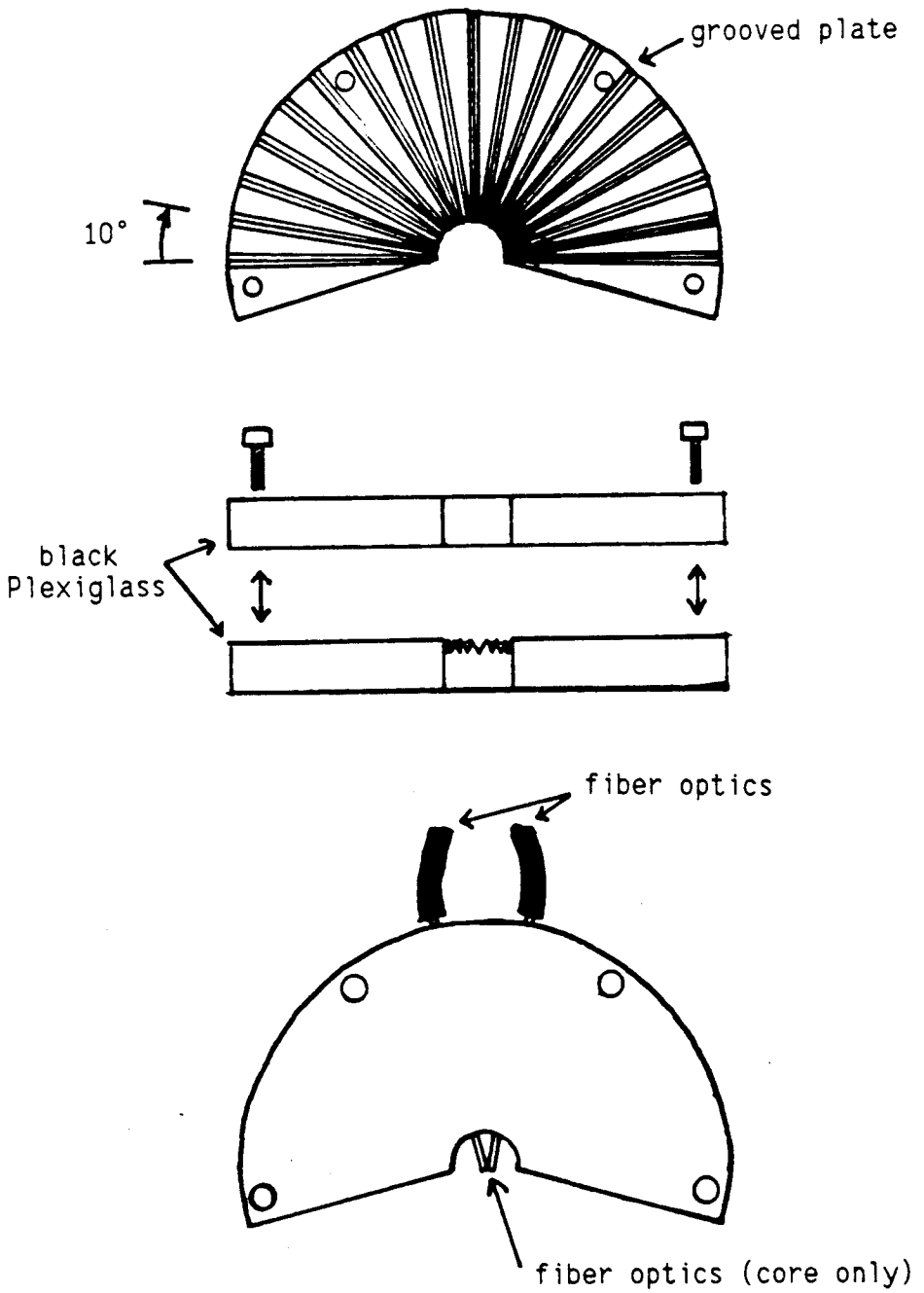

Figure I.16. Fiber optic holder constructed for the fiber optic angle study. The fiber optics are stripped of all external buffer and cladding and then "sandwiched" in the holder so that the two tips just touch each other.

black cloth.

Figure I.17 shows the blank-corrected fluorescence signal, the dark-corrected blank signal, and the resulting S/B as a function of the angle between the two fiber optics. The net fluorescence signal shows a maximum in the region of 20° while the blank signal is ca. constant from 20° to 80°. Thus, the S/B is primarily a function of the relative fluorescence collection efficiencies of the different probe configurations (angles). The 20° angle was selected for use in the fiber optic probe constructed for use with the fiber optic fluorometer.

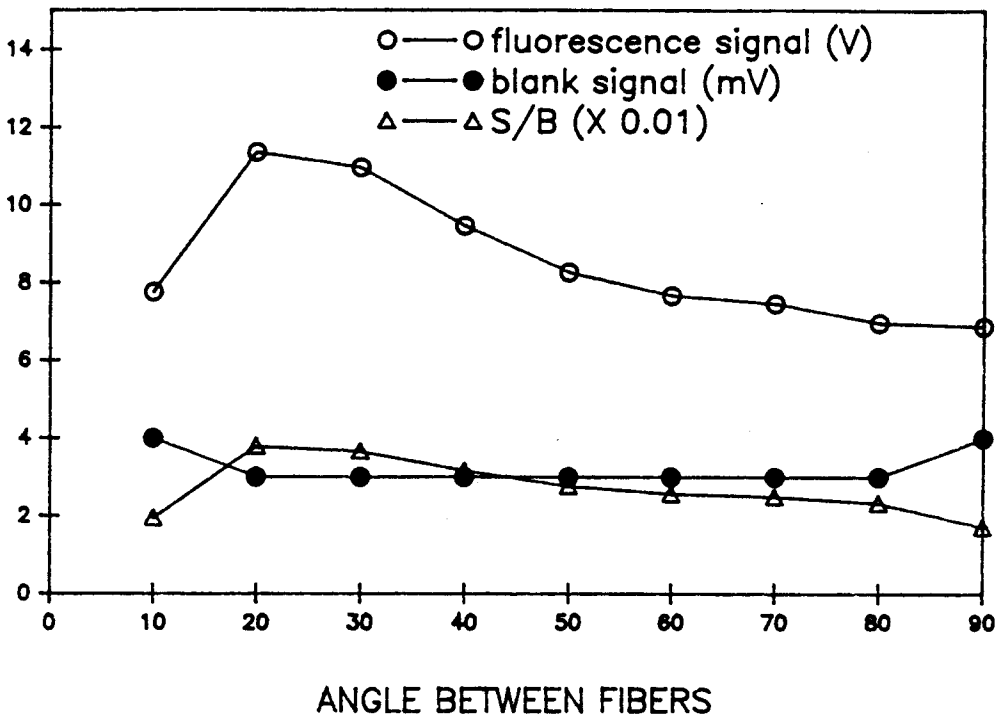

Figure I.17. The fluorescence signal, blank signal, and S/B as a function of fiber optic angle.

REFERENCES

1. Melles Groit Optics Guide 3, 1985, 169-166.

2. PTR SDM-1 Silicon Detector Module Users Guide, Rev. 1.0, 1986.

3. Ingle, Jr., J.D.; Crouch, S.R. "Spectrochemical Analysis", Prentice Hall, Englewood Cliffs, 1988, 554-556.

4. Bower, N.W., Ingle, Jr., J.D. Anal. Chem. 1975, 47, 2069-1072.

5. RCA 1P28 Specification Sheet, Aug. 1975.

6. RCA 4840 Specification Sheet, Oct. 1975.

APPENDIX II

SOFTWARE LISTING

```
'DEC 23, 1988
'DATA ACQUISTION USING CTM-5 COUNTER BOARD
'WAVELENGTH SCANNING VIA PTR SCAN CONTROLLER
'*************************************************************************
'DECLARE VARIABLES
'*************************************************************************
        DIM CTM(10)                             'COUNTER VARIABLES
        DIM COUNT(5000)                         'DATA ARRAY
        BSA% = &H300                            'BASE ADRESS OF CTM-5 BOARD
        S = 0                                   'COUNTER FOR SCAN ACCESS
        E$ = "1"                                '
        S$ = "100"                              '
        D$ = "D"                                'SCANNING PARAMETERS
        I$ = "I"                                '
        N$ = "-1"                               '
        O$ = "+1"                               '
        Y$ = "800"                              '
        X$ = "300"                              '
        W$ = "100"                              '
        CC = 0                                  '
        FILE$ = "-"                             '
        DEX% = 1                                '
        CTM(1) = 1                              '
        CTM(2) = 60                             '
        PTNM = 1                                '
'*************************************************************************
'MAIN MENU
'*************************************************************************
MENU:
        CLS
        LOCATE 6, 24: PRINT "ENTER              FOR FUNCTION"
        LOCATE 7, 24: PRINT "=====      ========================="
        LOCATE 9, 24: PRINT "  1       PTR WAVELENGTH SCAN (ONLY)"
        LOCATE 11, 24: PRINT "  2          COMPUTER DVM (ONLY)"
        LOCATE 13, 24: PRINT "  3           SCAN ACQUISITION"
        LOCATE 15, 24: PRINT "  E                TO EXIT"
        LOCATE 18, 24: INPUT "ENTER CHOICE:"; C$
        IF VAL(C$) = 1 THEN GOTO ONE
        IF VAL(C$) = 2 THEN GOTO TWO
        IF VAL(C$) = 3 THEN GOTO THREE
        IF C$ = "E" OR C$ = "e" THEN GOTO FINISH
        BEEP: BEEP
        GOTO MENU
ONE:
        CLS
        IF S = 0 THEN GOSUB SCANI
        S = S + 1
        GOSUB SCANM
        CLS
        GOTO MENU
TWO:
        CLS
```

```
        IF CC = 0 THEN GOSUB INITCTM
        CC = CC + 1
        GOSUB CTMENU
        GOTO MENU
THREE:
        CLS
        IF S = 0 THEN GOSUB SCANI
        S = S + 1
        IF CC = 0 THEN GOSUB INITCTM
        CC = CC + 1
        GOSUB BOTHMENU
        GOTO MENU
FINISH:
        END

'************************************************************************
'SCAN ACQUISITION ROUTINES
'************************************************************************
 BOTHMENU:
        CLS
        W = VAL(W$)
        TEMP = (PTNM * W)
        TEMP = (TEMP / 60)
        TEMP = (TEMP / 1000)
        CTM(3) = (1 / TEMP)
        LOCATE 1, 1: PRINT "LAMBDA 1 ="; X$; "nm"
        LOCATE 1, 20: PRINT "LAMBDA 2 ="; Y$; "nm"
        LOCATE 1, 40: PRINT "SCAN RATE ="; W$; " nm/min"
        LOCATE 2, 1: PRINT "GATE PERIOD ="; CTM(3); " ms"
        LOCATE 2, 45: PRINT "PRESENT FILE IS A:"; FILE$; DEX$
        LOCATE 6, 23: PRINT "ENTER              FOR FUNCTION"
        LOCATE 7, 23: PRINT "=====        ======================="
        LOCATE 9, 23: PRINT "  1           TO SET SCAN PARAMETERS"
        LOCATE 10, 23: PRINT "          (init. & final lambda & scan
rate)"
        LOCATE 12, 23: PRINT "  2      SPECIFY pts/nm (= SCAN
RATE/GATE )"
        LOCATE 14, 23: PRINT "  3            SET FILE PARAMETERS"
        LOCATE 16, 23: PRINT "  4                ACQUIRE SCAN"
        LOCATE 18, 23: PRINT "  E                   TO EXIT"
        LOCATE 23, 1: PRINT "PRESENT FILE DESCRIPTION ( TO BE
SAVED):"; DESCRIPT$
        LOCATE 20, 23: INPUT "ENTER CHOICE :"; CH$
        IF CH$ = "1" THEN GOSUB SCANA
        IF CH$ = "2" THEN GOSUB 22
        IF CH$ = "3" THEN GOSUB 33
        IF CH$ = "4" THEN GOSUB 44
        IF CH$ = "E" OR CH$ = "e" THEN GOTO EE
        GOTO BOTHMENU
22 :
        CLS
        LOCATE 12, 23: INPUT "ENTER PTS/NM (=SCAN RATE/GATE PERIOD)";
PTNM
        RETURN
```

```
33 :
        CLS
        LOCATE 12, 23: INPUT "CHANGE FILE DESCRIPTION ONLY? (Y OR
       N)"; O$
        IF O$ = "y" OR O$ = "Y" THEN GOTO DESCPT
        LOCATE 14, 23: INPUT "ENTER FILE NAME (8 CHAR MAX)"; FILE$
        LOCATE 15, 23: INPUT "ENTER INITIAL INDEX VALUE (1-100)";
       DEX%
        DEX$ = STR$(DEX%)
        IF DEX% > 9 AND DEX% < 100 THEN
           NCHAR = 2
           ELSEIF DEX% < 9 THEN
           NCHAR = 1
        END IF
        DEX$ = RIGHT$(DEX$, NCHAR)
DESCPT:
        LOCATE 17, 23: PRINT "TYPE FILE DESCRIPTION TO BE SAVED
       (15-20 CHAR)"
        LOCATE 19, 15: LINE INPUT DESCRIPT$
        RETURN

44 :
        W = VAL(W$)                          'NM/MIN
        TEMP = (PTNM * W)                    'TEMP = PT/MIN
        TEMP = (TEMP / 60)                   'TEMP = PT/SEC
        TEMP = (TEMP / 1000)                 'TEMP = PT/ms
        CTM(3) = (1 / TEMP)                  'ctm(3) = GATE PERIOD IN ms
        X = VAL(X$)                          'CALCULATE # OF DATA POINTS
        Y = VAL(Y$)
        C = (Y - X)
        C = ABS(C)
        CTM(4) = (C * PTNM)                  'ctm(4) = # OF DATA POINTS
        C = (C * 8)                          'C = # OF STEPS (PTR STEPS)
        GOSUB LOADD                          'LOAD COUNTERS.
        GOSUB SCANGO                         'BEGIN SCAN.
        GOSUB ARM                            'ARM COUNTERS (AQUIRE).
        GOSUB STORE                          'STORE DATA.
        U$ = "EO"                            'TURN CONTROLLER
        PRINT #1, U$                         'CURRENT OFF.
        INPUT #1, A$, B$
        RETURN
EE:
        RETURN
'*************************************************************************
'CTM ROUTINES
'*************************************************************************

'-------------------------------------------------CTM-5 MENU-----
CTMENU:
        CLS
        LOCATE 1, 1: PRINT "GATE PERIOD ="; CTM(1); "sec"
        LOCATE 1, 50: PRINT "MEASUREMENT PERIOD ="; CTM(2); "sec"
        LOCATE 2, 25: PRINT "DESTINATION FILE IS  A:"; FILE$; DEX$
```

```
        LOCATE 6, 22: PRINT "ENTER        FOR FUNCTION"
        LOCATE 7, 22: PRINT "=====      ================="
        LOCATE 9, 22: PRINT "  1        CHANGE GATE PERIOD"
        LOCATE 10, 22: PRINT "          OR MEASUREMENT PERIOD"
        LOCATE 12, 22: PRINT "  2       EDIT DESTINATION FILE"
        LOCATE 14, 22: PRINT "  3           ACQUIRE DATA"
        LOCATE 16, 22: PRINT "  E              TO EXIT"
        LOCATE 23, 1: PRINT "PRESENT FILE DESCRIPTION (TO BE
       SAVED):"; DESCRIPT$
        LOCATE 18, 22: INPUT "ENTER CHOICE"; CH$
        IF VAL(CH$) = 3 THEN GOSUB 3
        IF VAL(CH$) = 2 THEN GOSUB 2
        IF VAL(CH$) = 1 THEN GOSUB 1
        IF CH$ = "E" OR CH$ = "e" THEN GOTO E
        GOTO CTMENU
E:
        RETURN
1 :
        CLS
        LOCATE 10, 20: PRINT "GATE PERIOD ="; CTM(1); "sec"
        LOCATE 11, 20: PRINT "MEASUREMENT PERIOD ="; CTM(2); "sec"
        LOCATE 13, 20: INPUT "NEW GATE PERIOD (SECONDS)"; CTM(1)
        LOCATE 14, 20: INPUT "NEW MEASUREMENT PERIOD (SECONDS)";
       CTM(2)
        RETURN
2 :
        CLS
        LOCATE 10, 20: PRINT "PRESENT DESTINATION FILE IS A:"; FILE$;
       DEX$
        LOCATE 12, 20: INPUT "CHANGE FILE DESCRIPTION ONLY (Y OR N)";
       O$
        IF O$ = "y" OR O$ = "Y" THEN GOTO DESCRIP
        LOCATE 14, 20: INPUT "ENTER NEW FILE NAME (7 CHAR. MAX)";
       FILE$
        LOCATE 15, 20: INPUT "ENTER INITIAL INDEX VALUE (1-100)";
       DEX%
        DEX$ = STR$(DEX%)
        IF DEX% > 9 AND DEX% < 100 THEN
           NCHAR = 2
           ELSEIF DEX% < 9 THEN
           NCHAR = 1
        END IF
        DEX$ = RIGHT$(DEX$, NCHAR)
DESCRIP:
        LOCATE 17, 20: PRINT "TYPE FILE DESCRIPTION TO BE SAVED
       (15-20 CHAR)"
        LOCATE 19, 15: LINE INPUT DESCRIPT$
        RETURN
3 :
        CTM(3) = (CTM(1) * 1000)          'Change gate period to ms
        CTM(4) = (CTM(2) / CTM(1))        'Calculate total number of
                                          'data points
        GOSUB LOADD
        CLS
```

```
        LOCATE 12, 35: PRINT "PLEASE WAIT"
        GOSUB ARM
        GOSUB STORE
        RETURN
'-----------------------------------------------INITIALIZE CTM-5 ----
INITCTM:
          'First perform master reset by writing OFFH to command
          'register;
          'C7-C5 = 111 (perform master control functions)
          'C4-C0 = 1 1111 (master reset)
        OUT BSA% + 1, &HFF
          'Now, to configure as desired
          'first point to master mode control register (via command
          'register); load data pointer register with 0001 0111 (17H)
          'C7-C5 = 000 (load data pointer register)
          'C4-3 = 10 (element pointer = master mode register)
          'C2-0 = 111 (group pointer = control)
        OUT BSA% + 1, &H17
           'then load master control mode register with
           '1100 1010 1111 0000 (CAF0H);
           'MM15 = 1 (BCD division on scalar)
           'MM14 = 1 (data pointer increment disabled)
           'MM13 = 0 (8-bit data)
           'MM12 = 0 (FOUT gate off)
           'MM11-8 = 1010 (FOUT divider = 10)
           'MM7-4 = 1111 (FOUT source = F5 (100Hz))
           'MM3 = 0 (compare 2 disabled)
           'MM2 = 0 (compare 1 disables)
           'MM1-0 = 00 (time of day disabled)
        OUT BSA%, &HF0: OUT BSA%, &HCA
           'Now, to configure individual counters.
           'Use counter #5 as gate for up counters, ie. load counter
           '5 with # milliseconds = accumulate time.
           'Configure counter #5 by (first) setting data pointer
           'register to point to counter 5's mode register, this
           'done by writing 05H to the command register.
           'C7-C5 = 000 (reference data pointer register)
           'C4-C3 = 00 (E2-E1 = 00, indicates a mode register)
           'C2-C0 = 101 (G4-G1 = 101, indicates counter 5)
        OUT BSA% + 1, &H5
           'So, now write counter 5 mode word to counter 5's mode
           'register.
           '(Base address is now counter 5's mode register, as
           'specified by previous command).
           'CM15-CM13 = 000 (counter is not gated)
           'CM12 = 0 (count on rising edge)
           'CM11-CM8 = 1110 (count source = F4 = 1Khz, one count = 1
           'millisec.)
           'CM7 = 0 (disable special gate)
           'CM6 = 0 (reload from load)
           'CM5 = 1 (count repetitively)
           'CM4 = 0 (binary count)
           'CM3 = 0 (count down)
           'CM2-CM0 = 010 (output toggled)
```

```
        OUT BSA%, &H22: OUT BSA%, &HE
           'Now, configure counters 1 & 2 as cascaded up counters
           '(1 = low byte and 2 = high byte).
           'Begin by pointg to counter 1 control register, write 01H
           'to command register.
           'C7-C5 = 000 (reference data pointer register)
           'C4-C3 = 00 (E2-E1, a mode register)
           'C1-C0 = 001 (G4-G1, counter 1)
        OUT BSA% + 1, &H1
           'Now, to configure counter 1 send mode word to base
           'address (which is now counter 1 mode register, as per
           'above).
           'Mode word is 0229H
           'CM15-CM13 = 000 (no gating)
           'CM12 = 0 (count on rising edge)
           'CM11-CM8 = 0010 (count input is source 2, pin # 19 =
           'output of V/F converter).
           'CM7 = 0 (disable special gate)
           'CM6 = 0 (reload from load)
           'CM5 = 1 (count repetitively)
           'CM4 = 0 (binary count)
           'CM3 = 1 (count up)
           'CM2-CM0 = 001 (active high T.C. pulse)
        OUT BSA%, &H29: OUT BSA%, &H2
           'Now, set mode of high byte counter (#2)
           'First point to counter 2 mode register by writing 02H to
           'command register (base address + 1)
           'C7-C5 = 000 (reference data pointer register)
           'C4-C3 = 00 (E2-E1, a mode register)
           'C2-C0 = 010 (G4-G1, counter #2)
        OUT BSA% + 1, &H2
           'Configure counter 2 to count overflow of counter 1.
           'Write mode word 0029H to counter 2 mode register, now
           'at base address as per above.
           'CM15-CM13 = 000 (no gating)
           'CM12 = 0 (count on rising edge)
           'CM11-CM8 = 0000 (count source is output of n-1 counter,
           'counter 1).
           'CM7 = 0 (disable special gate)
           'CM6 = 0 (reload from load)
           'CM5 = 1 (count repetitively)
           'CM4 = 0 (binary count)
           'CM3 = 0 (count up)
           'CM3-CM0 = 001 (active high T.C. pulse)
        OUT BSA%, &H29: OUT BSA%, &H0
        RETURN
'-----------------------------------------LOAD COUNTERS----------
LOADD:
           'First ensure that counter 5 toggle is set high.
           'Write EDH to command register (at BSA% + 1).
           'C7-C3 = 1110 1 (set output bit of specified counter)
           'C2-C0 = 101 (specify counter 5)
        OUT BSA% + 1, &HED
           'Next point to counter 5 load register by writing 0DH to
```

```
            'command register (base address + 1).
            'C7-C5 = 000 (data pointer register)
            'C4-C3 = 01 (E2-E1, a load register)
            'C2-C0 = 101 (G4-G1, counter 5)
         OUT BSA% + 1, &HD
            'Now load gate time (as entered by user as integrate time,
            'at this pt. must be in ms) by writing appropriate value
            '(low bye first, high byte second) to counter 5 load
            'register now at base address as per above command.
            'Variable holding this parameter is ctm(3).
         CTM(5) = INT(CTM(3) / 256)
         CTM(6) = CTM(3) - (CTM(5) * 256)
         OUT BSA%, CTM(6): OUT BSA%, CTM(5)
            'Load both counters 1 & 2 with 0000, first counter 1.
            'Point to counter 1's load register by writing 09H to
            'command register (BSA% + 1).
            'C7-C5 = 000 (reference data pointer)
            'C4-C3 = 01' (load register of specified counter)'
            'C2-C0 = 001 (specify counter 1)
         OUT BSA% + 1, &H9
            'Write 0000 to counter 1 load register (now at BSA%)
         OUT BSA%, &H0: OUT BSA%, &H0
            'Now for counter 2.  Point to counter 2's load register.
         OUT BSA% + 1, &HA
            'Load it with 0000.
         OUT BSA%, &H0: OUT BSA%, &H0
         RETURN
'-----------------------------------------COUNT (ARM)-------------
ARM:
            'Set loop counter.
         XX = 1
AGAIN:
            'Make sure counter 5 output bit is high.
         OUT BSA% + 1, &HED
            'Load and arm counter 5 by writing 70H to command register
            'C7-C5 = 011 (load and arm selected counters)
            'C4-C0 = 1 0000 (select counter 5)
            'Delay, then load and arm counter 1 & 2.
         OUT BSA% + 1, &H70
         FOR I = 1 TO 6
         NEXT I
         DUMMY = ABS(I)
         OUT BSA% + 1, &H63
            'Now poll for counter 5's output bit to toggle low.
            'Check by reading status register (BSA% + 1)
POLL:
         P = INP(BSA% + 1)
         IF P > 128 OR P = 128 THEN P = P - 128
         IF P > 64 OR P = 64 THEN P = P - 64
         IF P > 32 OR P = 32 THEN GOTO POLL
            'Once its low, first priority is to latch counters by
            'writing save (93H) to command register (BSA% + 1).
            'C7-C5 = 100 (disarm & save specified counters)
            'C4-C0 = 1 0011 (specify counters 5, 2, & 1)
```

```
        OUT BSA% + 1, &H93
           'Now read count values from hold registers.'
           'Write 11H to command register (BSA% + 1)
           'C7-C5 = 000 (reference data pointer)
           'C4-C3 = 10 (E2-E1, a hold register)
           'C2-C0 = 001 (G4,G1, counter 1)
        OUT BSA% + 1, &H11
           'Read counter 1 low byte first, high byte second
           'Hold register for counter 1 is now at BSA%
        LOW1 = INP(BSA%): HIGH1 = INP(BSA%)
           'Point to counter 2's hold register.
        OUT BSA% + 1, &H12
           'Read counter 2 low byte first, high byte second.
        LOW2 = INP(BSA%): HIGH2 = INP(BSA%)
           'Calculate count (now need to include HIGH2%)
        SUM! = LOW1 + (HIGH1 * 256) + (LOW2 * 65536)
           'Place sum in array.
        COUNT(XX) = SUM!
           'See if done.
        YY = (80 - XX)
        IF YY = 0 THEN GOTO DONE2
        XX = (XX + 1)
        PRINT XX; YY
        GOTO AGAIN
DONE2:
        RETURN
'------------------------------------------ FILE SAVE-------------
STORE:
        PRINT XX
        IF DEX% > 9 AND DEX% < 100 THEN
           NCHAR = 2
           ELSEIF DEX% < 9 THEN
           NCHAR = 1
        END IF
        DEX$ = RIGHT$(DEX$, NCHAR)
        FILES$ = "A:" + FILE$ + DEX$ + ".WR1"
        OPEN FILES$ FOR OUTPUT AS #2
        SECOND$ = "FIRST # = # DATA POINTS"
        FIRST$ = "SECOND # = GATE PERIOD (ms)"
        PRINT #2, FILE$
        PRINT #2, DESCRIPT$
        PRINT #2, SECOND$
        PRINT #2, FIRST$
        PRINT #2, CTM(4)
        PRINT #2, CTM(3)
        FOR I = 1 TO CTM(4)
           PRINT #2, COUNT(I)
        NEXT
        CLOSE #2
        DEX% = (DEX% + 1)
        DEX$ = STR$(DEX%)
        RETURN

'*************************************************************************
```

```
'SCAN SUBROUTINES
'*************************************************************************

'----------------------------------------SCAN INITIALIZATION ------
SCANI:
        ON ERROR GOTO ERROR1
        OPEN "com1:9600,n,8,2,rs,ds" FOR RANDOM AS #1
        PRINT #1, ""                            'Send dummy prompt
        INPUT #1, A$                            'Read PTR message
HERE1:
        PRINT "PLEASE WAIT"                     'Potential error here
              A$ = "f1"                         'Go to high limit
        PRINT #1, A$
        INPUT #1, A$, B$, C$                    'Clear buffer
        FOR I = 1 TO 70000!                     'Wait for MC to finish
        NEXT
        A$ = "f0"                               'Go to low limit
        PRINT #1, A$
        INPUT #1, A$, B$                        'Clear buffer
        FOR I = 1 TO 70000!                     'Wait fo MC to finish
        NEXT
        Z$ = "z"
        PRINT #1, Z$                            'Get location of f0
        INPUT #1, A$, F$                        '(step # of f0)
        ON ERROR GOTO ERROR2                    'Potential error here
HERE2:
        OPEN "ofset.txt" FOR INPUT AS #2        'Read previous location
        INPUT #2, E!                            'of zero order (step
        CLOSE #2                                'offset from f0)
        P$ = "+"
        PRINT #1, P$; E!                        'Goto zero order
        INPUT #1, A$, B$                        '(clear buffer)
        FOR I = 1 TO 1000
        NEXT                                    'Wait for movement
        PRINT #1, Z$                            'Get present location
        INPUT #1, A$, G$                        '(count) of zero order
        A = VAL(F$)                             'F$=F0 count (location)
        B = VAL(G$)                             'G$=zero order location
        E! = B - A                              'E!=present offset
        RETURN
'-----------------------------------------SCAN  MAIN MENU -------
SCANM:
       CLS
       LOCATE 5, 24: PRINT "ENTER                FOR FUNCTION"
       LOCATE 6, 24: PRINT "=====              ================="
       LOCATE 8, 24: PRINT "  O               OPTIMIZE ZERO ORDER"
       LOCATE 10, 24: PRINT "  W             GOTO SINGLE WAVELENGTH"
       LOCATE 12, 24: PRINT "  I         INCREMENT AROUND PRESENT
SETTING"
       LOCATE 14, 24: PRINT "  S            PERFORM WAVELENGTH
SCANNING"
       LOCATE 16, 24: PRINT "  E                          EXIT"
       LOCATE 20, 24: INPUT "TYPE CHOICE "; A$
       IF A$ = "I" OR A$ = "i" THEN GOTO INCRE
```

```
        IF A$ = "W" OR A$ = "w" THEN GOTO SINGLE1
        IF A$ = "O" OR A$ = "o" THEN GOTO OPT1
        IF A$ = "S" OR A$ = "s" THEN GOTO SCAND
        IF A$ = "E" OR A$ = "e" THEN GOTO QUITS
        CLS : PRINT "INVALID CHOICE, TRY AGAIN"
        GOTO SCANM
SCAND:  GOSUB SCANA
        GOSUB SCANGO
        CLS
        LOCATE 16, 24: PRINT "PLEASE WAIT FOR SCAN TO FINISH PRIOR"
        LOCATE 17, 24: PRINT "    TO ENTERING NEXT COMMAND"
        LOCATE 20, 24: INPUT "ANOTHER SCAN (Y or N)"; H$
        IF H$ = "y" OR H$ = "Y" THEN GOTO SCAND
        GOTO SCANM
QUITS:  PRINT #1, I$; S$                        'Reset controller
        INPUT #1, A$, B$                        'to slew speed
        PRINT #1, D$; E$                        'for later use
        INPUT #1, A$, B$                        '& turn controller
        U$ = "EO"                               'current off.
        PRINT #1, U$                            '
        INPUT #1, A$, B$                        '
RETURN                                          '
'----------------------------------- ZERO ORDER OPTIMIZATION ----
OPT1:
        PRINT #1, I$; S$                        'Slew speed
        INPUT #1, A$, B$
        PRINT #1, D$; E$
        INPUT #1, A$, B$
        U$ = "E1"                               'Controller current on
        PRINT #1, U$
        INPUT #1, A$, B$
        A$ = "FO"                               'Go home
        PRINT #1, A$
        INPUT #1, A$, B$                        'Clear buffer
        FOR I = 1 TO 70000!                     'Wait
        NEXT
        P$ = "+"
        PRINT #1, P$; E!                        'Goto initial
        INPUT #1, A$, B$                        'location of
        FOR I = 1 TO 10000                      'zero order
        NEXT
        CLS
        I = 0                                   'increment counter = 0
        LOCATE 4, 24: PRINT "              ZERO ORDER OPTIMIZATION
      ROUTINE "
        LOCATE 8, 24: PRINT "NOW AT ORIGINAL LOCATION OF ZERO ORDER"
        LOCATE 10, 24: PRINT "TO OPTIMIZE ZERO ORDER, MAXIMIZE SIGNAL
      BY STEPPING + OR -"
        LOCATE 11, 24: PRINT "AROUND INITIAL LOCATION.  TO STEP +,
      TYPE (U) FOR UP, TO"
        LOCATE 12, 24: PRINT "STEP -, TYPE (D) FOR DOWN.  WHEN
      MAXIMUM SIGNAL IS OBSERVED"
        LOCATE 13, 24: PRINT "OPTIMIZATION IS COMPLETE AND TYPE (M)."
        GOSUB INCR1                             'Goto increment subroutine
```

```
        PRINT #1, Z$                          'Get new location (count)
        INPUT #1, A$, G$                      'of (optimized) zero order
        B = VAL(G$)
        E! = B - A                            'Calculate new offset
        OPEN "OFSET.TXT" FOR OUTPUT AS #2     '(steps from F0) and write
        PRINT #2, E!                          'to file.
        CLOSE #2
        CLS
        GOTO SCANM                             'Return to scan menu
'---------------------------------- MONITOR SINGLE WAVELENGTH ------
SINGLE1:
        CLS
        INPUT "INPUT DESIRED WAVELENGTH (nm)", X$
        GOSUB LAMBDA1
        GOSUB FIND1
        PRINT "PRESENT WAVELENGTH SETTING IS"; L; "nm"
        GOTO SCANM
'--------------------INCREMENT AROUND PRESENT SETTING-------------
INCRE:
        CLS
        GOSUB FIND1
        PRINT "INITIAL WAVELENGTH IS"; L; "nm"
        PRINT
        PRINT "TO VARY AROUND PRESENT WAVELENGTH, TYPE (U) FOR UP AND
       (D)"
        PRINT "FOR DOWN.  WHEN WAVELENGTH SETTING IS OPTIMIZED, TYPE
       (M)."
        PRINT
        GOSUB INCR1
        GOSUB FIND1
        CLS : PRINT "NOW AT"; L; "nm"
        GOTO SCANM
'------------------------------------------- SCANNING --------
SCANA:
        CLS
        LOCATE 8, 24: INPUT "INPUT STARTING WAVELENGTH (nm)"; X$
        LOCATE 10, 24: INPUT "INPUT FINAL WAVELENGTH (nm)"; Y$
SCANB:
        LOCATE 12, 24: PRINT "POSSIBLE SCAN RATES (nm/min): 1, 5, 10,
      25, 50, 100, 150, 200, 500"
        LOCATE 14, 24: INPUT "INPUT SCAN RATE FROM LIST"; W$
        IF W$ = "1" THEN GOTO RATE1
        IF W$ = "5" THEN GOTO RATE2
        IF W$ = "10" THEN GOTO RATE3
        IF W$ = "25" THEN GOTO RATE4
        IF W$ = "50" THEN GOTO RATE5
        IF W$ = "100" THEN GOTO RATE6
        IF W$ = "150" THEN GOTO RATE7
        IF W$ = "200" THEN GOTO RATE8
        IF W$ = "500" THEN GOTO RATE9
        PRINT "SCAN RATE MUST BE ON LIST"
        GOTO SCANB
RATE1:
        M$ = "150": V$ = "1"
```

```
        GOTO SCANC
RATE2:
        M$ = "30": V$ = "1"
        GOTO SCANC
RATE3:
        M$ = "30": V$ = "2"
        GOTO SCANC
RATE4:
        M$ = "6": V$ = "1"
        GOTO SCANC
RATE5:
        M$ = "3": V$ = "1"
        GOTO SCANC
RATE6:
        M$ = "3": V$ = "2"
        GOTO SCANC
RATE7:
        M$ = "1": V$ = "1"
        GOTO SCANC
RATE8:
        M$ = "3": V$ = "4"
        GOTO SCANC
RATE9:
        M$ = "3": V$ = "10"
SCANC:
        Y = VAL(Y$)
        X = VAL(X$)
        C = Y - X
        GOSUB LAMBDA1
        IF C < 0 THEN P$ = "-"
        C = ABS(C)
        C = C * 8
        GOSUB FIND1
        PRINT C
        PRINT "NOW AT STARTING WAVELENGTH ("; L; "nm)"
        INPUT "IS THIS CORRECT ? (Y or N)"; J$
        IF J$ = "Y" OR J$ = "y" THEN GOTO CHECK
        GOSUB INCRS
        IF A$ = "A" OR A$ = "a" THEN GOTO SCANA
CHECK:
        RETURN
SCANGO:
        CLS
        PRINT C
        LOCATE 10, 10: INPUT "TO BEGIN SCAN, HIT RETURN "; A$
        U$ = "E1"
        PRINT #1, U$
        INPUT #1, A$, B$
        PRINT #1, I$; V$
        INPUT #1, A$, B$
        PRINT #1, D$; M$
        INPUT #1, A$, B$
        PRINT #1, P$; C
        INPUT #1, A$, B$
```

```
        P$ = "+"
        RETURN
'------------------------------ GOTO WAVELENGTH SUBROUTINE -----
LAMBDA1:
        U$ = "E1"                          'Controller current on
        PRINT #1, U$
        INPUT #1, A$, B$
        PRINT #1, I$; S$                   'Slew speed
        INPUT #1, A$, B$
        PRINT #1, D$; E$
        INPUT #1, A$, B$
        K = VAL(X$)                        'Calculate # of steps from
        K = (K * 8)                        'zero order
        K = (K + B)                        'Plus zero order offset
        K = (K - A)                        '(steps) from F0
        K! = K
        A$ = "F0"                          'Goto F0
        PRINT #1, A$
        INPUT #1, A$, B$                   'Clear buffer
        FOR I = 1 TO 70000!
        NEXT                               'Wait
        P$ = "+"
        PRINT #1, P$; K!                   'Goto selected wavelength
        INPUT #1, A$, B$                   '(K!=# steps from F0)
        FOR I = 1 TO 70000!
        NEXT                               'Wait to get there
        U$ = "E0"                          'Turn controller current off
        PRINT #1, U$                       'and clear buffer
        INPUT #1, A$, B$
        RETURN
'--------------------------- SCANNING INCREMENT SUBROUTINE ------
INCRS:
        PRINT "TYPE (A) TO BEGIN SCAN FROM SCRATCH"
        PRINT "TYPE (I) TO INCREMENT AROUND PRESENT SETTING"
        INPUT "CHOICE "; A$
        IF A$ = "A" OR A$ = "a" THEN GOTO SCRATCH
MORE:
        PRINT "TO INCREMENT, TYPE (U) FOR UP, (D) FOR DOWN, (M) WHEN
       FINISHED"
        PRINT "REMEMBER, EACH STEP=.125 nm"
        GOSUB INCR1
        GOSUB FIND1
        PRINT "NOW AT"; L; "nm"
        INPUT "INCREMENT SOME MORE (Y or N)"; A$
        IF A$ = "Y" OR A$ = "y" THEN GOTO MORE
SCRATCH:
        RETURN
'------------------------------------------ LOCATE SUBROUTINE ---
FIND1:
        PRINT #1, Z$                       'Get present location (count),
        INPUT #1, A$, L$                   'convert count to nm (8counts=1nm)
        L = VAL(L$)                        'and save nm location in L
        L = (L - B) / 8
        RETURN
```

```
'---------------------------------------- INCREMENT SUBROUTINE -----
INCR1:
        U$ = "E1"                   'Controller current on
        PRINT #1, U$
        INPUT #1, A$, B$            'Clear buffer
        I = 0                       'Set increment counter to 0
        PRINT "TYPE COMMAND IN RESPONSE TO QUESTION MARK PROMPT."
INCR2:
        INPUT A$
        IF A$ = "M" OR A$ = "m" THEN GOTO INCR3
        IF A$ = "U" OR A$ = "u" THEN GOTO INCR4
        PRINT #1, N$                'Step -1
        INPUT #1, A$, B$            'Clear buffer
        I = I - 1                   'Increment counter
        PRINT "PRESENT POSITION W.R.T. INITIAL LOCATION IS", I
        GOTO INCR2
INCR4:
        PRINT #1, O$                'Step +1
        INPUT #1, A$, B$            'Clear buffer
        I = I + 1                   'Increment counter
        PRINT "PRESENT POSITION W.R.T. INITIAL LOCATION IS", I
        GOTO INCR2
INCR3:
        PRINT "OPTIMIZATION COMPLETE"
        U$ = "E0"                   'Turn controller current
        PRINT #1, U$                'off
        INPUT #1, A$, B$            'Clear buffer
        CLS
        RETURN
'---------------------------------------------- ERROR TRAPS ---------
ERROR1:
        PRINT #1, ""
        INPUT #1, A$
        RESUME HERE1
ERROR2:
        PRINT "?"
        RESUME NEXT
```